Pliocene Vegetation and Climate of Arctic Norway and the Variability of the Norwegian Atlantic Current

Sina Panitz

Doctor of Philosophy

2016

Northumbria University at Newcastle

Pliocene Vegetation and Climate of Arctic Norway and the Variability of the Norwegian Atlantic Current

Sina Panitz

A thesis submitted in partial fulfilment of the requirements of the University of Northumbria for the degree of Doctor of Philosophy

Research undertaken in the Faculty of Engineering and Environment

October 2016

Microscopic "creatures"

unlike each other, but with similar features.

Released into the air by flowers and trees,

or swimming in the sun-lit waters of the seas.

While admiring them in all their glory,

they are telling me their long story.

Abstract

The Pliocene Epoch (5.33–2.59 Ma) is characterised by climatic conditions similar to those predicted for 2100, with enhanced warming in the (sub-)Arctic. The climate evolution at high latitudes is not well understood due to the sparsity of time-continuous palaeoenvironmental records. This study provides new records of Pliocene vegetation changes in Arctic Norway and the variability of the Norwegian Atlantic Current based on analyses of terrestrial and marine palynomorphs from ODP Site 642 (Norwegian Sea, 67°N) to assess climate variability and identify different scale forcing mechanisms.

The Piacenzian pollen record (3.60–3.14 Ma) shows vegetation changes between cool temperate and boreal forests during warmer-than-present and similar-to-present climate phases, respectively, implying shifts of the northern deciduous/mixed forest limit of 4–8° latitude. During warm phases, warmest month temperatures were 8–14°C higher than present. The development of peatlands during cooler phases may have amplified the cooling through CO_2-drawdown and positive vegetation-snow feedbacks. The high regional and hemispheric-wide climate variability highlights the importance of well-dated, high-resolution records for regional to global palaeoenvironmental reconstructions and data-model comparisons.

Long-term Pliocene vegetation changes (5.03–3.14 Ma) reveal a continuous decline of thermophilic elements over successive warm phases, supporting the notion of long-term climate cooling caused by decreasing CO_2 concentrations. This cooling is superimposed on shifts between cool temperate and boreal climate phases on multi-millennial timescales. Minima in eccentricity (400-ka), together with low-amplitude obliquity/precession cycles are associated with the development of boreal conditions. At 4.56 Ma, a marked decline in pollen influx suggests atmospheric circulation changes in response to the shoaling of the Central American Seaway, a hypothesis supported by model results. Subsequently, changes in northward heat transport via the North Atlantic Current strongly affected vegetation changes. The Pliocene climate evolution represents the later part of late Neogene cooling instead of a reversal of that trend.

Dinoflagellate cyst assemblage changes (3.320–3.137 Ma) indicate variations in Atlantic and Arctic water influence, corresponding to cool temperate and boreal terrestrial climatic conditions in Arctic Norway, respectively. These records emphasise a high climate variability on glacial-interglacial timescales and linkage of both marine and terrestrial environmental changes.

I

List of contents

List of figures

List of tables

List of plates

List of Abbreviations

ABF – Acritarch Burial Flux

AMOC – Atlantic Meridional Overturning Circulation

ANN – Artificial Neural Network

A.s.l. – above sea level

C – Cold water

CA – Coexistence Approach

CAS – Central American Seaway

CCA – Canonical Correspondence Analysis

CMT – Coldest Month Temperature

DCA – Detrended Correspondence Analysis

DBF – Dinoflagellate cyst (dinocyst) Burial Flux

Dinocysts – Dinoflagellate cysts

DSDP – Deep Sea Drilling Project

EGC – East Greenland Current

GDGT – Glycerol Dialkyl Glycerol Tetraether

GSR – Greenland-Scotland Ridge

HadCM3 – Hadley Centre coupled atmosphere-ocean Climate Model

IN – Inner Neritic

IODP – Integrated Ocean Drilling Program

IRD – Ice-Rafted Debris

NAC – North Atlantic Current

NCC – North Cape Current

NHG – Northern Hemisphere Glaciation

NLR – Nearest Living Relative

NwAC – Norwegian Atlantic Current

MAP – Mean Annual Precipitation

MAT – Mean Annual Temperature

Mbsf – Metre below sea floor

MCR – Mutual Climatic Range

MIS – Marine Isotope Stage

MPd – Monthly Precipitation of the driest month

MPw – Monthly Precipitation of the warmest month

mPWP – mid-Piacenzian Warm Period

MPwt – Monthly Precipitation of the wettest month

O – Oceanic

OCCP – Ocean Controls on high-latitude Climate sensitivity – a Pliocene case study

ODP – Ocean Drilling Program

ON – Outer Neritic

PAR – Pollen Accumulation Rate

PC – Principal Component

PCA – Principal Component Analysis

PlioMIP – Pliocene Model Intercomparison Project

PRISM – Pliocene Research, Interpretation and Synoptic Mapping

PZ – Pollen Zone

RBC – Round Brown Cyst

RDA – Canonical Redundancy Analysis

SSA – Small Spiny Acritarchs

SST – Sea Surface Temperature

W – Warm water

WA – Weighted-Averaging regression

WA-PLS – Weighted-Averaging Partial Least Squares regression

WGC – West Greenland Current

WMT – Warmest Month Temperature

WSC – West Spitzbergen Current

Acknowledgements

Declaration

I declare that the work contained in this thesis has not been submitted for any other award and that it is all my own work. I also conform that this work fully acknowledges opinions, ideas and contributions from the work of others. The work was conducted in collaboration with Uni Research Climate and the Bjerknes Centre for Climate Research in Bergen, Norway, contributing to the project "OCCP – Ocean Controls on high-latitude Climate sensitivity – a Pliocene case study".

Any ethical clearance for the research presented in this thesis has been approved. Approval has been sought and granted by the University Ethics Committee on the 7th of April 2014.

I declare that the Word Count of this Thesis is 41,919 words.

Name: Sina Panitz

Signature:

Date: 13.02.2017

Publications from this thesis

Chapter 3 of this thesis has been published: **Panitz, S.**, Salzmann, U., Risebrobakken, B., De Schepper, S. and Pound, M. J., 2016. Climate variability and long-term expansion of peatlands in Arctic Norway during the late Pliocene (ODP Site 642, Norwegian Sea). Clim. Past, 12, 1043–1060, doi:10.5194/cpd-11-5755-2015.

Chapter 1: Introduction

1.1   Project overview

1.1.1   Rationale

Present-day climate warming as a consequence of anthropogenic greenhouse gas emissions is particularly pronounced at high latitudes. Since the mid-19th century, the Arctic north of 60° latitude has warmed at a rate about twice as high as that of the global average (IPCC, 2013). This effect is known as Arctic amplification. The Arctic is more sensitive to climatic changes because of positive feedback mechanisms that are primarily associated with sea ice and snow cover, but also changes in vegetation, the extent of permafrost and the freshwater balance (Miller et al., 2010; Screen and Simmonds, 2010; Serreze and Francis, 2006). Several scenarios of future global warming, considering different radiative forcings under a range of CO_2 concentrations, project a global temperature rise in the order of 2–4°C by 2100, with warming being highest in the Arctic and over land (IPCC, 2013). One component of the enhanced warming at high latitudes is the northward migration of vegetation zones. A change from tundra vegetation to boreal, or even deciduous, forests acts as a positive feedback due to reductions in surface albedo and higher evapotranspiration rates (Pearson et al., 2013). While the extent of future Arctic vegetation changes under different climate scenarios can only be estimated by models, the reconstruction of vegetation during past warm intervals using proxy data provides the opportunity to better understand climate variability and to test climate models used to project future climate change (Haywood et al., 2011; Miller et al., 2010).

The Pliocene Epoch (5.33–2.59 Ma, Gibbard et al., 2010) represents the most recent interval in the Earth's history that is characterised by climatic conditions similar to those that current climate models project for the end of the 21st century (Dowsett et al., 2013a; Haywood et al., 2016; IPCC, 2013; Salzmann et al., 2013, 2011). In comparison to earlier past warm intervals, such as the Miocene or Paleocene-Eocene Thermal Maximum, the Pliocene world exhibits more similarities to the present, facilitating environmental interpretations and comparisons with present-day conditions and future projections (Haywood et al., 2011; Salzmann et al., 2009). For example, continents were located at or near their modern positions during the Pliocene and much of the Pliocene biota is still extant (Salzmann et al., 2011). In addition, a large number of

proxy data is available for the Pliocene and the geographical distribution of marine and terrestrial study sites is much more complete when compared to earlier past warm intervals (Dowsett et al., 2015; Haywood et al., 2016; Salzmann et al., 2013, 2011). However, distinct differences in boundary conditions between the present and the Pliocene (e.g. topography, ocean gateway configurations, the size of polar ice sheets and orbital configurations) hamper a direct comparison between projected and past climatic changes (Haywood et al., 2011; Salzmann et al., 2011). Furthermore, future climatic changes represent a forced perturbation to the climate system while the climate of the Pliocene was in equilibrium to long-term CO_2-forcing (Crowley, 1996; Haywood et al., 2011). Nevertheless, Pliocene environmental reconstructions are still one of the best methods available in order to understand the natural temporal variability and magnitude of climate changes, as well as processes operating in a warmer-than-present world.

Just as today, Pliocene warming was characterised by significant temperature increases at high latitudes as opposed to only minor temperature changes in the tropics and subtropics (Dowsett et al., 2010; Miller et al., 2010). Such latitudinal differences in the magnitude of warming resulted in a reduced equator-to-pole temperature gradient, suggesting increased meridional atmospheric and oceanic heat transport (Dowsett et al., 2013a; Salzmann et al., 2011). In the high northern latitudes, the Greenland ice sheet was markedly reduced in size and the Arctic may have been seasonally free of sea ice (Kleiven et al., 2002; Knies et al., 2014a). Boreal forest reached the Arctic coast, resulting in a less extensive distribution of tundra areas when compared to present (Salzmann et al., 2008). The associated reduction of surface albedo when compared to present together, with radiative forcing, resulted in enhanced high-latitude warming (Lunt et al., 2012).

The species composition of Northern Hemisphere boreal and temperate forests was much more homogenous during the Pliocene when compared to present. Species that are now restricted to North America and/or Southeast Asia displayed a circumpolar distribution (Svenning, 2003; Wen, 1999). Geographical barriers that existed over the course of the Cenozoic are the main result for the modern regionalisation of angiosperms (Xing et al., 2015). Nevertheless, climate change was responsible for the extinction of some temperate tree taxa in Europe at the end of the Pliocene (Svenning, 2003). Pliocene vegetation changes are characterised by profound northward shifts of vegetation zones at mid- to high latitudes. In Norway, temperate taxa grew at least 7° latitude north of their present limit and the prevalence of mixed forests in Svalbard

suggests a latitudinal northward shift of vegetation by about 10° (Willard, 1996, 1994). A late Pliocene (Piacenzian, 3.60–2.59 Ma, Gibbard et al., 2010) vegetation record from Ellesmere Island off East Greenland shows the presence of boreal forest to forest-tundra with mean summer temperatures at least 6°C higher than present (Bennike et al., 2002). On the west of Greenland, boreal forest reached the Arctic coast and terrestrial surface temperatures are estimated to have been up to 19°C higher than present during the Pliocene (Ballantyne et al., 2010, 2006; Rybczynski et al., 2013). While these records suggest stable, warmer-than-present climatic conditions during the Pliocene, their low resolution, poor age control and/or low temporal coverage hamper the reconstruction of Pliocene climate variability.

Despite warmer-than-present conditions, glaciation events have been documented during the Pliocene, highlighting the instability of Pliocene warmth (De Schepper et al., 2014). Most evidence for glacial advances around the Nordic Seas originates from ice-rafted debris (IRD) deposits in marine records (Jansen et al., 2000; Kleiven et al., 2002). The most pronounced event in Pliocene benthic oxygen isotope records is Marine Isotope Stage (MIS) M2 (Lisiecki and Raymo, 2005). This glacial event has been linked to a southward shift of the North Atlantic Current (NAC) (De Schepper et al., 2013). However, the terrestrial extent of MIS M2 and other events remains uncertain due to the scarcity of terrestrial glacial deposits and evidence in vegetation records (Andreev et al., 2014; Gao et al., 2012).

During the late Miocene and Pliocene, ocean gateway changes, particularly the opening of the Bering Strait and the shallowing of the Central American Seaway (CAS), resulted in profound oceanographic and climatic changes in the North Atlantic region. The Bering Strait opened around 5.5–5.4 Ma with water flowing from the Arctic to the Pacific Ocean (Gladenkov et al., 2002). The reversal towards a northward flow of Pacific water into the Arctic Ocean via the Bering Strait around 4.5 Ma within the early Pliocene (Zanclean, 5.33–3.60 Ma, (Gibbard et al., 2010)) has been associated with the shoaling of the CAS between 4.7 and 4.2 Ma (De Schepper et al., 2015; Haug et al., 2001; Verhoeven et al., 2011). As a result of the reversal, the inflow of cooler and fresher Pacific water led to the establishment of a proto-East Greenland Current (EGC) and thus the onset of a near-modern Nordic Seas circulation (De Schepper et al., 2015; Verhoeven et al., 2011). Around 3.9 Ma, Arctic sea ice reached its modern summer limit for the first time, possibly favoured by circum-Arctic mountain uplift and freshwater input from the Pacific and Siberian rivers (Knies et al., 2014a). The latter has

been proposed to be associated with an increased Atlantic Meridional Overturning Circulation (AMOC) and thus northward heat and moisture transport caused by the shoaling of the CAS (De Schepper et al., 2009a; Driscoll and Haug, 1998; Haug and Tiedemann, 1998; Osborne et al., 2014; Steph et al., 2006). A strengthened AMOC has been proposed to be responsible for the amplified warming at high latitudes when compared to mid- to low latitude regions during the Pliocene (Dowsett et al., 2013a, e.g. 1992; Robinson et al., 2011). However, recent modelling studies suggest that its strength was slightly reduced or similar to its present state (Hill, 2015; Zhang et al., 2013a). This is supported by alkenone-based sea surface temperature (SST) reconstructions in the Piacenzian, which suggest radiative forcing as the main cause of high-latitude warmth (Bachem et al., 2016). Nevertheless, shifts in the position/strength of the NAC and variations in northward heat transport during the Piacenzian have been documented in marine palaeoenvironmental reconstructions (De Schepper et al., 2009a; Lawrence et al., 2009). The effects of these changes in the northward heat transport on high-latitude vegetation and terrestrial climate are unknown.

Data-model comparison studies currently reveal a cold bias of modelled SST and surface air temperature reconstructions in the Northern Hemisphere high latitudes (Dowsett et al., 2013a; Salzmann et al., 2013). In the North Atlantic and Nordic Seas, proxy-based SST estimates reveal average values up to ~13°C higher than present during the mid-Piacenzian warm period (mPWP, 3.264–3.025 Ma, Dowsett et al., 2016; Robinson, 2009). This magnitude of polar amplification is not reflected in any of the applied models (Dowsett et al., 2013a). A recent modelling study suggests that the Norwegian Atlantic Current (NwAC), which is an extension of the NAC and strongly influences the climate of Scandinavia, may have been cooler than present as a result of altered geographical boundary conditions (Hill, 2015). The mismatch between data and models has been partly ascribed to the comparison of time-averaged proxy data to model simulations that represent a discrete time interval (Dowsett et al., 2013a; Salzmann et al., 2013). In order to reduce uncertainties in environmental reconstructions and climate modelling, an orbitally-defined time slice within the Piacenzian centred around 3.205 Ma (MIS KM5c) has been chosen for future palaeoclimate research (Haywood et al., 2013a).

To address the uncertainties with regard to Pliocene climate variability, the magnitude of glaciation events, and the role of oceanic and atmospheric forcing, high-resolution records of land cover changes and related ocean conditions are needed for the Nordic

Seas area. That terrestrial climatic conditions were not as stable as previously thought has been revealed by a high-resolution pollen record from the northeast Siberian Arctic, showing vegetation changes on orbital time scales (Andreev et al., 2014). Furthermore, the selection of a time slice for data-model comparison requires well-dated, high-resolution proxy records (Dowsett et al., 2013a; Haywood et al., 2013a; Salzmann et al., 2013).

1.1.2   Aim, research questions and objectives

This study presents the first Pliocene high-resolution records of vegetation changes in Arctic Norway and the variability of the NwAC. The main aim of this study is to assess terrestrial and marine high-latitude climate variability in Norway and the Norwegian Sea during the warmer-than-present Pliocene.

The following Research Questions (RQs) are formulated:

> **RQ 1:** What was the temporal variability and extent of vegetation changes in Arctic Norway during the Pliocene?

> **RQ 2:** What was the magnitude of Pliocene terrestrial temperature variations and is there any evidence for glaciation events in Norway?

> **RQ 3:** What was the variability of the Norwegian Atlantic Current during the Piacenzian?

> **RQ 4:** Are vegetation changes in Arctic Norway linked to the variability of the Norwegian Atlantic Current and/or atmospheric forcing mechanisms?

The reconstructions of vegetation and surface-ocean conditions are based on terrestrial and marine palynomorph assemblage changes in the sediments of Ocean Drilling Program (ODP) Hole 642B (67°N, 3°E) in the Norwegian Sea. A previous analysis of pollen has been conducted on nine samples in Hole 642C by Willard (1994). From the presence of pollen from coniferous and deciduous tree taxa, including temperate elements, Willard (1994) inferred the prevalence of a mixed forest at the northern limit of the deciduous forest zone in northern Norway. Here, a total of 128 samples are spread across the Pliocene section of the core (5.03–3.14 Ma) to establish a high-resolution record of vegetation and climate changes. In addition, dinoflagellate cyst (dinocysts) assemblage changes are investigated for an interval (3.35–3.14 Ma) within the Piacenzian and compared to vegetation changes. The age model for ODP Hole 642B

is based on magnetostratigraphy and correlation of benthic oxygen isotope signal to the global benthic $\delta^{18}O$ stack (Lisiecki and Raymo, 2005; Risebrobakken et al., 2016), enabling the correlation of environmental changes to other well-dated sites within the North Atlantic region and circumpolar Northern Hemisphere.

This PhD project contributes to the "Pliocene Model Intercomparison (PlioMIP)/Pliocene Research, Interpretation and Synoptic Mapping (PRISM)" project (Dowsett et al., 2016; Haywood et al., 2016) and PAGES workgroup "Pliocene climate variability over glacial-interglacial timescales; PlioVAR (McClymont et al., 2015). In addition, the work was conducted in close collaboration with Uni Research Climate and the Bjerknes Centre for Climate Research in Bergen, Norway, investigating Pliocene Arctic climate in the Nordic Sea as part of the project "OCCP – Ocean Controls on high-latitude Climate sensitivity – a Pliocene case study". The records of palynomorph assemblage changes, analysed in this study, will be compared to oxygen isotope data from planktonic foraminifera and alkenone-derived SSTs from the same core analysed at Uni Research Climate and the Bjerkness Center for Climate Research (Bachem et al., 2016; Risebrobakken et al., 2016).

1.1.3   Thesis structure

This thesis consists of six Chapters. The first chapter provides an overview of the modern vegetation and oceanography in the North Atlantic region and summarises Pliocene vegetation and oceanographic records and evidences for glaciations in this region. In Chapter 2, materials and methods are described. Chapter 3 presents vegetation and climate changes in northern Norway during the Piacenzian. The evolution of vegetation and climate during the Pliocene and possible controls are investigated in Chapter 4. In Chapter 5, the variability of the Norwegian Atlantic Current, as derived from dinocyst assemblage changes during the Piacenzian, is discussed and the data is compared to vegetation changes in northern Norway. The main conclusions of this research project are highlighted in Chapter 6.

1.2   Modern environment and oceanography of the North Atlantic region

1.2.1   Vegetation and climate

1.2.1.1 Temperate to polar zones

At present, the Northern Hemisphere mid- to high latitudes are characterised by a relatively strong latitudinal temperature gradient that is reflected in the vegetation
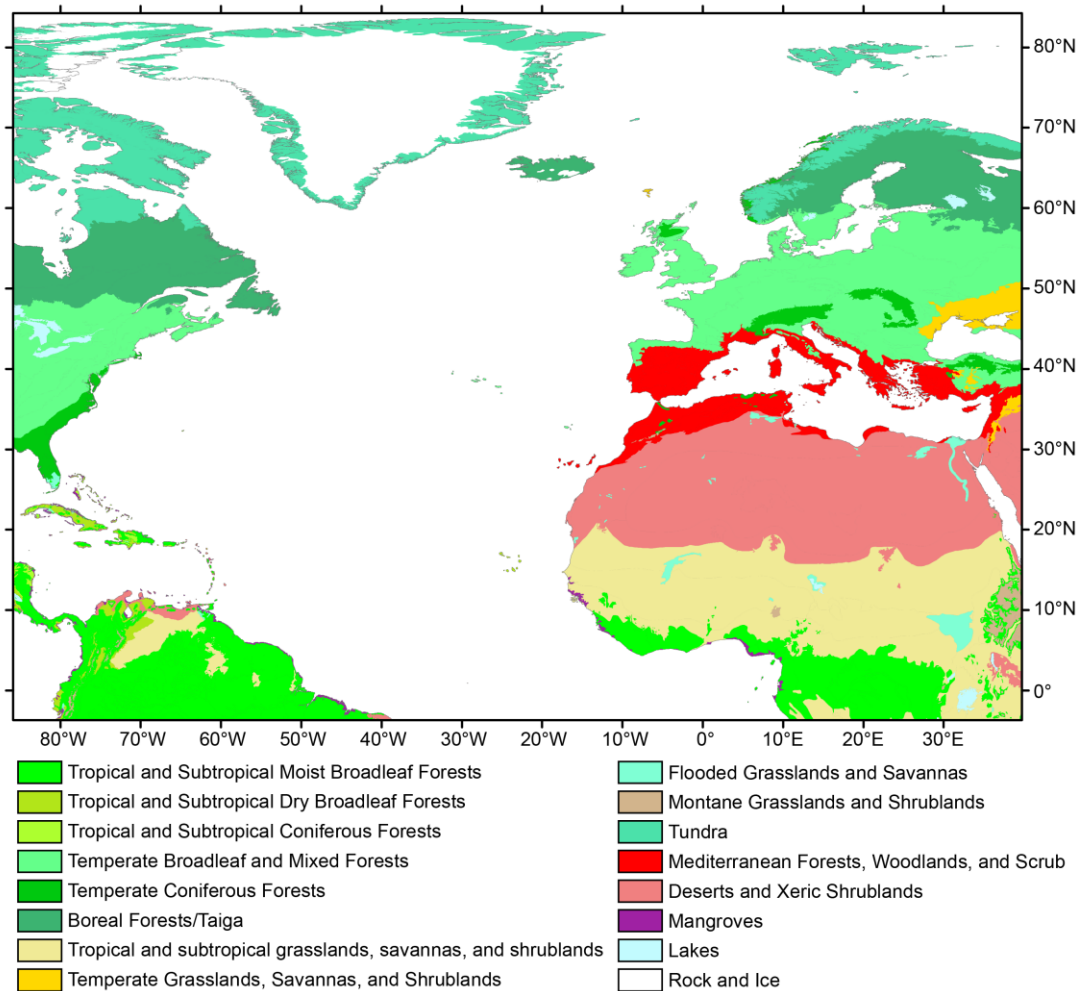
Figure 1.1: Biome distribution in the North Atlantic region. Data obtained from Olson et al. (2001).

distribution. The temperate deciduous forests of Central Europe pass into boreal forests at c. 60°N and tundra vegetation prevails beyond c. 68°N in northern Scandinavia (Figure 1.1). In southern Norway, the deciduous forest reaches its northernmost limit in the world due to the influence of the warm waters of the NAC (Diekmann, 1994; Moen, 1999). In addition to the latitudinal climatic gradient, climate and vegetation of Norway change with increasing altitude of the Scandinavian mountains with mixed to boreal forests in the lowlands and alpine tundra at higher elevations (Moen, 1999, 1987).

The climate of the temperate deciduous forest zone is continental to maritime with warm (16–22°C on average), moist summers and cold (-4°C to -15°C on average) winters. Precipitation is relatively evenly distributed around the year, ranging between 500–2500 mm (Archibold, 1995; Gurevitch et al., 2002). At present, the composition of Northern Hemisphere temperate and boreal forests is characterised by a strong regionalisation of thermophilic taxa in comparison to past periods of the Cenozoic. The flora of central Europe is relatively depauperate when compared to that of North

America and eastern Asia. In Europe, the dominant tree genera include *Betula*, *Carpinus*, *Corylus*, *Fagus*, *Quercus* and *Ulmus*. In contrast, the temperate deciduous forests of eastern North America are much more diverse with more than 120 tree species. Predominate tree genera include *Acer*, *Aesculus*, *Betula*, *Carya*, *Castanea*, *Fraxinus*, *Juglans*, *Liriodendron*, *Magnolia* and *Tilia* (Gurevitch et al., 2002). This regionalisation of thermophilic tree taxa is mainly the result of the establishment of geographical barriers throughout the Cenozoic and long-term cooling of climate which led to extensive glaciations in the Northern Hemisphere high latitudes (Svenning, 2003; Xing et al., 2015). During most of the Cenozoic, thermophilic taxa that are presently endemic to North America and/or eastern Asia (e.g. *Carya*, *Sciadopitys* and *Tsuga*) also thrived in Europe (e.g. Fauquette et al., 1999; Ferguson and Knobloch, 1998; Mohr, 1984; Rousseau et al., 1995; Willard, 1994; Zagwijn, 1960).

Northern Hemisphere boreal forests show a circumpolar distribution and are characterised by cold, dry climates with a large annual temperature range and a short growing season. Mean summer temperatures are above 10°C for 30–120 days and mean winter temperatures as low as -30°C (Archibold, 1995). Precipitation can, however, be quite variable and reaches highest values in coastal areas and along mountain ranges. Four coniferous tree genera, namely *Abies*, *Larix*, *Picea* and *Pinus*, dominate the circumpolar boreal forests (Gurevitch et al., 2002). In northern Europe, the boreal forest stretches from c. 58°N to 68°N. *Pinus* and *Picea* are the most abundant tree genera in Scandinavia with *Alnus* and *Betula* also being widely distributed (Archibold, 1995; Moen, 1999). Mixed forests form the transition between pure deciduous and coniferous forests and are part of the boreal zone. In Scandinavia, the mixed forest zone extends between c. 58°N and 63°N (Moen, 1999). At the northern boundary of the boreal forest zone, a belt of birch trees forms the tree line, beyond which shrub willow (*Salix*) and heath communities extend (Archibold, 1995; Moen, 1999).

Beyond the northern boundary of the boreal forest the growth of woody plants is restricted due to warmest month temperatures below 10°C, frost-free conditions for only 2–6 months of the year and low precipitation (Archibold, 1995; Gurevitch et al., 2002). The vegetation consists of shrubs, grasses, sedges, mosses and lichens. These shrublands transition into treeless tundra vegetation at higher latitudes and altitudes where permafrost is continuously present (Figure 1.1) (Gurevitch et al., 2002). The climate is cold, dry (<250 mm/yr) and windy, with maritime influences in coastal areas

(Archibold, 1995). The alpine flora of Scandinavia is similar to that of the Arctic (Archibold, 1995; Moen, 1999).

At higher latitudes in the boreal and tundra regions of the northern hemisphere, the cool and moist climate favours the extensive development of peatlands. Peatlands form where evaporation rates are low and the water table remains at or near the surface for most of the year. The peatlands of Scandinavia together with those found in Canada and Russia constitute almost 90% of the total Earth's peatland area (Archibold, 1995). In Norway, blanket bogs are more widespread when compared to Sweden and Finland, where fens and mires are the dominant wetland type, due to higher rainfall. The most common species in these bogs are peat mosses (*Sphagnum*) (Archibold, 1995; Moen, 1999).

1.2.1.2 Vegetation composition of Norway and orography

As a result of the influence of the NAC and warm westerly and south-westerly winds, the climate of Norway is maritime, with mild winters and higher Mean Annual Temperatures (MATs) than any other area at comparable latitudes (Diekmann, 1994). Due to its geographic location and the Scandinavian mountains that run from north to south, the climate and vegetation of Norway changes along three gradients: latitudinal, altitudinal and continental (Moen, 1987). While MATs decrease with increasing latitude as well as altitude and continentality, precipitation decreases from west to east, being highest along the southwest coast of Norway (Diekmann, 1994).

At present, mountains reach a maximum elevation of 1500 m in northern Norway (Nordland) with the tree line being lowest near the coast (400–500 m above sea level (a.s.l.)) and reaching elevations of up to 800 m a.s.l. further inland (Moen, 1999). In this area, MATs and Warmest Month Temperatures (WMTs, July) range
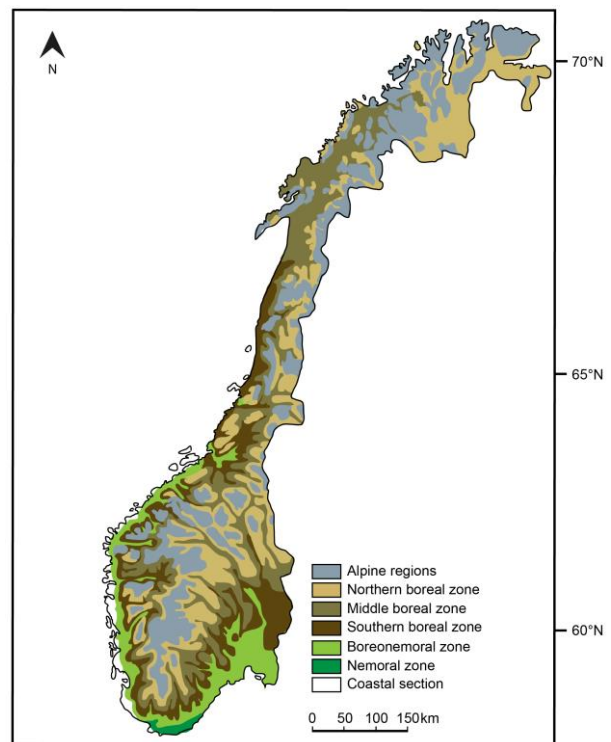
Figure 1.2: Vegetation of Norway modified after Moen (1987).

9

between 4–6 °C and 12–16°C along the coast and -6–-4°C and 0–4°C at the higher altitudes, respectively (Moen, 1999). Bodø (67°N) and Mo i Rana (66°N) are the closest meteorological stations to ODP Hole 642B, from which climate data is available for the last 30 years from the Meteorological Institute of Norway. The weather station near Bodø is situated near the coast, 11 m a.s.l. Mo i Rana is located at the head of a fjord around 50 km east of the coast, with the weather station lying 70 m a. s. l. At both stations, present-day MATs average -0.5°C with values ranging between ~ -2.5 and 1.7°C and WMTs reach 9.8°C on average, ranging between 5.8 and 13.8°C (Norwegian Meteorological Institute and Norwegian Broadcasting Corporation, 2014). In Norway, precipitation follows a strong east-west gradient. Mean Annual Precipitation (MAP) ranges from 1000 to 2500 mm along a broad south-north stretching coastal belt and only drops below 1000 mm further inland. In the area around Bodø and Mo i Rana, MAP is 1000–1500 mm (Diekmann, 1994; Moen, 1999).

Most of Norway is covered by boreal and alpine vegetation today (Figure 1.2). To the south, the boreal zone transitions into the temperate deciduous forests of Central Europe. In the north (~70°N) and at higher elevations, the boreal zone is limited by the tree line formed by the birch tree *Betula pubescens* and borders the Arctic and alpine tundra (Moen, 1999, 1987). The altitudinal limit of the tree line above which alpine tundra dominates decreases gradually from ~1200 m a.s.l. in the southern Scandinavian mountains to sea level in northernmost Norway (Moen, 1999). The flora becomes less diverse and forest productivity, as well as tree density, declines from south to north (Moen, 1987). Temperate deciduous forest is only found along the far south coast and is characterised by the absence of *Picea abies* (Figure 1.2) (Diekmann, 1994; Moen, 1987).

The boreal zone is divided into four subzones (boreonemoral, southern, middle and northern boreal zone; Figure 1.2) that follow climatic gradients. The climate is characterised by cold winters, long-lasting snow cover and a short growing season (Moen, 1987). The southernmost boreal zone (boreonemoral) mainly consists of *Pinus sylvestris* and *Picea abies*, with thermophilic deciduous trees (e.g. *Acer platanoides*, *Fraxinus excelsior*, *Quercus* spp., *Tilia cordata* and *Ulmus glabra*) abundant under favourable local climatic conditions, especially on south-facing slopes (Diekmann, 1994). Presently, the boreonemoral zone extends over a continuous area in southern Norway, but also occurs sporadically up to ~64°N (Moen, 1987). The northern boreonemoral limit is defined by the northernmost distribution of *Quercus* forest, but

the absence of oak forest in central Norway may also be due to topographical barriers (Diekmann, 1994; Moen, 1987).

In the southern boreal zone, deciduous forest (*Alnus* spp., *Betula* spp. and *Corylus avellana*) is still present and wide areas are covered by raised bogs. The latitudinal boundary between the southern and middle boreal zone, with the latter being dominated by coniferous forests, is located at ~67°N (Figure 1.2). Raised bogs reach their upper altitudinal limit in this zone (Moen, 1987). Along the coast, the middle boreal zone extends to about 70°N where it transitions into the northern boreal zone, consisting of sparsely growing coniferous forest, a broad belt of birch forest (especially at higher altitudes in southern to central Norway), and peatlands (Moen, 1987). Beyond the northern boreal zone, alpine regions with grass-heaths communities extend at higher altitudes and latitudes (Moen, 1987).

Moen (1987) and Diekmann (1994) both separate a coastal section along the west and southwest coast of Norway that is distinct in climate and vegetation (Figure 1.2). Climatically, the coastal area is associated with mild winters, relatively cool summers and frequent precipitation. The modern vegetation, however, has been significantly altered by human activity, with the present dominance of open heathland (*Calluna vulgaris*) ascribable to logging and continuous burning and grazing cycles (Moen, 1987). Atlantic raised bogs that naturally lack any marginal forest stretch along the coast and the remaining forest stands are composed of *Alnus* spp., *Betula* spp., *Corylus avellana*, *Fraxinus excelsior*, *Pinus sylvestris* and *Quercus* spp. (Diekmann, 1994; Moen, 1987).

1.2.2   Oceanography of the Nordic Seas

1.2.2.1 Surface circulation and water masses

The relatively warm waters of the NwAC which is an extension of the NAC are responsible for the mild climate of Scandinavia (Diekmann, 1994; Moen, 1999). The NAC originates near 40°N at the east coast of North America where it separates from the Gulf Stream and flows northeastward before turning eastward near 50°N (Figure 1.3) (e.g. Lozier et al., 1995; Orvik and Niiler, 2002). In the eastern North Atlantic, a component of the NAC turns southward and joins the subtropical gyre. The northeastward-flowing NAC splits into two major branches that enter the Nordic Seas via the Iceland-Faroe Ridge and Faroe-Shetland Channel (Hansen and Østerhus, 2000; Orvik and Niiler, 2002). Upon entering the Norwegian Sea, these two branches form the
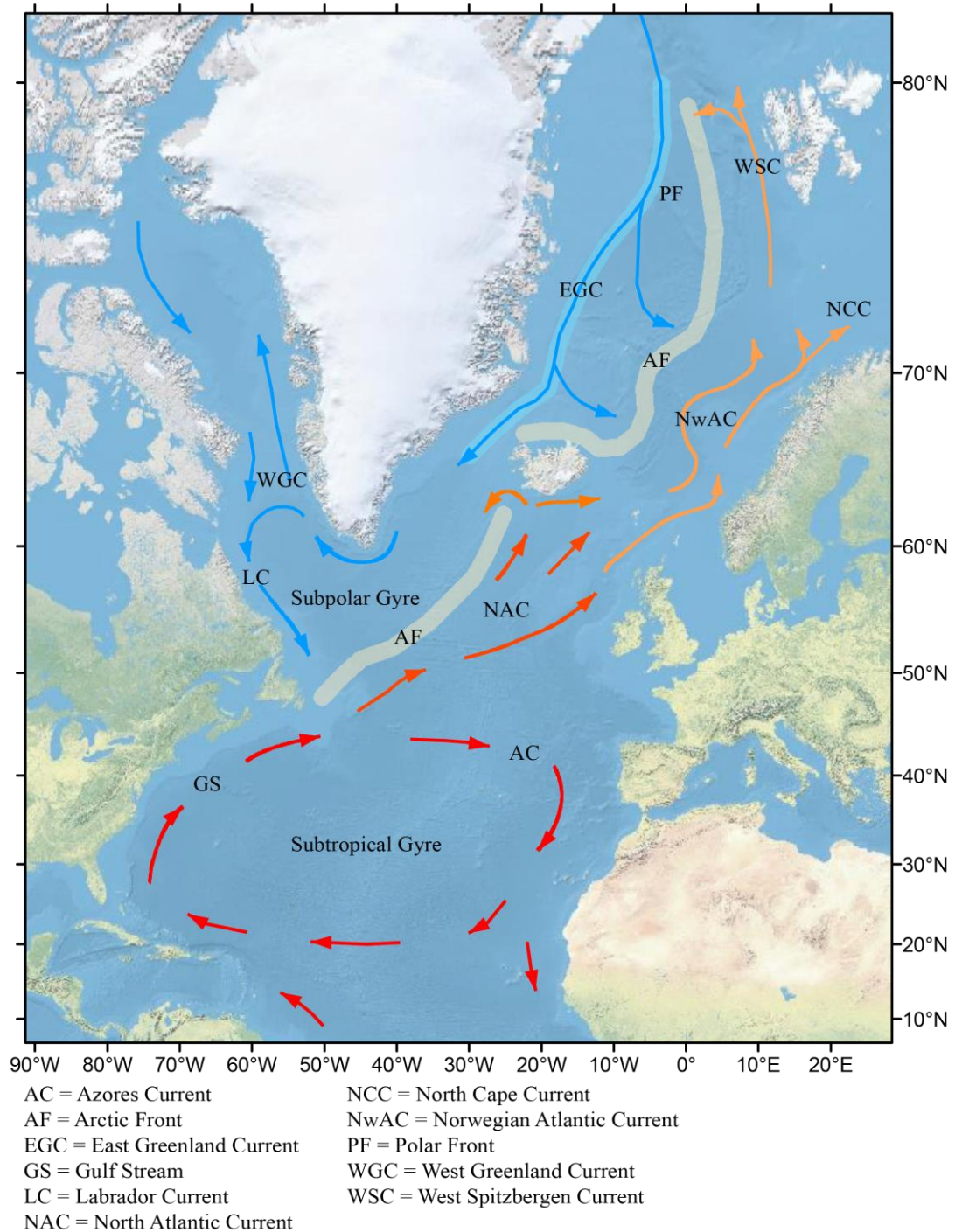
Figure 1.3: Modern ocean surface circulation in the North Atlantic and Nordic Seas. Colour coding is indicative of the relative temperature of the surface water masses: red = very warm; dark orange = warm; light orange = moderately warm; blue = cold.

NwAC (Figure 1.3). The western branch follows the topographic slope of the Vøring Plateau whereas the eastern branch flows along the Norwegian shelf edge, partly branching into the North Sea (Orvik and Niiler, 2002). North of Norway, the main flow of the eastern branch of the NwAC continues northwestwards towards the Fram Strait and into the Arctic Ocean where it is called the West Spitzbergen Current (WSC). A

smaller branch bifurcates into Barents Sea and forms the North Cape Current (NCC) (Figure 1.3) (Marret and Zonneveld, 2003; Orvik and Niiler, 2002). At present, the Barents Sea is an important area for the formation of cool and dense bottom water (Blindheim and Østerhus, 2005). Cold surface waters from the Arctic enter the Nordic Seas through the Fram Strait via the EGC which flows southward along the east coast of Greenland (Figure 1.3). Some of the waters of the EGC are diverted into adjacent basins and seas along the path, before the remaining part exits the Nordic Seas through the Denmark Strait (Blindheim and Østerhus, 2005).

The Nordic Seas are characterised by a steep zonal climatic gradient and its water masses can be divided into three domains from east to west: Atlantic domain, Arctic domain and Polar domain (Swift, 1986). Warm and saline (6–10°C, 35.1–35.3psu in summer) Atlantic waters cover the Norwegian Sea and are separated from the Arctic domain by the Arctic Front which runs from SW to NE north of Iceland and ends in the Fram Strait (Figure 1.3). The waters of the Arctic domain have relatively low temperatures and salinities (0–4°C, 34.6–34.9psu) and extend over much of the Greenland Sea and the northern Iceland Sea. The Arctic domain is separated from the Polar domain by the Polar Front which follows the north-to-south flowing EGC (Figure 1.3). The waters of the Polar domain to the west of the EGC are colder and less saline (<0°C, 30–34psu) than those of the Arctic domain (Swift, 1986).

1.2.2.2   Modern dinoflagellate cyst assemblage distribution

Dinoflagellates are unicellular organisms that live in marine as well as freshwater environments. Together with diatoms and coccolithophorids, they constitute the majority of the marine phytoplankton, and thus primary productivity. The feeding strategies of dinoflagellates include autotrophy, heterotrophy, symbiosis and parasitism (Marret and Zonneveld, 2003; Rochon et al., 1999). Some dinoflagellates produce resting cysts with walls made of organic, calcareous or siliceous substances during their life cycle. These cysts have a high potential for preservation in the geological record. Of all known dinoflagellates only 13–16% produces resting cysts. The majority of these produces organic-walled cysts (Head, 1996a). Most fossil dinocysts belong to the orders Gonyaulacales and Peridiniales. They are differentiated based on the tabulation pattern of the cyst (Evitt, 1985). Gonyaulacoid cysts are produced by autotrophic dinoflagellates and protoperidinioid cysts by heterotrophic species, with the latter cysts being characterised by a brown colour (e.g. Schreck et al., 2013; Verhoeven and

Louwye, 2013). Heterotrophic dinocysts are more sensitive to oxidation which may alter the fossil assemblages (e.g. De Schepper et al., 2004; Zonneveld et al., 2007).

Datasets of the modern global distribution of organic-walled dinocysts and correlations to oceanic waters masses and surface-water parameters provide a reference for palaeoenvironmental reconstructions (Marret and Zonneveld, 2003; Matthiessen, 1995; Rochon et al., 1999; Zonneveld et al., 2013). Matthiessen (1995) presents the first overview of the distribution of recent dinocysts in the Norwegian-Greenland Sea, revealing four assemblages (Figure 1.4). The first assemblage covers the Norwegian Sea and is characterised by high relative abundances of the cysts of *Protoceratium reticulatum* (*Operculodinium centrocarpum* sensu Wall and Dale 1966) (>60%) and a high species diversity. Other species include *Ataxiodinium choane*, *Bitectatodinium tepikiense*, *Nematosphaeropsis labyrinthus*, *Peridinium faeroense* and *Spiniferites* spp. The second assemblage follows the East Greenland continental shelf, shows a low diversity and is mainly composed of brown protoperidinioid cysts (e.g. *Brigantedinium simplex*). The third assemblage stretches across

Figure 1.4: Modern dinoflagellate cyst assemblages in the surface sediments of the Nordic Seas from Matthiessen (1995). Striated areas outline the regions where the most abundant species comprise at least 60% of the assemblages for 1, 2 and 4, and 30% for assemblage 3. **1:** cyst of *Protoceratium reticulatum*, **2:** *Brigantedinium* spp. and *Islandinium minutum*, **3:** *Impagidinium pallidum* and *Nematosphaeropsis labyrinthus*, **4:** *Peridinium faeroense*.

the Greenland and Iceland Seas and shows high relative abundances of *Impagidinium pallidum* and *N. labyrinthus*, suggesting that these species prefer cold oceanic environments. *Brigantedinium* spp. and cysts of *P. reticulatum* regionally form an important component of the assemblage. The fourth assemblage is found on the north Icelandic shelf and slope and the Iceland-Faeroe Ridge, and is characterised by the predominance of *P. faeroense*. The distribution of these assemblages can be correlated

to the prevailing water masses in the Norwegian-Greenland Sea (Figure 1.3, 1.4). Assemblage 1 follows the North Atlantic water domain, although not perfectly, in the Norwegian Sea. The polar domain along the EGC is characterised by assemblage 2. The distribution of assemblage 3 coincides with Arctic water masses in the Greenland and Iceland Seas. The shelf water masses of Iceland are represented by assemblage 4 (Matthiessen, 1995).

1.3   Pliocene environment and oceanography of the North Atlantic region

1.3.1   Climate and vegetation evolution from the Miocene to Pleistocene

The Pliocene Epoch (5.332–2.588 Ma) is the latter of two epochs within the Neogene Period (23.03–2.588 Ma) in the Cenozoic Era (65.5 Ma to present) and is divided into the Zanclean (5.332–3.600 Ma) and Piacenzian (3.600–2.588 Ma) Ages (Table 1.1) (Gibbard et al., 2010). The Pliocene Epoch follows on the Miocene Epoch (23.03–5.332 Ma) and precedes the Pleistocene Epoch (2.588–0.012 Ma) within the Quaternary Period (2.588 Ma to present; Table 1.1).

Geographically and climatically, the Pliocene represents a transitional stage between the Miocene and the modern world.

Table 1.1: Chronostratigraphic chart of the upper Cenozoic (modified after Gibbard et al. (2010)).

Era	Period	Epoch	Age	Age (Ma)
Cenozoic	Quaternary	Holocene		0.012
		Pleistocene	'Tarantian'	
			'Ionian'	
			'Calabrian'	
			Gelasian	2.588
	Neogene	Pliocene	Piacenzian	3.600
			Zanclean	5.332
		Miocene	Messinian	
			Tortonian	
			Serravalian	
			Langhian	
			Burdigalian	
			Aquitanian	23.03

Mountain uplift and the opening and closing of oceanic gateways during the Miocene led to the development of a modern-like tectonic setting by the beginning of the Pliocene (Potter and Szatmari, 2009). The climate evolved from significantly warmer-than-present conditions with no or much smaller ice caps on the poles during the Miocene to the cooling climate throughout the Pliocene to the glacial-interglacial stages of the Pleistocene (Zachos et al., 2001, 2008).

From the Middle to Late Miocene, climate progressively cooled. On land, warmest climatic conditions during the Middle Miocene are reflected by the presence of cool temperate mixed forests at the high northern latitudes which had been replaced by cold

evergreen needle-leaf forests by the end of the Miocene (Pound et al., 2012 and references therein). Late Miocene pollen and plant debris from the Hovgård Ridge west of Spitzbergen show the presence of swampy, taiga-like coniferous forests at 77–78°N (Boulter and Manum, 1997). In northwest Europe, conifer swamp forests with *Sciadopitys* and *Taxodium* and mixed forests persisted under subtropical to warm temperate conditions during the Middle to Late Miocene (Larsson et al., 2011; Mosbrugger et al., 1994; Pound and Riding, 2015). In the ocean, SST records and palaeoenvironmental reconstructions based on marine palynomorphs also document a continuous cooling trend towards the Pliocene (De Schepper et al., 2015; LaRiviere et al., 2012; Schreck et al., 2013). This cooling trend persisted throughout the Pliocene and culminated in the onset of Northern Hemisphere Glaciation (NHG) at 2.7 Ma (Kleiven et al., 2002; Mudelsee and Raymo, 2005; Ravelo et al., 2004). The earlier glaciation event at 3.3 Ma has been regarded as a failed onset of NHG (De Schepper et al., 2013, 2009a; Lisiecki and Raymo, 2005).
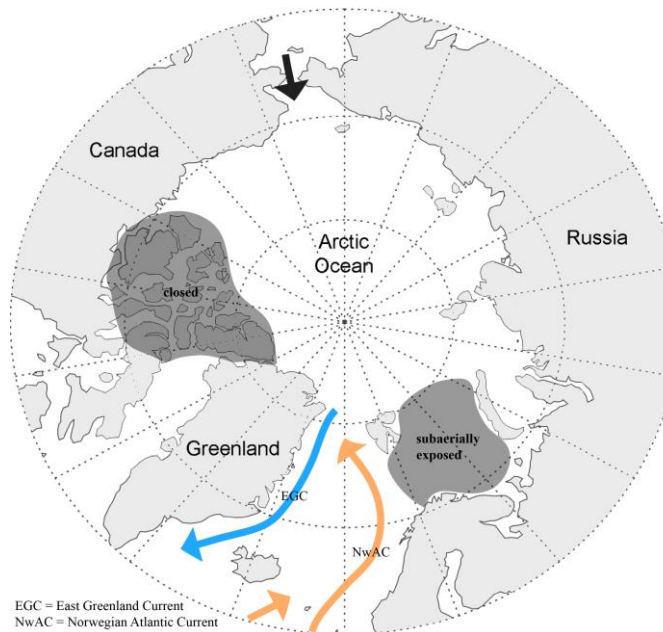
Figure 1.5: Pliocene oceanographic setting for the Arctic Ocean and Nordic Seas. Northward flow of Pacific water into the Arctic Ocean via the Bering Strait commenced around 4.5 Ma. Colour coding is indicative of the relative temperature of the water masses. Light orange = subpolar; blue = polar.

1.3.2 Palaeoceanographic boundary conditions

Palaeoceanographic boundary conditions in the North Atlantic were slightly altered during the Pliocene when compared to present. Tectonic changes throughout the time interval influenced the development and pathways of major currents, which consequently affected climate.

The effect of the closure of the CAS on Pliocene high-latitude warmth and initiation of NHG has been extensively studied (De Schepper et al., 2013; Haug and Tiedemann, 1998; Molnar, 2008; Steph et al., 2010, 2006). Most recent studies suggest that deep-water through-flow from the Pacific to the Atlantic halted during the Middle Miocene and that a further shoaling occurred between ~4.8 and 4.2 Ma (Haug and Tiedemann,

1998; Haug et al., 2001; Montes et al., 2015; Steph et al., 2010). The latter shoaling phase has been associated with the establishment of a modern-like EGC in the Nordic Seas as a consequence of northward flow of Pacific waters through the Bering Strait (Figure 1.5) (Verhoeven et al., 2011).

The Greenland-Scotland Ridge (GSR) extends east and west from Iceland and has a maximum depth of ~850 m. At present, the relatively shallow depth of the GSR restricts the deep water flow from the Nordic Seas to the North Atlantic. A complete submergence of the ridge took place around 12 Ma (Poore et al., 2006). During the Pliocene, the GSR was about 250 m deeper than present, resulting in a stronger overflow of deep water masses (Poore et al., 2006). Modelling studies have shown that a deeper GSR increased water temperatures in the Nordic Seas (Hill, 2015; Robinson et al., 2011). While Robinson et al. (2011) propose that the warmer water temperatures were caused by a strengthened AMOC as a result of a deeper GSR, Hill (2015) shows a weaker overturning circulation and suggest that the warming may solely be explained by palaeogeographic changes.

In the Arctic Ocean, the Canadian Arctic Archipelago was closed and the Barents Sea was subaerially exposed during the Pliocene (Figure 1.5) (Butt et al., 2002; Matthiessen et al., 2009). Thus, the Bering Strait and Fram Strait were the only connections of the Pacific and Atlantic Ocean to the Arctic Ocean, respectively. In the Nordic Seas, the subaerially exposed Barents Sea prevented the branching of the NwAC off northern Norway and increased heat transport to the Arctic Ocean (Figure 1.5) (Butt et al., 2002; Hill, 2015).

1.3.3 Pliocene vegetation and climate records

1.3.3.1 Zanclean (5.33–3.60 Ma)

For the Zanclean, reconstructions of atmospheric CO_2 concentrations using alkenones and boron isotopes in planktic foraminifera average between ~400–300 ppm at different sites in the North Pacific and North Atlantic Ocean (Bartoli et al., 2011; Martínez-Botí et al., 2015; Pagani et al., 2010; Seki et al., 2010). Terrestrial records from the high latitudes in the North Atlantic region provide evidence of mixed to boreal forests, indicating distinct warmer-than-present climatic conditions (Rybczynski et al., 2013; Verhoeven et al., 2013).
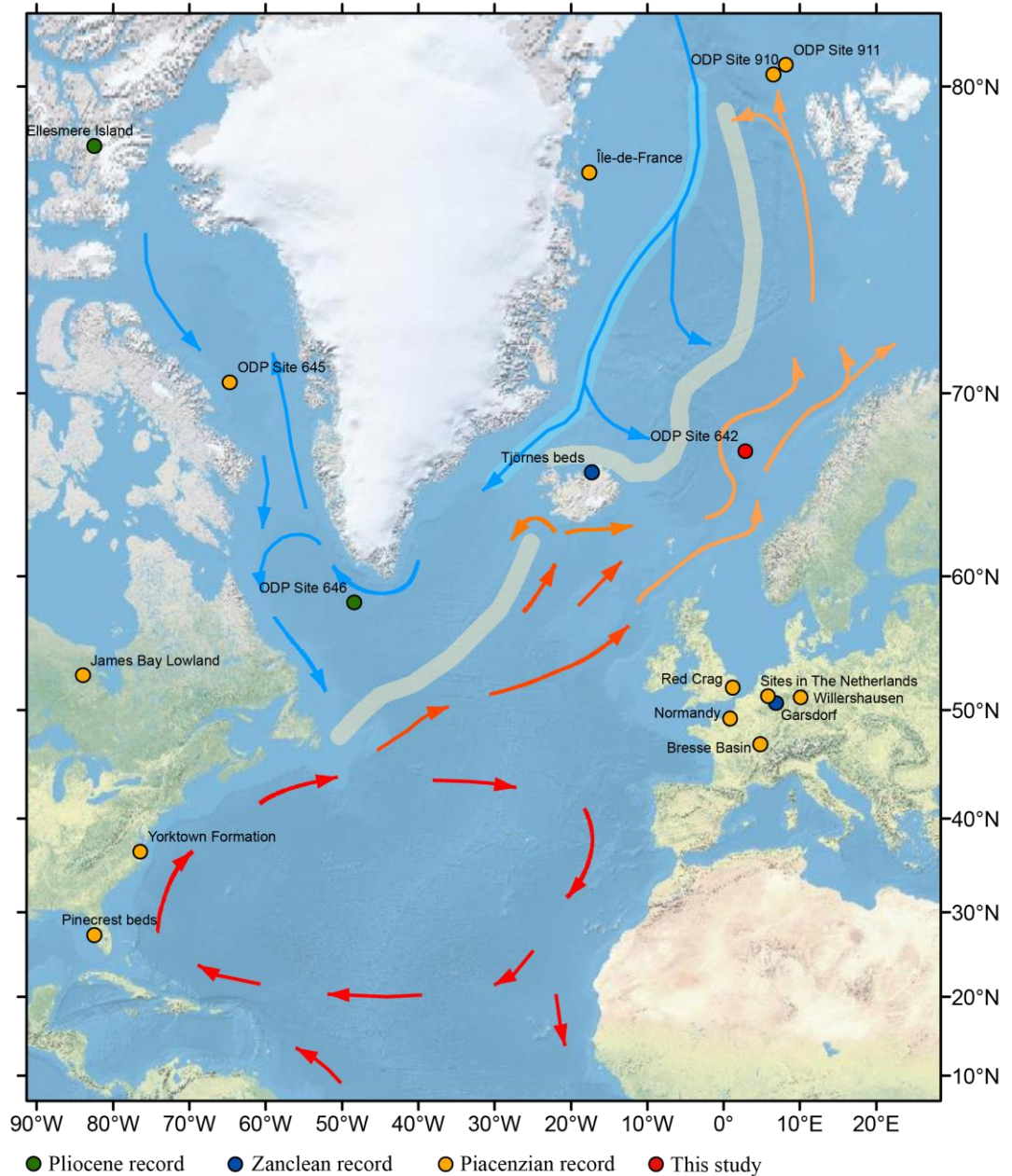
Figure 1.6: Location of Pliocene vegetation records discussed in the text and modern-day ocean surface circulation in the North Atlantic and Nordic Seas. Colour coding is indicative of the relative temperature of the surface water masses: red = very warm; dark orange = warm; light orange = moderately warm; blue = cold.

In western Germany (51°N), a Zanclean microflora is described from the overlying beds of the Rhenish brown coal region which are exposed in the open-cast mines of Frechen and Fortuna Garsdorf (Figure 1.6; Table 1.2) (Mohr, 1984). Mixed forests with *Fagus* as the most common element and other taxa such as *Abies*, *Alnus*, *Carpinus*, *Carya*, *Liquidamber*, *Pterocarya*, *Picea*, *Quercus*, *Tsuga* and *Ulmus* persisted under warmer-than-present condition (Mohr, 1984).

Off southwest Greenland, the pollen assemblages from ODP Site 646 (58°N) reflect the prevalence of mixed forests with temperate elements under humid cool temperate climate conditions in southeastern Canada and possible Greenland during the Plio-Pleistocene (Figure 1.6; Table 1.2) (de Vernal and Mudie, 1989a). Represented taxa include *Alnus*, *Betula*, *Lycopodium*, *Picea*, *Pinus*, Polypodiaceae, *Sciadopitys*, *Sphagnum*, *Tsuga* and *Quercus*.

In northern Iceland, the Tjörnes section (66°N) was deposited in a shallow marine environment before 4 Ma (Figure 1.6; Table 1.2) (Verhoeven et al., 2013). Diverse plant communities persisted throughout the Zanclean in a maritime temperate climate without a dry season, and warm summers comparable to the present western European climate. Fluctuating sea levels due to tectonic activity is regarded as the main cause of vegetation changes (Verhoeven et al., 2013). During sea level lowstands the coastal plain consisted of dry heathland and coastal marshes (Cyperaceae) with deciduous trees growing on well-drained levees (*Acer*, *Betula*, *Juglans*, *Ostrya*, *Pterocarya*, *Sambucus Tilia* and *Ulmus*) – the composition of these lowland forests changed over time – and the lower levee borders (*Alnus*, *Corylus* and *Myrica*). Gymnosperm forest (*Abies*, *Larix*, *Picea*, *Pinus* and *Tsuga*) was present in the hinterland. The continuous presence of the warm-loving taxa *Ilex* indicates that July temperatures were at least 8°C higher than present. Verhoeven et al. (2013) suggest that the maritime temperate climate in northern Iceland was possibly favoured by an intensification of the Gulf Stream after the shoaling of the CAS between 4.7–4.2 Ma. In an earlier study, Willard (1994) also inferred the presence of a mixed conifer-hardwood forest, prevailing under warm-temperate conditions.

Tree-ring analysis on larchs found in peat deposits on Ellesmere Island (79°N), Canada, reveal an increase of MATs of 18.3±4.1°C when compared to present during the Zanclean (Figure 1.6; Table 1.2) (Ballantyne et al., 2010, 2006; Csank et al., 2011). While the deposits were previously dated to 5–4 Ma based on mammalian fossils (Csank et al., 2011 and references therein), re-dating using the terrestrial *in situ* cosmogenic nuclide dating burial methods suggests a minimum age of 3.4–3.8 Ma with a possible age range of 3.0–4.8 Ma (Rybczynski et al., 2013). Considering both age estimates, deposition during the Zanclean seems to be plausible. During the time of deposition boreal forest prevailed in the region. The reconstructed climatic conditions, including average growing season temperatures, MATs, meteoric water values and

relative humidity, are comparable to conditions presently found 15–20° further south (Csank et al., 2011).

1.3.3.2 Piacenzian (3.60–2.59 Ma)

Atmospheric CO_2 reconstructions based on alkenones and boron isotopes in planktic foraminifera for the Piazencian yield values between ~400 and 300 ppm (Bartoli et al., 2011; Martínez-Botí et al., 2015; Pagani et al., 2010; Seki et al., 2010); values similar to those reconstructed for the Zanclean. During interglacials of the mPWP, CO_2 concentration reached values up to ~400 ppm, suggesting that the warmth of the mPWP was at least partly driven by radiative forcing (Bartoli et al., 2011).

A global biome reconstruction for the Piacenzian shows that evergreen taiga and temperate forests were still situated further north in the Northern Hemisphere, thus covering areas that are presently vegetated by tundra (Salzmann et al., 2013, 2008). The evergreen taiga forests were dominated by *Picea* and *Pinus*, transitioning into mixed and deciduous forests with thermophilic elements (e.g. *Carpinus*, *Quercus*, *Sciadopitys* and *Tsuga*) towards the south (Andreev et al., 2014; Salzmann et al., 2008; Willard, 1994). Further south in the mid- to low latitudes the zonal vegetation distribution was more similar to today but with more thermophilic elements (e.g. *Engelhardia*, *Liquidamber* and *Sequoia*) in the mid-latitudes, indicating a reduced latitudinal temperature gradient (Salzmann et al., 2013, 2008).

In southwestern Florida, terrestrial and marine proxies of the Pinecrest Beds (27°N) show that climatic conditions were comparable to present day during the Piacenzian (Figure 1.6; Table 1.2) (Willard, 1994; Willard et al., 1993). Pollen assemblages were dominated by *Pinus*, with relative high abundances of Cupressaceae, Taxaceae and *Quercus*.

Further north at the eastern U.S. Atlantic coastal plain, pollen assemblages from the shallow marine deposits of the Yorktown Formation (37°N), southeastern Virginia, show the presence of a *Quercus-Carya-Pinus* forest in this region during the Piacenzian (Figure 1.6; Table 1.2) (Willard, 1994). The vegetation composition is similar to that of today, but indicative of slightly warmer (MAT of ca. 2–2.5°C) and wetter (+ ~250 mm/year) climatic conditions compared to present. *Sciadopitys* disappears at the end of the Piacenzian in these deposits (Willard, 1994).

Table 1.2: Compilation of Pliocene pollen records in the North Atlantic region. For locations see Figure 1.6.

Site	Location	Age (Ma)	Vegetation	Climate	Temperature	References
Pinecrest Beds	27°N, 82°W	4.5–2.6	Mixed forests (Cupressaceae, *Pinus*, *Quercus*, Taxaceae)	Subtropical to warm temperate	Present to cooler	Willard (1994); Willard et al. (1993)
Yorktown Formation	37°N, 76°W	3.5–2.6	Mixed forests (*Quercus-Carya-Pinus*)	Subtropical	January: +3–5°C, MAT: +2–2.5 °C	Willard (1994)
Bresse Basin	47°N, 5°E	3.2–2.6	Mixed forests (e.g. *Alnus*, *Carya*, *Fagus*, *Pinus*, *Pterocarya*, *Quercus*, *Tsuga*)	Cool temperate	n/a	Rousseau et al. (1992)
Normandy	49°N, 1°E	3.3–2.6	Mixed forests (e.g. *Alnus*, *Carya*, Cupressaceae, *Pinus*, *Pterocarya*, *Sciadopitys*, *Sequoia*, *Tsuga*)	Cool temperate	n/a	Rousseau et al. (1995)
Garsdorf	51°N, 7°E	5.3–2.6	Mixed forests (e.g. *Carpinus*, *Fagus*, *Picea*, *Quercus*, *Tsuga*)	Warm temperate	MAT: 11–15°C, January: -1–10°C, July: 15–23°C	Mohr (1984)
The Netherlands	~51°N, 6°E	3.2–2.6	Mixed forests (e.g. *Alnus*, *Carya*, *Nyssa*, *Pinus*, *Sciadopitys*, *Sequoia*, *Tsuga*)	Cool temperate	MAT: 13–18°C (+3–8°C)), January: 2–4.5°C (+ <2°C), July: 24–29°C (+8–11°C)	Donders et al. (2007); Zagwijn (1960)

Willers-hausen	52°N,10°E	2.6–3.2	Mixed forests (*Alnus*, *Carpinus*, *Carya*, *Fagus*, *Picea*, *Pinus*, *Quercus*, *Sciadopitys*, *Tsuga*)	Warm temperate	MAT: 13.9±2.7°C	Mohr (1986); Salzmann et al. (2013)
Red Crag	52°N, 1°E	2.6–3.0	Mixed forests (e.g. *Carya*, *Corylus*, *Ilex*, *Pinus*, *Pterocarya*, *Sciadopitys*, *Tsuga*)	Cool temperate	12.8±1.3°C	Head (1998); Salzmann et al. (2013)
James Bay Lowland	53°N, 84°W	3.5–3.0	Mixed (e.g. *Carya*, *Pinus*, *Quercus*, *Tsuga*) to boreal (e.g. *Betula*, *Picea*, *Pinus*) forests	Cool temperate to subarctic	MAT_{mixed}: 8–12°C (+9–13°C), MAT_{boreal}: 0–3°C (+1–4°C)	Gao et al. (2012)
ODP Site 646	58°N, 48°W	5.3–2.6	Mixed forests (e.g. *Alnus*, *Betula*, *Picea*, *Pinus*, *Sciadopitys*, *Tsuga*)	Humid cool temperate	MAT: + >3.5°C, January: +5–10°C	de Vernal and Mudie (1989a); Willard (1994)
Tjörnes Beds	66°N, 17°W	5.3–4.0	Coastal marshes (Cyperaceae) and mixed forests (e.g. *Alnus*, *Ilex*, *Larix*, *Pinus*, *Tsuga*)	Maritime Temperate	January: + 1.3°C, July: + 8°C	Verhoeven et al. (2013)
ODP Site 642	**67°N, 3°E**	**3.1–5.0**	**Mixed (e.g. *Alnus*, *Betula*, *Pinus*, *Quercus*, *Sciadopitys*) to boreal forests with peatlands (*Sphagnum*)**	**Cool temperate**	**MAT: 5–14°C (+5–14°C), January: -8–1.4°C (+0.5–10°C), July: 18–24°C (+8–14°C)**	**Willard (1994); This study**

ODP Site 645	70°N, 65°E	Piacenzian (early Pleistocene)	Coniferous forest to tundra (e.g. *Betula*, Ericaceae, *Picea*, *Pinus*, *Sphagnum*)	Cool temperate to subarctic	n/a	de Vernal and Mudie (1989b)
Île-de-France Island	78°N, 18°W	3.6–2.6	Boreal forest to forest-tundra (*Picea*, *Thuja*)	Subarctic	July: >10°C (+6°C)	Bennike et al. (2002)
Ellesmere Island	79°N, 82°W	3.4–3.8 (3.0–4.8)	Boreal forests (*Larix*)	Subarctic	-1.4±4.0°C (+18.3±4.1°C)	Ballantyne et al. (2010); Csank et al (2011); Rybczynski et al. (2013)
ODP Site 910 & 911	80°N, 7°E & 80°N, 8°E	5.3–2.6	Boreal forests to shrub tundra (e.g. *Betula*, *Larix Picea*, *Pinus*, *Pterocarya*, *Sciadopitys*, *Tsuga*)	Subarctic	n/a	Willard (1996); Knies et al. (2014b)

In France (47–49°N), pollen assemblages in two terrestrial Piacenzian sediment sequences show the presence of cool temperate mixed and coniferous forests (Figure 1.6; Table 1.2) (Rousseau et al., 1995, 1992). Mixed forests in the Bresse Basin were composed of *Alnus*, *Carpinus*, *Carya*, *Fagus*, *Pterocarya*, *Quercus*, *Tsuga* and *Ulmus* (Rousseau et al., 1992). In Normandy, coniferous forest (*Abies*, Cupressaceae, *Picea* and *Pinus*) with thermophilic elements (*Carya*, *Carpinus*, *Castanea*, *Ilex*, *Juglans*, *Liquidamber*, *Mycria*, *Nyssa*, *Pterocarya*, *Quercus*, *Sciadopitys*, *Sequoia*, *Tilia*, *Tsuga* and *Ulmus*) predominated during the late Piacenzian (Rousseau et al., 1995).

Diverse Piacenzian microfloras, including genera of North American and East Asian affinity (*Carya*, *Liquidamber*, *Nyssa*, *Pterocarya*, *Sciadopitys*, *Sequoia*, *Taxodium*-type and *Tsuga*) are found in the Netherlands (51°N) and have been widely used to assign continental stages for the Neogene in NW Europe (Figure 1.6; Table 1.2) (Andrew and West, 1977; Head, 1998; Popescu et al., 2006, 2010; Zagwijn, 1992, 1960). However, a revision of these stages using multivariate statistics has shown that the pollen assemblages are influenced not only by climate but also by the fluvial depositional setting, taphonomic effects and other environmental conditions (Donders et al., 2007). The only significant division is the palynological change at the Pliocene-Pleistocene boundary which is marked by a decline in subtropical wetland taxa and the lowest occurrence of *Nyssa* (Donders et al., 2007). The Piacenzian vegetation of the Netherlands fluctuated between the predominance of swamp forests which consisted of taxa such as *Alnus*, *Nyssa*, *Sequoia* and *Taxodium* and drier forests composed of *Pinus*, *Sciadopitys*, *Tsuga* and *Quercus* (Zagwijn, 1960).

Sink-hole deposits in Willershausen in central Germany (52°N) dated to the late Piacenzian/early Pleistocene (3.2–2.4 Ma) reveal a diverse assemblage of plant- and animal-remains, thriving under warm temperate climatic conditions (Figure 1.6; Table 1.2) (Ferguson and Knobloch, 1998; Mohr, 1986). The surrounding area was vegetated by carr forests (e.g. *Alnus*, *Nyssa*, *Pterocarya* and *Salix*), broad-leaved (e.g. *Acer*, *Betula*, *Carpinus*, *Carya*, *Fagus*, *Quercus*, *Tilia* and *Ulmus*) and coniferous forests (e.g. *Picea*, *Pinus*, *Pseudotsuga*/*Larix*, *Sciadopitys*, *Taxus* and *Tsuga*) in well-drained areas (Ferguson and Knobloch, 1998).

In southeastern England, the Red Crag Formation at Walton-on-the-Naze, Essex (52°N), was deposited between 3.0–2.6 Ma under mild- (to warm-) temperate climatic conditions (Figure 1.6; Table 1.2) (Head, 1998). The pollen assemblages in two distinct

samples from different horizons reveal a high abundance of *Pinus* pollen with temperate coniferous (*Sciadopitys* and *Tsuga*) and deciduous (*Carya*, *Corylus*, *Ilex*, *Juglans*, *Myrica*, *Pterocarya*, *Quercus*, *Tilia* and *Ulmus*) elements (Head, 1998).

In the mid-latitude James Bay Lowland (53°N), Canada, till deposits dated to 3.5 Ma (3.6–3.4 Ma) are indicative of glaciation (Figure 1.6; Table 1.2) (Gao et al., 2012). After deglaciation, rapid warming led to the expansion of mixed forests (*Carya*, *Liquidamber*, *Pinus*, *Pterocarya*, *Quercus* and *Tsuga*) which resemble those presently growing in North Carolina. During cooler periods boreal forests (*Abies*, *Betula*, *Picea* and *Pinus*) prevailed in the area. These forests suggest that MATs were 1–13°C higher than present. Over the entire postglacial period from 3.5 to 3.0 Ma, a continuous cooling is observed by the gradual increase in *Betula*, *Picea* and *Pinus* and the decline of *Quercus* and *Taxodium* (Gao et al., 2012).

At ODP Site 646 (58°N) off southwest Greenland, the relative abundance of temperate tree taxa (*Quercus*, *Sciadopitys* and *Tsuga*) decreases during the Piacenzian, leading to the dominance of boreal vegetation in the early Pleistocene (Figure 1.6; Table 1.2) (de Vernal and Mudie, 1989a; Willard, 1994). The presence of these temperate taxa during the Piacenzian is indicative of a northward shift of the northern boundary of the deciduous as well as boreal forest zone and thus higher than present January temperatures (+5–10°C) and MATs (at least +3.5°C) (Willard, 1994).

In Norway, a mixed conifer-hardwood forest at the northern limits of the deciduous forest zone has been inferred from pollen assemblages in the sediments of ODP Hole 642C (67°N) (Figure 1.6; Table 1.2) (Willard, 1994). The assemblages are dominated by *Pinus*. Other represented taxa include *Abies*, *Alnus, Betula, Picea*, *Quercus, Sciadopitys* and *Tsuga* (Figure 1.7). Non-arboreal taxa (Asteraceae, Cyperaceae, Ericaceae and Ranunculaceae) constitute up to 20% of the assemblage. *Ilex* and *Pterocarya* are present but are not included in the counts (Willard, 1994). During the Piazencian the Scandinavian mountains had already been uplifted. They were, however, lower than present (Anell et al., 2009; Knies et al., 2014b). Anell et al. (2009) report uplift of ~1 km in northern Norway and 1–1.5 km in the southern Scandinavian mountains during the Neogene. These estimates correspond to the height of the Scandinavian mountains of 500 to 1000 m, as was used for the PRISM3 reconstruction of Pliocene climate (Sohl et al., 2009), reducing them by 500–1000 m in altitude compared to present.
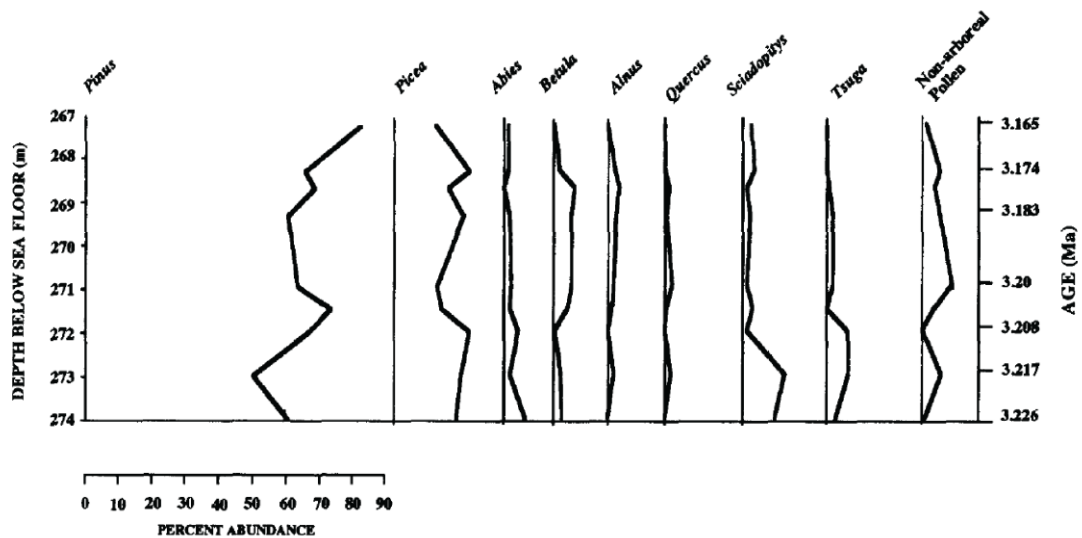
Figure 1.7: Pollen assemblages in nine Piacenzian samples from ODP Hole 642C (Willard, 1994).

In Baffin Bay west of Greenland, a palynological study of late Pliocene/early Pleistocene sediments of ODP Site 645 (70°N) reveals the presence of a relatively dense coniferous forest to forest tundra vegetation on Greenland and Baffin Bay Island under a humid, cool-temperate to subarctic climate (Figure 1.6; Table 1.2) (de Vernal and Mudie, 1989b). The vegetation described by de Vernal and Mudie (1989b) presumably prevailed during the early Pleistocene as the base of the Pleistocene has since been formally lowered from 1.8 Ma to 2.6 Ma (Gibbard et al., 2010; Palmer, 1983). The forests are represented by pollen assemblages of *Abies*, *Alnus*, *Betula*, Ericaceae, *Pinus* and *Picea*. High percentages of *Sphagnum* spores suggest the presence of extensive peatlands. The assignment to the early Pleistocene is supported by ice-rafted debris deposits that are recorded in the area surrounding Baffin Bay, indicative of glaciations events. De Vernal and Mudie (1989) propose that a humid climate contributed to high precipitation and the accumulation of ice.

A multi-proxy study of shallow marine deposits in the northern part of the subarctic Île-de-France (78°N) offshore northeast Greenland suggest that summer temperatures were about 6°C higher than at present (Figure 1.6; Table 1.2) (Bennike et al., 2002). Based on seed and wood fragments from *Picea* and *Thuja*, Bennike et al. (2002) infer the presence of boreal forest or forest-tundra in the northern part of the Island during the Piacenzian. Today, woody plants do not occur on the northern island because of perennial snow cover and frost.

26

In the Arctic Ocean (80°N), Piacenzian pollen assemblages changes from ODP Site 910 and 911 on the Yermak Plateau northwest of Svalbard, which is presently vegetated by tundra, reveal warmer-than-present climatic conditions and a northward latitudinal shift of vegetation by about 10° latitude (Figure 1.6; Table 1.2) (Willard, 1996). Boreal forest or shrub tundra with deciduous elements (*Abies*, *Alnus*, *Betula*, *Corylus*, *Castanea*, Cupressaceae, Cyperaceae, Ericaceae, *Larix*, *Picea*, *Pinus*, Poaceae, *Sciadopitys*, *Salix* and *Tsuga*) grew in the source area, which is most likely Spitsbergen, but could also be northernmost Norway or northeastern Greenland.

1.3.3.3 Northern Hemisphere high-resolution records

High-resolution terrestrial data for the Pliocene, identifying climatically-induced variations in vegetation, surface temperatures and precipitation are generally rare (Salzmann et al., 2013, 2008). However, existing records show that climate was not stable during the Pliocene, exhibiting climate changes of the order of several thousands of years (Andreev et al., 2014; Brigham-Grette et al., 2013; Demske et al., 2002; Gao et al., 2012; Popescu et al., 2010; Williams et al., 2009; Willis et al., 1999a).

During the Pliocene, subtropical forests to open subdesertic landscapes covered the West Mediterranean region (Fauquette et al., 1999). The climate was warmer than present across the whole region. Precipitation, however, was higher than present in the north and similar to, or slightly higher, than today in the south. Cooling events at 4.5 and 3.5 Ma are observed at some sites (Fauquette et al., 1999).

In the southwestern Black Sea, Deep Sea Drilling Project (DSDP) Site 380 (42°N) provides a high-resolution record of vegetation and climate changes during the Pliocene (Popescu et al., 2010). During the Zanclean, a warm and humid climate favoured the expansion of forest in the areas adjacent to the western Black Sea. Open environments with an increased abundance of herbs and steppe elements are indicative of cooler climatic conditions between MIS MG2 (3.34 Ma) and G1 (2.63 Ma), covering most of the Piacenzian Stage (Popescu et al., 2010).

In the continental interior of northeastern Eurasia, a sediment core recovered from Lake Baikal (53°N) reveals the prevalence of mixed coniferous forest in the Baikal region during the Piacenzian, interrupted by pronounced advances of open vegetation due to cooler and drier intervals (Demske et al., 2002). At present this region is characterised by boreal and mountain taiga and marks the transition between continuous and discontinuous permafrost. Modern climate is influenced by the Siberian High, bringing

cold and dry air masses in winter and moisture-bearing air masses carried by the westwind drift in summer (Demske et al., 2002). During the Piacenzian short-term climatic deterioration occurred at 3.39 Ma, between 3.28 and 3.26 and at 3.03 Ma with major cooling starting after 3 Ma. In the prevailing vegetation these cooling events are reflected by an increase in *Selaginella selaginoides* and *Lycopodium* and a decline in the relative abundance of *Tsuga* (Demske et al., 2002). Vegetation changes around Lake Baikal can be correlated to the benthic oxygen isotope signal at ODP Site 846 in the eastern equatorial Pacific. The advance of open vegetation coincides with glacial MISs KM2 (c. 3.12 Ma) and G20 (c. 3.0 Ma) during the mPWP. Evidence for vegetation changes during the global cooling event of MIS M2 is weak (Demske et al., 2002). The establishment of cool and dry climatic conditions after 3.15 Ma are associated with the development of the Siberian High caused by the intensifying NHG (Demske et al., 2002).

Figure 1.8: Location of Lake El'gygytgyn, NE Siberia in relation to ODP Site 642.

In northeastern Russia, a Piacenzian high-resolution pollen record from Lake El'gygytgyn (67°N), which formed after a meteorite impact at 3.6 Ma, shows vegetation changes on orbital time scales (Figure 1.8) (Andreev et al., 2014; Brigham-Grette et al., 2013; Herzschuh et al., 2016). With a modern MAT of -10°C the region around the lake is covered by shrub tundra with *Birch* and *Salix*, growing above deep permafrost (Brigham-Grette et al., 2013). Between 3.5 and 3.35 the area around Lake El'gygytgyn was vegetated with *Picea-Larix-Abies-Tsuga* forests. After 3.4 Ma coniferous trees gradually disappeared and were replaced by tundra, although localised stands of trees were still present (Andreev et al., 2014). During glacial event MIS M2 (c. 3.3 Ma) a treeless tundra and steppe dominated the region. Surface temperatures were not "glacial" but as warm as, or slightly warmer, than the Holocene average (Brigham-

Grette et al., 2013). Thereafter, *Larix-Pinus-Picea* forests expanded but open habitats developed during several cool intervals. Forests covered the area until about 2.7 Ma when they finally disappeared from the region, enhancing cooling by an increased land surface albedo (Andreev et al., 2014; Brigham-Grette et al., 2013). Climate reconstructions based on the pollen spectra for the mPWP indicate WMTs 3–6°C and MAP <100 to >200 mm higher than present. The warmest interval occurred between 3.6 to 3.4 Ma when WMTs were 7–8°C higher compared to today. Until 2.2 Ma warm Arctic summers persisted and seasonal rather than perennial Arctic sea ice cover existed due to polar amplification (Brigham-Grette et al., 2013).

1.3.4   Pliocene sea surface temperature records

1.3.4.1 Zanclean (5.33–3.60 Ma)

The 'Pliocene climatic optimum' (4.4–4.0 Ma) has been identified as the warmest interval during the Zanclean in globally distributed geochemical records of SSTs (Fedorov et al., 2013). The oceans and atmosphere were characterised by a reduced Equator-to-pole gradient due to similar-to-present SST in the tropics and markedly warmer temperatures in the high-latitudes. The tropical warm pool was much broader, exhibiting weaker upper-ocean stratification, hence a deeper thermocline, and a weak zonal temperature gradient in the all three oceans (Brierley et al., 2009; Fedorov et al., 2013). In the North Atlantic, SSTs were 4–8°C higher than present in the mid- to high latitudes (Fedorov et al., 2013). At ODP Site 999 (13°N) in the Caribbean Sea, estimates of subsurface temperature based on the Mg/Ca ratio in the shell of the planktonic foraminifer *Neogloboquadrina dutertrei* show a warming of surface waters and/or deepening of the thermocline between 4.8 and 4.3 Ma (Figure 1.9; Table 1.3) (Steph et al., 2010). The authors link this warming to the development of the Caribbean Warm Pool in response to the shoaling of the CAS (Haug and Tiedemann, 1998). In the Iceland Sea, annual SSTs derived from alkenones at ODP Site 907 were between 3 and 10°C higher than present with cooling commencing after 4.5 Ma (Figure 1.9) (De Schepper et al., 2015).

1.3.4.2 Piacenzian (3.60–2.59 Ma)

At DSDP Site 603 (36°N) in the western North Atlantic (Figure 1.9; Table 1.3), SSTs derived from Mg/Ca ratios of *Globigerina bulloides* are similar to present with only small fluctuations (De Schepper et al., 2013).

In the Mediterranean Sea (37–39°N), a composite alkenone-based SST record based on four Piacenzian sections (Punta Piccola, San Nicola, Singa and Vrica) reveal values 5–6°C higher than present and low-amplitude variability between 3.5 and 2.6 Ma (Herbert et al., 2015). The variance in SST changes is mainly controlled by precession, suggesting that local insolation was the main driver and that glaciations before the onset of NHG did not affect the region (Herbert et al., 2015).

Changes in the position and strength of the NAC during the Piacenzian have been recorded at Integrated Ocean Drilling Program (IODP) Site U1313 (41°N, reoccupation of DSDP Site 607) which is located just north of the subtropical gyre (Figure 1.9; Table 1.3) (Naafs et al., 2010). During the early Piacenzian, mean annual SSTs were on average 2–3°C higher-than-present, reflecting northward transport of warm waters by an intense NAC. SSTs decreased by 5°C between 3.45 and 3.29 Ma and culminated in MIS M2. Lower SSTs at Site U1313 indicate the influence of the NAC and thus a weakened northward heat transport. The return of warm and oligotrophic conditions at 3.29 Ma, coinciding with the beginning of the mPWP, suggests that northward heat transport via the NAC had been resumed (Naafs et al., 2010). In the eastern North Atlantic, IODP Site U1308 (50°N, reoccupation of DSDP Site 609) and ODP Site 610 (53°N) are situated in the path of NAC, showing Mg/Ca- and alkenone-based SSTs up to 10°C higher than present with a cooling of 3–4°C occurring during MIS M2 (Figure 1.9; Table 1.3) (De Schepper et al., 2013, 2009a).

A high-resolution alkenone-based SST record in the northeastern North Atlantic (ODP Site 982, 58°N) shows that surface water masses were up to ~6°C higher than present with high-amplitude variations (up to 8°C) on obliquity cycles (Figure 1.9; Table 1.3) (Lawrence et al., 2009). The high SSTs are presumably the result of increased atmospheric and oceanic heat transport towards higher latitudes caused by changes in regional atmospheric pressure gradients due to a reduced ice cover in the Northern Hemisphere. Such changes may have been induced by orbitally-driven changes in solar insolation (Lawrence et al., 2009 and references therein). The high variability of SST changes, similar to those of the late Pleistocene, contrasts benthic and planktonic δ^{18}O records that suggest relatively stable warm conditions. Lawrence et al. (2009) suggest that the signal observed at ODP Site 982 is either indicative of strong (sea) ice albedo feedbacks at the high northern latitudes or, more likely, represents a feature unique to this site with its position under the NAC. Changes in the strength and position of the NAC on orbital timescales would create the observed high-amplitude variations in
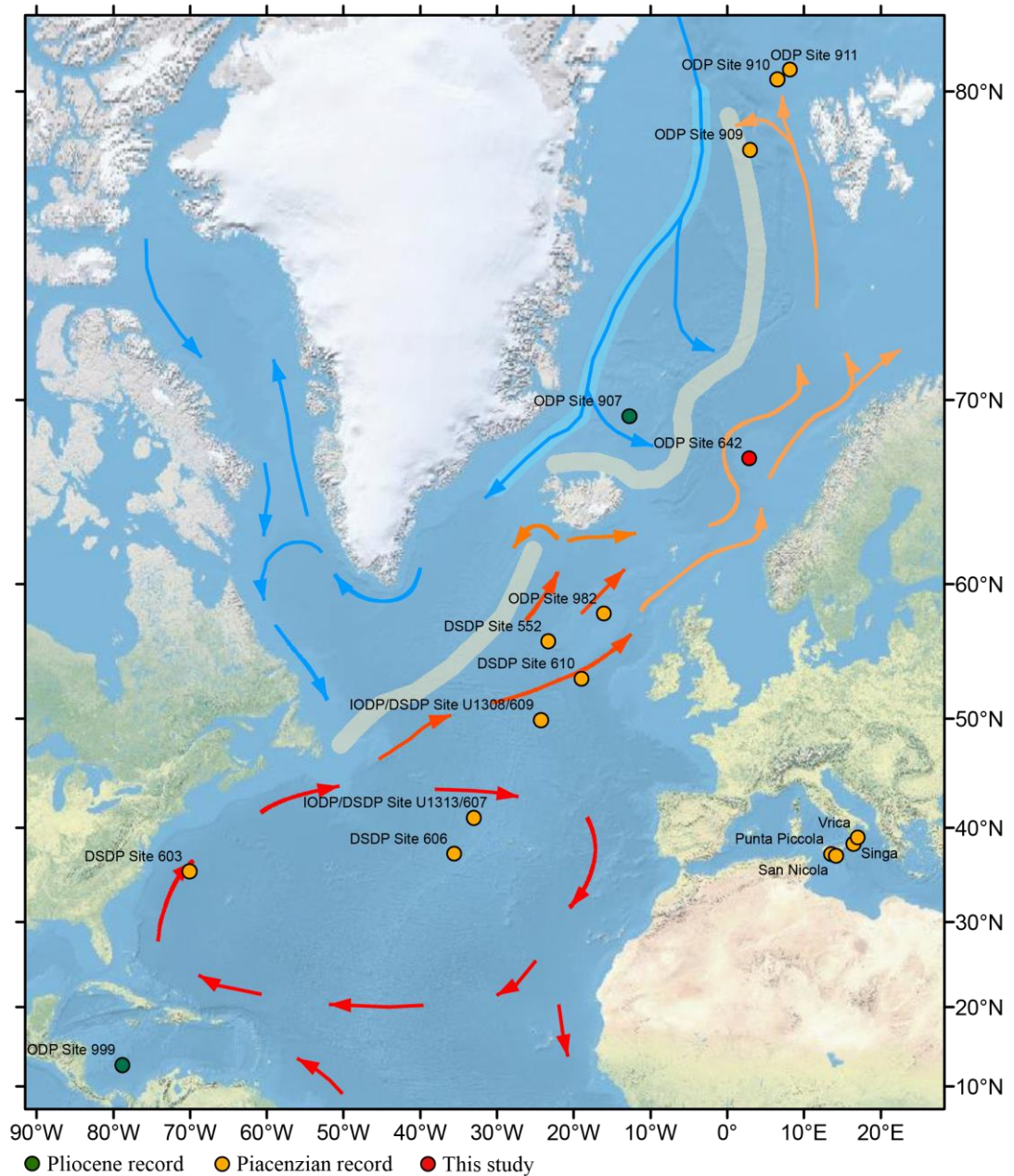
Figure 1.9: Location of Pliocene sea surface temperature records discussed in the text and modern-day ocean surface circulation in the North Atlantic and Nordic Seas. Colour coding is indicative of the relative temperature of the surface water masses: red = very warm; dark orange = warm; light orange = moderately warm; blue = cold.

SSTs. SSTs decrease by 4.5°C between 3.5 and 2.5 Ma, supporting the notion that the onset of NHG was gradual and possibly reflecting the growth of a modern-like Greenland ice sheet. During the Piacenzian, SST changes led the benthic δ^{18}O signal, indicating a larger contribution of ice volume as opposed to temperature to the δ^{18}O signal (Lawrence et al., 2009). Sea surface temperatures for the mPWP were derived from multiple proxies at four sites in the mid-latitudes of the North Atlantic to evaluate potential biases with regard to the recorded environmental signal (e.g. spring/summer or

31

annual SSTs, temperatures at certain depths) and proxy calibrations (Robinson et al., 2008). The four DSDP sites used in the study are Site 606 (37°N) at the northern margin of the subtropical gyre, Site 607 (41°N) at the transition between the subtropical gyre and the NAC, Site 609 (50°N) and Site 552 (56°N) ~1500 km off the United Kingdom in the path of the NAC (Figure 1.9; Table 1.3). The SST estimates are based on foraminiferal assemblages, foraminiferal Mg/Ca and alkenones and show an increase in the magnitude of warming with increasing latitude. At the lower latitude sites 606 and 607, the average mean annual SSTs reflected by alkenones are ~1.5°C higher than present. At the higher latitude sites 609 and 552 the warming of mean annual SSTs amounts to 3.4 and 5.3°C relative to modern values, respectively, across the studied interval (Robinson et al., 2008).

In the Norwegian Sea (ODP Hole 642B, 67°N), a recently published alkenone-based SST reconstruction for the mPWP shows summer SSTs 2–3°C higher than the Holocene average (Figure 1.9; Table 1.3) (Bachem et al., 2016). The study identified radiative forcing due to higher atmospheric CO_2 concentrations as the most likely cause for the higher SSTs in the Norwegian Sea. Bachem et al. (2016) suggest that the northward heat transport via the NAC was not enhanced during the mid-Piacenzian because of the presence of a Holocene-like subpolar gyre, restricting the inflow of warm Atlantic waters into the Norwegian Sea. The authors exclude a weaker ice-albedo feedback and altered palaeogeographic boundary conditions as a cause for the higher-than-present SSTs as the mPWP warming in the Norwegian Sea is close to the global average. Spectral analysis shows that the SST variability can partly be attributed to obliquity and precession forcing (Bachem et al., 2016).

Other proxy-based SST reconstructions from the Nordic Seas region show a pronounced warming during the mPWP with average values up to ~13°C higher than present (Dowsett et al., 2013a). Summer SSTs based on alkenones and Mg/Ca ratios in foraminifera shells were estimated in samples from ODP Hole 907A (69°N) in the Iceland Sea, Hole 909C (78°N) in the Fram Strait and 911A (80°N) northwest of Svalbard in the Arctic Ocean (Figure 1.9). The samples from Site 907 and 909 have an age of 3.0–3.3 Ma and the estimated SSTs from all sites are considered to represent warm peak average and not mean conditions. The average SST estimates for the mPWP were ~12°C at Site 907, ~13°C at Site 909 and ~18°C at Site 911 (Table 1.3) (Robinson, 2009). The age model of the northernmost site has since been updated, assigning the samples from Site 911 analysed by Robinson (2009) an age of 3.6 Ma

Table 1.3: Compilation of Pliocene sea surface temperature (SST) records in the North Atlantic. Orange, bold SST estimates represent spring to summer temperatures while the others are indicative of annual SSTs. For location see Figure 1.9.

Site	Location	Age (Ma)	proxy	SST (anomaly)	References
ODP Site 999	13°N, 79°W	5.3–2.6	Mg/Ca ratio	16–27±0.5°C	Steph et al. (2010); De Schepper et al. (2013)
DSDP Site 603	36°N, 70°W	3.33–3.19	Mg/Ca ratio	**15–23±1.5°C (-5.5–+2.5°C)**	De Schepper et al. (2013)
DSDP Site 606	37°N, 36°W	3.29–2.97	Foraminifera, Mg/Ca ratio, alkenones	Faunal: 18.5°C (February) & **25.6°C (August)**, Mg/Ca: **25.2°C**, Alkenones: 22.0±0.2°C; (+1.1–4.7°C)	Robinson et al. (2008)
Southern Italy (Mediterranean Sea)	37–19°N, 14–17°W	3.5–2.6	alkenones	24–28°C (+5–6°C)	Herbert et al. (2015)
IODP Site U1313/DSDP Site 607	41°N, 33°W	3.29–2.97 and 3.65–2.6	Foraminifera, Mg/Ca ratio, alkenones	Faunal: 14.8°C (Februrary) & **21.9°C (August)**, Mg/Ca: **18.0–23.4°C**, alkenones: 20.2°C, (-1.0–4.6°C) and 17–24°C (-1.3–7.7°C)	Robinson et al. (2008); Naafs et al. (2010)
IODP Site U1308/DSDP Site 609	50°N, 24°W	3.29–2.97 and 3.34–3.26	Foraminifera, Mg/Ca ratio, alkenones	Faunal: 18.2°C (Februrary) & **26.4°C (August)**, Mg/Ca: **14.2°C and 13–19±1.5°C**, alkenones: 17.5°C, (-3.4–9.8°C) and 15–21±1.5°C (+2–8°C)	Robinson et al. (2008); De Schepper et al. (2013, 2009a)

Site	Coordinates		Proxy	Temperature	Reference
DSDP Site 610	53°N, 19°W	3.33–3.23	Mg/Ca ratio, alkenones	**12–17±1.5°C**, 14–22±1.5°C (+ <10°C)	De Schepper et al. (2013, 2009a)
DSDP Site 552	56°N, 23°W	3.29–2.97	Foraminifera, Mg/Ca ratio, alkenones	Faunal: 11.7°C (Februrary) & **20.4°C (August)**, Mg/Ca: **11.6–14.7°C**, alkenones: 16.9°C, (+2.6–7.1°C)	Robinson et al. (2008)
ODP Site 982	58°N, 16°W	4.0–2.7	Alkenones	**13–20±.2°C (+ <7°C)**	Lawrence et al. (2009)
ODP Site 642	**67°N, 3°E**	**3.26–3.14**	**Alkenones**	**11.5–15.6±1°C (+ <4°C)**	**Bachem et al. (2016)**
ODP Site 907	69°N, 13°W	5.33–3.55 and 3.3–3.0	Alkenones and Mg/Ca	Alkenones: 4.8–12.2±1.5°C +3–10.4°C and 8±1°C (+~5), Mg/Ca: **10.7–12.3±0.9°C (+ 3–5°C)**	De Schepper et al. (2015); Robinson (2009); Schreck et al. (2013)
ODP Site 909	79°N, 3°W	3.3–3.0	Alkenones and Mg/Ca	**10.5–16.9±2°C (+11–18°C) and 12.7±2°C (+13°C)**	Robinson (2009)
ODP Site 910	80°N, 7°W	5.33–2.6	GDGT*	4.4–10.1°C (+3–9°C)	Knies et al. (2014a)
ODP Site 911	80°N, 8°W	3.6	Alkenones	**16.1–19.2±1.4°C (+17–20°C)**	Robinson (2009)

*GDGT = Glycerol Dialkyl Glycerol Tetraether

(Mattingsdal et al., 2013). The high SST estimates at Site 907 and 909, equating to summer temperatures ~8–12°C higher than present, preclude the existence of perennial sea ice during the mPWP (Table 1.3) (Robinson, 2009). The latter is supported by biomarker measurements of IP_{25} ('Ice Proxy with 25 carbon atoms' which is biosynthesised by certain sea ice diatoms) at ODP Hole 910C (80°N) on the Yermak Plateau, northwest of Svalbard, showing low IP_{25} concentrations (Figure 1.9). Estimates of SSTs at the site using glycerol dialkyl glycerol tetraethers (GDGTs) and hydroxyl GDGTs reveal values of ~4–6°C, which cover the upper range of modern summer SSTs on the southern Yermak Plateau (Table 1.3) (Knies et al., 2014a). At ODP Hole 907A, summer SSTs based on alkenones for the mPWP show values of ~8°C, which are ~3°C warmer than present (Table 1.3) (Schreck et al., 2013).

1.3.5   Pliocene dinoflagellate cyst and acritarch records

1.3.5.1 Zanclean

Dinocyst assemblage changes from the shallow marine, fossiliferous Tjörnes Beds in northern Iceland (66°N) reveal two major palaeoceanographic events in the northern Atlantic (Figure 1.10; Table 1.4) (Verhoeven and Louwye, 2013). The first, around 4.8 Ma, is marked by a change in the dominance of heterotrophic (e.g. *Barssidinium pliocenicum*, *Trinovantedinium* spp. and *Selenopemphix dionaeacysta*) to autotrophic (e.g. *Protoceratium reticulatum*, *Habibacysta tectata*, *Impagidinium* sp. and *Spiniferites* spp.) dinocysts, indicating a decrease in nutrients, probably as a result of the movement of the Polar Front away from the area. The second event at c. 4.5 Ma is marked by re-entrance of heterotrophic dinocysts and can be ascribed to the reversal in Pacific water flow through the Bering Strait as a consequence of the shoaling of the CAS between 4.7 and 4.2 Ma (Haug et al., 2001; Verhoeven and Louwye, 2013). This event was first documented by the invasion of Pacific molluscs to the Nordic Seas (Verhoeven et al., 2011 and references therein), and has now also been detected in dinocysts record. Heterotrophic species (e.g. *Barssidinium pliocenicum*, *Echinidinium euaxum*, *Brigantedinium* spp. and *Trinovantedinium glorianum*) show an abrupt return and the abundance of cold-water species (e.g. *Filisphaera filifera*) increases, indicating the influx of cold, nutrient-rich waters to the site. A sudden appearance of acritarchs (*Cyclopsiella? trematophora*, *Cymatiosphaera? invaginata* and *Halodinium scopaeum*) is probably related to several environmental factors such as low water depth, high energy and nutrient levels. The high abundance of heterotrophic dinocysts pre-dates the
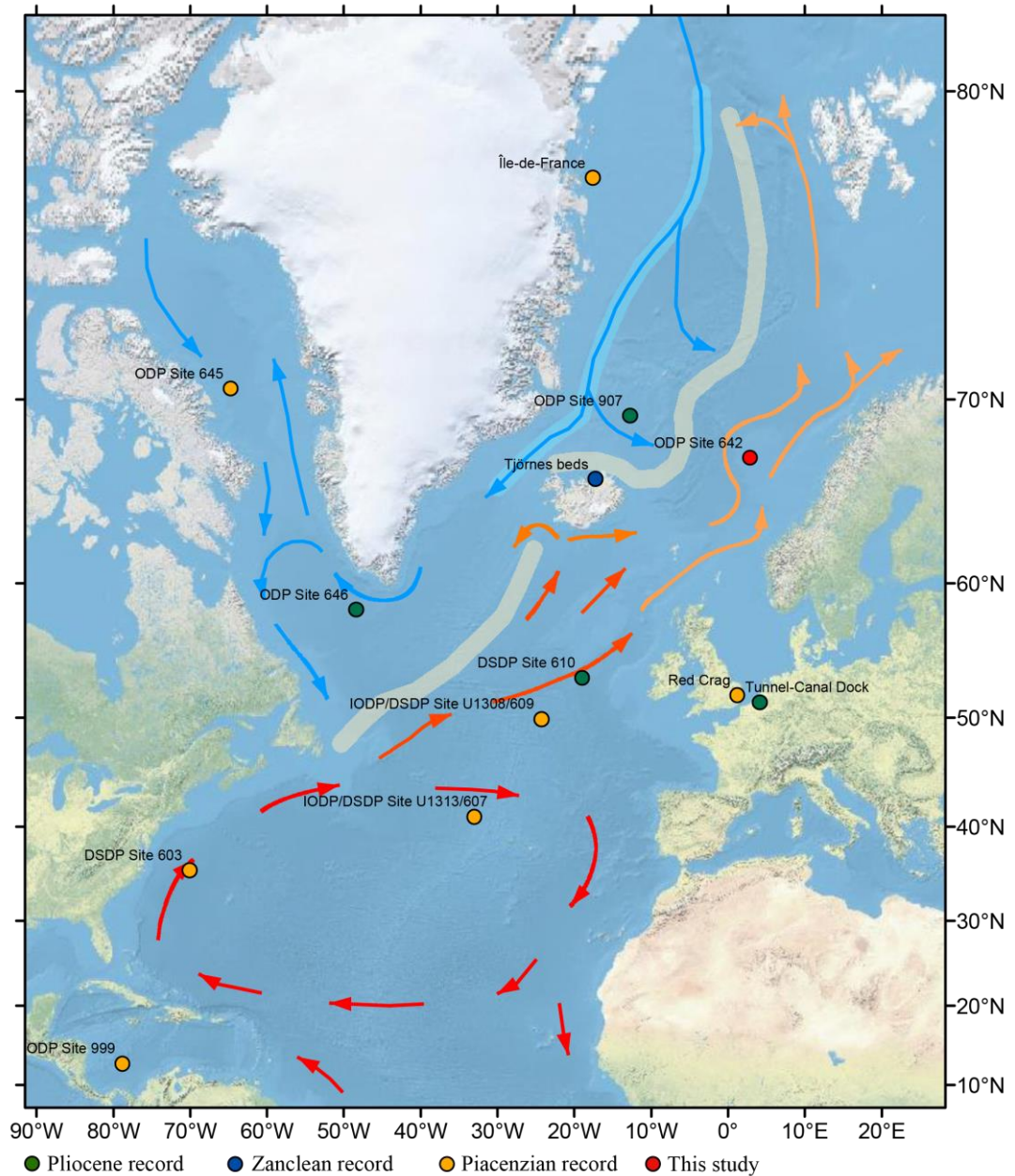
Figure 1.10: Location of Pliocene dinoflagellate cyst records discussed in the text and modern-day ocean surface circulation in the North Atlantic and Nordic Seas. Colour coding is indicative of the relative temperature of the surface water masses: red = very warm; dark orange = warm; light orange = moderately warm; blue = cold.

invasion of Pacific molluscs, suggesting that Pacific water was already present in the area before the first molluscs arrived (Verhoeven and Louwye, 2013).

Northeast of Iceland, a marked species turnover is recorded between 4.5 and 4.3 Ma in marine palynomorph assemblage changes in the sediments of ODP Hole 907A (69°N) (Figure 1.10; Table 1.4) (Schreck et al., 2013).

The turnover is reflected in the disappearance of the majority of species and followed by an abrupt decline in palynomorph accumulation at 4.2 Ma. *Nematosphaeropsis labyrinthus* disappears abruptly at 4.2 Ma. The disappearance of species is probably related to the establishment of the modern-like EGC which was initiated by the northward flow of Pacific waters through the Bering Strait into the Arctic Ocean as a result of the shallowing CAS (Verhoeven et al., 2011). The subsequent decline in palynomorph accumulation presumably reflects a combination of palaeoceanographic changes, including decreased palynomorph productivity, enhanced bottom-water oxygenation due to enhanced deep-water formation and the presence of sea ice (Schreck et al., 2013).

The development of a modern Nordic Seas circulation between 4.5–4.2 Ma is evident in dinocyst and acritarch assemblage changes at ODP Hole 642B (67°N) in the Norwegian Sea and ODP Hole 907A (69°N) in the Iceland Sea (Figure 1.10; Table 1.4) (De Schepper et al., 2015). Between 5.0 and 4.5 Ma, dinocysts at ODP Hole 642B are characteristic of a nutrient-rich outer shelf environment (e.g. *Batiacashpaera micropapillata* complex, *Spiniferites/Achomosphaera* spp., Protoperidinioids and *Nematospaeropsis labyrinthus*) that was under the influence of warm temperate waters. This is indicated by species such as *Operculodinium israelianum*, *O.? eirikianum*, *O. tegillatum* and *Melitasphaeridium choanophorum. Cymatiosphaera? invaginata* and occasionally *Lavradosphaera crista* and Cyst type I by de Vernal and Mudie (1989a) are the most abundant acritarchs. After 4.5–4.2 Ma, cooler but still warmer-than-present waters prevail above the site which is evident in the change in the predominance of taxa, with cysts of *Protoceratium reticulatum*, *Spiniferites/Achomosphaera* spp., *N. labyrinthus* and *Filisphaera filifera* being most abundant. Despite being a cosmopolitan species, cysts of *P. reticulatum* show notably high abundances in cold/temperate, nutrient-rich North Atlantic waters such as those associated with the NAC or NwAC (De Schepper et al., 2015; Marret and Zonneveld, 2003). Thus, the increase in the relative abundance of *P. reticulatum* at Site 642 after 4.5 Ma is interpreted as the first development of a modern-like NwAC (De Schepper et al., 2015). In the Iceland Sea, temperate sea water conditions are also recorded between 5.0 and 4.5 Ma with dinocyst assemblages similar to those at ODP Site 642. After 4.5 Ma, cool-water species dominate the assemblage and a marked decline in the relative abundance of warm-water species and dinocyst concentrations leads to the absence of dinocysts after 4.14 Ma, indicating the presence of cold water masses and unfavourable conditions for dinocysts

Table 1.4: Compilation of Pliocene dinoflagellate cyst records in the North Atlantic region. For locations see Figure 1.10.

Site	Location	Age (Ma)	Water mass conditions and timing of major changes	References
ODP Site 999	13°N, 79°W	3.36–3.25	Before and after MIS M2: nutrient-rich waters During MIS M2: oligotrophic waters	De Schepper et al. (2013)
DSDP Site 603	36°N, 70°W	3.34–3.19	Warm temperate	De Schepper et al. (2013)
IODP Site U1313/DSDP Site 607	41°N, 33°W	3.40–3.22	Warm, oligotrophic waters	De Schepper et al. (2013)
IODP Site U1308/DSDP Site 609	50°N, 24°W	3.34–3.18	Before and after MIS M2: warm waters During MIS M2: oligotrophic waters	De Schepper et al. (2013, 2009a)
Tunnel-Canal Dock	51°N, 4°E	5.0–2.6	Cool/mild to warm temperate	De Schepper et al. (2009b);
Red Crag	52°N, 1°E	2.6–3.0	Mild to warm temperate	Head (1998)
DSDP Site 610	53°N, 19°W	3.33–3.24	Before and after MIS M2: warm waters During MIS M2: subpolar waters	De Schepper et al. (2013, 2009a)
ODP Site 646	58°N, 48°W	5.3–2.6	Cool temperate to subarctic	de Vernal and Mudie (1989b)
Tjörnes Beds	66°N, 17°W	5.3–4.0	<4.8 Ma: decrease in nutrients; <4.5 Ma: nutrient-rich, cold waters	Verhoeven and Louwye (2013)
ODP Site 642	**67°N, 3°E**	**5.33–3.13**	**>4.5–4.2 Ma: nutrient-rich, warm temperate waters** **<4.5–4.2 Ma: temperate waters**	**This study;** **De Schepper et al. (2015)**

Site	Location	Age (Ma)	Description	Reference
ODP Site 907	69°N, 13°W	5.33–4.25	4.5–4.2 Ma: distinct species turnover and disappearance of the majority of species	De Schepper et al. (2015); Schreck et al. (2013)
ODP Site 645	70°N, 65°E	Piacenzian (early Pleistocene)	Subarctic	de Vernal and Mudie (1989b)
Île-de-France Island	78°N, 18°W	3.6–2.6	Polar to subpolar possibly with seasonal sea ice cover	Bennike et al. (2002)

(De Schepper et al., 2015; Schreck et al., 2013). This transition has been associated with the establishment of a proto-EGC and is in accordance with dinocyst assemblages changes observed in the Tjörnes Beds, northern Iceland at 4.5 Ma (De Schepper et al., 2015; Verhoeven and Louwye, 2013). Therefore, the development of the modern Nordic Seas circulation seems to be linked to the onset of northward flow of Pacific waters through the Bering Strait which may in turn be related to the shoaling of the CAS (De Schepper et al., 2015).

1.3.5.2 Piacenzian

The role of ocean circulation in causing the glaciation during MIS M2 has been determined from dinocyst assemblages changes and SSTs estimates at five sites in the North Atlantic, covering the time interval between 3.40 and 3.18 Ma (De Schepper et al., 2013, 2009a). The sites are located along the trajectory of the NAC and include ODP Site 999 (13°N) in the Caribbean Sea, DSDP Site 603 (36°N) in the western North Atlantic, IODP Sites U1313 (41°N) and U1308 (50°N) and DSDP Site 610 (53°N) in the eastern North Atlantic (Figure 1.10; Table 1.4). Before and after MIS M2, the inflow of nutrient-rich Pacific waters into the Caribbean Sea is evident from the high abundances of Round Brown Cysts (RBCs) and high dinocyst concentrations at Site 999. During MIS M2, heterotrophic dinocyst species are absent and dinocyst concentrations are low, indicating that oligotrophic conditions prevailed (De Schepper et al., 2013). At Site 603 no major dinocysts assemblages changes are recorded between 3.34 and 3.19 Ma, indicating a continuous flow of the Gulf Stream. *Protoceratium reticulatum* and the warm water taxa *Impagidinium acuelatum*, *I. paradoxum*, *I. patulum*, *I. solidum* and *Polysphaeridium zoharyi* are the predominant species (De Schepper et al., 2013). During the Piacenzian, warm and oligotrophic surface waters persisted at Site U1313 as shown by the presence of *I. acuelatum*, *I. paradoxum*, *I. patulum* and *Invertocysta* spp. Dinocyst assemblages at the site remain unchanged over MIS M2 but SST derived from alkenones show a slight cooling whereas those based on Mg/Ca ratios of *Globigerina bulloides* are indicative of warmer mixed layer temperatures. Together, these changes are interpreted as evidence for a southward shift of the NAC (De Schepper et al., 2013). At sites U1308 and 610, the dinocyst assemblages are characterised by high abundances of *P. reticulatum* and the persistent presence of *Spiniferites mirabilis* during warm intervals of the Piacenzian. Other common species include *Invertocysta* spp., *Impagidinium* spp. (excl. *I. pallidum*) and *Nematosphaeropsis labyrinthus* at Site U1308 and *Spiniferites*/*Achomosphaera* spp. and

N. labyrinthus at Site 610. Just before and during glacial MIS M2 the relative abundance of *P. reticulatum* drops below 10% at both sites, reflecting a southward shift, or slowdown of the NAC. At U1308, *P. reticulatum* is replaced by *N. labyrinthus*, *I. aculeatum* and *I. paxadoxum*, suggesting the persistence of high summer temperatures but a change to more oligotrophic conditions. Such a change may have been caused by a southward deflection of the NAC (De Schepper et al., 2013, 2009a). This is confirmed by a cooling of annual alkenone-based SSTs of 3–4°C (De Schepper et al., 2013). At Site 610, the dinocysts assemblages during MIS M2 mainly consist of *Bitectatodinium tepikiense*, *Filisphaera filifera*, *I. pallidum*, *N. labyrinthus* and cysts of *Pentapharsodinium dalei*. With the exception of *N. labyrinthus*, all taxa are cool-tolerant, neritic species. Nevertheless, warm-water taxa (e.g. *Melitasphaeridium choanophorum* and *Tectatodinium pellitum*) are still present. These changes in dinocysts assemblages coincide with a decline in alkenone-based SSTs of 3–4°C (De Schepper et al., 2013, 2009a). The authors suggest that the cooling at the northern sites together with only slight, to no, changes at the low-latitude sites is indicative of a reduced northward heat transport, resulting in the establishment of a steep latitudinal gradient during MIS M2. De Schepper et al. (2013) propose that the Pacific-to-Atlantic through-flow via an open CAS exceeded a threshold prior to MIS M2, which led to a reduction in the AMOC and a weakened NAC. This resulted in a southward deflection of the NAC and allowed the expansion of modern-like ice sheets on Greenland, Svalbard/Barents Sea and North America. The cooling is suggested to have caused a sea-level lowering which in turn resulted in a closure of the CAS. A closed CAS enabled the establishment of the Caribbean warm-water pool, which eventually re-invigorated the Gulf Stream and NAC. Northward heat transport led to the retreat of ice sheets and SST ~3°C higher-than-present at the eastern North Atlantic sites during the mPWP (De Schepper et al., 2013).

Shallow marine sediments (Tunnel-Canal Dock section) exposed in the Antwerp harbour area in northern Belgium (51°N) were deposited at the southern margin of the North Sea Basin during the Pliocene (Figure 1.10; Table 1.4) (De Schepper et al., 2009b, 2004; Louwye et al., 2004). The Lillo Formation has been assigned to the late Zanclean and Piacenzian and can be divided into four members. The lowest is the Luchtbal Sands Member whose depositional age has been estimated to 3.71–3.21 Ma. The overlying members (Oorderen, Kruisschans and Merksem Sands) are suggested to be a single depositional sequence and have an age of 3.71–2.6 Ma (De Schepper et al., 2009b; Louwye et al., 2004). The Luchtbal Sands Member is dominated by

Achomosphaera/Spiniferites spp. indet and cysts of *Protoceratium reticulatum*. The presence of cold-tolerant (*Filisphaera filifera*) and open-ocean (*Impagidinium* spp.) species is indicative of the influence of cool waters from the northern North Sea Basin. The rare occurrence of protoperidinioids in this unit can probably be ascribed to syn- or post-depositional oxidation and/or mechanical degradation in a high-energy depositional environment (De Schepper et al., 2009b). The Oorderen and Kruisschans sands members were deposited nearer to the shore under warm temperate neritic conditions. Increasing abundances of *Operculodinium israelianum* reflect a shallowing water depth. Represented thermophilic species include *Achomosphaera andalousiensis*, *Barssidinium pliocenicum*, *Lingulodinium machaerophorum* and *Tectatodinium pellitum* (De Schepper et al., 2009b; Louwye et al., 2004). The Merksem Sands Member represents the last unit of the transgressional succession, deposited very close to the shore under warm- or mild-temperate conditions before the onset of NHG. Several thermophilic species (e.g. *B. pliocenicum*, *L. machaerophorum*, *O. israelianum* and *T. pellitum*), including the acritarch *Nannobarbophora walldalei* are indicative of warm surface water conditions during deposition (De Schepper et al., 2009b).

The dinocyst assemblages of the Red Crag Formation (52°N) in southeastern England are indicative of a restricted marine environment and the inflow of more saline North Atlantic water masses into the southern North Sea Basin during the Piacenzian Figure 1.10; Table 1.4) (Head, 1998). A sample 2 m above the base of the Walton Crag deposits (3.2– >2.6 Ma), which is the uppermost unit of the Red Crag Formation, is characterised by high abundances of *Bitectatodinium tepikiense*, *B. raedwaldii*, *Lingulodinium machaerophorum*, *O. israelianum*, cysts of *Protoceratium reticulatum* and *Spiniferites/Achomosphaera* spp. High proportions of *B. tepikiense* and *L. machaerophorum* suggest mild to warm temperate surface waters with slightly higher temperatures than today. Other thermophilic taxa include *Barssidinium pliocenicum*, *Bitectatodinium raedwaldii*, *Operculodinium*? *eirikianium* and the acritarch *Nannobarbophora walldalei*. *L. macherophorum* and *O. israelianum* are presently both associated with estuarine environments and the former also with elevated nutrient levels. Notable is the absence of the cold-tolerant species *Filisphaera filifera* and *Habibacysta tectata* (Head, 1998).

The dinocyst assemblages at ODP Site 646 (58°N), southwest Greenland, reveal boreal cool temperate to subarctic surface water conditions with an influence of warmer North Atlantic water from the south during the Piacenzian (Figure 1.10; Table 1.4) (de Vernal

and Mudie, 1989a). The predominance of *Brigantedinium simplex*, *Filisphaera filifera*, *Nematosphaeropsis labyrinthea* and cysts of *Protoceratium reticulatum* is indicative of subarctic surface waters. *Batiacasphaera minuta* (as *Batiacasphaera sphaerica*), *Corrudinium devernaliae* (as *Corrudinium* sp. I), *Operculodinium? eirikianum* (as *Operculodinium longispinigerum*) and *Operculodinium tegillatum* (as *Operculodinium crassum*) have their last common occurrences around the Zanclean/Piacenzian boundary. *Cymatiosphaera? invaginata* (as *Cymatiosphaera* sp. I) and *Lavradosphaera crista* (as Incertae sedis I) are the predominate acritarchs during the Piacenzian (De Schepper and Head, 2009; de Vernal and Mudie, 1989a). An almost continuous inflow of the NAC into the eastern Labrador Sea is inferred from the presence of warm temperate to subtropical taxa such as *Impagidinium aculeatum*, *I. patulum* and *Spiniferites mirabilis*. High dinocyst and acritarch concentrations suggest high primary productivity. The presence of the acritarch *Cymatiosphaera*, protoperidinioid cysts (*Brigantedinium* spp., *Lejeunecysta* spp. and *Selenopemphix* spp.) and tasmanites (green algae) may reflect influxes from neritic environments (de Vernal and Mudie, 1989a).

At ODP Hole 907A (69°N) in the Iceland Sea, depleted palynomorph assemblages prevail throughout most of the Piacenzian (Figure 1.10; Table 1.4). Almost mono-specific assemblages predominated by *Spiniferites* spp. occur at 3.6 Ma, 3.4 Ma and 3.3 Ma while all other samples taken until 2.5 Ma are barren (<10 cyst/sample). Decreased productivity, sea ice cover and enhanced overturning are possible explanation for the depleted assemblages, indicating that similar to modern sea surface conditions had been established well before the first major expansion of the Greenland ice sheet at 3.3 Ma (Schreck et al., 2013).

At ODP Site 645 (70°N), Baffin Bay oceanographic conditions have been described for the late Pliocene/early Pleistocene with most of the record probably dating to the early Pleistocene (see Section 1.3.3.2; Figure 1.10; Table 1.4). The oldest dinocyst assemblages of this record are characterised by *Batiacashpaera minuta* (as *Batiacasphaera sphaerica*), *Brigantedinium* spp., *Filisphaera filifera*, *Operculodinium* cf. *tegillatum* (as *Operculodinium* cf. *crassum*) and *Habibacysta tectata* (as *Tectatodinium* sp. I) (de Vernal and Mudie, 1989b; Head, 1994). These assemblages are indicative of subarctic surface water conditions and support an early Pleistocene age. The acritarch *Cymatiosphaera? invaginata* (as *Cymatiosphaera* sp. I) is very abundant at Site 645 (de Vernal and Mudie, 1989b).

Polar to subpolar conditions with the possibility of seasonal sea ice prevailed in the coastal waters offshore Île-de-France (77.5°N), Northeast Greenland, as inferred from molluscs, dinocyst and diatom assemblages (Figure 1.10; Table 1.4) (Bennike et al., 2002). At present the island is surrounded by perennial pack ice except for a polynya bordering its south side. Thermophilic molluscs that are found in the Piacenzian deposits are also indicative of warmer-than-present sea water conditions (Bennike et al., 2002). The authors suggest that an intensified NAC brought warmer waters further north. The dinocyst assemblages are dominated by the extinct species *Filisphaera filifera* and cosmopolitan species *Brigantedinium* spp, complicating the environmental interpretation. Nevertheless, *F. filifera* is predominant at Pliocene and lower Pleistocene high latitude sites in the North Atlantic, suggesting that it is a cold-tolerant species. Assemblages that are dominated by *Brigantedinium* spp., with a low number of other protoperidinioid cysts are also mainly associated with polar and subpolar environments.

1.3.6   Glaciations within the Pliocene

1.3.6.1 Zanclean

Isolated glaciations are recorded in the Nordic Seas area during the Zanclean (De Schepper et al., 2014 and references therein). At c. 5.0–4.7 Ma glaciation events are observed on Iceland, and IRD pulses from Greenland and Scandinavia are detected in the Irminger Basin and Iceland Sea, and Norwegian Sea, respectively. The glacial event coincides with MIS Si6 and/or Si4, but its causes are unclear (De Schepper et al., 2014). Substantial oceanographic and topographic changes possibly promoted the initiation of glaciations (De Schepper et al., 2015; Knies et al., 2014a).

The closure of the CAS, in conjunction with tectonic changes in the circum-Arctic region is proposed to have led to the emergence of seasonal sea ice from c. 4 Ma onwards as shown by an increase in the biomarker IP_{25} in ODP Hole 910C on the Yermak Plateau, NW Spitzbergen (Knies et al., 2014a, 2014b). The opening and closure of oceanic gateways such as the Bering Strait, Fram Strait and CAS in the late Miocene/early Pliocene and circum-Arctic uplift is proposed to have triggered the expansion of Arctic sea ice (Knies et al., 2014a, 2014b). The inflow of cool, fresh Pacific water through the Bering Strait and enhanced freshwater discharge into the Arctic Ocean via Siberian rivers as a consequence of a shoaling CAS might have further facilitated sea ice growth (Knies et al., 2014a).

The expansion of Arctic sea ice at c. 4 Ma coincides with another glacial expansion in the Northern Hemisphere. Glacial deposits on Greenland, Iceland and British Columbia indicate the existence of mountain glaciers while increased IRD deposits in the Iceland and Norwegian Sea suggests an expansion of Scandinavian glaciers. This glacial event can likely be attributed to circum-Arctic uplift (De Schepper et al., 2014; Knies et al., 2014a, 2014b).

1.3.6.2 Piacenzian

The Zanclean/Piacenzian transition is marked by the gradual onset of Northern Hemisphere glaciations, starting at 3.6 Ma (De Schepper et al., 2014; Mudelsee and Raymo, 2005; Ravelo et al., 2004). Glacial growth in the North Atlantic and Nordic Seas area is either directly documented from terrestrial deposits or indirectly from marine records (De Schepper et al., 2014). The analysis of 45 globally distributed δ^{18}O records from benthic and planktonic foraminifera shows a gradual increase of 0.4‰ over the time interval from 3.6 to 2.4 Ma, equating to a sea level fall of 43±5 m (Mudelsee and Raymo, 2005). IRD pulses on the Yermak Plateau indicate that glaciers episodically expanded on the sub-aerially exposed Barents Sea between c. 3.5 and 2.4 Ma (Knies et al., 2009). At 3.5 Ma (3.4–3.6 Ma) a major glacial advance is also recorded in the James Bay Lowland, Canada (Gao et al., 2012).

According to marine records, a pronounced glacial event occurred at c. 3.3 Ma (MIS M2) (De Schepper et al., 2014, 2013; Lisiecki and Raymo, 2005; Mudelsee and Raymo, 2005). The event is evident in 11 of the 25 globally distributed high-resolution benthic δ^{18}O records analysed by Mudelsee and Raymo (2005). In the Northern Hemisphere it has been recorded by increases in IRD at ODP Site 907 off East Greenland, suggesting an expansion of the Greenland ice sheet (Kleiven et al., 2002). From 3.5 Ma onwards small IRD peaks have also been documented at ODP Site 644/642 in the Norwegian Sea, which have been interpreted to indicate the presence of Scandinavian glaciers large enough to reach the coast and calve icebergs (Kleiven et al., 2002). Bachem et al. (2016) present new IRD data from Hole 642B for the mPWP. As the IRD peaks are only small and alkenone-derived SSTs were higher than present, they suggest that Scandinavia is unlikely to be the source area. Instead, icebergs might have come from sea-terminating ice masses on East Greenland. This is supported by the IRD record from ODP Site 907 which shows larger, contemporaneous IRD peaks compared to those at Site 642 (Bachem et al., 2016; Kleiven et al., 2002). Terrestrial evidence for the extent of glaciation during MIS M2 is sparse but existing records document relatively

cool climatic conditions (Andreev et al., 2014; Demske et al., 2013; Popescu et al., 2010).

Glacial MIS M2 has been linked to a weakening of the NAC as a consequence of an opening of the CAS between 3.4–3.3 Ma (De Schepper et al., 2013, 2009a). The large through-flow from the Pacific to the Atlantic weakened the NAC and hence the northward heat transport. This resulted in cooling of the North Atlantic and permitted continental ice sheet growth. The closing of the CAS, caused by the sea level fall during full glaciation, led to the establishment of the Caribbean Warm Pool. The warming of Caribbean surface water resulted in a re-establishment of the NAC and northward heat transport, which led to deglaciation and the warm climate of the mPWP (De Schepper et al., 2013).

1.4   Summary

Pliocene vegetation and SSTs records in the North Atlantic region are characterised by an amplified warming relative to present at higher latitudes (Bennike et al., 2002; Rybczynski et al., 2013; Willard, 1994). In the Nordic Seas region, the low resolution and/or dating uncertainties of terrestrial records have, however, limited our understanding of the variability of climatic changes on multi-millennial to glacial-interglacial timescales. As the polar regions are particularly sensitive to environmental changes due to positive feedback mechanisms (Miller et al., 2010), further well-dated, high-resolution terrestrial and marine records are required to better understand the spatial extent of Pliocene climate changes. Only limited data on Pliocene vegetation changes is available for the Norwegian Sea regions (Willard, 1994), which represents an important region for the exchange of heat between the North Atlantic and Arctic Ocean via the NwAC (Bachem et al., 2016; De Schepper et al., 2015; Risebrobakken et al., 2016). Up to today, the role of changes in the strength of the AMOC and thus the NAC/NwAC in contributing to the enhanced warming in the Nordic Seas region in comparison to mid- and low-latitude region during the Pliocene is still being debated (Dowsett et al., 2009; Raymo et al., 1996; Risebrobakken et al., 2016; Sarnthein et al., 2009; Zhang et al., 2013a). With ODP Site 642 being located in the path of the NwAC, the site is ideally situated to record changes in the northward heat transport during the Pliocene. Here, a new high-resolution record of Pliocene vegetation changes in northern Norway is presented together with a new dinocyst record, documenting changes in the NwAC during the mPWP. These records provide new data on the magnitude of warming and climate variability in the Norwegian Sea region during the Pliocene and

allow for a direct comparison of terrestrial and marine changes to identify atmospheric and/or oceanographic forcing mechanisms.

Chapter 2: Site Location, Materials and Methods

2.1 Geographical setting

ODP Hole 642B was drilled during ODP Leg 104 in 1985. The site is located on the Outer Vøring Plateau in the Norwegian Sea about 400–450 km west of Norway (67°13.2'N, 2°55.8'E, 1286 m water depth; Shipboard Scientific Party (1987); Figure 2.1). A branch of the NwAC flows northward on either side of the plateau. The eastern branch follows the continental slope of Norway and the western branch flows around the Vøring Plateau. Atlantic Water is spread between both branches and lies above the site (Nilsen and Nilsen, 2007). The branches of the NwAC are an extension of the NAC which in turn is a continuation of the Gulf Stream (Orvik and Niiler, 2002). The eastern branch of the NwAC enters the Nordic Seas across the Iceland-Faroe Ridge while the western branch flows through the Faroe-Shetland Channel (Hansen and Østerhus, 2000).

2.2 Samples, preparation and analysis

The Pliocene section of ODP Hole 642B consists of nannofossil ooze, with minor diatom-nannofossil ooze and mud units. The sediment is moderately to heavily
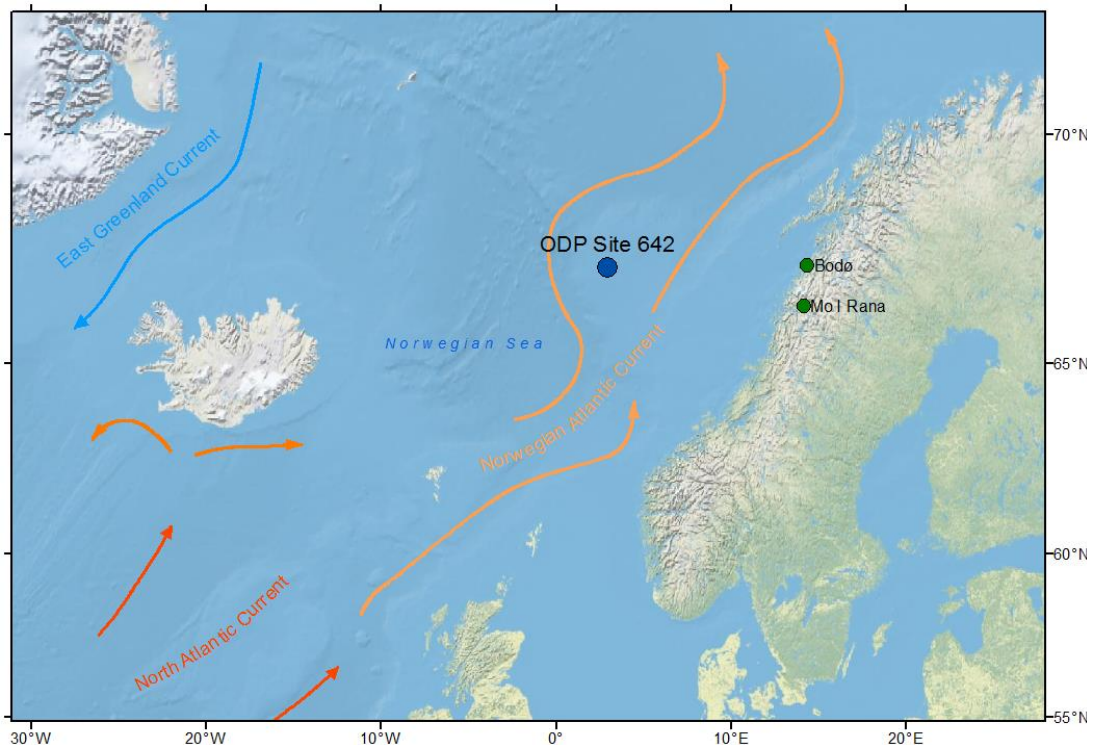
Figure 2.1: Location of ODP Site 642 in the Norwegian Sea. Meteorological stations used for present-day climate data are located in Bodø and Mo i Rana in Nordland, northern Norway. Colour coding indicates the relative temperature of currents: dark orange = warm; light orange = moderately warm; blue = cold.

bioturbated. From the Miocene to the Pleistocene, the deposition shifts from predominately siliceous to calcareous sediments (Shipboard Scientific Party, 1987). Samples were taken from core sections 9H1 to 10H6 between 83.55 and 66.95 metres below sea floor (mbsf) in 1 to 100 cm steps, depending on sample availability and required resolution (see also Risebrobakken et al., 2016).

All samples were pre-sieved in Bergen, Norway, through a 63 μm mesh to retain foraminifera for oxygen isotope analysis (Risebrobakken et al., 2016). A potential bias in the pollen data due to the loss of larger Pinaceae grains caused by pre-sieving has been excluded by comparison of sieved and unsieved samples. Samples were prepared for palynological analysis at the Palynological Laboratory Services Ltd, North Wales, and Northumbria University, Newcastle, using standard palynological techniques (Faegri and Iversen, 1989). In order to calculate pollen concentrations one (two) *Lycopodium clavatum* spore tablet(s) was (were) added to each sample (Stockmarr, 1971). The following batches of *Lycopodium* tablets were used: No. 483216, 3862 and 12496. As the sediment was processed in beakers, it was left to settle for 6–8 hours according to Stokes' law in between washes. The entire procedure from the unprocessed sample to the pollen slide took between 1.5 to 2 weeks. First, the <0.063 μm fraction was dry weighed. For most samples, 5–10g of sediment was weighed but amounts vary between 1.5 to 21.9g of sediment. At this stage, one (two) *Lycopodium* tablet(s) was (were) added to the beaker before 20% HCl was used to dissolve carbonates. After settling, the sediment was washed with deionised water and left to settle up to five times until the solution was neutral, ensuring the removal of Ca^{2+} -ions in order to avoid the formation of fluorosilicates. Concentrated HF (48%) was used to remove silicates. The sediment was repeatedly swirled and left in HF for 3–4 days. After decanting HF, the residue was washed once with deionised water and subsequently with hot HCl to remove fluorosilicates that might have formed. The sediment was back-sieved with deionised water through a 10 μm screen and transferred into tubes. The residue was stained with Safranin-O by adding two drops to the tube. After 1.5 minutes, the tube was filled with water and centrifuged. The water was decanted and the residue washed an additional two times in order to remove most of the Safranin-O. After the final wash, a few drops of a glycerol and water (1:1) mixture with diluted $CuSO_4$ was added to transfer the residue to storage glass vials. The vials were centrifuged and the liquid removed with a pipette before the residue was mounted on glass slides with glycerol-gelatine jelly. The slides were put upside down into a slide box which was placed into
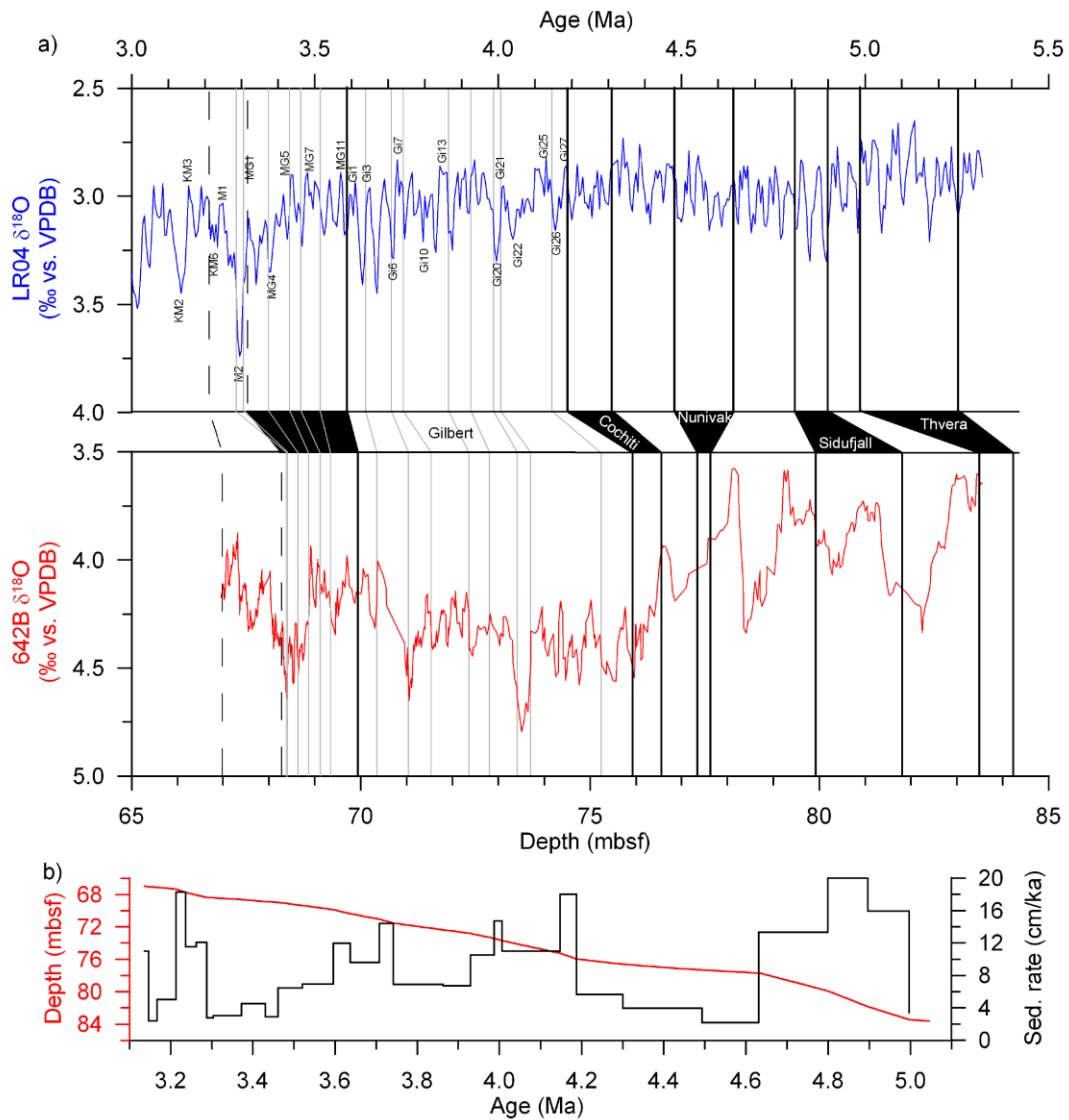
Figure 2.2: Age model for ODP Hole 642B from Risebrobakken et al. (2016). (a) Global LR04 benthic oxygen isotope stack (blue) versus age from Lisiecki and Raymo (2005) and (b) five-point running mean of *Cassidulina teretis* oxygen isotope values ($\delta^{18}O_{C.t.}$) from ODP Hole 642B (red) versus age. Vertical black lines indicate the location of magnetic reversals, with magnetic periods marked in black and white between the two panels. Two magnetic reversals (dashed lines) were not used as tie points for the age model. Grey lines represent tie points obtained from the correlation between the $\delta^{18}O_{C.t.}$ curve to the LR04 stack. Indicated marine oxygen isotope stages correspond to those defined by Lisiecki and Raymo (2005). (b) Age-depth model for ODP Hole 642B (red line) and sedimentation rates.

an oven (c. 60°C) for 5–6 hours to ensure the settling of palynomorphs against the cover slip. The microscopic analysis was carried out using a Leica Microscope (DM 2000 LED) at magnifications of 400x and 1000x.

2.3   Age model

The Pliocene age model for ODP Hole 642B is based on the magnetic stratigraphy of Bleil (1989) updated to the Astronomically Tuned Neogene Time Scale (ATNTS) 2012 (Hilgen et al., 2012), and further correlation of the benthic oxygen isotopes to the global

LR04 benthic $\delta^{18}O$ stack (Figure 2.2) (Lisiecki and Raymo, 2005; Risebrobakken et al., 2016). The age model was established for the sediment sequence between 83.61 and 66.94 mbsf, corresponding to 5.05 to 3.14 Ma. The core is barren of foraminifera between 88.43 and 83.61 mbsf (Risebrobakken et al., 2016) and a major hiatus exists after 3.14 Ma (Jansen and Sjøholm, 1991). Between 4.147 (MIS MG7/MG8) and 3.136 Ma (MIS KM3/KM2) the age model is fully constrained by isotopes. Across glacial MIS M2, the benthic $\delta^{18}O$ signal is not any heavier than during other times of the Pliocene, pointing to the possibility of a hiatus for the globally coldest part of MIS M2. However, a restricted local response to M2 cannot be excluded (Risebrobakken et al., 2016) (see also Chapter 3 and 5 for further discussions).

2.4   Analysis of palynomorphs

2.4.1   Pollen and spores

Pollen was counted in a total of 128 samples from ODP Hole 642B between 83.55 and 66.95 mbsf or 5.03 and 3.14 Ma. Identification was aided by the pollen reference collection at Northumbria University and the following literature: Erdtman et al. (1961); Moe (1974); Faegri and Iversen (1989); Beug (2004); Demske et al. (2013). In-situ *Lycopodium clavatum* spores were differentiated from the reference spores by distinct differences in shape and colour (Plate 2.1). The group *Juniperus*-type only contains pollen grains that are split open whereas Cupressaceae contains those that are still closed or have a papilla (Demske et al., 2013). Reworked pollen and spores were identified based on
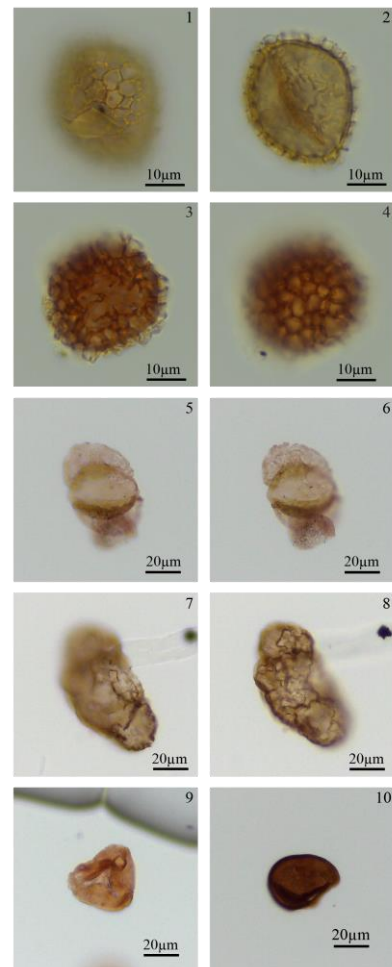
Plate 2.1: Comparison of in-situ *Lycopodium clavatum* spores and marker grains, and examples of reworked Pinaceae pollen and spores from ODP Hole 642B. All images were taken in bright field illumination. Sample number and England Finder coordinates are given for each grain. 1–2: in-situ *Lycopodium clavatum* spores, 9H2 90-91, B35/4; 3–4: *Lycopodium clavatum* marker grains, 9H2 90-91, C37/1; 5–8: reworked Pinaceae pollen, 9H2 15-16, Y36/0 and R38/4; 9: reworked trilete spore, 9H3 115-116, K65/4; and 10: reworked monolete spore 9H2 15-16, V41/3.

the thermal maturity of the exine as seen by their dark orange to brown colours, and/or their presence outside their stratigraphic range. In addition to a discolouration to yellow/orange colours, particularly reworked bisaccates showed a high degree of compression, a faint alveolar structure of air sacks and mineral imprints (Plate 2.1) (de Vernal and Mudie, 1989a, 1989b; Willard, 1996). Cenozoic uplift phases and shifting depocentres as documented in Eidvin et al. (2014) are restricted to the basins off the Norwegian coast and should not have affected the coring site which is located on the Outer Vøring Plateau.

Pollen diagrams were generated with the software Tilia Vers. 1.7.16 (Grimm, 1990). Pollen percentages were calculated on the total pollen sum excluding *Pinus* pollen, unidentified and reworked pollen and spores. Percentages of *Pinus* pollen was calculated based on the total pollen sum including *Pinus*. Stratigraphically constrained cluster analysis (CONISS) was used to delimit local pollen assemblage zones (Grimm, 1990, 1987). The zonation follows the method of Grimm (1987), with cutting the dendrogram at a certain height, so that the different clusters are characterised by a within-zone variability below a certain value. Further subzones were defined if they were considered to be of interpretative value.

Pollen accumulation rates (PARs) were calculated based on the following formula:

(1) $$PAR = C_P \text{ x } \rho \text{ x } S$$

with PAR in grains/(cm^2 ka), C_P being the pollen concentration (grains/g), ρ the dry bulk density (g/cm^3) and S the sedimentation rate (cm/ka).

Rarefaction was applied to estimate the number of taxa at a constant count of grains (Birks and Line, 1992). Diversity was assessed using the Shannon index which takes into account the relative abundance of a taxon as well as the number of taxa. The Shannon index is zero if the assemblage is dominated by a single taxon and shows high values for assemblages with many taxa that are each represented by few individuals (Hammer et al., 2001). Both rarefaction and diversity were calculated in PAST3 (PAleontologial STatistics, Hammer et al., 2001).

2.4.2 Dinoflagellate cysts

Dinocysts were counted in 44 samples from ODP Hole 642B between 68.45 and 66.95 mbsf or 3.32 and 3.14 Ma. A taxonomic list of species encountered in the Piacenzian sediments of ODP Hole 642B with full authorial citations is provided in Table 2.1.

Nomenclature follows that of Fensome et al. (2008) and the following literature: De Schepper and Head (2014, 2009, 2008a); De Schepper et al. (2009b, 2004); Head and Norris (2003); Head and Westphal (1999); Head (2003, 1997, 1996b, 1994, 1993); Louwye et al. (2004); Paez-Reyes and Head (2013); Schreck and Matthiessen (2013); Verhoeven and Louwye (2012); Wrenn (1988). *Brigantedinium* spp. comprises all (sub)spherical brown protoperidinioid cysts with an intercalary (sub)polygonal archeopyle and without processes (Reid, 1977). Round brown cysts (RBCs) include (sub)spherical brown protoperidinioid cysts with neither processes nor a visible polygonal archeopyle. Round brown spiny dinocysts without a visible archeopyle are included in *Echinidium* spp. Species within the genus *Spiniferites* were differentiated if possible, depending on orientation and preservation.

The dinocyst burial flux (DBF) was calculated based on the dinocyst concentrations using the following formula:

(1) $$\text{DBF} = C_D \times \rho \times S$$

with DBF in cysts/(cm^2 ka). C_D is the dinocyst concentration (cysts/g), ρ the dry bulk density (g/cm^3) and S the sedimentation rate (cm/ka). The comparison of DBF with dinocyst concentrations gives an indication of the influence of productivity and/or sedimentation rate on the observed fluctuations. If DBF and dinocyst concentration show the same pattern, the changes in concentrations can be interpreted to reflect changes in productivity (Hennissen et al., 2014).

2.4.3 Acritarchs

In this study, five formally described acritarchs (*Cymatiosphaera*? *aegirii*, *C.*? *icenorum*, *C.*? *invaginata*, *Lavradosphaera crista* and *Nannoborbosphora walldalei*) have been found in the majority of the Piacenzian samples of ODP Hole 642B. *C.*? *icenorum*, *C.*? *invaginata* and *L. crista* together with small spiny acritarchs (SSA) are the most abundant species and show a high variability in their relative proportions.

Acritarch species are used as an indicator for marine productivity, stratification and/or water temperature (De Schepper and Head, 2014; de Vernal and Mudie, 1989a, 1989b; Schreck et al., 2013). Here, the acritarch burial flux has been calculated based on the formula:

(2) $$\text{ABF} = C_A \times \rho \times S$$

with ABF in cysts/(cm^2 ka), C_A representing the acritarch concentration (cysts/g), ρ the dry bulk density (g/cm^3) and S the sedimentation rate (cm/ka).

Table 2.1: Taxonomic names with full authorial citations of dinoflagellate cyst and acritarch taxa from ODP Hole 642B between 68.45 and 66.95 metres below sea floor.

Dinoflagellate cysts

Achomosphaera andalousiensis Jan du Chêne 1977 emend. Jan du Chêne and Londeix 1988

Achomosphaera andalousiensis subsp. *andalousiensis* Jan du Chêne 1977 emend. Jan du Chêne and Londeix 1988

Achomosphaera andalousiensis subsp. *suttonensis* Head 1997

Achomosphaera ramulifera (Deflandre 1937) Evitt 1963

Amiculosphaera umbraculum Harland 1979

Ataxiodinium choane Reid 1974

Ataxiodinium Reid 1974

Ataxiodinium zevenboomii Head 1997

Barssidinium Lentin, Fensome and Williams 1994

Barssidinium graminosum Lentin, Fensome and Williams 1994

Barssidinium pliocenicum (Head 1993) Head 1994 emend. De Schepper and Head 2004

Batiacasphaera micropapillata complex sensu Schreck and Matthiessen (2013)

Bitectatodinium raedwaldii Head 1997

Bitectatodinium? *serratum* Head, Norris and Mudie 1989

Bitectatodinium sp. A of De Schepper et al. (2017)

Bitectatodinium Wilson 1973

Bitectatodinium tepikiense Wilson 1973

Brigantedinium Reid 1977 ex Lentin and Williams 1993

cf. *Cerebrocysta*? *namocensis* Head, Norris and Mudie 1989

Corrudinium harlandi Matsuoka 1983

Corrudinium? *labradori* Head, Norris and Mudie 1989

Corrudinium Stover and Evitt 1978

Cyst of *Pentapharsodinium dalei* Indelicato and Loeblich III 1986

Cysts of *Protoceratium reticulatum* (Claparède and Lachmann, 1859) Bütschli 1885

Dapsilidinium pseudocolligerum Stover 1977

Echinidinium Zonneveld 1997 ex Head, Harland and Matthiessen 2001

Filisphaera filifera Bujak 1984

Filisphaera microornata (Head, Norris and Mudie 1989) Head 1994

Filisphaera Bujak 1984

Habibacysta tectata Head, Norris and Mudie 1989

Heteraulacacysta sp. A of Costa and Downie (1979)

Impagidinium aculeatum (Wall 1967) Lentin and Williams 1981

Impagidinium pallidum Bujak 1984

Impagidinium paradoxum (Wall 1967) Stover and Evitt 1978

Impagidinium patulum (Wall 1967) Stover and Evitt 1978

Impagidinium solidum Versteegh and Zevenboom in Versteegh 1995

Impagidinium sp. 2 of De Schepper and Head (2009)

Impagidinium Stover and Evitt 1978

Invertocysta lacrymosa Edwards 1984

Invertocysta sp. 1

Invertocysta Edwards 1984 /*Amiculosphaera* Harland 1979

Lejeunecysta catomus ? Harland et al. 1991

Lingulodinium machaerophorum (Deflandre and Cookson 1955) Wall 1967

Melitasphaeridium choanophorum (Deflandre and Cookson, 1955) Harland and Hill 1979

Melitasphaeridium sp. A of De Schepper and Head (2008)

Melitasphaeridium (Deflandre and Cookson, 1955) Harland and Hill 1979

Nematosphaeropsis labyrinthus (Ostenfeld 1903) Reid 1974

Nematosphaeropsis lativittata Wrenn 1988

Nematosphaeropsis Deflandre and Cookson 1955 emend. Williams and Downie 1966

Operculodinium? *eirikianum* var. *eirikianum* Head 1997

Operculodinium centrocarpum s.s. (Deflandre and Cookson, 1995) Wall 1967/*Operculodinium israelianum* (Rossignol 1962) Wall 1967

Operculodinium janduchenei Head, Norris and Mudie 1989

Operculodinium Wall 1967 emend. Matsuoka, McMinn and Wrenn 1997

Pyxidinopsis braboi De Schepper, Head and Louwye 2004

Round brown cysts

Selenopemphix conspicua de Verteuil and Norris 1992

Selenopemphix dionaeacysta Head, Norris and Mudie 1989

Selenopemphix cf. *islandensis* Verhoeven and Louwye 2012

Selenopemphix nephroides (Benedek 1972) Bujak in Bujak et al. 1980

Selenopemphix nephroides - small variety (c. 20µm)

Selenopemphix Benedek 1972 emend. Bujak in Bujak et al. 1980

Spiniferites elongatus Reid 1974

Spiniferites falcipedius Warny and Wrenn 1997

Spiniferites mirabilis (Rossignol 1964) Sarjeant 1970

Spiniferites membranaceus (Rossignol 1964) Sarjeant 1970

Spiniferites ramosus (Ehrenberg 1838) Mantel 1854

Spiniferites Mantell 1850 emend. Sarjeant 1970 /*Achomosphaera* Evitt 1963

Tectatodinium pellitum (Wall 1967) Head 1994

Trinovantedinium glorianum (Head, Norris and Mudie 1989) de Verteuil and Norris 1992

Trinovantedinium Reid 1977 emend. de Verteuil and Norris 1992

Tuberculodinium vancampoae (Rossignol 1962) Wall 1967

Dinocyst spp.

Acritarchs

Cymatiosphaera? *icenorum* De Schepper and Head 2014

Cymatiosphaera? *invaginata* Head, Norris and Mudie 1989

Lavradosphaera crista De Schepper and Head 2008

Nannobarbophora walldalei Head 1996

Acritarchs are often encountered in marine palynomorphs assemblages but little attention has been given to stratigraphical ranges and palaeoenvironmental preferences of individual species. In recent years, acritarchs have increasingly been used in stratigraphical and palaeoecological studies especially in the mid- to high latitudes of the North Atlantic (De Schepper and Head, 2014, 2009, 2008a, 2008b; De Schepper et al., 2015; Schreck et al., 2013, 2012; Verhoeven and Louwye, 2013).

To determine their palaeoecological requirements, the abundances of *C.? aegirii*, *C.? icenorum* and *L. crista*, relative to the total sum of marine palynomorphs, have been compared to SST estimates based on Mg/Ca ratios of the planktonic foraminifer *Globigerina bulloides* (De Schepper and Head, 2014). De Schepper and Head (2014) determined the relationship between acritarch abundances and SSTs at three sites in the North Atlantic: IODP Site U1313, IODP Site U1308 and DSDP Hole 610A. All species show their highest abundances at the mid-latitude site (U1308 and 610A), where less oligotrophic conditions and lower SSTs (10–17C°) prevail when compared to Site U1313 at the subtropical gyre.

N. walldalei is a neritic species that occurs in tropical to warm- or mild-temperate regions. Its occurrence in oceanic records might be due to long distance transport (Head and Westphal, 1999; Head, 2003).

2.5   Data analysis

2.5.1   Pollen and spores

2.5.1.1   Transport of pollen and spores to the site

Pollen is transported into the marine environment by wind, rivers, ice and/or ocean currents. A schematic illustration of the possible transport routes of pollen and spores to marine sediments is shown in Figure 2.3. Owing to differences in production, dispersal strategies and grain morphology, pollen assemblages in marine sediments represent a fraction of the terrestrial species diversity. Taxa of wind-pollinated plants generally predominate and their relative proportion increases with the distance from the coast (Mudie and McCarthy, 2006; Mudie, 1982). Bisaccate pollen grains, especially those of *Pinus*, are over-represented due to the preferential transport of these grains over long distances. In contrast, pollen from deciduous trees and shrubs are generally under-represented as a result of their smaller size and higher density (Heusser, 1983; Mudie and McCarthy, 2006). Nevertheless, pollen distributions in marine surface samples

along coastal transects around the world reveal a good reflection of the vegetation (Hooghiemstra et al., 2006; Montade et al., 2011; Mudie, 1982; van der Kaars and De Deckker, 2003). Regional differences in climate, atmospheric and oceanographic circulation systems, however, have to be considered when interpreting marine pollen assemblages (Dupont, 2011; Mudie and McCarthy, 2006).

For ODP Site 642, the source area is considered to be predominately northern Norway as it is the closest landmass to the site. As the central part of Norway (county of Nordland) ranges in width only between c. 50 and 150 km, the boreal forests of northern Sweden and Finland could be additional source areas. While the Scandinavian mountains likely act as a boundary in westward pollen transport from northern Scandinavia, long-distance transport of *Pinus* grains from the boreal forests in northern Sweden and Finland to Site 642 cannot be excluded. Due to the relatively short travel distances of pollen from deciduous trees (<200 km) (Mudie and McCarthy, 2006), these grains are suggested to only originate from the Norwegian coast. In spring, when most plants disperse pollen and spores, wind from the east/south prevails in Norway (e.g. Hall, 2003), suggesting that the mixed to boreal forests in southwestern Norway could be an additional source area.

In Figure 2.3, the main processes that affect pollen transport to Site 642 are highlighted. Due to the predominance of easterly winds during spring, and northward transport of freshwater plumes by the Norwegian Coastal Current within 100 km off the coast (Mork, 1981), pollen transport by wind is considered to account for most of the pollen deposition at the site. Lateral transport of pollen by ocean currents has been shown to be negligible on continental scales (Dupont, 2011 and references therein). As the site is located on a plateau, bottom currents and/or gravity flows should have had a minor influence on the pollen assemblages. In the Norwegian Sea, these sedimentary processes have been suggested to affect palynomorph assemblages in the basins along the continental slopes (Matthiessen, 1995; Wall et al., 1977). On the Vøring Plateau, bioturbation occurs within the upper 10 cm of sediment (Romero-Wetzel, 1989).

2.5.1.2 Quantitative climate reconstructions based on pollen data

Most quantitative Quaternary climate reconstructions based on pollen assemblages rely on a modern pollen-climate calibration data set, relating pollen occurrences and abundances in modern surface samples to vegetation and climate (e.g. Seppä et al., 2004; Tarasov et al., 2011). Such reference datasets have been developed on a regional
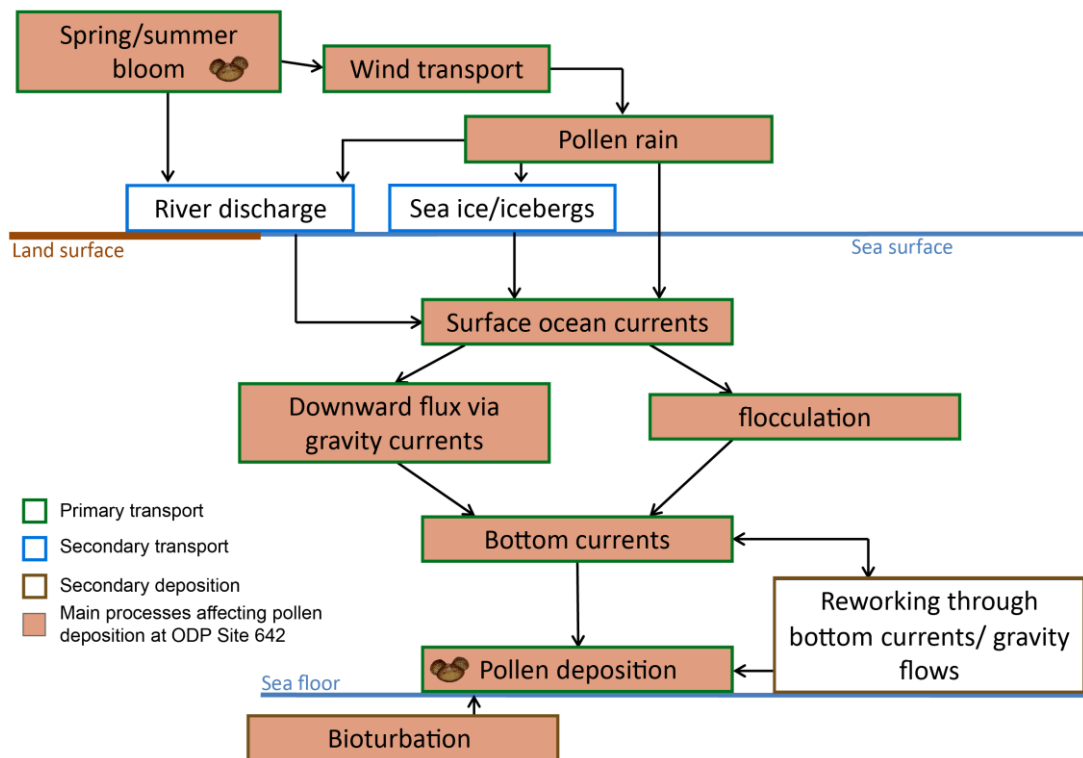
Figure 2.3: Schematic illustration of processes that can affect pollen transport and deposition in the marine environment.

to continental scale for application to Quaternary pollen records (Cheddadi et al., 1998a; Davis et al., 2013; Herbert and Harrison, 2016; Li et al., 2007; Tarasov et al., 2011; Whitmore et al., 2005). The development of a reference dataset requires the assessment of the relationship between the distribution of pollen taxa and the environmental variables using multivariate regression methods. Commonly used methods include detrended correspondence analysis (DCA) to establish the compositional variation in the dataset followed by canonical redundancy analysis (RDA) if species response is linear, or canonical correspondence analysis (CCA) if species response is unimodal (Legendre and Birks, 2012). The application of RDA/CCA allows to determination of variation in the dataset that is explained by one or more environmental variable(s) (e.g. Li et al., 2007; Seppä et al., 2004). For the reconstruction of palaeoclimate parameters, multivariate calibration methods are used to develop transfer functions (Juggins and Birks, 2012). Among these methods, the modern analogue technique (Guiot, 1990) has been widely applied to fossil pollen records (Cheddadi et al., 1998b; Davis et al., 2003; Guiot et al., 1989; Tarasov et al., 2011; Willard et al., 2001). This technique finds modern analogues for fossil assemblages based on a dissimilarity coefficient. By taking the (weighted) average of a climatic parameter of a certain number of modern analogues, environmental variables are reconstructed for the fossil assemblages (Guiot,

1990; Simpson, 2012). Other multivariate techniques include artificial neural network (ANN) (Davis et al., 2003; Peyron et al., 1998), weighted-averaging regression (WA) and weighted-averaging partial least squares regression (WA-PLS) (Herzschuh et al., 2010; Juggins and Birks, 2012; Li et al., 2007; Seppä et al., 2004). While ANNs can deal with non-linear problems, e.g. pollen-climate relationship, WA-PLS has the advantage of taking into account the unimodal distribution of species in relation to environmental variables (Bartlein et al., 2011; Juggins and Birks, 2012). Mathematical details, advantages and disadvantages of the different methods are discussed in Bartlein et al. (2011); Birks (2010, 1998); Birks et al. (2012); Seppä and Bennett (2003).

In pre-Quaternary epochs, the use of transfer functions is often strongly hampered by non-analogue assemblages of fossil plant remains (e.g. Fauquette et al., 1998). Alternatives are methods based on morphology such as leaf physiognomy and nearest living relatives (NLRs) of fossil taxa (Mosbrugger and Utescher, 1997; Uhl et al., 2007). For pre-Quaternary pollen assemblages, two NLR methods, the coexistence approach (CA) (Mosbrugger and Utescher, 1997; Utescher et al., 2014) and mutual climatic range technique (MCR) (Thompson et al., 2012) are commonly used for the quantitative reconstruction of climatic parameters. Both methods use the modern climatic tolerances of the NLRs of the fossil taxa present in an assemblage to determine the climatic range in which these taxa could coexist, the so called coexistence interval (Utescher et al., 2014). Only the presence/absence of a taxon is considered. Datasets of modern plant distribution and climatic parameters are available for North America (Thompson et al., 1999) and Eurasia (Utescher and Mosbrugger, 2013). Here, the CA is applied using the database for Eurasian plant species, which, in comparison to the North American database, includes tree species that are endemic to Asia (e.g. *Pterocarya* and *Sciadopitys*) and climate data for ferns and mosses. The CA can be used to estimate Mean Annual Temperature (MAT), Coldest Month Temperature (CMT), Warmest Month Temperature (WMT), Mean Annual Precipitation (MAP), Monthly Precipitation of the warmest month (MPw), Monthly Precipitation of the wettest month (MPwt) and Monthly Precipitation of the driest month (MPd). The application of the CA to modern floras and comparison to data from meteorological stations has shown that there is a very good match for the climate parameters MAT, WMT, CMT and MPwt. Reconstructions for MPd showed reasonable values whereas estimates for MAP and MPw differed substantially from the real values (Mosbrugger and Utescher, 1997). The CA has been criticised for incorrect or unprecise palaeoclimate reconstructions due to

inconsistencies when applied to modern floras (Grimm and Denk, 2012), and more recently also for its underlying assumptions and the lack of a statistical framework (Grimm and Potts, 2016). Nevertheless, the CA is a valuable tool for the reconstruction of pre-Quaternary terrestrial climatic conditions (Utescher et al., 2014). As the CA is based on presence/absence and not relative abundances, taphonomic bias is reduced. Further advantages include the straightforward use of climatic tolerances of modern taxa, the absence of additional calibrations and the identification of inconsistences when a high number of taxa is used (Utescher et al., 2014). The CA has mainly been applied to fossil pollen assemblages in terrestrial or shallow marine deposits (Ballantyne et al., 2010; Bruch et al., 2011; Ivanov et al., 2007; Olivares et al., 2004; Pound et al., 2015; Quan et al., 2014; Utescher et al., 2012, 2000). The application of the CA to pollen assemblages in marine sediments may be hampered by alterations of the pollen association caused by differential transport and taphonomy (Eldrett et al., 2014; Kotthoff et al., 2014). Further limitations for quantitative climate reconstructions, applying to both terrestrial and marine deposits, include the presence of pollen taxa from plants growing in different communities due to considerable relief in the study area, long-distance transport, large source area and/or relict taxa (Utescher et al., 2014). Additionally, the modern climate requirements of relict taxa – plants that once showed a much wider distribution but are presently restricted to certain areas (e.g. *Sciadopitys*) (e.g. Fauquette et al., 1998; Head, 1998; Popescu, 2001; Schulz and Stutzel, 2007; Willard, 1994) – might not represent their potential distribution (Utescher et al., 2014).

2.5.1.3 Principal Component Analysis

Principal Component Analysis (PCA) was applied to the transformed species abundance data to identify groups of variables (taxa) that are highly correlated, and the main gradients of variance (Legendre and Birks, 2012). The abundance data was normalised in PRIMER (Clarke and Gorley, 2006) to reduce asymmetry before applying PCA using PAST3 (Hammer et al., 2001). The data transformation accounts for the unimodal response of species to environmental variables (Legendre and Birks, 2012). PCA is the method of choice as it has been widely used in other studies to aid interpretation of Pliocene pollen assemblages changes (Demske et al., 2002; Jiménez-Moreno et al., 2013; Popescu, 2001; Willis et al., 1999b). Due to large differences in the relative abundance of taxa, the inclusion of all taxa yields many components, with the first two only explaining a small proportion of the variance. Taxa occurring rarely and those with limited climatic information were successively excluded from the analysis until the first

two components explained as much of the variance as possible. This resulted in the final inclusion of 18 taxa that are representative of the main Pliocene pollen assemblage changes and the variance of which is relatively well explained by the first two components.

2.5.1.4 Spectral Analysis

In order to analyse cyclicity within the vegetation changes spectral analysis was applied to the Pliocene pollen record using PAST3 (Hammer et al., 2001). The analysis was performed on the time interval between 4.366 and 3.137 Ma only, due to a 173,000 years-long hiatus before 4.366 Ma. The average resolution across the analysed interval is c. 11,200 years. Therefore, the data was interpolated on 11,000-year time steps prior to the analysis. Spectral analysis was performed on the relative abundance changes of taxa that show major variations within the pollen record and contain important climatic information. These include: Asteraceae, conifers excluding *Pinus*, Ericaceae, *Lycopodium* spp., *Picea*, *Pinus*, *Sciadopitys*, *Sphagnum* and *Tsuga* as well as the sum of Asteraceae, Ericaceae and *Lycopodium* spp. Low-frequency cyclicities are detected in the relative abundance changes which are indicative of periods in the order of 166,700 to 1,000,000 years.

2.5.1.5 Climate model

In order to allow for further interpretation of the pollen data and to reconstruct potential changes in pollen transport by wind, climate model outputs from the Hadley Centre coupled atmosphere-ocean climate model (HadCM3) have been investigated. HadCM3 is an IPCC AR4 (Intergovernmental Panel on Climate Change – Fourth Assessment Report) class climate model (as described in Gordon et al., 2000) and has been shown to reproduce well the large scale features of Pliocene climate (Haywood et al., 2013b). It has been used for a number of Pliocene climate modelling studies and was the first coupled atmosphere-ocean climate model (Haywood and Valdes, 2004) to run using boundary conditions defined by the PRISM project based at the US Geological Survey (see Dowsett, 2007). The simulations shown here have PRISM2 boundary conditions (following Dowsett et al., 1999) and an altered CAS as described and presented in Lunt et al. (2008a, 2008b). Here, two simulations of surface wind speeds and atmospheric pressure are used to ascertain the impact of closing the CAS on atmospheric circulation in the Nordic Sea region: (i) a Pliocene simulation with an open CAS and (ii) a Pliocene simulation with a closed CAS. The experiments were run by the palaeoclimate

modelling community at the University of Leeds (Prof. Alan Haywood and Dr Aisling Dolan) and the University of Bristol (Prof. Dan Lunt).

2.5.2   Dinoflagellate cysts

2.5.2.1   Dinoflagellate cysts as palaeoceanographic indicators

The distribution of dinocysts in marine sediments depends on surface water (e.g. temperature, salinity, nutrients, sea ice cover and turbulence) and sedimentary conditions (e.g. redox state) (Marret and Zonneveld, 2003; Rochon et al., 1999; Zonneveld et al., 2013). Gaining information about the relationship between species distribution and environmental variable enables the use of dinocyst assemblages for the reconstruction of past sea surface conditions, both qualitatively and quantitatively. Using CCA, temperature has been identified as the most important variable in controlling the distribution of dinocysts globally, with nitrate, salinity, phosphate and bottom water oxygen also being important variables (Zonneveld et al., 2013). The correlation of cyst distribution and environmental variables further allows the identification of ecological affinities of specific species with regard to temperature, salinity and nutrients, among others (Zonneveld et al., 2013). Correlations between cyst distribution in recent sediments and environmental parameters have been statistically assessed on a regional to global scale in order to establish transfer functions for palaeoenvironmental reconstructions (de Vernal et al., 2013a; Radi and de Vernal, 2008; Rochon et al., 1999). For salinity, the morphology of cysts, namely process length variations of cysts of *Protoceratium reticulatum*, have been used to establish predictive models (Jansson et al., 2014; Mertens et al., 2010). In the North Atlantic region, regionally established transfer functions for temperature, salinity, sea ice and productivity have been widely applied to Quaternary sediment sequences (e.g. Bonnet et al., 2010; de Vernal et al., 2013b, 2006, 2001; Radi and de Vernal, 2008; Van Nieuwenhove et al., 2016). In high-latitude marine environments, dinocysts represent an important proxy for surface water mass conditions due to their better preservation and higher diversity in comparison to calcareous and siliceous microfossils (de Vernal et al., 2013b, 2001, 1998; Expedition 302 Scientists, 2006; Matthiessen et al., 2009, 2005).

The application of transfer functions to pre-Quaternary records is hampered by the increasing number of extinct species and uncertainties about potential ecological adaptations of extant species (De Schepper et al., 2011). Instead, the palaeoecological affinities of extinct dinocyst species have been inferred from co-occurring species with

known environmental requirements (Head, 1997, 1996b), statistical correlation of dinocyst distributions to quantitative data from other proxies (Versteegh and Zonneveld, 1994) and the palaeogeographical distribution (e.g. Matthiessen and Brenner, 1996). This has led to the use of palaeoecological indices for the identification of palaeoenvironmental changes (De Schepper et al., 2015, 2009b; Verhoeven and Louwye, 2013; Versteegh and Zonneveld, 1994). Furthermore, palaeoenvironmental interpretations are based on dinocyst assemblage changes, with focus on certain indicator species (De Schepper et al., 2015; Hennissen et al., 2014).

When interpreting recent and fossil dinocyst assemblages, factors other than the environmental conditions in the surface water must be considered. These factors include (1) selective fossilization, (2) encystment rates, (3) transport by currents, (4) biochemical degradation and (5) reworking (Matthiessen, 1995; Wall et al., 1977). Here, non-ecological factors that affect the cyst composition in the Norwegian Sea are briefly discussed. Cysts of *P. reticulatum* is an ubiquitous species in the Nordic Seas and Arctic Ocean, tolerating a wide range of environmental conditions (de Vernal et al., 2001; Rochon et al., 1999). The high abundances of cysts of *P. reticulatum* in the Norwegian Sea can be ascribed to a combination of high cyst productions and transport from neritic to oceanic environments, resulting in an over-representation of this species (Dale, 1976; Matthiessen, 1995). Transport of this species from the North Atlantic via the NAC and NwAC also increases its representation in the Norwegian Sea (Matthiessen, 1995; Rochon et al., 1999). Protoperidinioid cysts are especially sensitive to oxidation (e.g. Zonneveld et al., 2007). At present, these cysts are the predominant component of the cyst flux in the Nordic Seas (Dale and Dale, 1992). Their under-representation in the sediment may be due to comparatively low cyst production and/or aerobic decay (Matthiessen, 1995). In the Nordic Seas, reworking of dinocysts probably mostly affects assemblages in the deep basins along continental slopes due to winnowing of bottom currents and submarine gravity flows (Matthiessen, 1995; Wall et al., 1977).

2.5.2.2 Environmental preferences of extant and extinct species

An extensive database of the distribution of extant dinocysts and their relationship to surface water properties for the North Atlantic and adjacent basins has been compiled by Marret and Zonneveld (2003) and Zonneveld et al. (2013). During the Pliocene, however, extinct species impede the palaeoecological and palaeoenvironmental interpretation of dinocyst assemblages. Initially, biogeographic distributions were used to infer the autecology of extinct species (Head and Westphal, 1999; Head, 1997,

1996b, 1994). In order to obtain quantitative palaeotemperature estimates, De Schepper et al. (2011) correlated abundances of extant and extinct Pliocene and Pleistocene dinocysts species to SST estimates based Mg/Ca ratios of the planktonic foraminifer *Globigerina bulloides* at four sites in the North Atlantic. A good agreement is found between the SST ranges of most extant species during the Pliocene and present (De Schepper et al., 2011). Of the species included in the analysis by De Schepper et al. (2011) the extant species *Bitectatodinium tepikiense*, cysts of *P. reticulatum*, *Impagidinium pallidum*, *Lingulodinium machaerophorum* and *Nematosphaeropsis labyrinthus* and the extinct species *Bitectatodinium raedwaldii*, *Filisphaera filifera* and *Habibacysta tectata* are continuously present in the Piacenzian assemblage of Hole 642B and their (palaeo)temperature requirements are briefly discussed. *B. tepikiense* is a temperate to subpolar species that exhibits a bi-hemispheric distribution (Zonneveld et al., 2013). In the Nordic Seas, this species is restricted to the Norwegian Sea (Matthiessen, 1995). In palaeogeographic reconstructions, *B. tepikiense* is often used as a cool-water indicator (De Schepper et al., 2009a; Head, 1998, 1996b; Versteegh and Zonneveld, 1994). The comparison of its present and past distribution in the North Atlantic in relation to temperature suggests a tolerance of higher temperatures in the past. Its more southerly occurrence during the Plio-/Pleistocene might, however, have been caused by long-distance transport (De Schepper et al., 2011). The Plio-/Pleistocene temperature range of the cosmopolitan species cysts of *P.reticulatum* and *N. labyrinthus* corresponds to the warmer end of its modern distribution (De Schepper et al., 2011; Zonneveld et al., 2013). The presently bipolar species *I. pallidum* represents an exception with regard to its modern and past SST requirements, suggesting that this species lived in warm Atlantic waters during the Plio-/Pleistocene (De Schepper et al., 2011; Zonneveld et al., 2013). At present, *L. machaerophorum* is found in coastal temperate to equatorial regions and in areas with high nutrient availability such as upwelling cells and river discharge plumes (Zonneveld et al., 2013 and references therein). During the Lower Pleistocene this species is mainly associated with Mg/Ca-based SSTs of >15°C in the North Atlantic (De Schepper et al., 2011). The neritic species *B. raedwaldii* only occurs in low abundances in the North Atlantic with indications for an affinity of relatively warm surface waters (De Schepper et al., 2011). The two extinct species, *F. filifera* and *H. tectata*, have been considered cool-tolerant species due to their common occurrences at high latitude sites during the Pliocene (Head, 1996b, 1994; Matthiessen and Brenner, 1996). However, with the high latitudes being considerably warmer than present their cool-water affinity remains questionable.

At the four North Atlantic sites, *F. filifera* exhibits a wide SST range of ~11–25°C, but because data from higher-latitude sites are missing the palaeoecological tolerances of this species cannot unequivocally be determined. *H. tectata* is most abundant at SSTs between 10 and 15°C (De Schepper et al., 2011).

2.5.2.3 Palaeoecological indices

Dinocyst species with known (palaeo)ecological affinities (Table 2.2) were used to calculate indices in order to characterise palaeoenvironmental changes. The Warm/Cold (W/C) index was determined based on the formula:

(3) $$W/C = nW/(nW + nC)$$

with n = number of species, W = warm-water species and C = cold-water species. Warm water taxa include *Achomosphaera andalousiensis* subsp. *suttonensis*, *Dapsilidinium pseudocolligerum*, *Impagidinium aculeatum*, *I. paxadoxum*, *I. patulum*, *I. solidum*, *Invertocysta lacrymosa*, *Lingulodinium machaerophorum*, *Melitasphaeridium choanophorum*, *Operculodinium*? *eirikianum* var. *eirikianum*, *Operculodinium centrocarpum/israelianum*, *Selenopemphix nephroides*, *Spiniferites mirabilis*, *Spiniferites membranaceus*, *Tectatodinium pellitum* and *Tuberculodinium vancampoae*. Cold-water indicators comprise *Bitectatodinium* sp. A of De Schepper et al. (2017) (grouped with *B. tepikiense*), *B. tepikiense*, *Filisphaera filifera*, *Filisphaera microornata*, *Impagidinium pallidum* and *Spiniferites elongatus* (De Schepper et al., 2015, 2011; Marret and Zonneveld, 2003; Verhoeven and Louwye, 2013; Versteegh and Zonneveld, 1994; Zonneveld et al., 2013).

Dinocyst species were also divided into inner neritic (IN), outer neritic (ON) and oceanic (O) species to evaluate the influence of water masses from the shelf and/or open ocean at the site. The IN/ON, IN/O and N/O indices were calculated according to equation 3. Inner neritic species include *L. machaerophorum*, *O. centrocarpum/israelianum*, *T. pellitum* and *T. vancampoae*. Typical outer neritic species are *Achomosphaera* spp. and *Spiniferites* spp. Oceanic species comprise *I. aculeatum*, *I. pallidum*, *I. paradoxum*, *I. patulum*, *I. solidum* and *Impagidinium* spp. (De Schepper et al., 2009b).

The diversity of the assemblages was assessed based on the number of taxa (richness) and the Shannon diversity index. Calculations were performed in PAST3 (PAleontological STatistics, Hammer et al., 2001).

The ratio of pollen to dinocyst concentrations (P/D; equation 3) is used as an indication for increased pollen influx.

Table 2.2: Dinoflagellate cyst species from ODP Hole 642B between 68.45 and 66.95 metres below sea floor and their palaeoecological affinities. P = Protoperidinioids; G = Gonyaulacoids; W = Warm water; C = Cold water; IN = Inner Neritic; ON = Outer Neritic and O = Oceanic.

Dinoflagellate cysts	P	G	W	C	IN	ON	O
Achomosphaera andalousiensis		x				x	
Achomosphaera andalousiensis subs. *andalousiensis*		x				x	
Achomosphaera andalousiensis subsp. *suttonensis*		x	x			x	
Achomosphaera ramulifera		x				x	
Amiculosphaera umbraculum		x					
Ataxiodinium choane		x					
Ataxiodinium spp.		x					
Ataxiodinium zevenboomii		x					
Barssidinium spp.	x						
Barssidinium graminosum	x						
Barssidinium pliocenicum	x						
Batiacasphaera micropapillata complex		x					
Bitectatodinium raedwaldii		x					
Bitectatodinium? *serratum*		x					
Bitectatodinium sp. A of De Schepper et al. (2017)		x		x			
Bitectatodinium spp.		x					
Bitectatodinium tepikiense		x		x			
Brigantedinium	x						
cf. *Cerebrocysta*? *namocensis*		x					
Corrudinium harlandi		x					
Corrudinium? *labradori*		x					
Corrudinium spp.		x					
Cyst of *Pentapharsodinium dalei*		x					
Cysts of *Protoceratium reticulatum*		x					
Dapsilidinium pseudocolligerum		x	x				
Echinidinium spp.	x						
Filisphaera filifera		x		x			
Filisphaera microornata		x		x			
Filisphaera spp.		x					
Habibacysta tectata		x					
Heteraulacacysta sp. A of Costa and Downie (1979)		x					
Impagidinium aculeatum		x	x				x
Impagidinium pallidum		x		x			x
Impagidinium paradoxum		x	x				x
Impagidinium patulum		x	x				x
Impagidinium solidum		x	x				x

	1	2	3	4	5	6	7
Impagidinium sp. 2 of De Schepper and Head (2009)		x					
Impagidinium spp.		x					x
Invertocysta lacrymosa		x	x				
Invertocysta sp. 1		x					
Invertocysta spp.		x					
Lejeunecysta catomus ?	x						
Lingulodinium machaerophorum		x	x		x		
Melitasphaeridium choanophorum		x	x		x		
Melitasphaeridium sp. A of De Schepper and Head (2008)		x					
Melitasphaeridium spp.		x					
Nematosphaeropsis labyrinthus		x					
Nematosphaeropsis lativittata		x					
Nematosphaeropsis spp.		x					
Operculodinium? eirikianum var. *eirikianum*		x	x				
Operculodinium centrocarpum s.s./ *Operculodinium israelianum*		x	x		x		
Operculodinium janduchenei		x					
Operculodinium spp.		x					
Pyxidinopsis braboi		x					
Round brown cysts	x						
Selenopemphix conspicua	x						
Selenopemphix dionaeacysta	x						
Selenopemphix cf. *islandensis*	x						
Selenopemphix nephroides	x		x				
Selenopemphix nephroides	x						
Selenopemphix spp.	x						
Spiniferites elongatus		x		x		x	
Spiniferites falcipedius		x				x	
Spiniferites mirabilis		x	x			x	
Spiniferites membranaceus		x	x			x	
Spiniferites ramosus		x				x	
Spiniferites/Achomosphaera spp.		x				x	
Tectatodinium pellitum		x	x		x		
Trinovantedinium glorianum	x						
Trinovantedinium spp.	x						
Tuberculodinium vancampoae		x	x		x		

Chapter 3: Climate variability and long-term expansion of peatlands in Arctic Norway during the late Pliocene

3.1 Introduction

Preceding the glacial-interglacial cycles of the Pleistocene, the Piacenzian Stage marks the last time interval in the Earth´s history that was characterised by a sustained warmer-than-present climate (Lisiecki and Raymo, 2005). The mPWP (3.264–3.025 Ma) has been subject of intensive palaeoclimate research due to its similarity to projections of future global warming and its near-modern palaeogeography, palaeoceanography and palaeobiology (Dowsett et al., 2010; Dowsett, 2007; Haywood et al., 2013a; IPCC, 2013; Salzmann et al., 2009). During the mPWP average global mean annual surface temperatures were about 2–3°C higher than present (Haywood et al., 2013b). As the duration of the mPWP exceeds orbital timescales its warmth was not driven by insolation changes, but rather by differences in the state of boundary conditions intrinsic to the climate system itself (Haywood et al., 2013a; Miller et al., 2010; Pound et al., 2014). Relatively high atmospheric CO_2 concentrations with values between 270–400 ppm have been identified as the most important cause of Piacenzian warmth while differences in orography, vegetation and ice sheets constitute the remaining proportion of warming relative to modern (Badger et al., 2013; Lunt et al., 2012; Martínez-Botí et al., 2015; Pagani et al., 2010; Seki et al., 2010).

In the North Atlantic and Nordic Seas, marine and terrestrial records reveal a strong warming at high latitudes during the Piacenzian. SSTs were up to 18°C warmer than present in the Nordic Seas as opposed to only ~2–4°C in the mid-latitudes (Dowsett et al., 2013a; Robinson, 2009). The amplified warming has been suggested to be related to an enhanced AMOC (Dowsett et al., 2016). However, model simulations indicate a similar-to-present AMOC during the mPWP, supporting the notion that the amplified warming in the Nordic Seas was a result of increased radiative forcing (Zhang et al., 2013a). On land, boreal taiga forests reached the coast of the Arctic Ocean during the Piacenzian, and tundra biomes were markedly reduced (Bennike et al., 2002; Rybczynski et al., 2013; Salzmann et al., 2008; Willard, 1996). In the high Artic, Pliocene deposits reveal MATs ~19°C warmer than present, favouring the growth of larch-dominated forests on Ellesmere Island (Ballantyne et al., 2010, 2006; Rybczynski et al., 2013). In contrast, vegetation changes were less profound in the mid-latitudes. The prevalence of mixed forests in eastern Arctic Canada during the Piacenzian

suggests a northward shift of the northern boundary of the deciduous forest zone by a minimum of 5° latitude, with MATs 3–5°C warmer than present (de Vernal and Mudie, 1989a; Willard, 1994). In Norway, warm-temperate taxa occur at least 7° latitude further north of their present limit, pointing towards substantially warmer conditions (Willard, 1994). A northward latitudinal shift of vegetation of about 10° is inferred from the presence of mixed to boreal forest on Svalbard during the Pliocene (Willard, 1996).

The mPWP has often been described as a relatively stable warm period with only minor temporal variations in climate and vegetation distribution (e.g. Willard, 1994; Thompson and Fleming, 1996). Until now, high resolution vegetation records with a robust age control are missing for the surroundings of the North Atlantic and Nordic Seas, and it is unclear whether the available palaeoclimate records represent the full variability or peak warm phases of the Piacenzian only. A recently published high resolution pollen record from Lake El'gygytgyn in the north-eastern Russian Arctic reveals major changes in the dominant biome distribution during the Piacenzian, ranging from temperate cool mixed forests to Arctic shrub tundra vegetation (Andreev et al., 2014; Tarasov et al., 2013).

Data-model comparison studies suggest that climate models currently underestimate the magnitude of mPWP warming that is evident in proxy-based SST reconstructions for the Nordic Seas (Dowsett et al., 2013a). The data-model discrepancy has been partly ascribed to the comparison of simulations that represent a discrete time interval to time-averaged proxy data (Dowsett et al., 2013a; Salzmann et al., 2013). A recent modelling study indicates that the Norwegian Current, which strongly affects the climate of Norway, may have been cooler than present when altered palaeogeographic boundary conditions are considered (Hill, 2015). In order to resolve these uncertainties a time slice centred around 3.205 Ma (MIS KM5c) has been proposed for future palaeoclimate research in the Piacenzian, requiring high resolution proxy records (Haywood et al., 2013a).

This study presents a new high-resolution reconstruction of Piacenzian vegetation and climate changes for Arctic Norway based on the recently re-dated sediment core ODP Hole 642B (Risebrobakken et al., 2016). The aim of this study is (1) to assess the evolution and temporal variability of vegetation and climate changes in Norway during the Piacenzian, (2) to determine their magnitude, and (3) to evaluate the potential of glacier and ice sheet build up on Scandinavia during cold intervals of the Piacenzian.

3.2 Materials and Methods

3.2.1 Sample information and pollen analysis

A total of 70 samples were taken from ODP Hole 642B of which 68 samples are situated between 69.90 and 66.95 mbsf (Shipboard Scientific Party, 1987), ranging in age between 3.60 and 3.14 Ma (Risebrobakken et al., 2016). The upper part of the sequence, which coincides with the PRISM interval, has been counted in high resolution (800 to 14,700 years) and covers the central part of interglacial MIS KM5c (3.205 Ma). The earlier part of the Piacenzian was analysed in lower resolution (6600 to 23,300 years) in order to document the main climatic states and trends. Additionally, two surface samples were taken from the same core at 0 and 3 cm below sea floor in order to compare the Piacenzian to modern pollen assemblages. The modern sample presumably covers less than 2000 years while the subsurface sample at 3 cm depth possibly reveals a maximum age of 6000 years. These assumptions are based on a modern sedimentation rate of <2 cm/kyr (Romero-Wetzel, 1989).

Pollen preservation is generally very good. An average of 510 pollen grains was counted per slide, or 185 grains excluding *Pinus*. On average 23 taxa were identified per sample. Only ten samples yielded counts below 300 grains. The presented cluster analysis does not include *Pinus* to highlight the assemblage changes in the other pollen and spores. Rarefaction was applied to estimate the richness at a constant count of grains (Birks and Line, 1992). Diversity was assessed using the Shannon index which takes into account the relative abundance of a taxon as well as the number of taxa. The Shannon index is zero if the assemblage is dominated by a single taxon and shows high values for assemblages with many taxa that are each represented by few individuals (Hammer et al., 2001). Both rarefaction and diversity were calculated in PAST (PAleontologial STatistics, Hammer et al. (2001)).

3.2.2 Climate reconstruction

To obtain quantitative estimates of Piacenzian climate, the CA of Mosbrugger and Utescher (1997) was applied. The method is described in Chapter 2. Climatic ranges have been quantified based on presence/absence of all taxa for MAT, CMT, WMT and MAP, using the Palaeoflora database (Utescher and Mosbrugger, 2013). To ensure accurate and reliable palaeoclimate estimates only samples with a minimum of ten NLR taxa were used to determine the palaeoclimatic range. This led to the exclusion of two
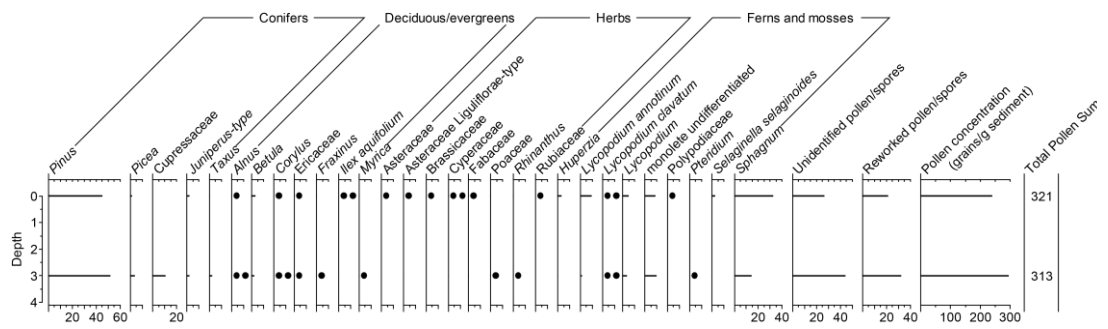
Figure 3.1: Pollen assemblages in the modern and mid-Holocene samples from ODP Hole 642B. Black circles are representative of single pollen or spore grains. Percentages of pollen and spores were calculated based on the pollen sum, excluding *Pinus*, unidentified and reworked pollen and spores. Depth is given in cm.

samples with a total count of less than 100 pollen grains. For this study a total of 37 taxa are used for the CA. All estimates are based on an average of 17 taxa per sample.

3.3 Results

3.3.1 Modern pollen assemblages

The analysed modern and mid-Holocene samples show pollen concentrations of 238 and 294 grains/g sediment, respectively (Figure 3.1). Percentages of *Pinus* pollen (45–52%) and *Sphagnum* spores (14–32%) are highest in the two samples. Pollen of other conifers (*Picea*, *Juniperus*-type and *Taxus*) are represented by proportions of less than 4%, but Cupressaceae pollen accounts for ~10% of the assemblage in the subsurface sample. The relative abundance of *Lycopodium* spores and undifferentiated monolete spores is also relatively high, with ~6–15% and ~9%, respectively. *Betula* is the most common deciduous tree pollen. *Alnus*, *Corylus*, Ericaceae, *Fraxinus, Ilex aquifolium* and *Myrica* pollen occur in very low numbers. Compared to the subsurface sample, the surface sample reveals a higher diversity of herb pollen (Asteraceae, Brassicaceae, Cyperaceae and Fabaceae). The proportion of reworked pollen and spores is relatively high in both samples (21–32%).

3.3.2 Piacenzian pollen assemblages
Pollen Zone 1 (69.9–69.0 mbsf, c. 3.60–3.47 Ma, 13 samples)

Pollen Zone (PZ) 1 is characterised by a high abundance of *Pinus* pollen (61–77%) and pollen from other conifer trees (*Picea,* Cupressaceae, *Juniperus*-type*, Sciadopitys* and *Tsuga*) (Figure 3.2; Plate 3.1). *Juniperus*-type*, Sciadopitys* and *Tsuga* pollen show their maximum abundances of the entire pollen record with up to ~22%, 18% and 10%, respectively, within this zone. Ericaceae pollen reaches a maximum of ~16% in the

71

middle of the zone and subsequently decreases to values of around 6% towards the upper part. *Alnus*, *Betula, Corylus*, *Quercus* and *Ulmus* pollen is frequently present whereas other deciduous tree pollen such as *Carpinus* and *Carya* occur only sporadically (Figure 3.2; Plate 3.1, 3.2). The abundance of herb pollen is generally low throughout PZ 1. The number of *Lycopodium* (including *L. annotinum*, *L. clavatum*, *L. inundatum* and *Lycopodium* spp. indet.) spores is relatively high in the early part (up to ~34%), declining continuously throughout the interval (Plate 2.1, 3.3). The relative abundance of *Sphagnum* spores is fairly constant, showing its lowest values (<22%) within the entire study interval. Spores of *Huperzia, Osmunda*, Polypodiaceae and undifferentiated monoletes are regularly found (Figure 3.2; Plate 3.3, 3.4). Rare pollen taxa only occur sporadically and the average diversity index across the zone is relatively low (Figure 3.3, 3.7). The number of taxa increases towards the upper part of the interval (Figure 3.7). Pollen concentrations mostly vary between ~1000–2000 grains/g sediment and peak at a maximum of 4300 grains/g sediment in the upper part of the zone. Reworked pollen and spores occur in low numbers with a maximum percentage of ~4% (Figure 3.2).

Pollen Zone 2 (69–68.54 mbsf, c.3.47–3.35 Ma, 9 samples)

The amount of *Pinus* remains high (65–75%) throughout PZ 2 while percentages of *Picea* pollen decreases (Figure 3.2). Pollen of other conifer trees (Cupressaceae, *Juniperus*-type, *Sciadopitys* and *Tsuga*) shows a sharp decrease in numbers at the lower pollen zone boundary (Figure 3.2). Ericaceae pollen increases to maximum values of ~18% in the upper part of the zone. The proportion of deciduous tree pollen is generally low. *Betula* pollen is consistently present while the proportion of *Alnus* and *Corylus* pollen peaks in the middle of PZ 2. Pollen of Asteraceae, especially Asteraceae Liguliflorae-type, shows maximum values of up to 31% in this zone while other herb pollen remains low in abundance (Figure 3.2; Plate 3.3). *Lycopodium* spores peak in the lower and upper parts of PZ 2, reaching proportions of up to 56%. A peak in the abundance of *Sphagnum* spores (43%) is observed in the lower part of the zone (Figure 3.2). *Osmunda* spores show highest abundance and subsequently decrease until it disappears from the assemblage in the upper part. *Huperzia* spores become more abundant and undifferentiated monolete spores are continuously present. *Pteridium* spores are also regularly found (Figure 3.2). The number of rare pollen taxa is very low and the number of taxa and the diversity index show similar values to PZ 1
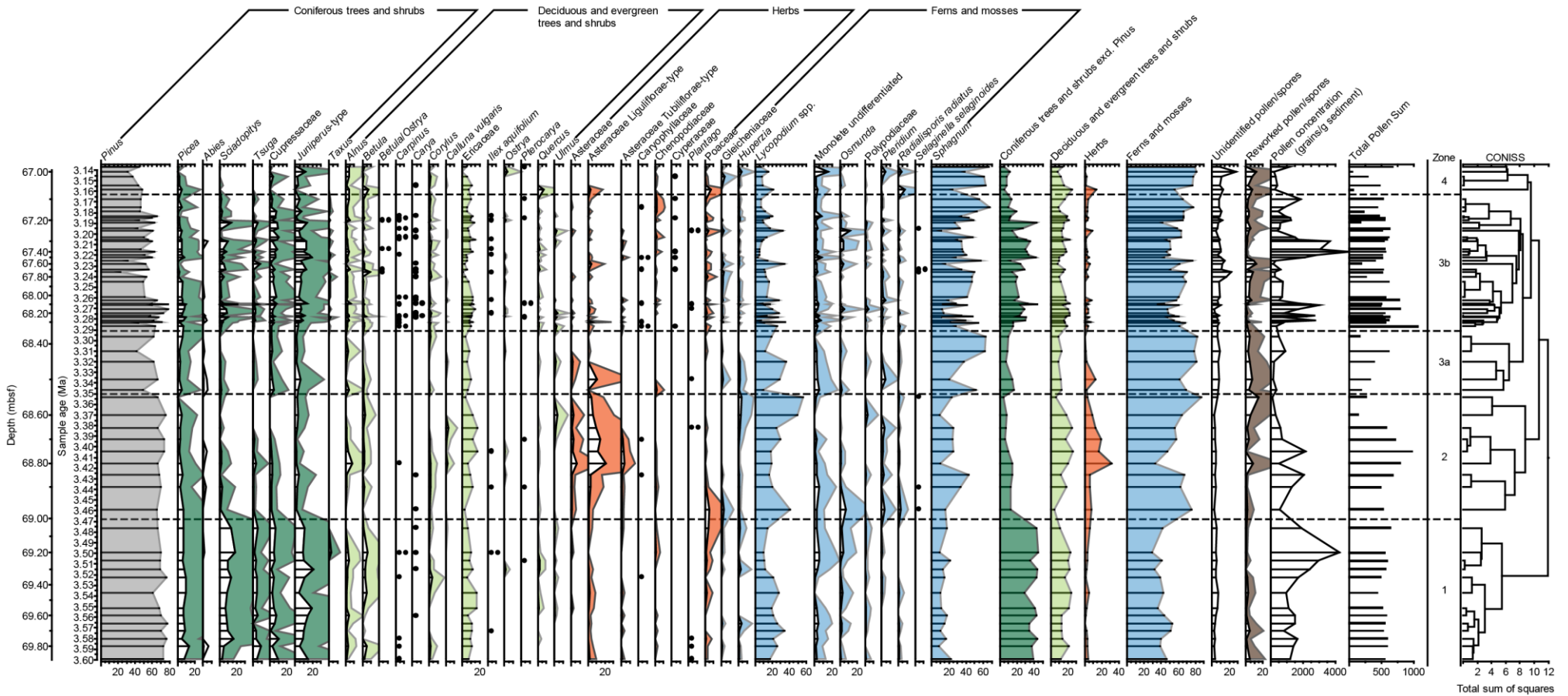
Figure 3.2: Pollen assemblages in the Piacenzian sediments of ODP Hole 642B. Non-patterned, coloured area represents 5-fold percentages. Black circles are representative of single pollen or spore grains. Percentages of pollen and spores were calculated based on the pollen sum, excluding *Pinus*, unidentified and reworked pollen and spores. *Pinus* was included in the pollen sum to calculate percentages of *Pinus*. The total pollen sum shown here comprises *Pinus* and unidentified pollen. Depth is indicated in metres below sea floor (mbsf).

73
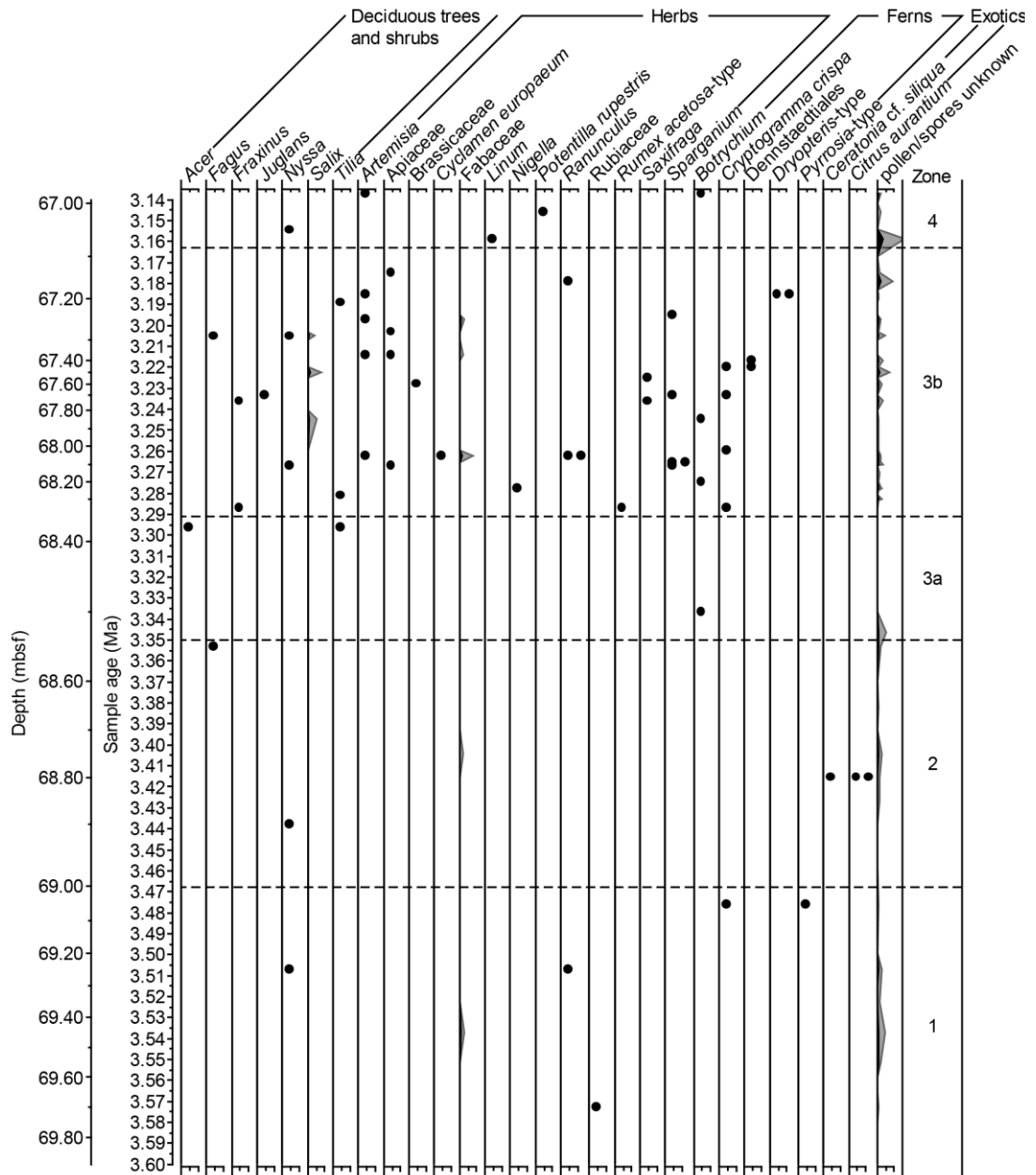
Figure 3.3: Pollen diagram showing taxa that occur in fewer than five samples. Grey areas represent five times the actual number. The exotic group marks taxa that have likely been transported to the site from the south. Depth is indicated in metres below sea floor (mbsf).

(Figure 3.3, 3.7). Pollen concentrations reach maximum values of ~2200 grains/g sediment within the zone. Reworked pollen and spores first reach a relatively high proportion (~9%) in the middle part of this zone and peak again, after declining to values of <3%, in the upper part of the zone (~15%) (Figure 3.2).

Pollen Zone 3a (68.54–68.365 mbsf, c. 3.35–3.29 Ma, 5 samples)

The proportion of *Pinus* pollen is slightly reduced when compared to PZ 1 and 2 with percentages ranging between 43 and 66% (Figure 3.2). Other conifer pollen remains low in abundance. Ericaceae pollen shows percentages of less than 10%. *Alnus*, *Betula* and *Corylus* pollen are continuously present whereas more temperate pollen taxa like *Carpinus* and *Carya* are absent. Asteraceae Liguliflorae-type pollen shows a pronounced peak (~10%) in the lower part of the zone while other herb pollen taxa only occur sporadically and in low numbers (Figure 3.2). *Lycopodium* spores reach their highest abundance in the lower part of the zone. A subsequent decline in the relative abundance of *Lycopodium* spores is accompanied by a distinct increase in *Sphagnum* spores, reaching proportions of up to ~63% in the upper part of the zone (Figure 3.7). The number of rare pollen taxa remains very low. The average diversity index is slightly higher when compared to PZ 1 and 2, whereas the number of taxa remains the same (Figure 3.7). Pollen concentrations are relatively low with maximum values of ~900 grains/g sediment (Figure 3.2).

Pollen Zone 3b (68.365–67.09, c. 3.29–3.16, 36 samples)

PZ 3b exhibits the highest sample density and shows a high variability which is superimposed by a prevailing change in abundances (Figure 3.2, 3.7). *Pinus* pollen shows relatively high values (43–79%) in the lower part of the zone alongside an increased proportion of pollen from other conifer trees (Cupressaceae, *Juniperus*-type, *Picea*, *Sciadoiptys* and *Tsuga*). Subsequently the proportion of *Pinus* pollen stays around 50% before steadily increasing to a maximum of ~65% in the upper part of the zone. Peaks in *Pinus* pollen are concurrent with higher abundances of the other conifer pollen (Figure 3.2, 3.7). The relative abundance of Ericaceae pollen does not exceed 15%. *Alnus*, *Betula, Corylus* and *Quercus* pollen occurs frequently in low percentages (<9%). Other deciduous tree pollen, such as *Carpinus, Carya, Ostrya, Pterocarya* and *Ulmus*, as well as pollen of the evergreen shrub *Ilex aquifolium* are found regularly within PZ 3b in low percentages (Plate 3.1, 3.2). Asteraceae Liguliflorae-type pollen
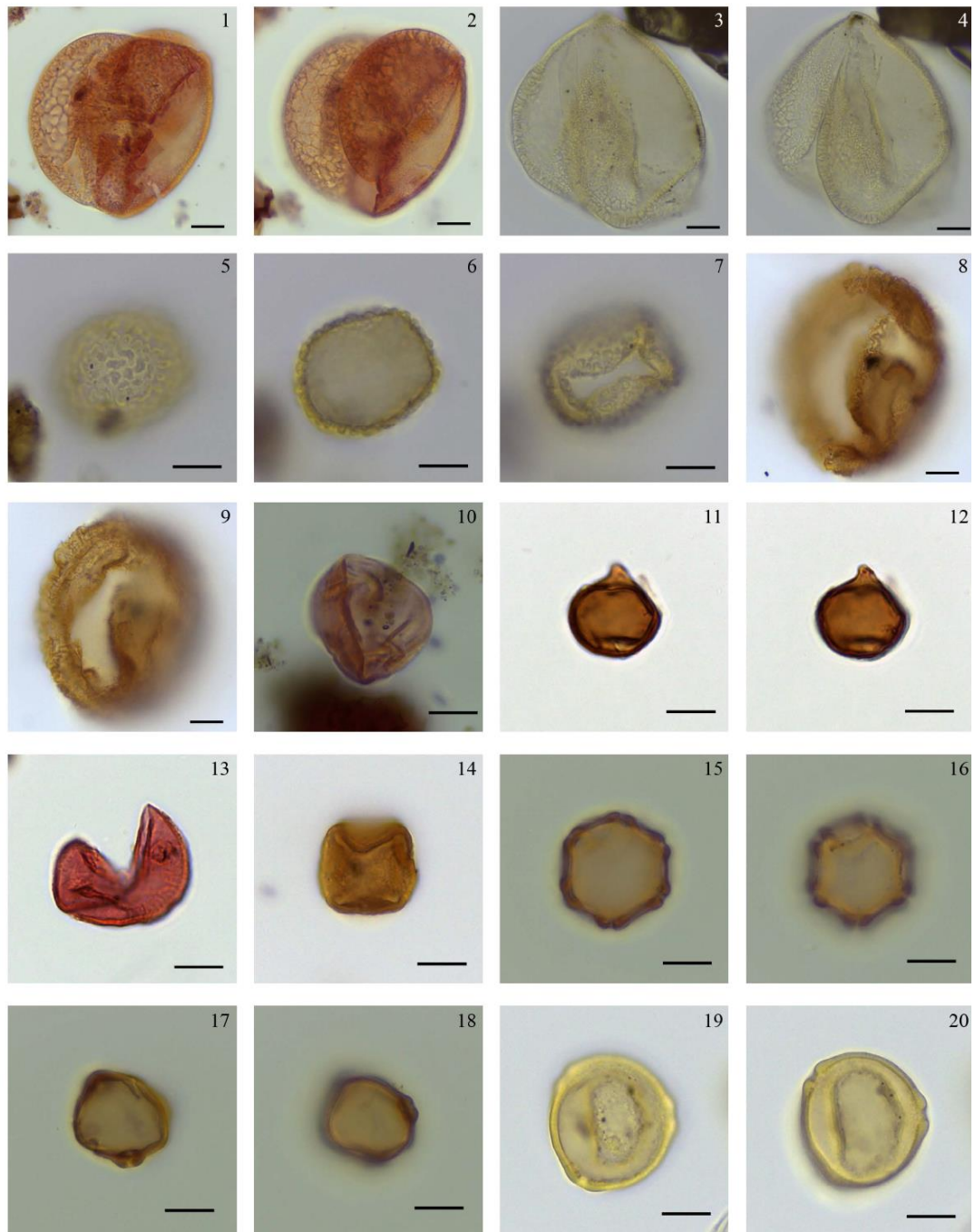
Plate 3.1: Selected pollen species from ODP Hole 642B. All images were taken in bright field illumination. Sample number and England Finder coordinates are given after species name. Scale bar represents 10 μm. 1–14: Pollen of coniferous tree and shrubs, 1–2: *Pinus*, 10H2 145-146, R65/0; 3–4: *Picea*, 10H4 115-116, S44/4; 5–7: *Sciadopitys*, 10H6 15-16, M33/4; 8–9: *Tsuga*, 9H4 80-81, O42/2; 10: Cupressaceae, pollen grain not split, 9H2 19-20, V39/3; 11–12: Cupressaceae, pollen grain with papilla, 9H2 130-131, T45/1; 13: *Juniperus*, 9H2 25-26, F57/0; 14: *Taxus*, 10H1 45-46, L52/0; 15–20: Pollen of deciduous trees, 15–16: *Alnus*, 9H2 90-91, C55/0, 17–18: *Betula*, 9H2 90-91, D57/1; and 19–20: *Carpinus*, 10H6 15-16, V56/0.

76
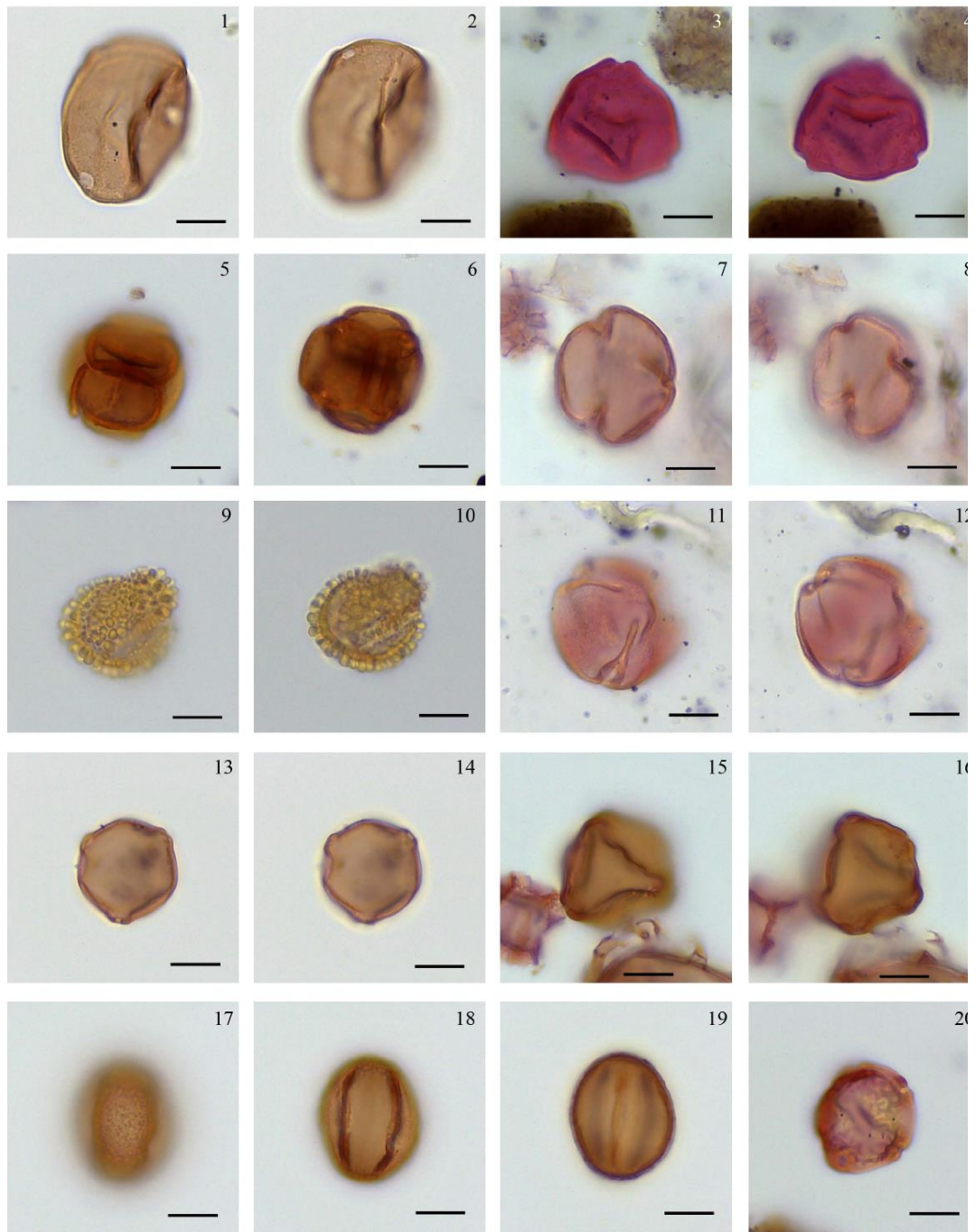
Plate 3.2: Selected pollen species from ODP Hole 642B. All images were taken in bright field illumination. Sample number and England Finder coordinates are given after species name. Scale bar represents 10 μm. 1–20: Pollen of deciduous and evergreen trees and shrubs, 1–2: *Carya*, 9H2 15-16, F39/2; 3–4: *Corylus*, 9H5 110-111, P34/4; 5–6: Ericaceae, 9H2 15-16, F39/2; 7–8: *Fagus*, 10H2 55-56, R50/0; 9–10: *Ilex aquifolium*, 9H2 15-16, K50/2; 11–12: *Nyssa*, 9H1 67-68, M44/2; 13–14: *Ostrya*, 9H2 95-96, R44/2; 15–16: *Pterocarya*, 9H2 135-136, L50/0; 17–19: *Quercus*, 9H2 130-131, V45/2; 20: *Ulmus*, 9H2 135-136, M37/0.
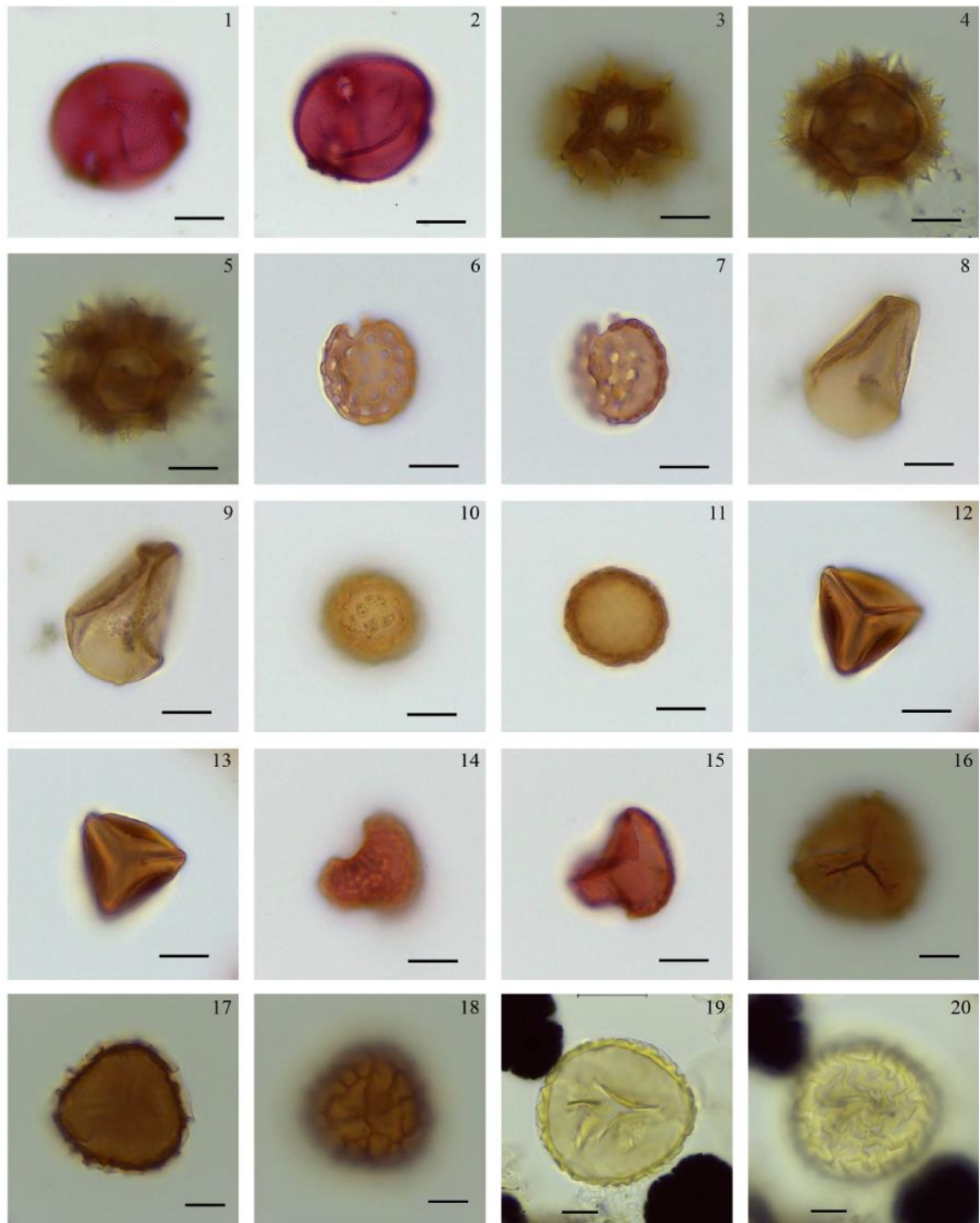
Plate 3.3: Selected pollen species from ODP Hole 642B. All images were taken in bright field illumination. Sample number and England Finder coordinates are given after species name. Scale bar represents 10 μm. 1–2: Pollen of deciduous trees, 3–11: pollen of herbs, 12–20: spores ferns and mosses. 1–2: *Tilia*, 9H7 61-62, M37/2; 3–5: Asteraceae Liguliflorae type, 9H2 90-91, K56/2; 6–7: Chenopodiaceae, 9H2 130-131, V49/3; 8–9: Cyperaceae, 10H1 45-46, N52/1; 12–13: Gleicheniaceae, 9H2 135-136, V38/1; 14–15: *Huperzia*, 9H3 25-26, R40/4; 16–18: *Lycopodium annotinum*, 9H2 15-16, F62/3; 19–20: *Lycopodium inundatum*, 10H4 115-116, W40/0.

78
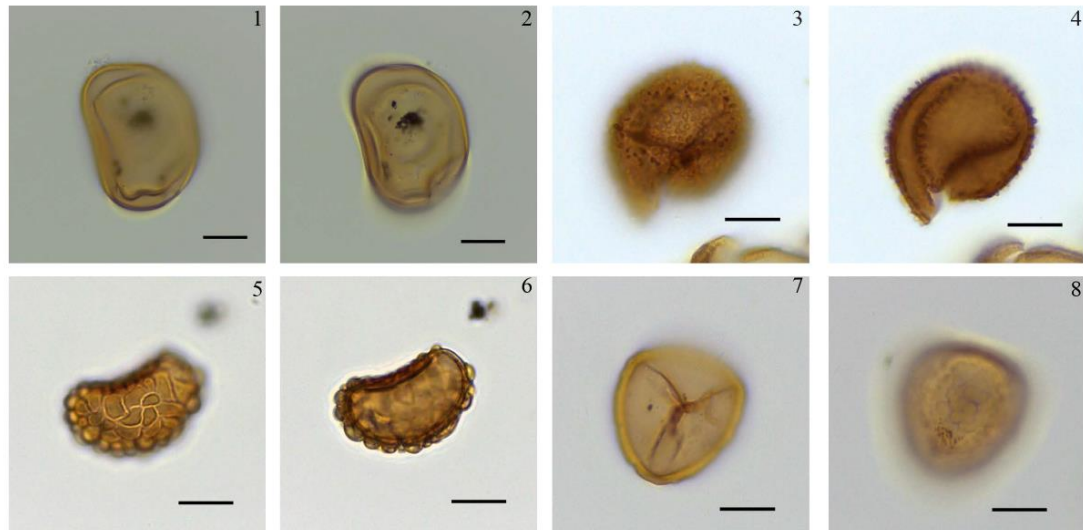
Plate 3.4: Selected pollen species from ODP Hole 642B. All images were taken in bright field illumination. Sample number and England Finder coordinates are given after species name. Scale bar represents 10 μm. 1–8: Spores of ferns and mosses, 1–2: psilate monolete undifferentiated, 9H2 15-16, O41/1; 3–4: *Osmunda*, 9H2 130-131, Q49/0; 5–6: *Polypodium*, 9H2 130-131, S37/2; 9–10: *Sphagnum*, 9H2 75-76, R40/0.

as well as the families Apiaceae and Cyperaceae first appears in this pollen zone (Figure 3.2). *Lycopodium* spores show a general decrease in abundance throughout the interval and alternate with high proportions of *Sphagnum* spores. After reaching a minimum of 11% the proportion of *Sphagnum* spores increases, reaching ~68% in the upper part (Figure 3.2). Spores of *Huperzia*, *Osmunda*, Polypodiaceae, *Pteridium* and undifferentiated monolete spores occur frequently (Figure 3.2). The number of rare pollen taxa is highest in this pollen zone (Figure 3.3). The number of taxa counted on a constant pollen sum is highly variable (Figure 3.7). In the lower part of the zone the diversity index shows a high variability with the same average value as PZ 3a. Subsequently, the average diversity of PZ 3b increases markedly (Figure 3.7). Pollen concentrations peak in the lower part (max. 300 grains/g sediment) and again in the middle part of the zone (max. 4900 grains/g sediment) (Figure 3.2). The proportion of reworked pollen and spores is highest between 68.05 and 67.55 mbsf, reaching values of up to ~13% and remaining below 7% outside the interval (Figure 3.2).

Pollen Zone 4 (67.09–66.95 mbsf, c. 3.16–3.14 Ma, 5 samples)

The amount of *Pinus* pollen varies between 32 and 48% and thus shows its lowest percentages within the entire Piacenzian record (Figure 3.2). Pollen concentrations are also relatively low (<580 grains/g sediment). While *Picea* and Ericaceae pollen decreases, *Juniperus*-type pollen percentages increase. Single pollen grains of never

exceeds 6% throughout the zone. Although still low in abundance comparatively more taxa of herb pollen is present in this interval. Pollen of *Artemisia* as well as the *Sciadopitys* are still found whereas pollen of *Tsuga* are absent. *Alnus, Betula* and *Corylus* pollen is consistently present while pollen of other deciduous trees (*Carya, Ostrya, Pterocarya,* and *Quercus*) only occurs sporadically. The diversity of herb pollen is reduced compared to PZ 3b (Figure 3.2). *Lycopodium* spores are relatively low in abundance (<21%) whereas the proportion of *Sphagnum* spores is high (up to ~62%) (Figure 3.2). *Huperzia* and undifferentiated monolete spores peak in the upper part of the zone. Rare pollen taxa are present in relatively low numbers (Figure 3.3). The number of taxa is comparable to PZ2 and 3a and the average diversity index remains unchanged when compared to PZ 3b (Figure 3.7). Pollen concentrations are low with values <1100 grains/g sediment. Reworked pollen reaches proportions of up to 12% (Figure 3.2).

3.3.3 Quantitative palaeoclimate estimates

Piacenzian temperature estimates using the CA show very wide ranges for every parameter in most samples (Figure 3.4). MATs based on the CA range on average from 5 to 14°C, suggesting MATs 5–14°C higher than present in comparison to climate data from the reference stations. However, the lower end of the estimated MATs is similar to the modern coastal temperatures (4–6°C) (Figure 3.4) (Moen, 1999). Maximum CMTs reach 4°C with estimates for the minimum values ranging between -8 and 1.4°C. These estimates are 1–11°C higher when compared to the present CMTs obtained from the reference stations but fall within the range to present-day coastal temperatures (Figure 3.4). Piacenzian WMTs range on average from 18 to 24°C for most pollen assemblages, implying summer temperatures were 8–14°C higher than present when compared to climate data from the reference stations. In comparison to coastal values, these estimates are at least 2–8°C higher than present (Figure 3.4) (Moen, 1999). For MAP, most reconstructed values overlap either with the whole modern day range or at least the upper end. However, 14 samples yield two ambiguous coexistence intervals due to the concurrent presence of *Sciadopitys* and *Calluna vulgaris* or *Selaginella selaginoides* (Figure 3.4, 3.5).

When applied to the modern and mid-Holocene samples, the reconstructed coexistence interval for MATs is too warm in comparison to the climate data from the reference stations as well as the data obtained from Moen (1999) (Figure 3.6). If the temperate taxa are excluded, the minimum values drop, resulting in a widening of the coexistence
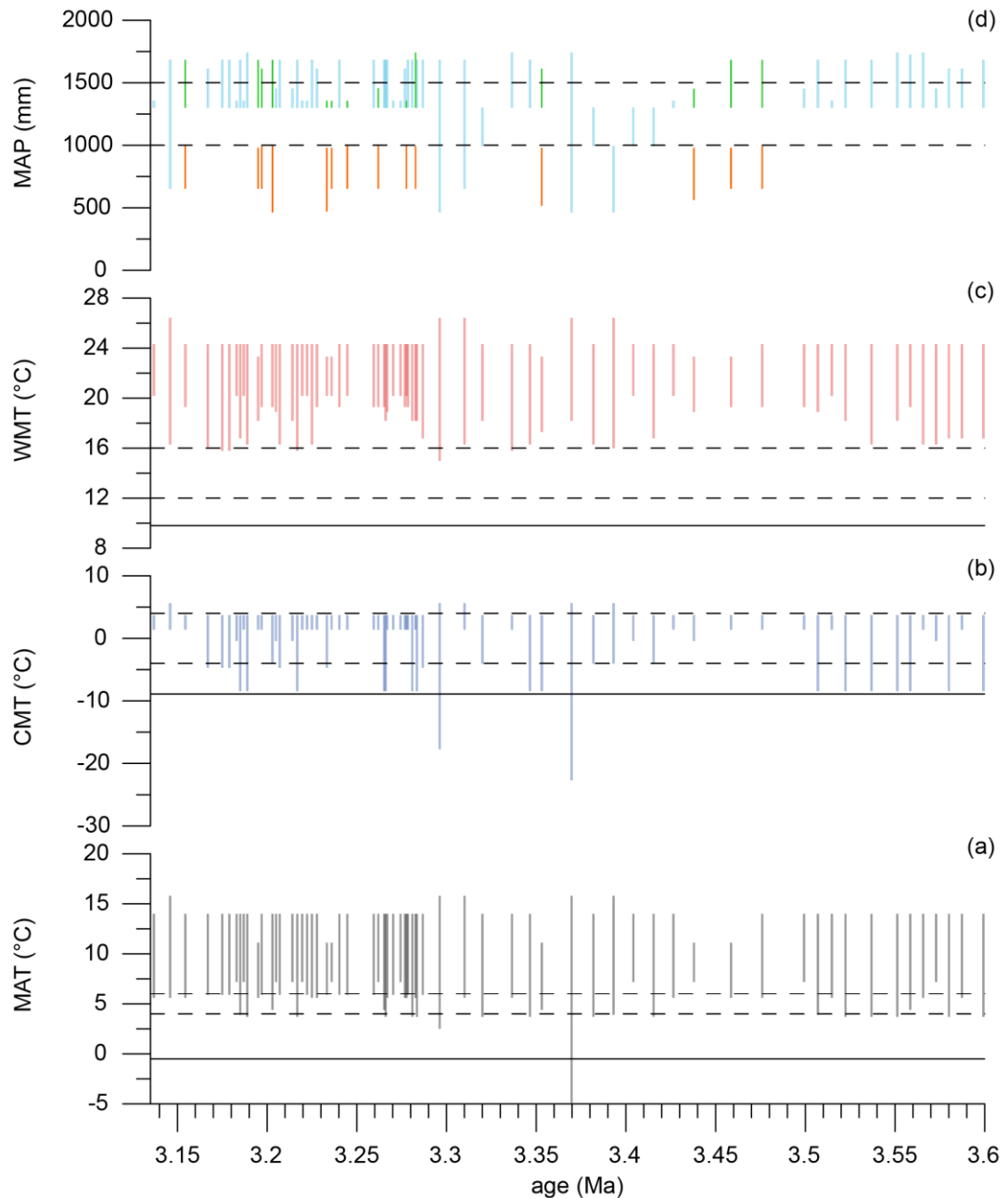
Figure 3.4: Estimates for (a) mean annual temperatures (MAT), (b) coldest month temperatures (CMT), (c) warmest month temperatures (WMT) and (d) mean annual precipitation (MAP) for the Piacenzian samples from ODP Hole 642B. Solid black lines in panels (a) to (c) represent the modern climate values from the meteorological stations in Bodø and Mo i Rana, Nordland, Norway (Figure 2.1) (Norwegian Meteorological Institute and Norwegian Broadcasting Corporation, 2014). Dashed lines represent the range of modern coastal temperatures (Moen, 1999). (d) light blue bars show unambiguous MAP ranges. Green and orange bars represent two ambiguous MAP ranges with *Sciadopitys* (green) and *Calluna vulgaris* and/or *Selaginella selaginoides* (orange) as climatic outliers (Figure 3.5).

interval and overlap with the modern data. Reconstructed CMTs coincide with modern coastal values for the sample at 3 cm depth but are higher than present for the surface sample (Figure 3.6). The coexistence interval also increases if the temperate taxa are
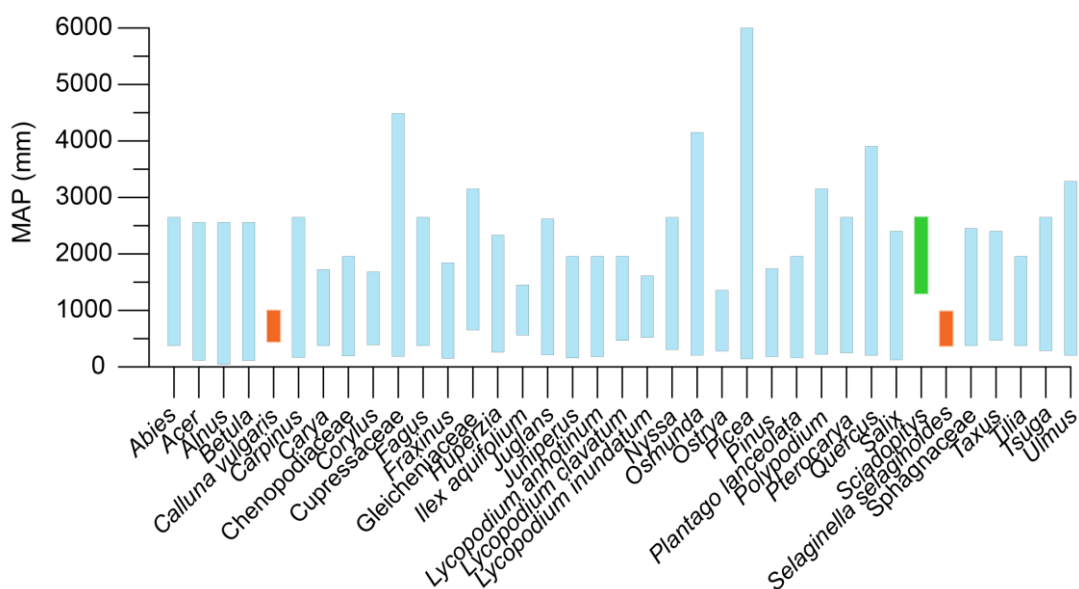
Figure 3.5: Mean annual precipitation (MAP) tolerances for taxa encountered in the Piacenzian samples from ODP Hole 642B. Green and orange bars show taxa that become climatic outliers if present in the same sample, producing two ambiguous coexistence intervals (Figure 3.4).

neglected. Estimates of WMTs match the upper end of the present-day coastal values of 12–16°C in both the modern as well as mid-Holocene sample (Figure 3.6) (Moen, 1999). For the surface sample, the reconstructed MAP range is lower than the modern range as a result of the presence of *Selaginella selaginoides*. The estimated MAP range for the mid-Holocene sample, however, overlaps with modern values (Figure 3.6).

3.4 Discussion

3.4.1 Modern pollen assemblages and vegetation

The modern and mid-Holocene samples from ODP Hole 642B were analysed in order to get a better understanding of the modern pollen signal in the marine sediments off Norway and to facilitate the interpretation of Piacenzian pollen assemblages. The pollen assemblages found in the two Holocene samples are representative of the modern vegetation of northern Norway, suggesting that northern Norway is the main source area for pollen and spores deposited at ODP Hole 642B. High abundances of *Pinus* pollen and *Sphagnum* spores reflect the extensive distribution of boreal forest and peatlands in northern Norway (Moen, 1999, 1987). Both fossil pollen grains are generally over-represented in marine sediments. This effect becomes more pronounced with increasing distance from the shore due to their preferential transportation over long distances (e.g. Heusser, 1983; Mudie and McCarthy, 2006). Nevertheless, percentages of *Pinus* pollen generally reflect its relative proportion in the vegetation community,
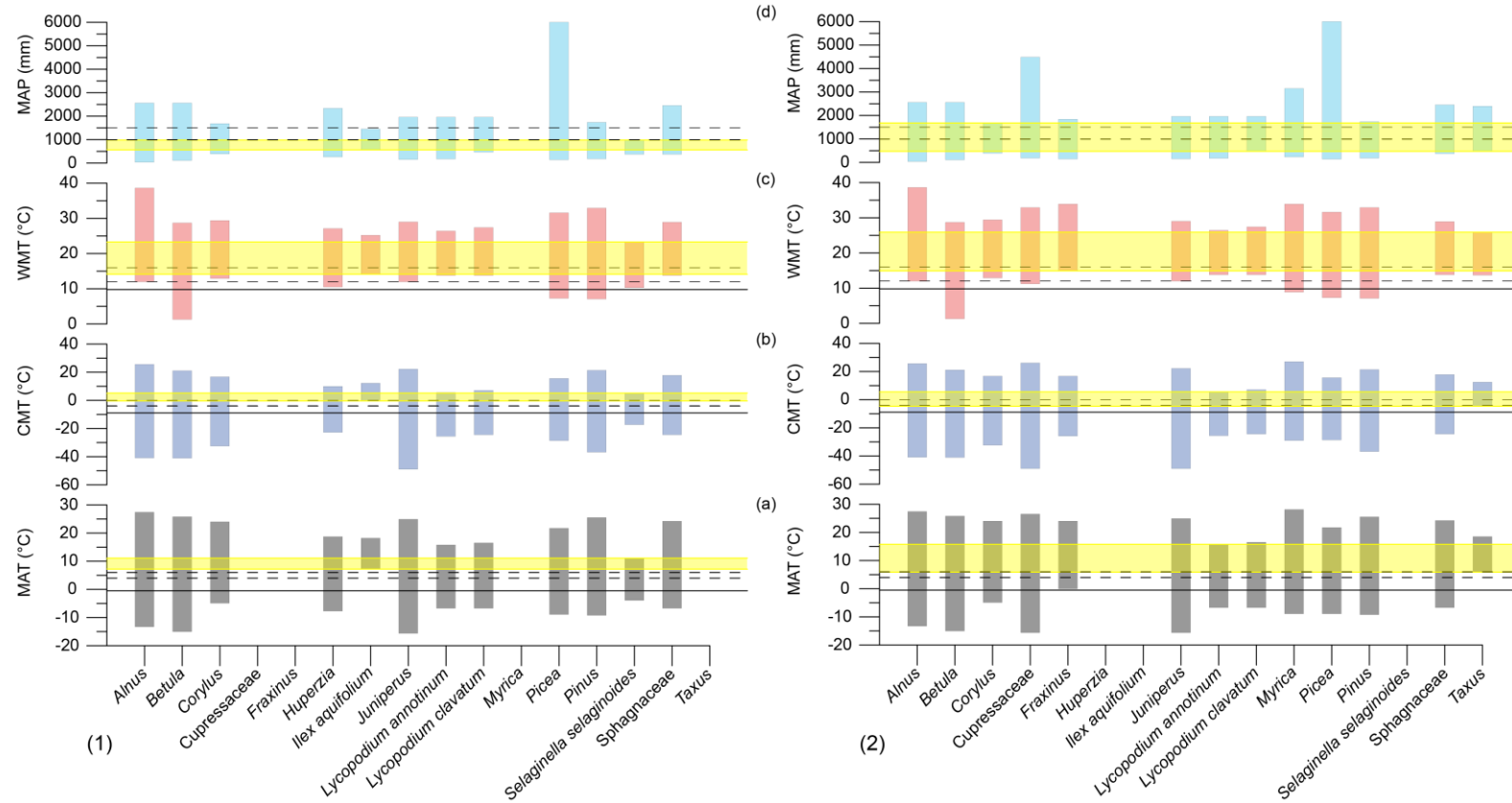
Figure 3.6: Climatic tolerances of taxa found in the (1) modern sample (0 cm) and (2) mid-Holocene sample (3cm) for (a) mean annual temperatures (MAT), (b) coldest month temperatures (CMT), (c) warmest month temperatures (WMT) and (d) mean annual precipitation (MAP). Yellow bars show the coexistence intervals for each parameter. Solid black lines in panels (a) to (c) represent the modern climate values from the meteorological stations in Bodø and Mo i Rana, Nordland, Norway (**Figure 2.1**) (Norwegian Meteorological Institute and Norwegian Broadcasting Corporation, 2014). Dashed lines represent the range of modern coastal temperatures (Moen, 1999). Listed taxa are found in both the modern and mid-Holocene samples.

and proportions of *Sphagnum* spores are highest where extensive peatlands are found onshore (e.g. Heusser, 1983; Mudie and McCarthy, 1994; Mudie, 1982). In contrast, pollen from deciduous trees is under-represented in marine sediments as this pollen is deposited closer to the source area (<200 km), as a result of their small size and high density (Mudie and McCarthy, 2006). With ODP Hole 642B being located ~400 km offshore, the contrast between the relative abundance of *Pinus* and deciduous tree pollen is especially pronounced. The pollen spectra at ODP Hole 642B are predominated by wind-pollinated taxa. Low abundance of deciduous trees can also be found in other marine records from the North Atlantic (Mudie and McCarthy, 2006). There is no evidence for large rivers in Norway during the Pliocene, which makes rivers as a significant transport medium for pollen to the site highly unlikely. Today, plumes of cold fjord water enter the Norwegian Sea in spring, but only extend less than 100 km offshore (Mork, 1981). However, modern-like fjords and glaciers which trigger such plumes almost certainly did not exist during the Pliocene.

The increase in *Sphagum* spores and slight decline in *Pinus* pollen in the mid- to late Holocene sample has been interpreted to reflect the expansion of peatlands that is observed in the late Holocene vegetation records from northern Norway (Bjune et al., 2004). Deciduous trees such as *Alnus* and *Betula* are common elements in terrestrial Holocene vegetation records (e.g. Bjune and Birks, 2008; Bjune, 2005) but are only represented in low numbers (<3%) in the marine surface pollen assemblages, complicating the quantification of their representation in the vegetation. The same applies for *Corylus* which is a thermophilic, oceanic climate species in Norway and reaches its upper limit in the middle boreal zone, thus extending up to 70°N (Bjune, 2005; Moen, 1987). Other thermophilic taxa such as *Fraxinus*, *Ilex* and *Taxus* that are restricted to southern Norway (<62.5°N) (Moen, 1999, 1987) are represented with a relative abundance of up to 2% in the modern and mid-Holocene pollen samples of Hole 642B, suggesting pollen input from a large source area. Human activity has, however, significantly altered the natural vegetation of Norway (Moen, 1999, 1987), resulting in the occurrence of species outside their natural habitat, which could explain the presence of *Fraxinus* and *Taxus* in the modern samples.

3.4.2 Late Pliocene climate reconstruction

According to the Piacenzian pollen assemblages and based on the modern vegetation distribution in Norway (Moen, 1999), the northern boundary of the boreonemoral and nemoral zone was shifted 4–8° latitude to the north during the two warmer-than-present

intervals in the Piacenzian (3.6–3.47 Ma and 3.29–3.18 Ma). Conditions rather similar to present characterised the interval between 3.47 and 3.29 Ma.

Palaeoclimate estimates for the Piacenzian using the Coexistence Approach suggest that MATs and WMTs were at least (minimum) 4°C and 8°C higher than today, respectively. These minimum estimates fit well with the reconstructed latitudinal shifts in forest zones and broadly corroborate previous temperature estimates from this site (Willard, 1994). Estimates for CMT and MAP overlap with modern climate data, either suggesting that values were similar to present or that changes are not detected due to limitations in the approach (e.g. Grimm and Potts, 2016). Factors which hamper accurate climate estimates from both the modern and mid-Holocene as well as Piacenzian samples include:

- *Uncertainties in pollen identification* allow a determination of many pollen taxa to genus level only. This yields wide climatic tolerances and ranges
- *Distance of site from the mainland* results in overall lower number of taxa and complicates the identification of the pollen source area
- *Near coastal Scandinavian mountains* cause a mixed pollen signal with taxa from different vegetation and climate zones along the altitudinal gradient
- *Lack of modern analogue*: several taxa are extinct in Europe, such as *Carya*, *Sciadopitys* and *Tsuga*, and their modern distribution might not reflect their climatic tolerances during the Pliocene.

Considering these limitations, the Piacenzian climate reconstruction based on the CA for northern Norway should be considered a low confidence estimate only.

3.4.3   Vegetation and climate at 3.60–3.47 Ma

At the onset of the Piacenzian, the occurrence of pollen from deciduous temperate elements (e.g. *Carpinus*, *Carya* and *Quercus*) together with high abundances of pollen from conifer trees, including temperate taxa such as *Sciadopitys* and *Tsuga*, suggest the presence of cool temperate deciduous to mixed forest in northern Norway. At present, *Quercus* spp. are a distinctly southern species in Norway, occurring in the nemoral and boreonemoral zones. During the earliest Piacenzian, the northern boundary of the boreonemoral zone was presumably positioned at least 4° further north when compared to today, reaching the Arctic Circle. Predominantly deciduous forest might even have prevailed in the lowlands of northern Norway, implying a northward shift of the northern limit of the nemoral zone by at least 8° latitude.

Sciadopitys and *Tsuga* are considered to be part of the cool temperate montane vegetation. Both species went extinct in Europe during the glacial-interglacial cycles of the Pleistocene but can still be found in East Asia and North America (e.g. Svenning, 2003; Wen, 1999). Only one species of *Sciadopitys* still exists at present, growing in the warm to cool temperate montane zone of Japan. There, *Sciadopitys* forests are associated with steep rocky ridges or slopes, requiring relatively dry habitat conditions in a humid climate (Ishikawa and Watanabe, 1986). In Neogene deposits from central Europe and Denmark, *Sciadopitys* is, however, known to be an element of peat-forming vegetation or conifer forests that grew in better drained or elevated areas, respectively, suggesting that its ecological requirements have changed (e.g. Figueiral et al., 1999; Schneider, 1995). In the Lake Baikal region, *Tsuga-Picea* forests are also ascribed to habitats at higher altitudes during the Piacenzian (Demske et al., 2002). The assignment of *Sciadopitys* and *Tsuga* to montane conifer forests is supported by the correlation of the relative percentage changes of these taxa to those of other high-altitude taxa (Cupressaceae, *Juniperus-type* and *Picea*; Figure 3.2) (e.g. Numata, 1974; Seppä and Birks, 2001).

Ericaceae shrubs, *Lycopodium* and *Sphagnum* mosses likely originated from both the understorey of the cool temperate to boreal forests, and alpine environments. The relative abundance of *Sphagnum* spores during the earliest Piacenzian is lower than that in the surface sample but similar to the subsurface sample (Figure 3.1, 3.2) which might be indicative of a less extensive distribution of peatlands.

Warmer-than-present climatic conditions between 3.55 and 3.48 Ma have also been recorded at Lake El'gygytgyn in the north-eastern Russian Arctic where *Larix*/*Pseudotsuga* forests predominated (Andreev et al., 2014; Brigham-Grette et al., 2013). In southern East Siberia, mixed coniferous forests grew under a relatively warm climate in the Lake Baikal region during the early Piacenzian (Demske et al., 2002).

3.4.4 Vegetation and climate at 3.47–3.35 Ma

A marked cooling around 3.47 Ma and a subsequent establishment of similar to present boreal conditions are inferred from a sharp drop in the relative abundance of conifer tree pollen (except *Pinus* pollen). A corresponding increase in the abundances of spores and pollen from herbs, shrubs and mosses (Asteraceae, Ericaceae, *Lycopodium* and *Sphagnum*; Figure 3.2) is interpreted to reflect the development of open environments at high altitudes, possibly similar to the modern low alpine vegetation, as a result of a

southward shift of the cool temperate mixed and boreal forest zones and accompanied lowering of the treeline. At present, the lower boundary of the low alpine zone, corresponding to the tree line, is reached at 400–800 m in the area around Bodø and Mo i Rana (Moen, 1999).

Maximum abundances of herb pollen, especially those of Asteraceae Liguliflorae-type are reached at 3.42 Ma, steadily declining towards 3.35 Ma (Figure 3.2, 3.7). They are indicative of drier conditions. At present, tall-herb meadows reach their distribution limit in the southern Arctic zone in northern Norway but are less common in the alpine regions (Moen, 1999). The high abundance of Asteraceae in ODP Hole 642B might reflect a vegetation community with no modern analogue. At present, alpine environments with abundant Asteraceae can only be found in the Southern Hemisphere. At Kosciuszko National Park, New South Wales, Australia, Asteraceae grows in alpine herbfields, grasslands, bogs and heath communities along with Ericaceae, *Huperzia*, *Lycopodium* and *Sphagnum* (Costin et al., 2000). Additionally, Asteraceae and Ericaceae pollen as well as *Lycopodium* and *Sphagnum* spores in the sediments of ODP Hole 642B may have originated from the field layer of forests covering the lower altitudes. These were more boreal in character during this time interval with *Pinus* as the dominant species, as indicated by low percentages of pollen from other conifers, including the temperate taxa *Sciadopitys* and *Tsuga* (Figure 3.2). The diversity index shows the lowest average value across this interval of relative cool climatic conditions (Figure 3.7).

The development of open environments at high altitudes is suggested to have occurred as a result of an altitudinal downward shift of vegetation belts as well as a southward displacement of vegetation zones. Taxa characteristic of the boreonemoral zone (e.g. *Quercus* and *Sciadopitys*) comprise low proportions in the pollen assemblage at ODP Hole 642B between c. 3.47 and 3.35 Ma (Figure 3.2), suggesting that patches of deciduous to mixed forests grew in the area. These patches presumably represent extensions of the northern boundary of the mixed forest zone. The prevalence of boreal forest together with patchy deciduous forest stands and low alpine environments at higher altitudes is indicative of climatic conditions similar to today. Assuming tree line elevations of 400–800 m, the northern Norwegian mountains were probably not high enough for mountain glaciers to establish between 3.47 and 3.35 Ma. Presently, glaciers only form in the high alpine zone, above 1000 m (Moen, 1999, 1987).

87
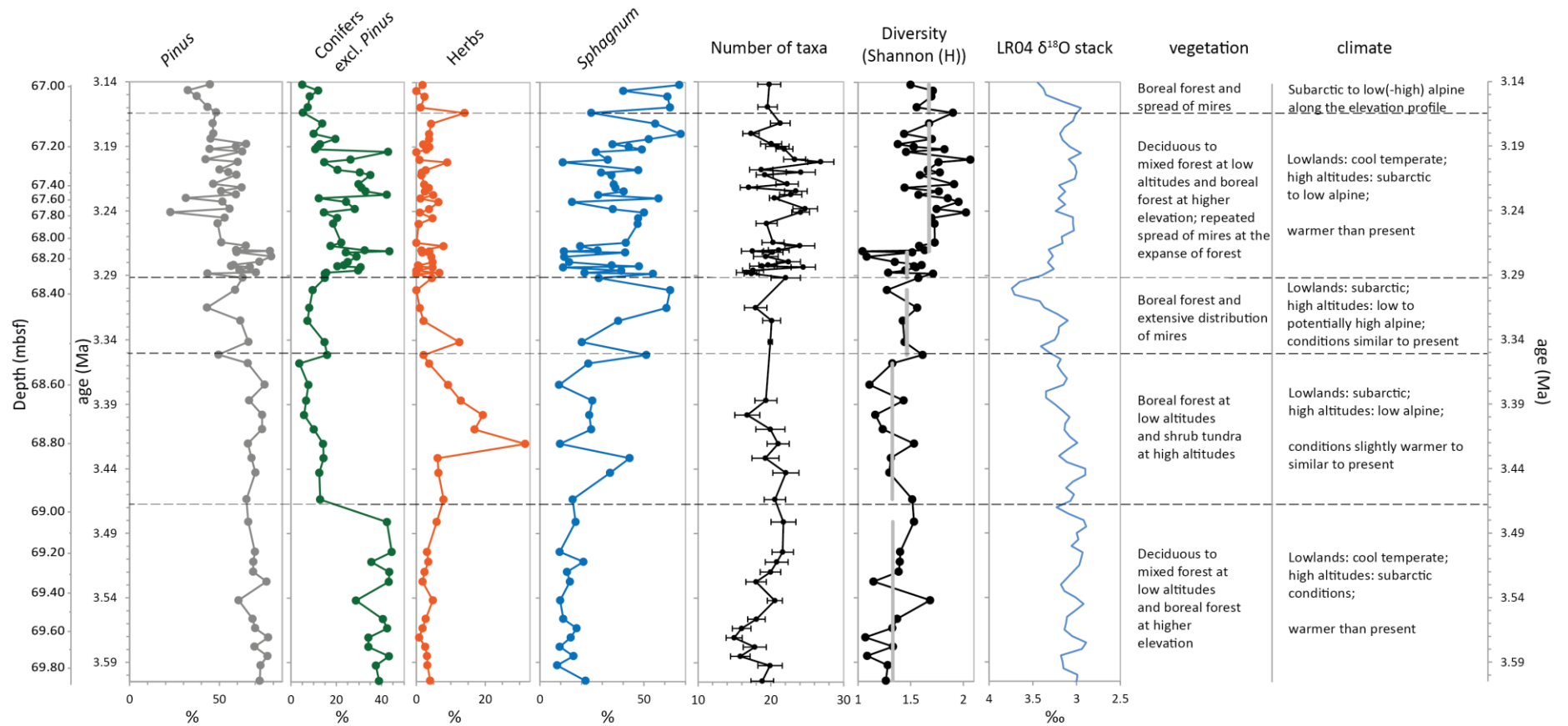
Figure 3.7: Summary diagram illustrating percentage changes in the main taxa or taxa groups, diversity based on the Shannon index, numbers of taxa rarefied at 300 individuals, the global benthic LR04 oxygen isotope stack (Lisiecki and Raymo, 2005) and description of the main vegetation configurations and climatic conditions. Vertical grey lines in the diversity graphs correspond to the average value across the interval. Dashed horizontal lines correspond to the main pollen zones shown in **Figure 3.2**.

While the ODP Hole 642B pollen record indicates cold conditions similar to present-day (Figure 3.2, 3.7), re-occurring warmer and cooler climate conditions are documented in the Lake El'gygytgyn and Lake Baikal region between 3.47 and 3.35 Ma (Andreev et al., 2014; Demske et al., 2002). As in ODP Hole 642B, the pollen percentages of thermophilic tree species (*Abies*, *Picea* and *Tsuga*) also decrease significantly between c. 3.48 and 3.45 Ma. At the same time, increased percentages of Cyperaceae and Poaceae pollen as well as *Sphagnum* and other spores indicate the development of open habitats, suggesting cooler and reoccurring drier and wetter climatic conditions around Lake El'gygytgyn (Andreev et al., 2014). The peak in *Sphagnum* spores at c. 3.43 Ma in ODP Site 642B coincides with an increase in *Sphagnum* spores in the Lake El'gygytgyn record, suggesting wetter climatic conditions both in northern Norway and the Siberian Arctic. A biome reconstruction for Lake El'gygytgyn suggests the first appearance of tundra during a cool interval, lasting from 3.39 to 3.31 Ma (Andreev et al., 2014). A thinning of the forests and spread of Ericaceae shrubs and Lycopodiaceae is also recorded at Lake Baikal at 3.47 Ma, but warm conditions prevail until 3.5 Ma (Demske et al., 2002). Between 3.5 and 3.38 Ma, drier but still relatively warm climatic conditions are inferred from a change of moist (*Abies*, *Picea* and *Tsuga*) to dry (*Juniperus*-type, *Larix*/*Pseudotsuga* and *Quercus*) forests (Demske et al., 2002). A strong cooling is observed in the Lake Baikal region at 3.39 Ma from a spread of boreal taxa and a maximum in *Selaginella selaginoides* (Demske et al., 2002).

The period of cooling in Scandinavia, north-eastern Russian Arctic and southern East Siberia corresponds to the time of deposition of till, and hence glaciation, in the James Bay Lowland, Canada (~52°N) at c. 3.5 Ma (3.6–3.4 Ma) (Gao et al., 2012), and also to enriched global benthic $\delta^{18}O$ (Lisiecki and Raymo, 2005). No major glacial events are, however, evident in the Nordic Seas during this time interval (Fronval and Jansen, 1996; Kleiven et al., 2002). Gao et al. (2012) propose that the lack of ice-rafted detritus in the Nordic Seas either indicates a significant contribution from the North American ice sheet to the elevated benthic $\delta^{18}O$ values or a restriction of glaciation to the continental interior of Greenland and Fennoscandinavia. The Piacenzian vegetation record for northern Norway suggests a wide distribution of boreal forest between 3.47 and 3.35 Ma. Considering the present-day average minimum elevation of glaciers (~1000 m) in northern Norway, and a lower height of the Scandinavian mountains

during the Pliocene, mountainous glaciation seems highly unlikely (Andreassen et al., 2012; Sohl et al., 2009).

In the North Atlantic, SSTs derived from alkenones decrease at 3.45 Ma at IODP Site U1313 (41°N, 33°W) just north of the subtropical gyre, suggesting a weakened northward heat transport via the NAC (Naafs et al., 2010). At ODP Site 982 (58°N, 16°W), which sits at the northern end of the NAC, a gradual cooling of SSTs (alkenones) is recorded from c. 3.5 Ma onwards (Lawrence et al., 2009). These SST records confirm the hemispheric-wide extent of climatic changes around c. 3.47 Ma.

3.4.5   Vegetation and climate at 3.35–3.29 Ma

After c. 3.35 Ma, the percentages of *Pinus* pollen drop below 50%, suggesting a decline in pine forest coverage and a further cooling of climate (Figure 3.2). Around 3.3 Ma, the high relative abundance of *Sphagnum* spores reflects a spread of peatlands and high precipitation (Figure 3.7). Additionally, the absence of temperate pollen taxa, e.g. *Carpinus*, *Carya*, *Sciadopitys* and *Tsuga*, is indicative of the predominance of boreal forest. The proportion of *Sphagnum* spores is about twice as high around 3.3 Ma than in the surface sample, suggesting a more extensive distribution of peatlands.

The upper limit of well-developed peatland communities is presently reached in the lower alpine zone. The maximum elevation of this zone ranges from 600 to 1400 m where the Scandinavian mountains reach a sufficient height (Moen, 1999, 1987). The clear boreal to alpine character of the vegetation around 3.3 Ma suggests that climatic conditions might have been cold enough to allow for the establishment of mountain glaciers in northern Norway. The cooling event at c. 3.3 Ma coincides with glacial MIS M2, a major global glaciation event. In the Northern Hemisphere a modern-like ice configuration with glaciation in Greenland, Iceland, the Barents Sea and Scandinavia is suggested for MIS M2 (De Schepper et al., 2014). However, the possibility of a hiatus in ODP Hole 642B over the most extreme part of MIS M2 must be considered (see section 2.3).

At Lake El'gygytgyn, a further increase in herbs and spores combined with a decrease in tree taxa is observed at 3.352 Ma, indicating enhanced cooling and relatively dry climatic conditions (Andreev et al., 2014). Between 3.310 and 3.283 Ma, tundra- and steppe-like vegetation dominated around the lake but tree and shrub vegetation was still present in the area. A high *Sphagnum* content also points to the existence of wetlands

around the lake (Andreev et al., 2014). In the lake Baikal region, cool climatic conditions still persisted until around 3.3 Ma (Demske et al., 2002).

3.4.6   Vegetation and climate at 3.29–3.16 Ma

After 3.29 Ma, cool temperate deciduous to mixed forests re-migrated to northern Norway as shown by the frequent presence of pollen from temperate deciduous taxa (e.g. *Carpinus*, *Carya, Pterocarya* and *Quercus*) and the increase in the relative abundance of conifer pollen (Figure 3.2). Between 3.29 and 3.26 Ma, pollen percentages of *Pinus* and conifers are high while those of *Sphagnum* spores are relatively low, suggesting a spread of forest at the expense of peatlands and thus warmer climatic conditions. A reestablishment of *Pinus-Larix-Picea* forests after MIS M2 is also documented at Lake El'gygytgyn and mixed coniferous forests spread in the Lake Baikal region (Andreev et al., 2014; Demske et al., 2002).

In the pollen record of ODP Hole 642B, an opening of the vegetation is seen at c. 3.26 Ma, when the relative abundance of *Pinus* pollen and *Lycopodium* spores decreases. The correspondingly increased proportion of *Sphagnum* spores suggests wetter and possibly also cooler climatic conditions (Figure 3.2). Thereafter, percentages of *Pinus* are quite variable, suggesting repeated warmer phases. Taxa diversity is higher during the warmest climatic conditions within the Piacenzian record (3.29–3.18 Ma) when compared to the preceding cool intervals (3.47–3.29 Ma). This coincides with a higher number of taxa in individual samples (Figure 3.7). In the north-eastern Russian Arctic, an opening of the vegetation and drier climatic conditions is inferred from the high amounts of herb pollen in the Lake El'gygytgyn record between c. 3.25 and 3.20 Ma (Andreev et al., 2014). This coincides with low *Pinus* pollen and high *Sphagnum* spore percentages in the sediments of ODP Hole 642B. Cooler climate conditions are also recorded in the Lake Baikal region during this interval (Demske et al., 2002). In northern Norway, climate oscillated between cooler and warmer phases. The high abundance of *Pinus* pollen in the sediments of ODP Hole 642B around 3.20–3.18 Ma coincides with a re-establishment of forests around Lake El'gygytgyn at c. 3.20 Ma (Andreev et al., 2014). The decline in the relative abundance of *Pinus* pollen and marked increase in the proportion of *Sphagnum* spores after 3.18 Ma suggest the establishment of cooler climatic conditions similar to those during MIS M2.

Over the entire 3.29–3.16 Ma interval, a wider distribution of cool temperate montane forests in northern Norway during warmer phases is indicated by peaks in the

abundances of *Sciadopitys* and *Tsuga* pollen, coinciding with high *Pinus* pollen contents (Figure 3.2). Thermophilic pollen taxa like *Carpinus*, *Carya*, *Ilex, Pterocarya* and *Quercus* occur frequently together with other rarely represented pollen of deciduous trees (e.g. *Acer, Fagus*, *Juglans*, *Nyssa* and *Tilia*; Figure 3.3; Plate 3.2, 3.3), pointing to the presence of nemoral to boreonemoral forests and a warm climate (Figure 3.2, 3.3). Relatively high numbers of *Juniperus*-type and Cupressaceae pollen suggest the prevalence of open shrub vegetation at higher altitudes throughout the interval (Bjune, 2005; Seppä and Birks, 2001). The high proportion of *Sphagnum* spores, peaks in herbs such as Asteraceae, Chenopodiaceae and Poaceae pollen and the regular occurrence of other herb pollen taxa also suggest the continuous presence of open environments (Figure 3.2). The relatively high abundance of *Sphagnum* spores also points to more humid conditions than during the previous intervals.

The negative correlation of *Pinus* and *Sphagnum* pollen percentages suggests distinct changes between a wider forest coverage and expansion of peatlands, presumably indicative of repeatedly warmer and cooler climatic conditions. The development of peatlands during Piacenzian intervals that show a similar-to-present vegetation distribution and climate might have contributed to the long-term decline in atmospheric CO_2 concentrations towards the Pleistocene (e.g. Lunt et al., 2008a; Martínez-Botí et al., 2015; Pound et al., 2015). At present circumarctic peatlands in the Northern Hemisphere form a major carbon sink (e.g. Gajewski et al., 2001; MacDonald et al., 2006). In addition, a change from a taiga- to tundra-dominated vegetation significantly increases surface albedo by expanding snow cover over the summer (Koenig et al., 2011 and references therein). The wider distribution in peatlands in northern Norway during the Piacenzian might have acted as a positive internal feedback mechanism that facilitated the development of an extensive Scandinavian ice sheet around 2.72 Ma (Kleiven et al., 2002).

The findings of this study corroborate a previous palynological analysis of nine samples from the Piacenzian section of ODP Hole 642C, indicating the presence of a mixed conifer-hardwood forest at the northern limits of the deciduous forest zone in Norway between c. 3.3 and 3.1 Ma (Willard, 1994). However, this high-resolution study indicates that the warmth of the Piacenzian was not as stable as previously thought, but was instead interrupted by cooler intervals, causing latitudinal and altitudinal shifts of the boundary between the deciduous and boreal forest zone.

In the North Atlantic, a return of warm conditions at 3.29 Ma is documented in the alkenone-based SST record of Site U1313, indicating an enhanced northward heat transport by the NAC (Naafs et al., 2010). A re-establishment of the NAC at 3.285 Ma, following the glacial maximum of MIS M2, is also seen in the alkenone- and Mg/Ca-derived SSTs as well as dinoflagellate assemblage changes at IODP Site U1308 (50°N, 24°W) and DSDP Site 610 (53°N, 19°W) further north (De Schepper et al., 2013). The warming documented at these sites is in agreement with this study. In contrast, Site 982 records a continuous cooling over this interval which might, however, be attributed to discrepancies in the age model (Khélifi et al., 2012; Lawrence et al., 2013, 2009).

3.4.7   Vegetation and climate at 3.16–3.14 Ma

The climate of Norway cooled further, as indicated by the steady decrease in the relative abundance of *Pinus* pollen, high proportions of *Sphagnum* spores and the sporadic occurrence of pollen from temperate taxa between c. 3.16 and 3.14 Ma (Figure 3.2, 3.7). The pollen assemblage shows a strong resemblance to that during MIS M2, suggesting similar or slightly colder climatic conditions when compared to today, and potentially creating conditions favourable for glacier build-up at high altitudes. Cool climate prevailed in the James Bay Lowland, Canada during that time, as indicated by the prevalence of boreal forests (Gao et al., 2012). A thinning of forests and deflection to cooler conditions is also observed at Lake Baikal at c. 3.18 and 3.15 Ma (Demske et al., 2002). In contrast, conifer forests grew under relatively warm climate conditions until 3.06 Ma in the Lake El'gygytgyn area (Andreev et al., 2014).

3.4.8   (Sub)Arctic vegetation evolution during the Piacenzian

During the Cenozoic, temperate to boreal forests showed a wide distribution in the Northern Hemisphere and were very uniform in their floristic composition (e.g. Wen, 1999; Xing et al., 2015). Palaeogeographic and palaeoclimatic changes during the Pliocene and Pleistocene led to today's disjunct distribution of tree genera in Europe, Asia and North America (e.g. Svenning, 2003; Xing et al., 2015). The Piacenzian flora of northern Norway exhibits a similar composition to that in Canada and Siberia at that time (e.g. Andreev et al., 2014; de Vernal and Mudie, 1989a; Pound et al., 2015). The reconstructed Piacenzian vegetation and climate changes in northern Norway are closely correlated with other vegetation records across the Northern Hemisphere (Table 3.1), indicating a hemispheric response to external and internal forcing. Vegetation changes at Lake El'gygytgyn strongly follow orbitally-induced glacial-interglacial cycles (Andreev et al., 2014; Brigham-Grette et al., 2013). For instance, the hemisphere-wide

Table 3.1: Summary of Piacenzian (sub)Arctic vegetation records. Time intervals correspond to the main pollen zones delimited in ODP Hole 642B. Piacenzian vegetation changes are compiled from the following: ODP Hole 642B (this study); the Lake El'gygytgyn record in the NE Russian Arctic (Andreev et al., 2014); Lake Baikal record in SE Siberia (Demske et al., 2002); Yukon, NW Canada (Pound et al., 2015) and James Bay Lowland, SE Canada (Gao et al., 2012).

Location/time interval	3.6-3.47 Ma	3.47-3.35 Ma	3.35-3.29 Ma	3.29-3.16 Ma	3.16-3.14 Ma
Northern Norway (ODP Hole 642B, 67°N)	Cool temperate to deciduous forest	Boreal forest and low alpine environments	Boreal forest and extensive peatlands	Cool temperate to boreal forests, long-term expansion of peatlands	Further decrease of forest coverage and spread of peatlands
Temperature	Warm	*Cool*	*Cool*	Warm	*Cool*
Precipitation	High	*Low*	High	High	High
North-eastern Russian Arctic (Lake El'gygytgyn, 67°N)	Diverse coniferous forest with temperate trees and shrubs and peatlands	3.48 Ma: decrease in thermophilic taxa; 3.48-3.42 Ma: predominance of boreal forest and open habitats, repeated wetter and drier intervals; 3.42-3.39 Ma: boreal forest; After 3.39 Ma: boreal forest and first appearance of tundra	After 3.35 Ma: further opening of the vegetation; 3.31-3.28 Ma: mostly treeless tundra- and steppe-like vegetation with forest patches and peatlands	3.28-3.25 Ma: boreal forest; 3.25-3.20 Ma: boreal forest with open habitats; 3.20 Ma: boreal forest	After 3.06 Ma: opening of the vegetation
Temperature	Warm	*Cool* / Warm	*Cool* / *Cool*	Warm	Warm / *Cool*
Precipitation	*Low*	High / High	*Low* / *Low*	High / *Low* / High	High

South-eastern Siberia (Lake Baikal, 53°N)	Mixed coniferous forests	At 3.47, 3.43 and 3.39 Ma: thinning of forest and predominance of boreal vegetation	After 3.3 Ma: Spread of coniferous forest	At 3.26 and 3.18 Ma: thinning of boreal forest and spread of boreal taxa	After 3.15 Ma: reduced forest coverage and development of open habitats
Temperature	Warm	Cool / Warm / Cool	Cool	Cool	Cool
Precipitation	High	Low / High / Low	Low / High	Low	Low

Canada (Yukon, 64°N and James Bay Lowland, 52°N)		James Bay Lowland: till deposits dated to 3.5 Ma (3.4 – 3.6 Ma)		Yukon: diverse boreal forest with wetlands/lakes	James Bay Lowland: boreal forest
Temperature		Cool		Warm	
Precipitation				High	

cooling at c. 3.48–3.47 Ma and c. 3.3 Ma coincide with MIS MG6 and M2, respectively (Andreev et al., 2014; Brigham-Grette et al., 2013; Lisiecki and Raymo, 2005).

The circum-arctic distribution of tundra/peatlands developed during the late Piacenzian and throughout the glacial-interglacial cycles of the Pleistocene (e.g. Andreev et al., 2014; Gajewski et al., 2001). The transition of high-latitude vegetation changes from forest to tundra environments during the late Piacenzian presumably amplified the cooling through vegetation-snow albedo feedbacks (e.g. Gallimore and Kutzbach, 1996; Koenig et al., 2011). The long-term cooling trend over the Piaceanzian that is observed in all records is in accordance with declining atmospheric CO_2 values from the Piacenzian towards the early Pleistocene (Bartoli et al., 2011; Martínez-Botí et al., 2015; Seki et al., 2010). Expansion of tundra biomes may have contributed to the drawdown of atmospheric CO_2, further enhancing cooling.

The main vegetation and climate changes during the Piacenzian observed in (sub)Arctic records are illustrated in Table 3.1. During the earliest Piacenzian diverse forest communities persisted under a warmer-than-present climate in northern Norway, the north-eastern Russian Arctic and southern East Siberia (Andreev et al., 2014; Demske et al., 2002). In all regions, cooling around 3.48–3.47 Ma is indicated by the development of open habitats. Till deposits in the James Bay Lowland, Canada provide evidence for glaciations between 3.6 and 3.4 Ma (Gao et al., 2012). A further opening of the vegetation and deterioration of climate is observed both in northern Norway and the north-eastern Russian Arctic after 3.35 Ma, culminating in the coldest recorded climatic conditions around 3.3 Ma. High *Sphagnum* spore content in ODP Hole 642B and the Lake El'gygytgyn record are indicatve of an extensive distribution of peatlands during the coldest interval (Andreev et al., 2014). Warm climatic conditions re-established after c. 3.29 Ma in northern Norway, the north-eastern Russian Arctic and southern East Siberian which were interrupted by cooler intervals until c. 3.18 Ma (Andreev et al., 2014; Demske et al., 2002). However, conifer forests prevail under relatively warm climatic conditions in the vicinity of Lake El'gygytgyn until 3.06 Ma. Piacenzian deposits from the Yukon Territory, Canada have been assigned to the mPWP and reveal the prevalence of diverse forests with wetlands/lakes (Pound et al., 2015). Between 3.18 and 3.14 Ma reduced forest coverage in northern Norway and in the Lake Baikal area, and the predominance of boreal forest in the James Bay Lowland are indicative of cool climatic conditions (Demske et al., 2002; Gao et al., 2012).

3.5   Conclusions

The Piacenzian high-resolution pollen record from ODP Hole 642B in the Norwegian Sea reveals repeated fluctuation of cool temperate and boreal conditions. Warmest month temperatures are estimated to be 8–14°C higher than present. The northern boundary of the boreonemoral to nemoral forest zone was shifted northward by at least 4–8° latitude during warmer-than-present intervals. Throughout the Piacenzian record (c. 3.6–3.14 Ma) three main climatic phases are observed:

- 3.60–3.47 Ma: Cool temperate deciduous to mixed forest prevails in northern Norway, suggesting a northward shift of vegetation boundaries of at least 4–8° latitude.

- 3.47–3.29 Ma: A southward shift of vegetation zones as well as a displacement of vegetation belts to lower altitudes indicates cooling. Low alpine environments develop in mountainous areas, suggesting climatic conditions similar to today. The cooling culminates at c. 3.3 Ma (around MIS M2), potentially creating conditions cold enough for glacier build-up at the highest summits.

- 3.29–3.14 Ma: Re-establishment of warmer-than-present climate conditions is indicated by re-migration of deciduous to mixed forest to northern Norway. Repeated warmer and colder phases are recorded until c. 3.18 Ma after which climate continuously cools and conditions similar to MIS M2 establish again. The development of peatlands might have contributed to the drawdown of atmospheric CO_2 before the start of Northern Hemisphere glaciation.

Chapter 4: Pliocene vegetation and climate evolution in Arctic Norway controlled by North Atlantic Current variability

4.1 Introduction

In the Nordic Seas region, the pronounced high-latitude warming in comparison to mid- to low-latitude regions documented in Pliocene (5.33–2.58 Ma) marine and terrestrial proxy records has often been ascribed to an enhanced oceanic and/or atmospheric northward heat transport (Bennike et al., 2002; Dowsett et al., 2013a; Robinson, 2009; Verhoeven et al., 2013). Existing Pliocene vegetation records in the Nordic Seas region and the Canadian Arctic Archipelago are indicative of rather stable warmer-than-present climatic conditions throughout the epoch (Bennike et al., 2002; Rybczynski et al., 2013; Verhoeven et al., 2013; Willard, 1994). This notion is likely an artefact of the short temporal coverage and/or low resolution of these records. Recently published Piacenzian high-resolution records in the Northern Hemisphere suggest more variable climatic conditions (Chapter 3) (Andreev et al., 2014; Gao et al., 2012). A high variability of terrestrial climate during the Pliocene is in better agreement with marine proxy studies from the North Atlantic and Nordic Seas, showing major oceanographic changes and highly variable SSTs (De Schepper et al., 2015; Lawrence et al., 2009; Naafs et al., 2010; Risebrobakken et al., 2016; Schreck et al., 2013). During the Zanclean, major oceanographic changes affected the Nordic Seas region. Around 4.5 Ma, the establishment of a modern-like EGC and NwAC, which is an extension of the NAC, led to the onset of a modern-like circulation with a strong zonal temperature gradient (De Schepper et al., 2015). These oceanographic changes have been attributed to the shallowing of the CAS and the related onset of Pacific to Atlantic water through flow via the Bering Strait (De Schepper et al., 2015; Verhoeven et al., 2011). After the establishment of modern-like oceanographic conditions, major variations in the strength and/or position of the NAC and thus northward heat transport are evident in Piacenzian high-resolution SST reconstructions. These changes have been related to atmospheric circulation changes forced by orbitally controlled insolation variations and ocean gateway changes (De Schepper et al., 2013; Lawrence et al., 2009; Naafs et al., 2010). Piacenzian vegetation changes in northern Norway show a strong coupling between Scandinavian climate changes and the northward transport of warm Atlantic water via the NAC (Chapter 3).

The Pliocene has been suggested to be an epoch characterised by global climate cooling based on benthic oxygen isotope and SSTs records (LaRiviere et al., 2012; Lisiecki and Raymo, 2005; Mudelsee et al., 2014). Sniderman et al. (2016) question the idea of the Pliocene being the last warmer-than-present period within a gradual cooling trajectory. Instead, the authors suggest that the Pliocene represents a discrete warming that interrupted the late Neogene cooling trend. In the Southern Hemisphere, a distinct warming and wetting of climate during the Zanclean is inferred from a biome turnover in southern Australia that corresponds to higher SSTs at low- and high- latitude sites, reversing the long-term cooling and aridification trend (Sniderman et al., 2016 and references therein). In globally distributed Pliocene SST records, the Zanclean has also been identified as an interval of peak warmth (Fedorov et al., 2013). However, most Pliocene marine and terrestrial studies in the North Atlantic region have focused on climatic changes during the Piacenzian period which represents an interval of global cooling due to the progressive expansion of Arctic sea ice and growth of the Greenland ice sheet (Kleiven et al., 2002; Knies et al., 2014a; Lunt et al., 2008a; Mudelsee and Raymo, 2005; Salzmann et al., 2008). The climate variability during the Zanlcean and impact of the onset of a modern-like Nordic Seas circulation around 4.50 Ma and the related development of a stronger zonal and meridional temperature gradient (De Schepper et al., 2015) on atmospheric circulation and terrestrial climate in the North Atlantic region is, however, unknown.

This study presents the first complete Pliocene high-resolution pollen record, reflecting vegetation changes in northern Norway. The aim of this study is to assess (1) the response of high-latitude vegetation and climate changes to the variability of the NAC, (2) the long-term controls and (3) the impact of the shoaling of the CAS on the vegetation and climate evolution in northern Norway. Furthermore, the study addresses the role of Zanclean climate changes within the long-term Pliocene climate evolution. A previous high-resolution study of vegetation changes in northern Norway shows highly variable climatic conditions during the Piacenzian between 3.60 and 3.14 Ma (Chapter 3). The Pliocene vegetation and climate reconstruction is based on pollen and spore assemblage changes in the sediments of ODP Hole 642B in the Norwegian Sea, spanning the time interval from 5.03 to 3.14 Ma.

4.2   Materials and Methods

A total of 128 samples were selected for pollen analysis between 83.55 and 66.95 mbsf from ODP Hole 642B (Shipboard Scientific Party, 1987), ranging in age between 5.03

to 3.14 Ma (Risebrobakken et al., 2016). For the majority of samples more than 300 pollen and spore grains were counted. Only 20 samples yielded a total count of less than 300 grains. The present cluster analysis includes all pollen and spores to identify the main pollen assemblages zones within the Pliocene record.

PCA was performed on the percentage data to identify the main pattern of variance in the pollen assemblage changes in order to determine the controlling environmental variables. In addition, spectral analysis was carried out over the time interval from 4.366 to 3.137 Ma in order to detect cyclicity. Climate model outputs were investigated to evaluate the effect of the closure of the CAS on atmospheric circulation. A more detailed description of methodologies is given in Chapter 2.

4.3   Results

4.3.1   Pliocene pollen assemblages
Pollen zone 1 (83.55–77.38 mbsf, 5.03–4.51 Ma, 13 samples)

PZ 1 shows high proportions of *Pinus* pollen (58–85%) (Figure 4.1). The relative abundance of coniferous tree and shrub pollen (*Abies*, Cupressaceae, *Juniperus* type, *Picea*, *Sciadopitys*, *Taxus* and *Tsuga*) excluding *Pinus* pollen ranges between 25 and 66%. Pollen of deciduous (*Alnus*, *Betula*, *Carpinus*, *Carya*, *Corylus*, *Pterocarya*, *Quercus* and *Ulmus*) and evergreen (*Calluna* and Ericaceae) trees and shrubs are always present, constituting up to 22% of the assemblages. Herb pollen (Asteraceae, Caryophyllaceae, Chenopodiaceae, Cyperaceae and Poaceae) are always present but do not exceed a relative abundance of 10%. Spores of ferns and mosses (*Lycopodium*, *Osmunda*, Polypodiaceae, *Pteridium* and undifferentiated monoletes) excluding *Sphagnum* spores show proportions ranging between 6 and 30%. Percentages of *Sphagnum* spores are relatively high with values between 6 and 35%. Notable are the very high pollen PARs (~7500–19,300 grains/(cm^2 ka)) throughout the majority of PZ 1 and the marked drop to values around ~100 grains/(cm^2 ka) at the end of the zone (Figure 4.2). The relative proportion of reworked pollen and spores is very low throughout most of PZ 1 (<3%), only showing higher values (3–9%) in the lowermost part.

Pollen zone 2 (77.38–76.60 mbsf, 4.51–4.30 Ma, 7 samples)

Very low PARs (< ~100 grains/(cm^2 ka)) occur in the lower part of PZ 2 (Figure 4.2). The total pollen sum is below 40 grains in four samples within this zone. Therefore,
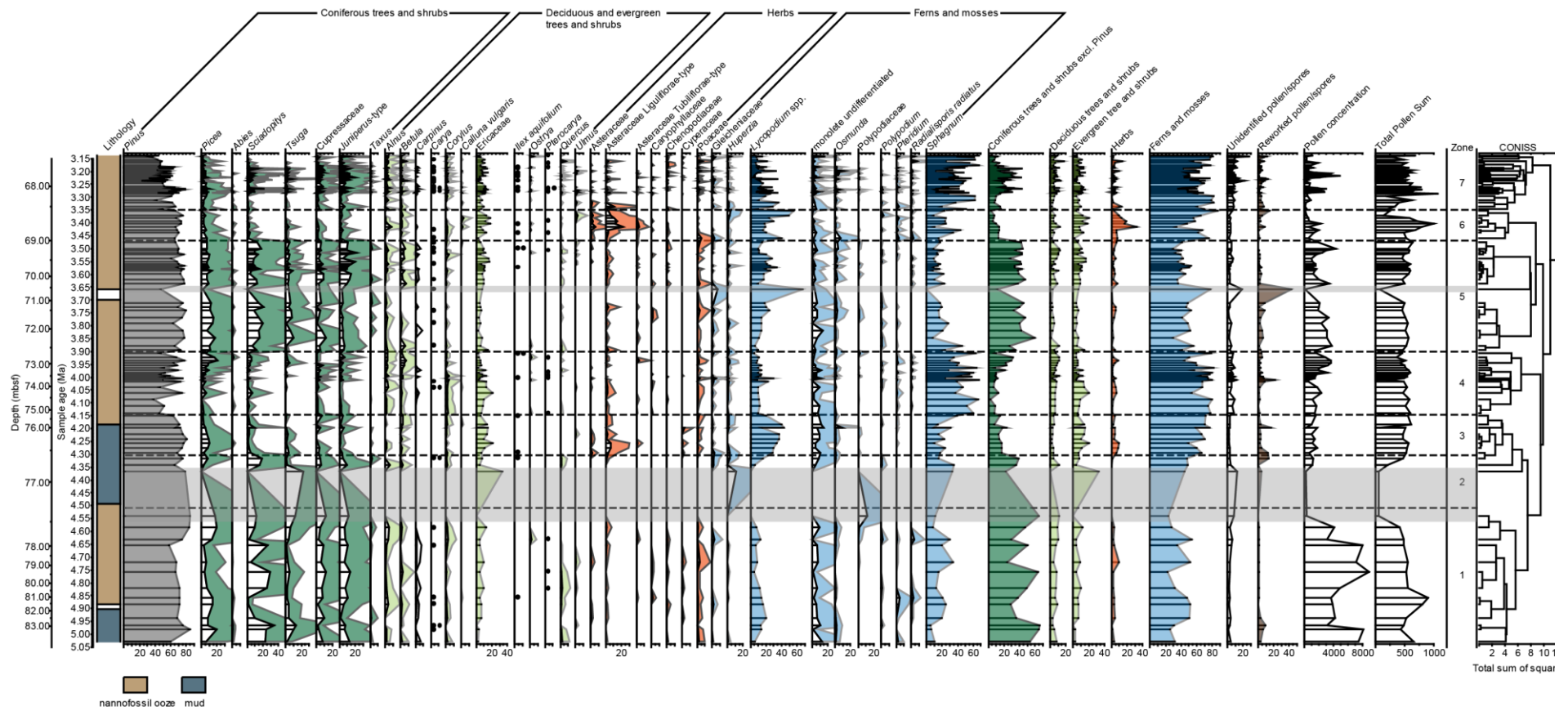
Figure 4.1: Pollen assemblages in the Pliocene sediments of ODP Hole 642B. Non-patterned, coloured area represents 5-fold percentages. Black circles are representative of single pollen or spore grains. Percentages of pollen and spores were calculated based on the pollen sum, excluding *Pinus*, unidentified and reworked pollen and spores. *Pinus* was included in the pollen sum to calculate percentages of *Pinus*. The total pollen sum shown here comprises *Pinus* and unidentified pollen. Depth is indicated in metres below sea floor (mbsf). Grey horizontal bars delimit samples with low pollen counts (<100). Samples with a total count of less than 40 grains are not shown. The lithology of the Pliocene section of Hole 642B was obtained from the original report (Shipboard Scientific Party, 1987).
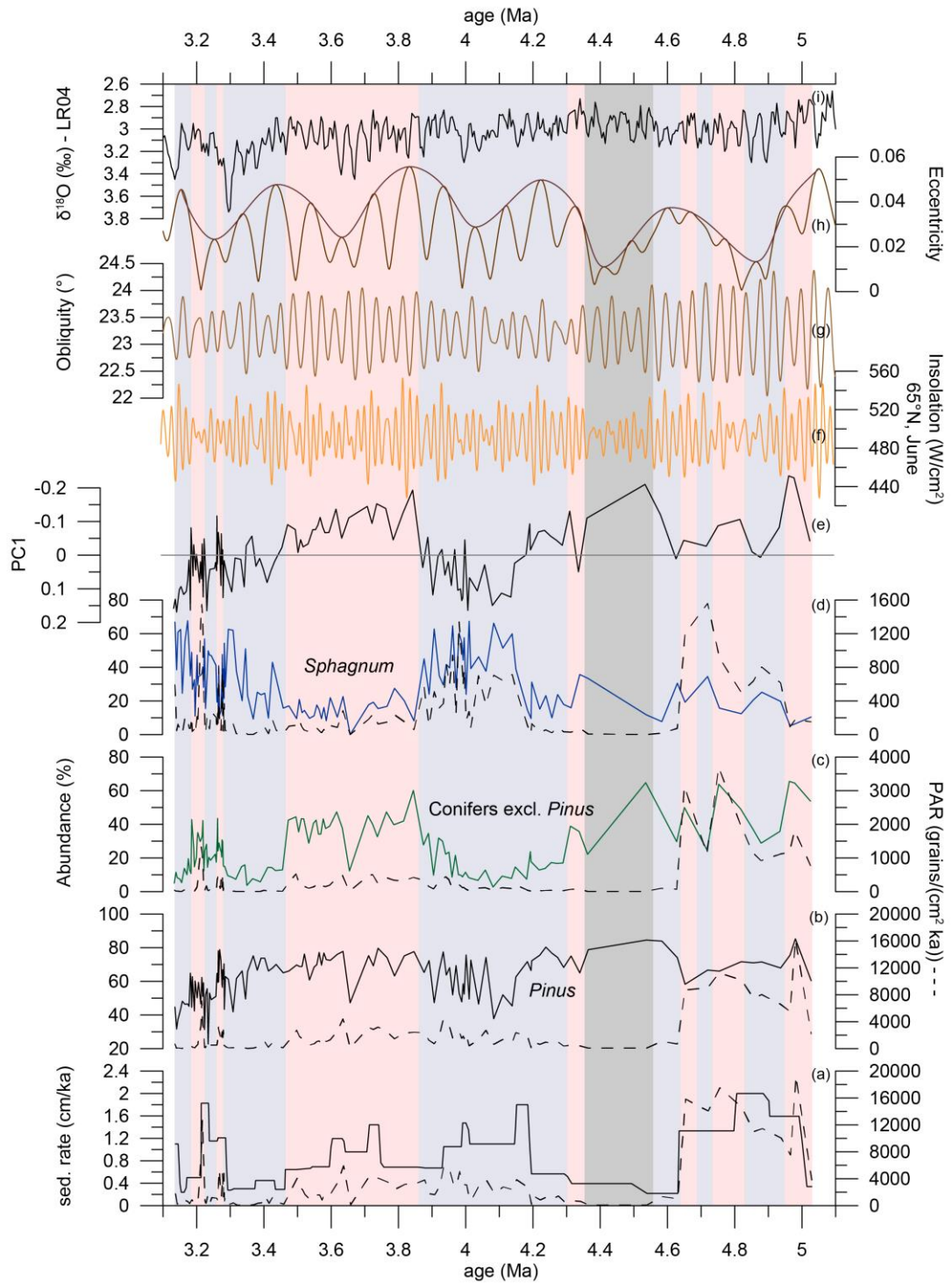
Figure 4.2: Comparison of (a–e) selected Pliocene pollen data from ODP Hole 642B to (f–h) orbital solutions (Laskar et al., 2004) and the global benthic oxygen isotope record (Lisiecki and Raymo, 2005). (a) Sedimentation rate (dashed line; Risebrobakken et al., 2016) and pollen accumulation rate (PAR, dashed line); (b–d) relative abundance changes of *Pinus*, conifers excluding *Pinus*, and *Sphagnum* (solid lines) and their PARs (dashed lines); (e) Principal Component (PC) 1 from Principal Component Analysis (see Figure 4.3). The blue and red shading indicates cooler (boreal) and warmer (cool temperate) intervals, respectively. The grey bar highlights the interval with low PARs and pollen counts.

relative abundances are not shown in Figure 4.1. Pollen and spore taxa that were present include *Alnus*, *Betula*, Ericaceae, *Fraxinus*, *Huperzia*, *Juniperus* type, *Pinus*, *Sphagnum* and *Tsuga*. Reworked pollen and spores were also found. The PAR reaches values between ~100 and 700 grains/(cm^2 ka) in the upper part of the zone. The three uppermost samples contain high abundances of *Pinus* pollen (65–79%) and pollen of conifers excluding *Pinus* (22–39%) and *Sphagnum* spores (16–36%).

Pollen zone 3 (76.60–75.29 mbsf, 4.30–4.15 Ma, 9 samples)

PARs vary between ~200 and 4000 grains/(cm^2 ka) and do not reach values as high as those attained during PZ 1 (Figure 4.2). Percentages of *Pinus* pollen (63–80%) are high throughout the zone (Figure 4.1). Pollen of coniferous trees and shrubs are relatively low (7–24%). Proportions of Asteraceae (2–8%) peak in the lower part of the zone. Abundances of Ericaceae (5–21%) pollen, *Lycopodium* (15–43%) and *Sphagnum* spores (10–39%) are relatively high. Reworked pollen and spores are highest (~13%) in the lower part of PZ 3. One sample in the upper part of the zone with a total pollen sum of <100 shows proportions of reworked pollen and spores of 17%.

Pollen zone 4 (75.29–72.60 mbsf, 4.15–3.90 Ma, 19 samples)

A slight decline in the relative abundance of *Pinus* pollen from 63% to a minimum of 38% is recorded in the lower part of PZ 4, which is accompanied by an increase in *Sphagnum* spores from 40% to 66% (Figure 4.1). Both percentages of *Pinus* pollen (38–78%) and *Sphagnum* spores (24–68%) reveal a high variability within the zone with *Pinus* pollen showing high proportions in the middle to upper part. Coniferous trees and shrub pollen remain low throughout PZ 4 but increase in the upper part, mainly due to a peak in *Picea* pollen. Ericaceae pollen show highest abundances in the middle part of the zone with a maximum of 21%. Relative proportions of herb pollen and *Lycopodium* spores are low, reaching maximum values of 8% and 14%, respectively. *Lycopodium* spores increase to 22% and 30% at two occasions. A single peak of reworked pollen and spores (22%) is documented in the middle part of the zone. PARs vary between ~850 and 5900 grains/(cm^2 ka) (Figure 4.2).

Pollen zone 5 (72.60–69.02 mbsf, 3.90–3.47 Ma, 25 samples)

PZ 5 is characterised by high abundances of *Pinus* pollen (61–80%) and pollen of other coniferous trees and shrubs (28–60%) (Figure 4.1). Pollen taxa of deciduous and evergreen trees and shrubs show relatively low abundances, reaching proportions of up

to 12% and 17%, respectively. Herb pollen (<8%) also constitute only a minor part of the assemblages. Percentages of *Lycopodium* spores range between 6 and 34% and those of *Sphagnum* spores reach values of 8–45%. Relative proportions of reworked pollen and spores are low (<8%) throughout the zone. A sample within the middle part of the zone, yielding counts of less than 100 grains, shows high percentages of reworked pollen and spores (43%). PARs range between ~150 and 5900 grains/(cm^2 ka) (Figure 4.2).

Pollen zone 6 (69.02–68.54 mbsf, 3.47–3.35 Ma, 9 samples)

The percentages of *Pinus* pollen (65–75%) are high throughout PZ 6 (Figure 4.1). The relative abundance of pollen of coniferous trees and shrubs drops sharply from 42% to 13% at the start of the zone. This decline coincides with a peak in *Lycopodium* spores (40%) which is followed by high percentages of *Sphagnum* spores (34–43%). Subsequently, the relative abundance of Asteraceae pollen increases to 32%, declining to values of 4% towards the upper part of the zone where they are replaced by *Lycopodium* spores (49–56%). PARs are relatively low (~45–1400 grains/(cm^2 ka)) (Figure 4.2). Reworked pollen and spores reach a maximum proportion of 15% in the upper part of the zone.

Pollen zone 7 (68.54–66.95 mbsf, 3.35–3.14 Ma, 46 samples)

PZ 7 is characterised by a long-term decline in the relative abundance of *Pinus* pollen (Figure 4.1). In comparison to the previous PZs, the proportions of coniferous tree and shrub pollen is low, but relatively high and variable percentages (up to 44%) are documented in the middle part of the zone. Pollen of deciduous and evergreen trees and shrubs is present with maximum proportions of 13% and 15% respectively. After an initial peak in percentages of Asteraceae pollen (12%) and *Lycopodium* spores (29–36%) in the lower part of PZ 7, the relative abundance of *Sphagnum* spores increases to 62%. Percentages of *Lycopodium* show an overall decline from a maximum of 36% in the lower part to values <20% in the upper part. The proportion of *Sphagnum* spores is highly variable, reaching highest values (up to 68%) in the uppermost part. Reworked pollen and spores show low (<13%) relative abundances. PARs range between ~60 and 12,700 grains/(cm^2 ka) (Figure 4.2).
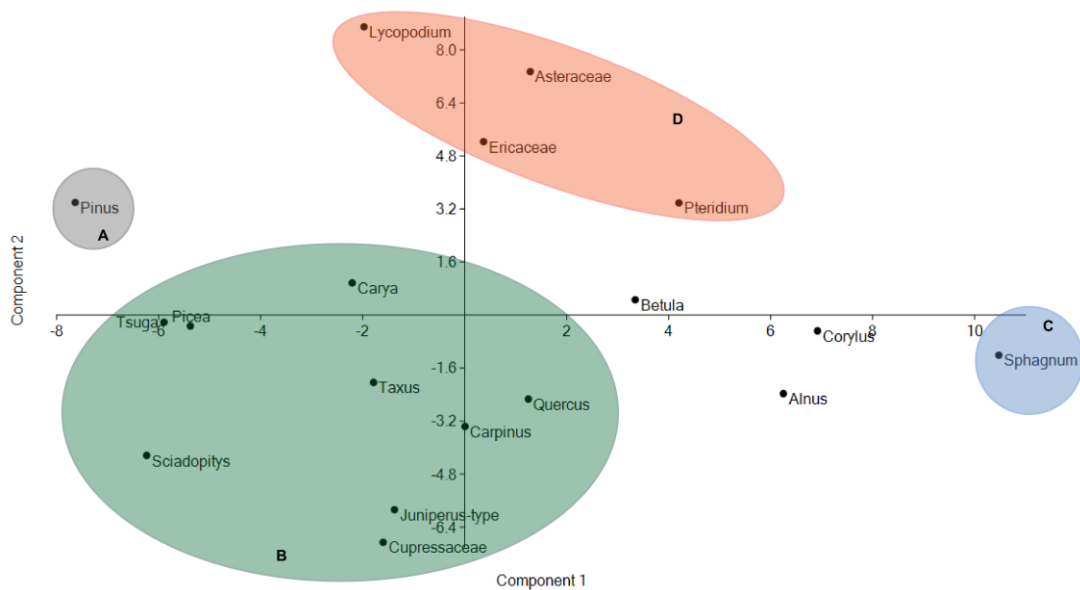
Figure 4.3: Principal Component Analysis using the most abundant taxa in the Pliocene pollen record of ODP Site 642B. The four identified groups include: (A) *Pinus* as a component of boreal and mixed forest, (B) mixed forests with thermophilic elements, (C) *Sphagnum* as the main element of peatlands and (D) tundra vegetation, consisting of herb fields and/or heather.

4.3.2 Principal Component Analysis

The first two components of the PCA using 18 taxa explain 34% of the variance with the first component accounting for 19% and the second for 15%. Four groups of pollen and spore types can be identified (Figure 4.3): (A) *Pinus* as a component of boreal and mixed forest, (B) mixed forests with thermophilic elements (e.g. *Carya*, *Quercus* and *Sciadopitys*), (C) *Sphagnum* as the main element of peatlands and (D) tundra vegetation, consisting of herbfields and/or heather (Asteraceae, Ericaceae and *Lycopodium* spp.). Taxa such as *Alnus*, *Betula* and *Corylus* grow in various vegetation zones, explaining their rather isolated position on the plot. Principal Component (PC) 1 is interpreted to reflect temperature, with warmer climatic conditions prevailing when loadings are low and thus *Pinus* and other coniferous and deciduous trees show high abundances. Cool climatic conditions, however, prevail when relative abundances of *Sphagnum* are high as indicated by high component loadings. The interpretation of PC 2 is more ambiguous due to pollen assemblages with high abundances of Asteraceae pollen that have no modern analogue (Chapter 3). With lower loadings of PC 2 being associated with higher abundances of *Sciadopitys*, which presently grows in a humid climatic (Ishikawa and Watanabe, 1986), this component may be indicative of precipitation changes.
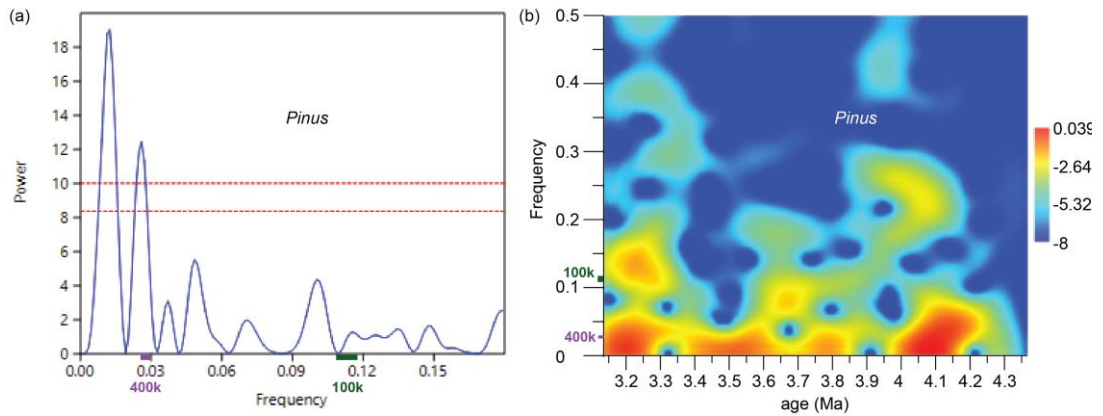
Figure 4.4: Spectral analysis of the relative abundance changes of (a) *Pinus* interpolated to 11,000 years and the corresponding evolutionary spectra (b). (a) Red dashed lines represent the 99% and 95% significance levels. (b) A size 32 Hanning window was used. The colours are indicative of the relative power. The purple and green bars along the frequency axes of both figures mark the frequency ranges of the 400,000-years and 100,000-years eccentricity cycles (data obtained from Laskar et al., 2004).

4.3.3   Spectral analysis

Low-frequency cyclicities in the order of 166,700 to 1,000,000 years are detected in the relative abundance changes of all taxa. A periodicity on orbital time scales, corresponding to the long eccentricity cycle, is only recorded in the relative abundance changes of Asteraceae and *Pinus* pollen. Here, only the spectral analysis of *Pinus* percentages changes is shown (Figure 4.4), as the assignment of Asteraceae pollen to a particular plant type or vegetation zone is uncertain.

4.3.4   Climate model results

Climate model outputs for vector mean surface wind speeds (10m) and atmospheric pressure (corresponding to ~750m and ~1500m) during spring (March, April, May) from simulations with an open CAS (hereafter referred to as OCAS) and closed CAS (hereafter referred to as CCAS) show differences in wind speeds and directions. In the OCAS experiment, southeasterlies to southwesterlies prevail along the coast of Norway in spring, with southeasterlies predominating at lower altitudes (10m and ~750m). In all OCAS simulations, a stationary front is located to the south of the core location (Figure 4.5). This zone of weak winds extends further northeast in the CCAS experiment, forming a low-velocity front east of the site location. In addition, wind speeds at the lower altitudes (10m and ~750m) are slightly reduced in the CCAS experiment, particularly in central Norway and further north. At higher altitudes (~1500m), northerly winds prevail above the site and southwesterlies affect the coast of Norway in the CCAS experiment (Figure 4.5).
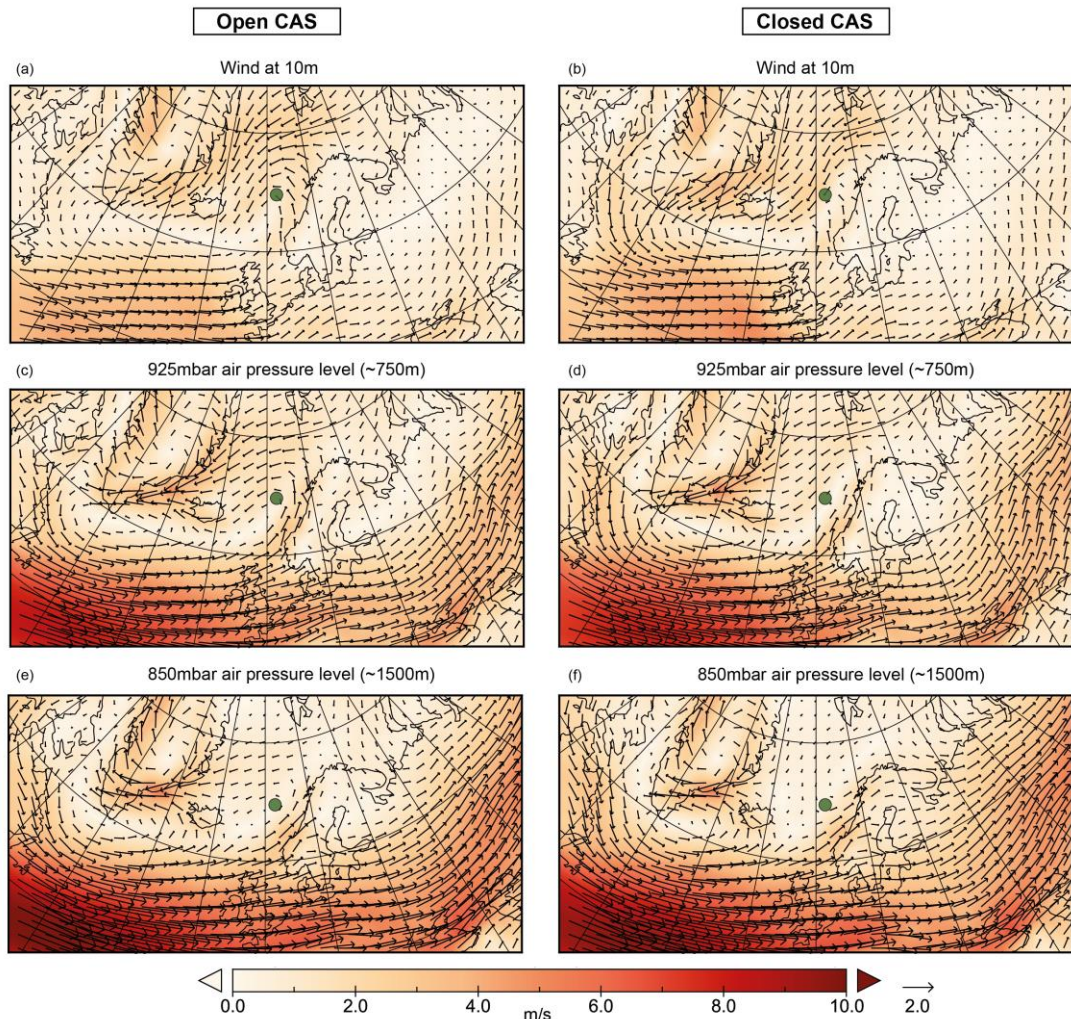
Figure 4.5: Model predictions for winds in spring (March, April, May) in the Nordic Seas region with an open and closed Central American Seaway (CAS). (a–b) winds at 10m altitude; (c–d) winds on the 925mbar pressure level, corresponding to an altitude of ~750m; and (e–f) winds on the 850mbar pressure level, corresponding to an altitude of ~1500m. The green circle marks the location of ODP Hole 642B in the Norwegian Sea (67°N, 3°E).

4.4   Discussion

4.4.1   Vegetation and climate evolution during the Pliocene

During the early Zanclean (5.03–4.51 Ma), the prevalence of cool temperate deciduous to mixed forests in northern Norway is indicated by the high abundance of *Pinus* pollen and the presence of thermophilic taxa (e.g. *Carpinus*, *Carya*, *Sciadopitys* and *Quercus*) (Figure 4.1). Whether pure deciduous or mixed forests existed in the lowlands of the Scandinavian mountains is not clear from the pollen signal due to the low abundances of deciduous elements. The latter is an artefact of the distance of the site from the shore which also results in the over-representation of *Pinus* pollen (Chapter 3) (Heusser and Balsam, 1985; Mudie and McCarthy, 2006). Cooler intervals at c. 4.90–4.85 Ma, 4.72 Ma and 4.63 Ma are marked by lower abundances of *Sciadopitys* pollen and higher

proportions of *Sphagnum* spores, suggesting the development of peatlands at higher altitudes as a result of a southward shift of vegetation zones and lowering of the treeline (Figure 4.4). Around 4.90–4.80 Ma, glacial expansions have been inferred from IRD deposits in the Nordic Seas and also around Antarctica (De Schepper et al., 2014 and references therein). In the Norwegian Sea, IRD deposits point to the presence of sea-terminating glaciers somewhere around the Nordic Seas at 5.0–4.9 Ma (Fronval and Jansen, 1996; Mangerud et al., 1996). Dinocyst assemblage changes from Hole 642B reveal the influence of warm temperate Atlantic water in the Norwegian Sea. Around 4.90 Ma, a slight cooling is evident in the warm/cold index (De Schepper et al., 2015). The prevalence of boreal forests in northern Norway around 4.90 Ma suggests that an extensive glaciation in Scandinavia is unlikely (Figure 4.1). However, variable climatic conditions between 5.03 and 4.51 Ma as seen in the abundance changes of *Sciadopitys* pollen and *Sphagnum* spores are in agreement with repeated cooling phases and related expansions of small-scale glaciations around the Nordic Seas (Fronval and Jansen, 1996).

At Hole 642B, very low PARs occur between 4.51 and 4.37 Ma (Figure 4.1, 4.2; see section 4.4.3 for discussion). The first sample above this interval contains high proportions of Ericaceae, *Pinus* and *Tsuga* pollen as well as *Huperzia* and *Sphagnum* spores, suggesting the presence of boreal forests and tundra environments in northern Norway. This interpretation should, however, be regarded with caution due to the low pollen counts. A subsequent increase in *Sciadopitys* pollen suggests the prevalence of cool temperate mixed forests – conditions similar to those before the interval with low PARs. A cooling is seen at 4.30 Ma by the development of herb fields/heathlands, consisting of Asteraceae, Ericaceae and *Lycopodium*, at higher altitudes, which is accompanied by a decline and subsequent absence of thermophilic elements (Figure 4.1). This cooling was possibly initiated by the development of a modern-like NwAC between 4.50 and 4.30 Ma that spread cooler but still temperate waters across the Norwegian Sea (De Schepper et al., 2015). At Hole 642B, the presence of the NwAC is indicated by the appearance of the dinocyst cyst of *Protoceratium reticulatum*, which is a tracer of Atlantic water in the Nordic Seas, and a prolonged decrease in the warm/cold index (Figure 4.6) (De Schepper et al., 2015). At ODP Site 907 in the Iceland Sea, the gradual disappearance of dinocyst species between 4.50 and 4.30 Ma is reflective of decreasing water temperatures and salinity due to the establishment of a proto-EGC (Schreck et al., 2013). The increased export of cool Arctic waters into the Nordic Seas
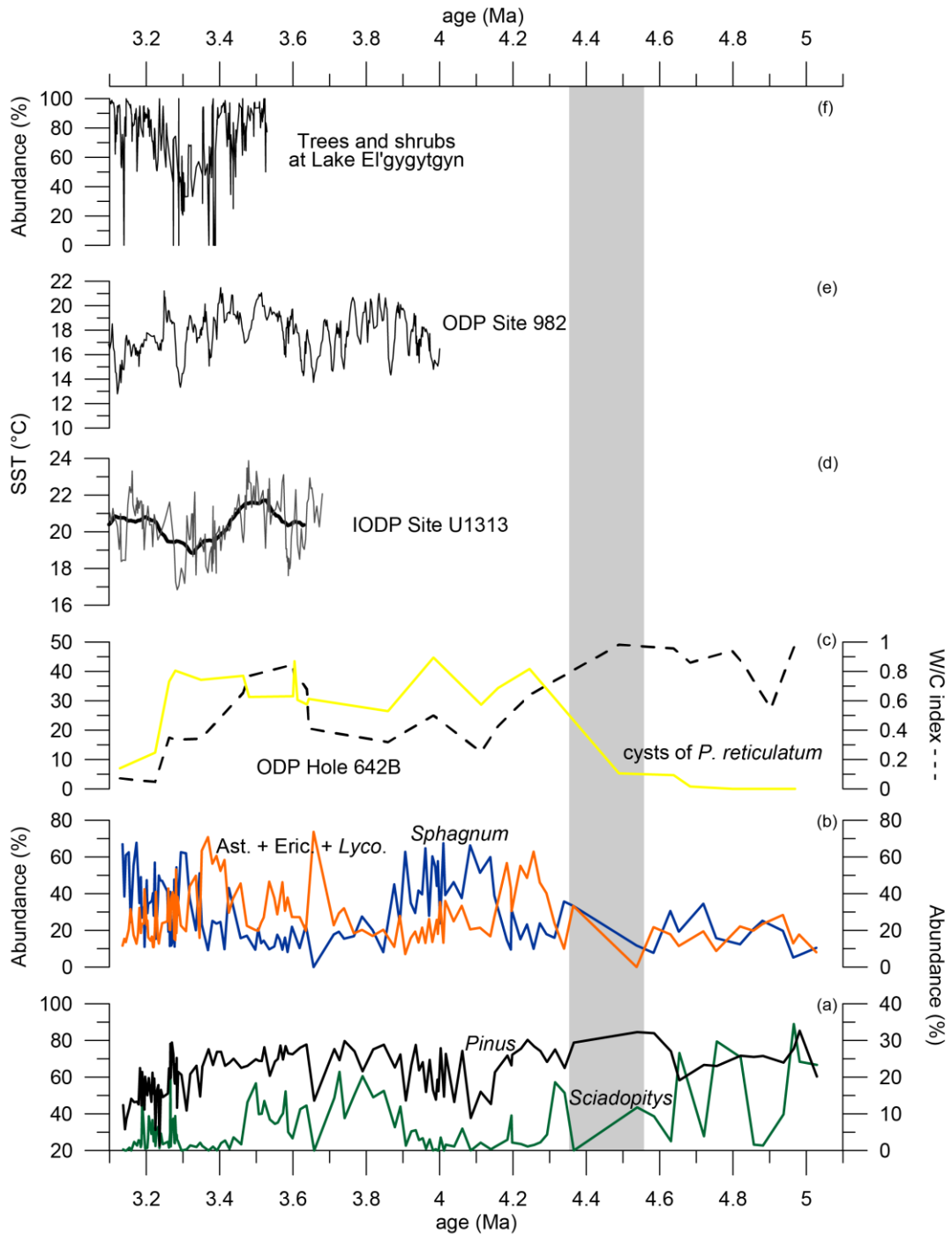
Figure 4.6: Comparison of (a–b) relative abundance changes of selected pollen data from ODP Hole 642B to other Pliocene marine and terrestrial proxy records in the Northern Hemisphere. (a–b) Relative abundance changes of *Pinus* pollen (black), *Sciadopitys* pollen (green), *Sphagnum* spores (blue) and the sum of Asteraceae and Ericaceae pollen and *Lycopodium* spores (orange); (c) relative abundance changes the dinocyst cyst of *Protoceratium reticulatum* (yellow) and the warm (W)/cold (C) water index (De Schepper et al., 2015); (d) alkenone-derived sea surface temperature (SST) estimates at IODP Site U1313 (grey) and the 100 ka moving average (Naafs et al., 2010); and (f) relative abundance changes of trees and shrubs at Lake El'gygytgyn in NE Siberia (Andreev et al., 2014). The grey bar highlights the interval with low pollen accumulation rates and counts.

109

via a modern-like EGC has been linked to the shoaling of the CAS which led to an increased North Pacific sea level relative to the Atlantic and reversed the water flow through the Bering Strait (De Schepper et al., 2015; Sarnthein et al., 2009; Schreck et al., 2013; Verhoeven et al., 2011). A cooling is also observed in the decrease in thermophilic trees and increase in herb taxa in Mediterranean pollen records around 4.50 Ma (Suc et al., 1995a, 1995b).

At 4.15 Ma, peatlands start to expand at the expense of herb fields/heathlands, and boreal forests prevail until 3.90 Ma in northern Norway. In the Norwegian Sea, an increase in cold water species across this interval is indicative of a continuous cooling (Figure 4.6) (De Schepper et al., 2015). After 4.20 Ma, harsh surface and/or deep water conditions at Site 907 prevent the deposition and/or preservation of dinocysts (De Schepper et al., 2015; Schreck et al., 2013). In northern Norway, this cooling phase is interrupted at 3.90 Ma, when the expansion of diverse mixed forests vegetation is indicative of the re-establishment of cool temperate conditions in the area (Figure 4.1). This warming coincides with the emergence of seasonal Arctic sea ice in the Eurasian sector of the Arctic Ocean (Knies et al., 2014a). The enhanced export of sea ice might have counterbalanced the northward heat transport by a stronger AMOC (Knies et al., 2014a), which in turn resulted in warmer climatic conditions in Scandinavia. This is supported by Pliocene stable oxygen and carbonate isotope records from Hole 642B, which are indicative of the presence of a warmer NwAC between 4.0 and 3.65 Ma (Risebrobakken et al., 2016).

The early Piacenzian pollen assemblages of Hole 642B reflect the presence of diverse cool temperate mixed forests in northern Norway which is indicated by the high abundance of coniferous taxa excluding *Pinus*. Temperate climatic conditions in Scandinavia between 3.60 and 3.47 Ma correspond to SSTs up to 6°C higher than present in the North Atlantic and Mediterranean Sea (Figure 4.6) (Herbert et al., 2015; Lawrence et al., 2009; Naafs et al., 2010). High SSTs along the path of the NAC are indicative of the northward transport of warm surface waters during the early Piacenzian (Lawrence et al., 2009; Naafs et al., 2010). At 3.48–3.47 Ma, a distinct cooling of ~4°C is observed in alkenone-derived SST estimates at IODP Site U1313 which is located at the north-eastern edge of the subtropical gyre (Figure 4.6). This cooling is followed by a short warming of less than 2°C at 3.45 Ma. A subsequent gradual decline in SSTs suggests a weakened NAC and thus northward heat transport (Naafs et al., 2010). At Hole 642B, a sharp decline in the relative abundance of coniferous trees and shrubs

excluding *Pinus* between 3.48 and 3.46 Ma, which leads to the predominance of boreal forest and subarctic climate conditions in northern Norway, coincides with the initial decrease in SSTs at Site U1313. A weakening of the NAC and northward heat transport might have led to a reduced influence of Atlantic water in the Nordic Seas, causing the establishment of boreal forests in the lowlands of the Scandinavian mountains and herb field/heathlands at higher altitudes in northern Norway. A northward shift of the NAC and accompanied re-establishment of northward heat transport is inferred from an increase in SSTs and dinocyst assemblages changes at several sites in the North Atlantic, corresponding to the onset of warm climatic conditions during the mPWP (3.264–3.025 Ma) (De Schepper et al., 2013; Dowsett et al., 2010; Naafs et al., 2010). This is in agreement with a return of cool temperate forests to northern Norway. Climatic conditions seem to be slightly colder in comparison to those before 3.47 Ma, as seen in colder average temperatures at Site U1313 and a lower relative abundance of *Sciadopitys* in the pollen assemblages of Hole 642B (Figure 4.6). Cool temperate to boreal climatic conditions prevail in northern Norway between 3.29 and 3.18 Ma. Peatlands at higher altitudes are a common part of the vegetation which is reflected in the high abundances of *Sphagnum* spores. The expansion of peatlands and decline in the prevalence of boreal forests are indicative of the cooling climate before the onset of NHG (Chapter 3).

As opposed to the repeated occurrence of prolonged warmer and cooler intervals during the Piacenzian in northern Norway, a long-term cooling of alkenone-derived SSTs at ODP Site 982 in the northern North Atlantic, starting at 3.5 Ma, is indicative of a gradual change of climate before the intensification of NHG (Lawrence et al., 2009). At Site 982, which is situated further north than Site U1313 in the path of the NAC just before it enters the Norwegian Sea, obliquity-driven high-amplitude SST variations during the Piacenzian are superimposed by a long-term cooling trend (Figure 4.6) (Lawrence et al., 2009). Lawrence et al. (2009) propose that the high amplitude variations at Site 982 were caused by changes in the position of the westerlies as a result of orbitally forced insolation changes. Slight displacements in the westerlies would have affected the position of the NAC and thus resulted in high-amplitude SST variations at Site 982 (Lawrence et al., 2009). The continuous cooling trend from 3.5 Ma onwards is in contradiction to the long-term SST evolution at Site U1313 and related changes in the strength of the NAC (Lawrence et al., 2009; Naafs et al., 2010). Naafs et al. (2010) suggest that the SST record from Site 982 either reflects displacements of the northern

end of the NAC or that the discrepancies might be explained by uncertainties in the age model for Site 982 (see Khélifi et al., 2012; Lawrence et al., 2013). Assuming that age model uncertainties between c. 3.5 and 3.3 Ma are negligible, the different climatic signal derived from Site 982 when compared to Site U1313 and 642 might be a result of the strong impact of the westerlies on SSTs at Site 982, modulating the position of the NAC.

In NE Siberia, a similar pattern to the climatic changes observed at Hole 642B and Site U1313 is recorded in the relative abundance changes of trees and shrubs in the vicinity of Lake El'gygytgyn (Figure 4.6) (Andreev et al., 2014). While the vegetation opens around c. 3.47 Ma and c. 3.45 Ma, a pronounced decline in the relative abundance of trees and shrubs does not take place until c. 3.39 Ma. Warmer conditions establish after c. 3.28 Ma, with relative abundances of trees and shrubs accounting for >50%. The similarity between the different records suggests that these climatic changes occurred across the Northern Hemisphere (Chapter 3).

Changes in vegetation and climate are also recorded in northwestern Africa around 3.48 Ma, with warmer and wetter conditions prevailing before and drier climatic conditions after 3.48 Ma (Leroy and Dupont, 1994, 1997). In northwestern Africa, a dry phase between 3.44 and 3.40 Ma shows a non-analogue vegetation which is characterised by high abundances of Asteraceae Liguliflorae in the pollen spectra (Leroy and Dupont, 1997). This phase coincides with cooler and possibly drier climatic conditions inferred from the appearance of Asteraceae Liguliflorae in the Hole 642B pollen record (Figure 4.1). The first extensive aridification in northwestern Africa at 3.26 Ma corresponds to the onset of the mPWP, and is marked by the establishment of cool temperate conditions in Norway. The correlation of pronounced climate changes at 3.48 Ma, 3.35 Ma, 3.27–3.26 Ma and 3.20 Ma in northwestern Africa and northern Norway highlights the hemispheric-wide extent of these changes.

4.4.2 Controls on long-term Pliocene vegetation and climate changes in northern Norway

The Pliocene pollen record from Hole 642B reveals four major changes in vegetation and climate in northern Norway, with cooler, boreal conditions developing at 4.30 Ma and 3.47 Ma and warmer, cool temperate conditions at 3.90 Ma and 3.29 Ma (Figure 4.1). These changes are indicative of repeated latitudinal shifts of the northern boundary of the deciduous forest zone. Possible controls on the long-term vegetation changes in

northern Norway, including declining atmospheric CO_2 concentrations and orbital forcing, will be discussed in the following sections.

4.4.2.1 Declining atmospheric CO_2 concentrations

Over the almost two-million-year-long record, the relative abundance of the thermophilic taxon *Sciadopitys* shows a continuous decrease in subsequent warm intervals (Figure 4.1, 4.2). At present, *Sciadopitys* is endemic to Japan where it thrives on well-drained slopes in a temperate and wet climate (Ishikawa and Watanabe, 1986). During the Neogene, *Sciadopitys* was a common element in the temperate forests of the Northern Hemisphere, forming part of lowland swamp environments to high-altitude forests (Fauquette et al., 1999; Figueiral et al., 1999; Philippe et al., 2002; Schneider, 1995). In northern Norway, the decline of this species throughout the Pliocene may be indicative of a progressive cooling of climate that is also evident in other Pliocene terrestrial and marine records (Fedorov et al., 2013; Gao et al., 2012; Herzschuh et al., 2016; Lawrence et al., 2009; Naafs et al., 2010; Verhoeven et al., 2013). This cooling is also reflected in the loadings of PC 1, showing an overall increase between 5.03 to 3.14 Ma (Figure 4.2). Decreasing atmospheric CO_2 concentrations have been suggested to be the main driver for the cooling throughout the Pliocene and the onset of NHG (Bartoli et al., 2011; DeConto et al., 2008; Lunt et al., 2008a; Martínez-Botí et al., 2015; Pagani et al., 2010; Seki et al., 2010; Tripati et al., 2009). However, the identification of a continuous decline in atmospheric CO_2 values in proxy records is difficult due to wide ranges, with values between ~270 and 400 ppm, and variations between proxies (Badger et al., 2013; Bartoli et al., 2011; Martínez-Botí et al., 2015; Pagani et al., 2010; Seki et al., 2010).

4.4.2.2 Orbital forcing

Climate changes on orbital timescales, with a predominance of obliquity peridiocities, have been identified in Pliocene environmental records, using a variety of proxies such as benthic oxygen isotopes, alkenones and pollen and spores (Andreev et al., 2014; Lawrence et al., 2009; Lisiecki and Raymo, 2005; Willis et al., 1999b). A recent modelling study suggests that orbital forcing has a strong impact on Pliocene climate variability on glacial-interglacial timescales with strong regional differences (Prescott et al., 2014). Spectral analysis of Pliocene vegetation changes in northern Norway reveals low-frequencies cyclicity, exceeding orbital time scales and suggesting that the observed climatic changes are not predominantly orbitally controlled. Notable is, however, the influence of the long (400 ka) eccentricity cycle on the relative abundance

changes of *Pinus* pollen which is particularly pronounced between 4.2 and 4.0 Ma and 3.3 and 3.1 Ma (Figure 4.4). During these intervals, the relative abundances of *Pinus* pollen is comparatively low, reflecting cooler climatic conditions. These minima in percentages of *Pinus* pollen correspond to minima in the 400-ka eccentricity cycle (Figure 4.2). A correlation of the onset of four different climate phases in the eastern Nordic Seas to eccentricity minima and concurrent low-amplitude insolation forcing, and thus precession, has also been inferred from low-frequency changes in stable oxygen and carbon isotope records from Hole 642B (Risebrobakken et al., 2016). In southwestern Romania, Zanclean vegetation changes between 4.90 and 4.30 Ma have been related to the 100-ka as well as 400-ka eccentricity cycle, with the former showing relatively low-amplitude changes (Popescu, 2001; Popescu et al., 2006). In this record, higher abundances of thermophilic (altitudinal) trees correspond to eccentricity maxima (minima) (Popescu et al., 2006). This relationship is the opposite to that observed at Hole 642B. However, in northwest Europe, cool periods during the Middle Miocene show a correlation to minima in the 400-ka eccentricity band (Utescher et al., 2012). The same relationship is documented in Miocene benthic stable oxygen isotope changes from ODP Site 1085 in the southereastern Atlantic, with middle to late Miocene glacial events corresponding to 400-ka eccentricity minima (Westerhold et al., 2005), as well as late Pliocene/early Pleistocene alkenone-derived SST changes in the Mediterranean Sea (Herbert et al., 2015). The magnitude of glacial expansion during 400-ka eccentricity minima has been suggested to be linked to low-amplitude variations in obliquity (Zachos et al., 2001) and precession (Herbert et al., 2015). At Hole 642B, low abundances of *Pinus* pollen between 4.2 and 4.0 Ma and 3.3 and 3.1 Ma are not only associated with 400-ka eccentricity minima but also with relatively low-amplitude variations in obliquity and precession, suggesting that the observed cooler intervals may be a response to the concurrence of eccentricity minima and low-amplitude obliquity and/or precession changes (Figure 4.2). The presence of the 400-ka eccentricity cycle in the Pliocene pollen record from Hole 642B supports the finding of a strong 400-ka signal in oxygen and carbon isotope records predating the onset of NHG (Clemens and Tiedemann, 1997; Westerhold et al., 2005; Zachos et al., 2001). De Boer et al. (2014) show that the pre-NHG 400-ka cycles are predominated by variations of the Antarctic ice sheet which are obscured during the Late Pleistocene by the variability of the Northern Hemisphere ice sheets. While an eccentricity forcing appears to be present in the Pliocene vegetation changes in northern Norway, the signal seems to be masked by

palaeogeographic and palaeoceanographic in the North Atlantic and Nordic Seas region (see also Risebrobakken et al., 2016).

4.4.3 Effects of the shoaling of the Central American Seaway on oceanographic and/or atmospheric circulation

During the early Zanclean, the pollen record of Hole 642B shows a pronounced decline in PARs, suggesting changes in pollen transport, deposition and/or preservation. At 4.56 Ma, PARs drop from very high (~7500–19,300 grains/(cm^2 ka)) to very low values (< ~100 grains/(cm^2 ka)). After 4.35 Ma, PARs slowly recover and subsequent peaks reach maximum values of ~12,700 grains/(cm^2 ka) (Figure 4.2). The main question is whether these changes are a result of taphonomic processes or oceanographic and/or atmospheric changes related to the shoaling of the CAS between 4.7 and 4.2 Ma (Haug et al., 2001).

Factors affecting transport, deposition and preservation of pollen grains in marine sediments, include pollen production, direction of prevailing winds, river transport, direction of marine currents, marine primary productivity, oxygen content and temperature of the water and time elapsing until deposition and burial (Bottema and Van Straaten, 1966; Dupont, 2011). There is no clear link between higher PARs and warmer intervals, suggesting that the changes in PARs are not only related to terrestrial productivity (Figure 4.2). The sharp decline in PARs at 4.56 Ma is unlikely to have been caused by changes in pollen production only, as the composition of pollen assemblages just before and after the interval with low PARs are very similar. Additionally, fluctuations between warmer and cooler intervals are evident throughout the subsequent Pliocene section and are not associated with major changes in PARs.

4.4.3.1 Influence of sedimentation rate, oxidation and primary productivity on pollen deposition and preservation

In marine sediments, pollen are generally well preserved in areas with low dissolved oxygen content and rapid sedimentation, reducing the exposure time to oxygenated water (Bottema and Van Straaten, 1966; Heusser and Balsam, 1977; Keil et al., 1994). Both, low oxidant concentrations and short oxidation exposure times result in a rapid decrease in pollen concentrations (Lebreton et al., 2010). Primary productivity can also affect pollen deposition and preservation, with a higher productivity, particularly in upwelling areas, resulting in a more effective sinking of particles and the presence of

less oxygenated bottom waters due to stronger decay of organic matter (Dupont, 2011 and references therein).

In the sediments of Hole 642B, pollen concentrations and PARs show a relatively good correlation to sedimentation rate (Figure 4.2), supporting the notion that preservation of organic material is positively related to sedimentation rate (Müller and Suess, 1979). Higher concentrations before 4.56 Ma may be indicative of the presence of less well oxygenated bottom water. Carbonate isotope ratios of planktonic and benthic foraminifera from Hole 642B are indicative of reduced deep water ventilation in the Norwegian Sea in comparison to the Holocene between 5.05 and 4.65 Ma (Risebrobakken et al., 2016). The authors relate the reduced ventilation to increased heat transport to the Arctic Ocean and reduced input of brine water as a result of a subaerially exposed Barents Sea. The carbonate isotope values might also have been influenced by a higher primary productivity and increased respiration between 5.05 and 4.65 Ma, as indicated by peaks in dinocyst and acritarch accumulation rates at the same site (De Schepper et al., 2015; Risebrobakken et al., 2016). As the relationship is not constant, increased ocean-atmosphere gas exchange and reduced bottom water ventilation are suggested to have had a stronger impact (Risebrobakken et al., 2016). The almost complete absence of pollen between 4.56 and 4.35 may have been caused by oxidation due to the presence of oxygenated bottom water at the site as a result of enhanced overturning. At Hole 642B, an increase in bottom water ventilation between 4.65 and 4.40 Ma, reaching values closer to the Holocene mean, corresponds to the subsidence of the Hovgård Ridge in the Fram Strait and the shoaling of CAS which both presumably resulted in an increased AMOC (Haug and Tiedemann, 1998; Haug et al., 2001; Knies et al., 2014b; Risebrobakken et al., 2016; Sarnthein et al., 2009). The changes in stable oxygen and carbonate isotope values, and dinocyst and acritarch accumulation rates at Hole 642B are also indicative of a gradual reduction in primary productivity and decay of organic matter (De Schepper et al., 2015; Risebrobakken et al., 2016). Thus, enhanced ventilation and lower primary productivity might have contributed to the lack of pollen between 4.56 and 4.35 Ma.

4.4.3.2 Changes in wind direction and/or strength

The predominant mode of pollen transport largely depends on the regional climate and the distance of the site from the source area (Mudie and McCarthy, 2006). In marine sediments, high pollen concentrations (5000–10,000 grains/cm^3) are usually found off the mouth of large rivers (Heusser and Balsam, 1977; Hooghiemstra et al., 2006). In

case of the presence of a prevailing wind system (e.g. westerlies, trade winds), aeolian transport accounts for high pollen influxes to marine sediments and past changes in influx can be used to reconstruct wind strength (Hooghiemstra et al., 2006; Leroy and Dupont, 1994; Mudie and McCarthy, 2006). Wind, and to a minor degree ocean currents, are suggested to be the main transport media of pollen to Hole 642B due to the predominance of wind-pollinated pollen (Chapter 3). River transport is negligible as there is no evidence for large river systems in Norway during the Pliocene, and further because of the distance of the site from the shore.

At present, the main atmospheric circulation pattern in the North Atlantic region is determined by the difference in pressure between the subtropical Azores high and the subpolar Icelandic low (Budikova, 2009; Furevik, 2000). Changes in the mean sea-level pressure fields – the North Atlantic Oscillation (NAO) – strongly affect ocean surface circulation. Together with the effect of deep-water formation and an estuarine circulation, wind stress is the main driver for the inflow of Atlantic water into the Nordic Seas (Furevik, 2000). In northern Norway, the prevailing winds change seasonally, with easterly to northeasterly winds predominating during summer and westerly to southwesterly winds prevailing during winter (Furevik, 2000; Hall, 2003). However, changes in the prevailing wind direction with the strongest effects during winter also occur over decadal timescales in response to major atmospheric circulation shifts (Furevik, 2000; Ottersen et al., 2001; Trigo et al., 2002). During positive NAO years, enhanced wind stress over the Nordic Seas causes a stronger inflow of Atlantic water into the Norwegian Sea and a narrowing of the NwAC (Blindheim et al., 2000; Furevik, 2000). The enhanced wind stress over the North Atlantic is associated with increased heat loss and thus cooling of the upper ocean which leads to inflow of cooler Atlantic water into the Norwegian Sea (Delworth and Dixon, 2000; Furevik, 2000). Simulations for the Piacenzian suggest that wind strength in the North Atlantic was stronger than present (Haywood et al., 2000; Li et al., 2015). A modelling study testing the climate effects of reduced sea ice shows a weakening of polar easterlies and enhanced cyclonic circulation over the Nordic Seas (Raymo et al., 1990). Lawrence et al. (2009) suggest that the Piacenzian high amplitude variations in SST estimates in the northern North Atlantic are caused by changes in the position of the NAC due to latitudinal shifts of the strongest westerlies. However, a compilation of observational and modelling studies highlights that a weakening of the meridional temperature gradient together with warmer air masses above the Arctic in a warmer climate may

117

lead to a weakening and southward displacement of the westerlies (Budikova, 2009). In the absence of a strong meridional and zonal oceanic temperature gradient during the early Zanclean, prevailing easterlies could explain the high PARs at Hole 642B. This is supported by a study on atmospheric circulation in Europe during the late Miocene based on vegetation reconstructions and model simulations, showing that westerlies mainly affected mainland Europe, with relatively weak easterly winds in northern Europe (Quan et al., 2014). Changes in the prevailing wind direction might have occurred with the establishment of a cooler proto-EGC and modern-like NwAC in the Nordic Seas around 4.50–4.30 Ma which was accompanied by the development of a stronger zonal temperature gradient (De Schepper et al., 2015). In the pollen record from Hole 642B, this may be reflected in the sharp decline in PARs at 4.56 Ma, suggesting limited pollen transport to the site.

To test the hypothesis of atmospheric circulation changes affecting pollen transport to Site 642, simulations of vector mean winds during spring for three different altitudes were compared from experiments with an OCAS and CCAS (see section 2.5.1.5 and 4.3.4; Figure 4.5). In the OCAS experiment, winds at lower altitudes (10m and ~750m) predominately come from the southeast, indicating that the pollen source area is central and southern Norway. The stationary front located to the south of the core location in all OCAS simulations may facilitate the sinking of pollen towards the sea surface (Figure 4.5). In the CCAS experiment, the low-wind-velocity zone extends northward and is situated to the east of the site location, which might inhibit the westward transport of pollen. Reduced winds speeds in central Norway and further north at the lower altitudes (10m and ~750m) in the CCAS experiment is also indicative of a hampered offshore pollen transport. At higher altitudes (~1500m) in the CCAS experiment, prevailing southwesterlies along the Norwegian coast and northerly winds above the site suggest a restricted pollen transport to the Site 642 (Figure 4.5). Thus, the combination of an extended stationary front to the east of the site location, reduced wind speeds and southwesterly winds with increasing altitude in the CCAS experiment create unfavourable conditions for pollen transport from Norway to Site 642. These simulations suggest that the main atmospheric circulation changed above Norway and the Norwegian Sea in response to the closure of the CAS, with wind directions being more favourable for pollen deposition at Site 642 when the CAS is open. With PRISM2 boundary conditions (see section 2.5.1.5), the OCAS experiment is, however, not a true representation of the Zanclean environment, mainly with regard to the size of Northern

Hemisphere ice sheets and the meridional temperature gradient. Nevertheless, the experiments show that the closure of the CAS has a pronounced effect on the prevailing wind directions in Norway and the Norwegian Sea.

4.4.4 Pliocene climatic changes in relation to the late Neogene climate evolution

In northern Norway, Pliocene vegetation and climate changes show distinct climate phases lasting between ~520 and 120 ka that are characterised by prevailing cool temperate, warmer-than-present or boreal, similar-to-present climates. Within these intervals, the climate variability is high, which is particularly expressed in marked abundance changes of the temperate taxon *Sciadopitys* and *Sphagnum* spores, with the latter being indicative of the distribution of peatlands and thus cooler/wetter climatic conditions (Figure 4.6). Highest abundances of *Sciadopitys* pollen during the early Zanclean suggest the occurrence of warmest climatic conditions during the studied interval. This is supported by dinocyst assemblages from the same site which are indicative of warm temperate conditions in the Norwegian Sea during the early Zanclean and a subsequent cooling of the water masses (Figure 4.6) (De Schepper et al., 2015). A low-resolution study of Oligocene to Pleistocene pollen assemblages in the sediments of DSDP Site 338 north of the Vøring Plateau in the Norwegian Sea shows a continuous decline in the proportions of angiosperm pollen and thus deciduous trees in the vegetation of Norway, suggesting a long-term cooling of climate (Koreneva et al., 1976). This is in agreement with the predominance of gymnosperm pollen in the Pliocene sediments of Hole 642B and the gradual decline in the relative abundance of *Sciadopitys* pollen (Figure 4.1). The long-term cooling of climate in northern Norway during the Pliocene supports the notion that the warmth of the Pliocene represents a portion of a gradual late Neogene cooling trajectory (LaRiviere et al., 2012; Mudelsee et al., 2014) instead of a reversal of that trend (Sniderman et al., 2016). However, a more detailed study of Miocene vegetation changes in Norway is required to evaluate the long-term Neogene terrestrial climate evolution in the subarctic Nordic Seas region.

4.5 Conclusions

The Pliocene pollen record (5.03–3.14 Ma) from ODP Hole 642B, reflecting vegetation changes in northern Norway, represents the first complete Pliocene record of terrestrial climatic changes. Prolonged warmer-than-present and cooler, more similar to present, climate phases are characterised by the prevalence of cool temperate and boreal forests, respectively. A long-term cooling of climate is indicated by the gradual decrease of the relative abundances of *Sciadopitys* pollen during subsequent warm phases, which may

be related to declining atmospheric CO_2 concentrations throughout the Pliocene. The development of boreal forest and peatlands at higher altitudes during cooler intervals coincides with minima in the 400-ka eccentricity cycle and low-amplitude variations in obliquity and precession. The following climate phases and their relation to palaeoceanographic and palaeoclimatic changes are inferred from the pollen record:

- 5.05–4.51 Ma: Cool temperate mixed forests prevail in northern Norway under a warmer-than-present climate. Boreal forests develop around 4.90 Ma, indicating subarctic climatic conditions. This cooling might be associated with a globally recognised cooling event that led to glacial expansion in the Arctic and Antarctica (De Schepper et al., 2014).

- 4.51–4.30 Ma: An interval with very low PARs between 4.51 and 4.37 Ma precludes the inference of vegetation and climate changes. The presence of boreal forests and tundra environments may be inferred from the few encountered pollen. Subsequently, cool temperate climatic conditions – similar to those before the interval with low PARs – are evident from the pollen assemblages.

- 4.30–4.15 Ma: Boreal forests persist in the lowlands of the Scandinavian mountains and herb fields/heathlands develop at higher altitudes, suggesting the establishment of subarctic climatic conditions in northern Norway. The cooling is possibly associated with the development of a modern-like NwAC and circulation pattern in the Nordic Seas as a result of the shoaling of the CAS and onset of Pacific-to-Arctic water flow through the Bering Strait (De Schepper et al., 2015).

- 4.15–3.90 Ma: Boreal forests prevail and peatlands expand at the expanse of herb fields/heathlands, suggesting cooler and/or wetter climatic conditions in northern Norway not unlike modern.

- 3.90–3.47 Ma: The re-establishment of cool temperate forests is indicative climate warming, which is possibly the result of sea ice expansion in the Arctic and the related enhancement of the overturning circulation and northward heat transport (Knies et al., 2014a). Warmer-than-present climatic conditions in northern Norway correspond to higher-than-present SSTs in the North Atlantic and Mediterranean Sea.

- 3.47–3.35 Ma: The persistence of cooler, boreal climatic conditions is evident from the prevalence of boreal forests and herb fields/heathlands at higher

altitudes. The cooling at 3.47 Ma coincides with a reduction in northward heat transport via the NAC. Concurrent vegetation changes in NE Siberia and NW Africa suggest a hemispheric-wide extent.

- 3.35–3.14 Ma: Peatlands expand and the prevalence of boreal forest declines, suggesting long-term cooling before the onset of NHG. A re-establishment of cool temperate climatic conditions at 3.29 Ma corresponds to a re-invigoration of the NAC and the onset of the mPWP.

The Hole 642B Pliocene pollen record is marked by a sharp decline in PARs at 4.56 Ma. Pollen accumulation does not recover until 3.35 Ma, with values remaining below those attained during the early Zanclean. Marine primary productivity is high and bottom water ventilation is reduced compared to the Holocene mean during the early Zanclean (Risebrobakken et al., 2016), possibly favouring pollen deposition and preservation at the site. A slight increase in ventilation and/or reduction in primary productivity between 4.65 and 4.40 (Risebrobakken et al., 2016) might have contributed to low PARs. Climate model experiments suggest that changes in the main atmospheric circulation pattern during spring as a consequence of the closure of the CAS might have inhibited pollen transport to the site. In these experiments, the closure of the CAS results in the presence of a stationary front east of the site, reduced wind speeds and the prevalence of southwesterly winds with increasing altitude, creating unfavourable conditions for offshore pollen transport.

Chapter 5: Reconstruction of mid-Piacenzian Norwegian Atlantic Current variability using marine palynomorphs

5.1 Introduction

As the most recent prolonged warm period in the Earth's history that exhibits similarities to climatic conditions predicted for the end of the 21st century, the mPWP (3.264–3.025 Ma) has been the focus of proxy reconstructions and climate modelling to compile a comprehensive picture of the magnitude and spatial scale of climatic changes and their drivers (Dowsett et al., 2016; Haywood et al., 2016). During the mPWP, global annual surface temperatures were 2.7–4.0°C higher than present, with estimates for atmospheric CO_2 concentration ranging between 270–410 ppm (Badger et al., 2013; Bartoli et al., 2011; Haywood et al., 2013b; Martínez-Botí et al., 2015; Seki et al., 2010). The most recent environmental reconstruction of the mPWP, the PRISM 4, highlights the need for high-resolution multi-proxy records with a regional and process-oriented approach (Dowsett et al., 2016). These are needed to provide a more complete palaeoenvironmental reconstruction and gain a better understanding of the climate variability within the mPWP (Dowsett et al., 2016, 2013b). Furthermore, there is significant disagreement between data and models over the magnitude of warming and degree of climate variability in the mPWP, highlighting the need for further investigations (Dowsett et al., 2013a; Haywood et al., 2013a; Salzmann et al., 2013).

In the Nordic Seas, proxy-based reconstructions reveal an enhanced SST increase when compared to low-latitude sites during the mPWP (Dowsett et al., 2013a; Robinson, 2009), which has often been ascribed to an increased northward heat transport via a stronger AMOC (Ravelo and Andreasen, 2000; Raymo et al., 1996). However, recent modelling and proxy studies suggest that radiative forcing due to increased greenhouse gas levels and palaeogeographic changes could account for the amplified warming in the Nordic Seas (Bachem et al., 2016; Hill, 2015; Risebrobakken et al., 2016; Zhang et al., 2013a, 2013b). The magnitude of warming varies between proxies and sites. At ODP Site 907 (69°N) in the Iceland Sea, the reconstruction of summer SSTs using the Mg/Ca ratio yields values 3–5°C higher than present (Robinson, 2009). An estimate of annual SSTs derived from alkenones at the same site is ~5°C higher than today (Schreck et al., 2013). At ODP Site 909 (79°N) northwest of Svalbard, summer SSTs using alkenones and the Mg/Ca ratio have been estimated to be ~11–18°C higher than present (Robinson, 2009). A warming of annual SSTs of 3–4°C is inferred from the distribution

of GDGTs at the nearby Site 910 (80°N) (Knies et al., 2014a). The warming is least pronounced in the Norwegian Sea. There, alkenone-derived summer SST estimates for the mPWP show an increase of 2–3°C in comparison to the Holocene average, with an obliquity-driven SST variability of up to 4°C (Bachem et al., 2016). Bachem et al. (2016) suggest that the inflow of warm Atlantic water into the Norwegian Sea via the NAC was similar to present and that radiative forcing is the main cause for the higher-than-present SSTs.

In the North Atlantic, variations in the strength and position of the NAC recorded in dinocyst assemblage changes and SST records have been suggested to have had a strong impact on high-latitude climate during the onset of the mPWP and the preceding glacial MIS M2 (c. 3.3 Ma) (De Schepper et al., 2013). The authors propose that a weakened NAC halted northward heat transport prior to the global ice volume expansion during MIS M2, whereas the re-establishment of an active, modern-like NAC corresponds to the onset of the mPWP (De Schepper et al., 2013). In northern Norway, the climate was too warm for the persistence of sea-terminating glaciers, even during MIS M2. There, fluctuations between cool temperate to boreal conditions occurred during the mPWP, indicating highly variable climatic conditions (Chapter 3). It remains unclear whether the Scandinavian terrestrial realm (vegetation, glaciers) and Nordic Seas SST changes are linked to variations in the inflow of Atlantic water into the Norwegian Sea or can merely be explained by insolation changes. In particular, evidence for changes in the inflow of Atlantic water and its effects on terrestrial climate is missing for the Norwegian Sea – a region crucial for heat exchange between the North Atlantic and Arctic Ocean.

Here, we integrate oceanographic and terrestrial environmental reconstructions in the Norwegian Sea region over a ~180 ka (3.320–3.137 Ma) time interval that covers MIS M2 to the beginning of MIS KM2 in order to investigate land-ocean interactions, enabling the identification of oceanographic and/or atmospheric forcing. This study presents a new record of dinocyst assemblage changes in the sediments of ODP Site 642 which will be compared with the pollen record (Chapter 3) as well as alkenone-derived SSTs and IRD records from the same site (Bachem et al., 2016). The aim is to build a conceptual model of marine and terrestrial environmental changes during the mPWP to advance our understanding of the processes (e.g. ocean current and/or orbitally forced insolation changes) that drive the observed climatic changes.

5.2 Dinoflagellate cyst and acritarch analysis

Dinocysts and acritarchs were analysed in 44 samples from ODP Hole 642B taken between 68.45 and 66.95 mbsf. Dinocysts and acritarchs were counted along with pollen and spores (Chapter 2, 3) on the same slides. At least 300 dinocysts were identified for each sample. Cysts of *Protoceratium reticulatum* with short processes were counted separately in 34 samples as their proportions are an indication of the salinity of the water masses, with process length being positively correlated to salinity (Jansson et al., 2014). The relative abundance of taxa is described as dominant (>60%), abundant (60–30%), common (30–10%), rare (10–1%) or present (1–0%) (Matthiessen, 1995).

5.3 Results

5.3.1 Dinoflagellate cyst assemblages

In ODP Hole 642B, 71 different dinocyst taxa were encountered in the Piacenzian sediments. The number of taxa in any one sample ranges between 19 and 34, showing a continuous decline throughout the studied interval. The highest number of taxa is recorded during MIS M1 and the lowest during MIS KM5; both are reflected in the Shannon diversity index (Figure 5.4). Selected dinocyst species are shown on Plate 5.1, 5.2, 5.3 and 5.4. Four taxa, namely cysts of *Protoceratium reticulatum*, *Filisphaera filifera*, *Habibacysta tectata* and *Spiniferites/Achomosphaera* spp. constitute between 52 to 87% of the assemblages. Other rare to common species include *Bitectatodinium raedwaldii*, *B. tepikiense*, *Lingulodinium machaerophorum*, *Impagidinium pallidum*, *Nematosphaeropsis labyrinthus*, *Pyxidinopsis braboi* and Round Brown Cysts. Together these eleven taxa always comprise at least 80% of the assemblage in any sample (Figure 5.1).

Cysts of *P. reticulatum*, *F. filifera* and *H. tectata* show marked relative abundance changes over the studied time interval (3.320 and 3.137 Ma), covering MIS M2 to the early part of MIS KM2 (Figure 5.1). During MIS M2, relative abundances of cysts of *P. reticulatum* are relatively constant between ~25–40%. Proportions of *F. filifera* are relatively high in the first half of MIS M2 with values around 10–15% and decline to values of <10% after 3.284 Ma. Relative abundances of cysts of *P. reticulatum* decline throughout MIS M1, before reaching minimum values of 8% in the first half of MIS KM6. At the start of MIS M1, percentages of *F. filifera* show a marked increase from 4 to 12% with values increasing to a maximum of 25% at 3.228 Ma within the early part
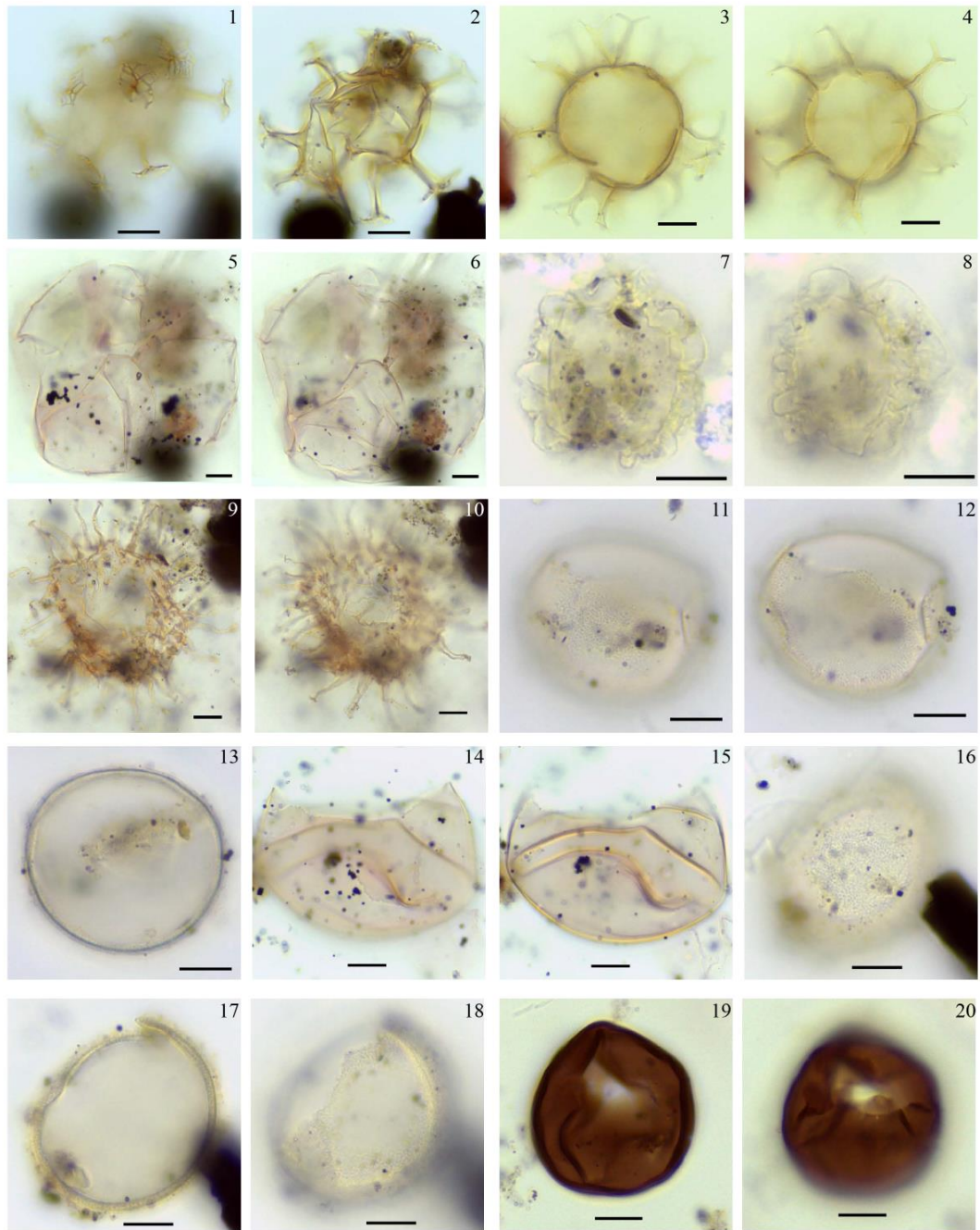
Plate 5.1: Selected dinoflagellate cysts species from ODP Hole 642B. All images were taken in bright field illumination. Sample number and England Finder coordinates are given after species name. Scale bar represents 10 μm. 1-2: *Achomosphaera andalousiensis* subsp. *suttonensis*, 9H2 55-56, T44/3; 3-4: *Achomosphaera* spp. indet, 9H2 45-46, P54/0; 5-6: *Amiculosphaera umbraculum*, 9H1 80-81, G38/3; 7-8: *Ataxiodinium choane*, 9H1 135-136, T42/4; 9-10: *Barssidinium graminosum*, 9H2 52-53, V35/2; 11-13: *Bitectatodinium raedwaldii*, 9H2 34-35, L32/0; 14-15: *Bitectatodinium serratum*, 9H1 80-81, N37/0; 16-18: *Bitectatodinium tepikiense*, 9H2 34-35, K32/2; 19-20: *Brigantedinium* spp. indet., 9H1 100-101; T34/1.
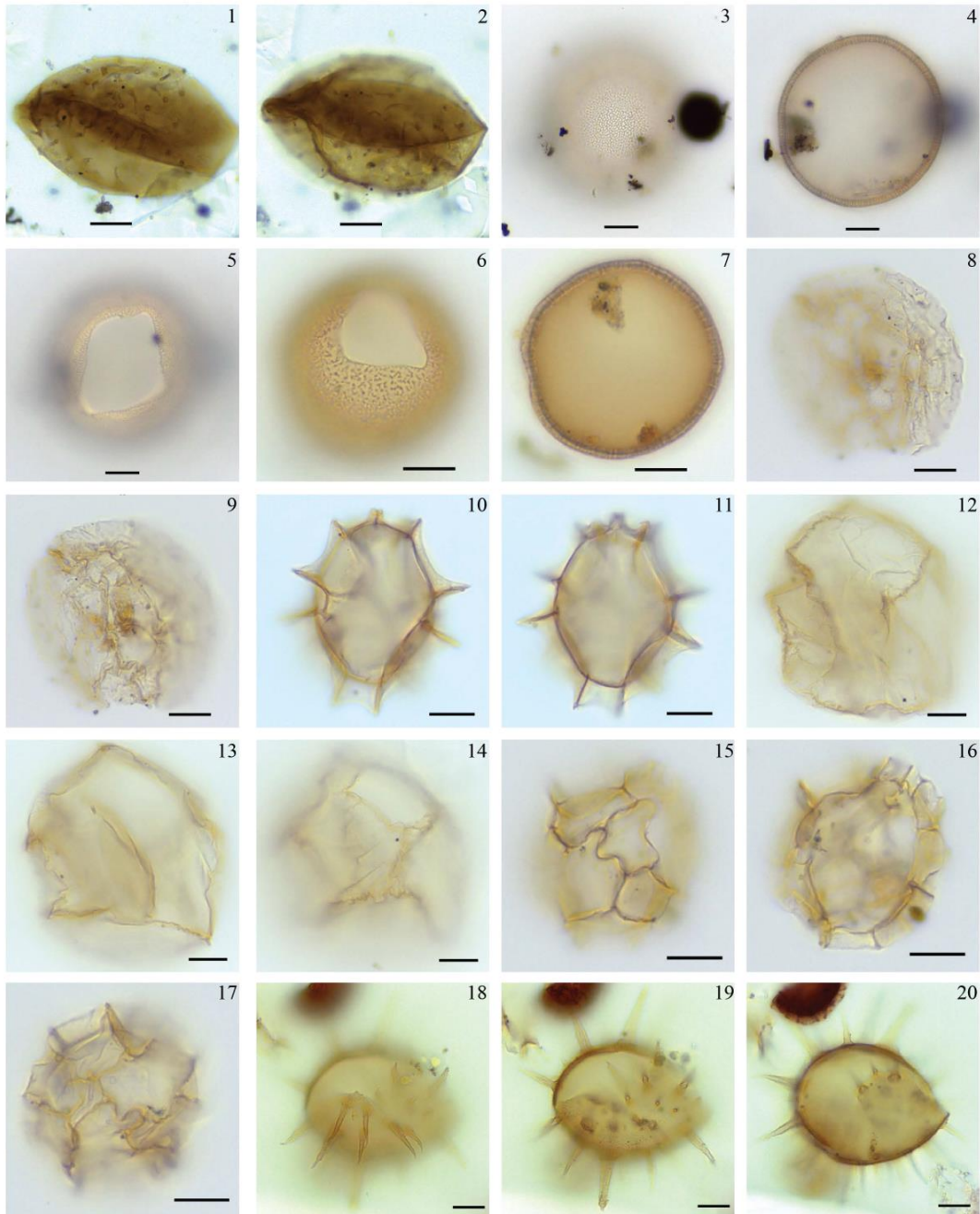
Plate 5.2: Selected dinoflagellate cysts species from ODP Hole 642B. All images were taken in bright field illumination. Sample number and England Finder coordinates are given after species name. Scale bar represents 10 µm. 1-2: *Echinidinium* spp. indet., 9H2 12-13, P38/2; 3-5: *Filisphaera filifera*, 9H2 34-35, Q44/4; 6-7: *Habibacysta tectata*, 9H1 85-86, S49/2; 8-9: *Heteraulacacysta* sp. A of Costa and Dowie (1979), 9H2 55-56, S41/1; 10-11: *Impagidinium aculeatum*, 9H2 55-56, M51/0; 12-14: *Impagidinium pallidum*, 9H2 35-36, Q36/0; 15-17: *Impagidinium paradoxum*, 9H2 55-56, N53/0; 18-20: *Lingulodinium machaerophorum*, 9H2 35-36, W42/4.
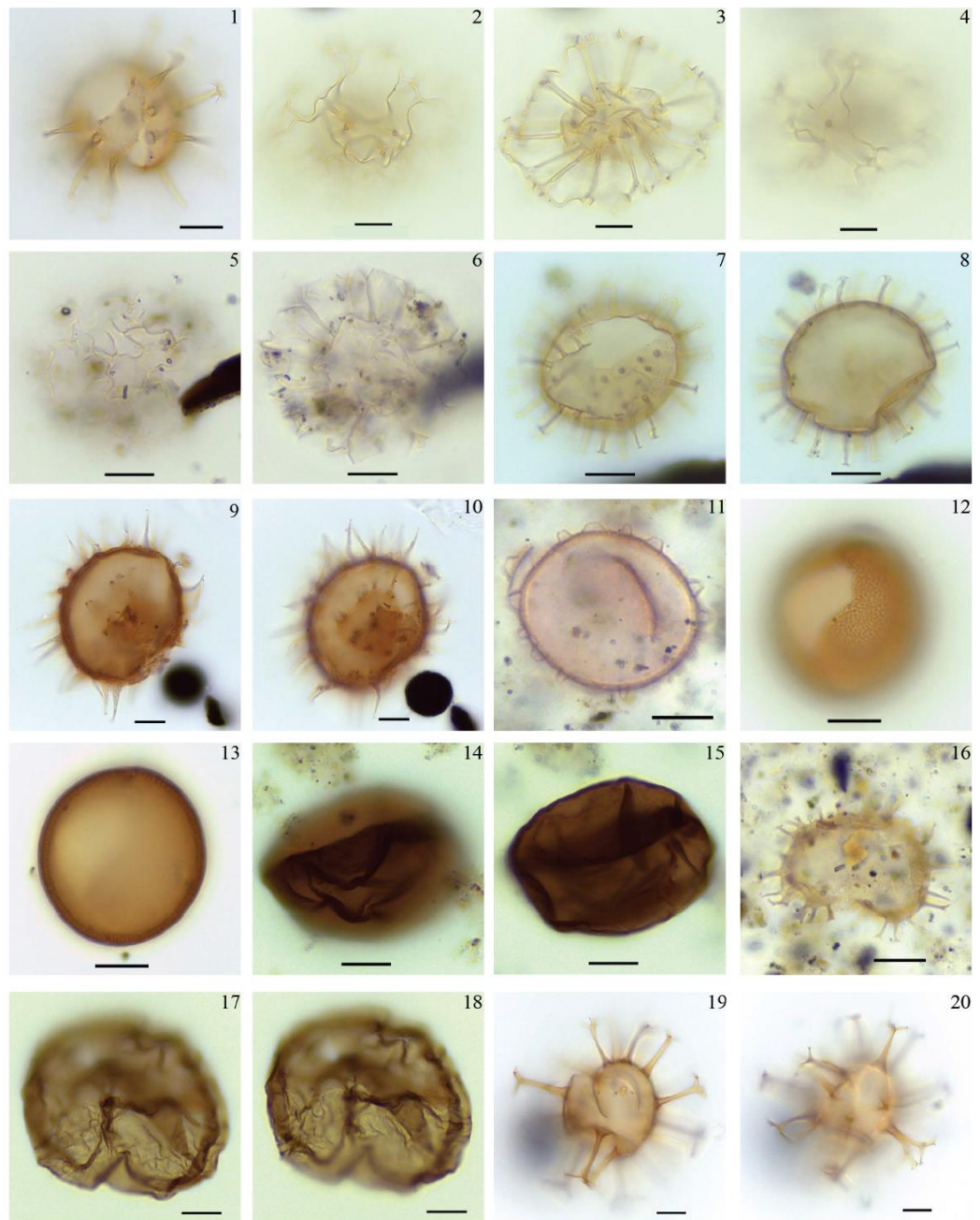
Plate 5.3: Selected dinoflagellate cysts species from ODP Hole 642B. All images were taken in bright field illumination. Sample number and England Finder coordinates are given after species name. Scale bar represents 10 µm. 1: *Melitasphaeridium choanophorum*, 9H2 25-26, M36/1; 2-4: *Nematosphaeropsis labyrinthus*, 9H2 34-35, Q34/0; 5-6: *Nematosphaeropsis lativittata*, 9H1 60-61-B, M47/2; 7-8: Cyst of *Protoceratium reticulatum*, 9H1 85-86, O43/1; 9-10: *Operculodinium centrocarpum/israelianum*, 9H2 15-16, S51/0; 11: *Operculodinium janduchenei*, 9H1 74-75, T39/4; 12-13: *Pyxidinopsis braboi*, 9H2 25-26, M34/4; 14-15: Round brown cyst, 9H1 100-101, S33/4; 16: *Selenopemphix dionaeacysta*, 9H2 38-39, T44/3; 17-18: *Selenopemphix nephroides*, 9H2 35-36, S55/2; 19-20: *Spiniferites* spp. indet.,9H2 45-46, K42/0.
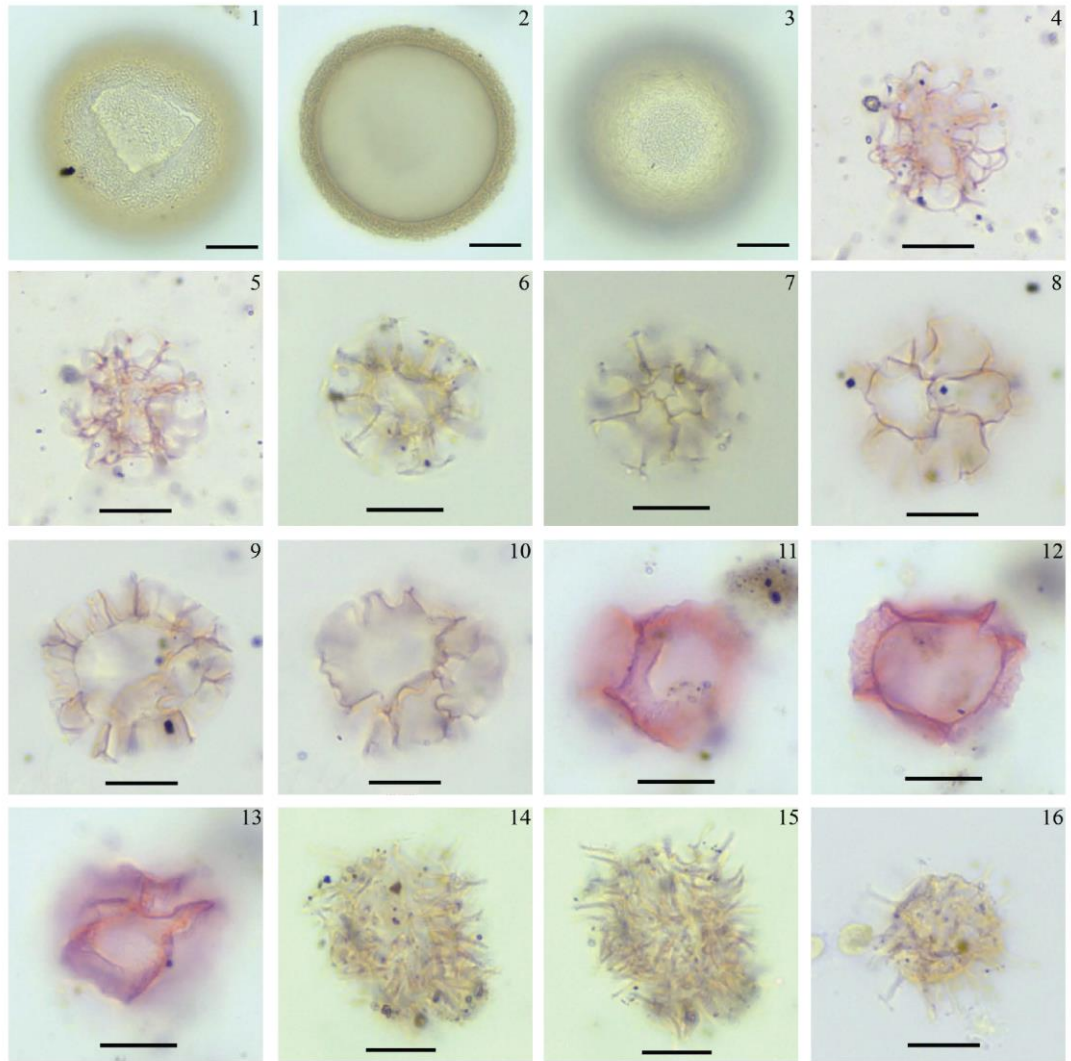
Plate 5.4: Selected dinoflagellate cysts and acritarch species from ODP Hole 642B. All images were taken in bright field illumination. Sample number and England Finder coordinates are given after species name. Scale bar represents 10 μm. 1-3: *Tectatodinium pellitum*, 9H1 76-77, J35/4; 4-5: *Cymatiosphaera? aegirii*, 9H1 67-86, N38/0; 6-7: *Cymatiosphaera? icenorum*, 9H2 34-35, K36/0; 8-10: *Cymatiosphaera? invaginata*, 9H1 115-116, W36/2; 11-13: *Lavradosphaera crista*, 9H1 90-91, O49/0; 14-15: *Nannobarbophora walldalei*, 9H2 48-49, M35/0; 16: Small spiny acritarch, 9H2 30-31, F42/0.

of MIS KM6. Proportions of *H. tectata* are very low (<4%) during MIS M2 but gradually increase throughout MIS M1 and reach values of up to 29% in the first half of MIS KM6. In the middle of MIS KM6 between 3.225 and 3.222 Ma, a sharp increase in the relative abundances of cysts of *P. reticulatum* from 13 to 48% occurs, which is accompanied by a marked decline in the relative abundances of *F. filifera* and *H. tectata*. Subsequently, relative abundances of cysts of *P. reticulatum* gradually increase to maximum values of 64% at 3.205 Ma within MIS KM5 while *F. filifera* and *H. tectata* both show proportions of less than 7%. After 3.205 Ma, relative abundances of cysts of *P. reticulatum* continuously decline. Proportions of *F. filifera* peak at 3.189 and
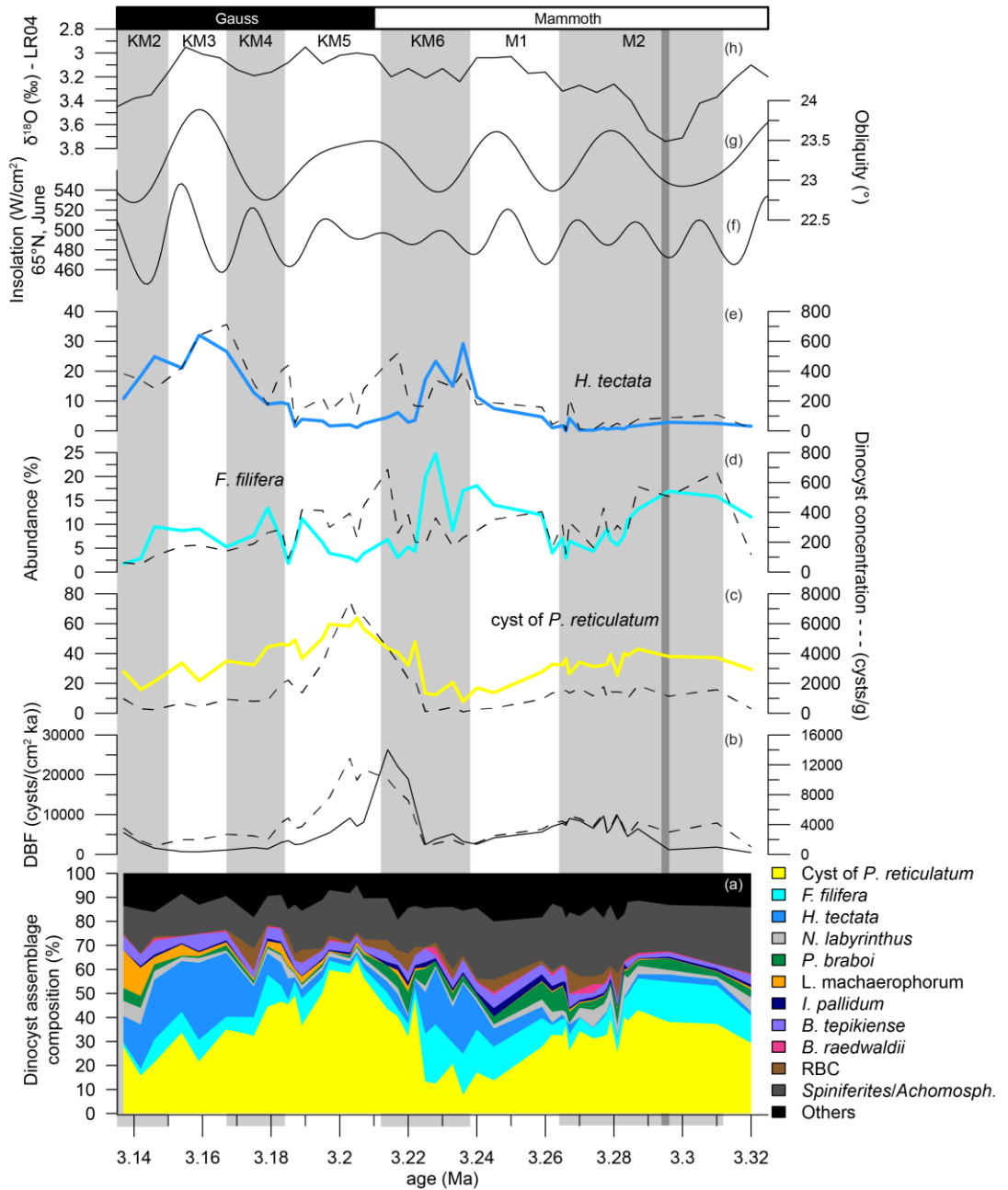
Figure 5.1: Abundances changes of selected dinoflagellate cyst (dinocyst) species from ODP Hole 642B (a–e) and orbital solutions for mean daily insolation (f) and obliquity (g) from Laskar et al. (2004) as well as the global benthic oxygen isotope stack (h) from Lisiecki and Raymo (2005). (a) Dinocyst assemblage composition in Hole 642B. cyst of *P. reticulatum* = *Protoceratium reticulatum*, *F. filifera* = *Filisphaera filifera*, *H. tectata* = *Habibacysta tectata*, *N. labyrinthus* = *Nematosphaeropsis labyrinthus*, *P. braboi* = *Pyxidinopsis braboi*, *L. machaerophorum* = *Lingulodinium machaerophorum*, *I. pallidum* = *Impagidinium pallidum*, *B. tepikiense* = *Bitectatodinium tepikiense*, *B. raedwaldii* = *Bitectatodinium raedwaldii*, RBC = round brown cysts and *Spinisph./Achomosph.* = *Spiniferites/Achomosphaera* spp.; (b) dinocyst burial flux (DBF) and total dinocyst concentration and (c–e) relative abundance and concentration of the dinocyst species cyst of *P. reticulatum*, *F. filifera* and *H. tectata*. Dark grey vertical bar indicates the possible presence of an hiatus over the most extreme part of marine isotope stage M2 (Risebrobakken et al., 2016).

129
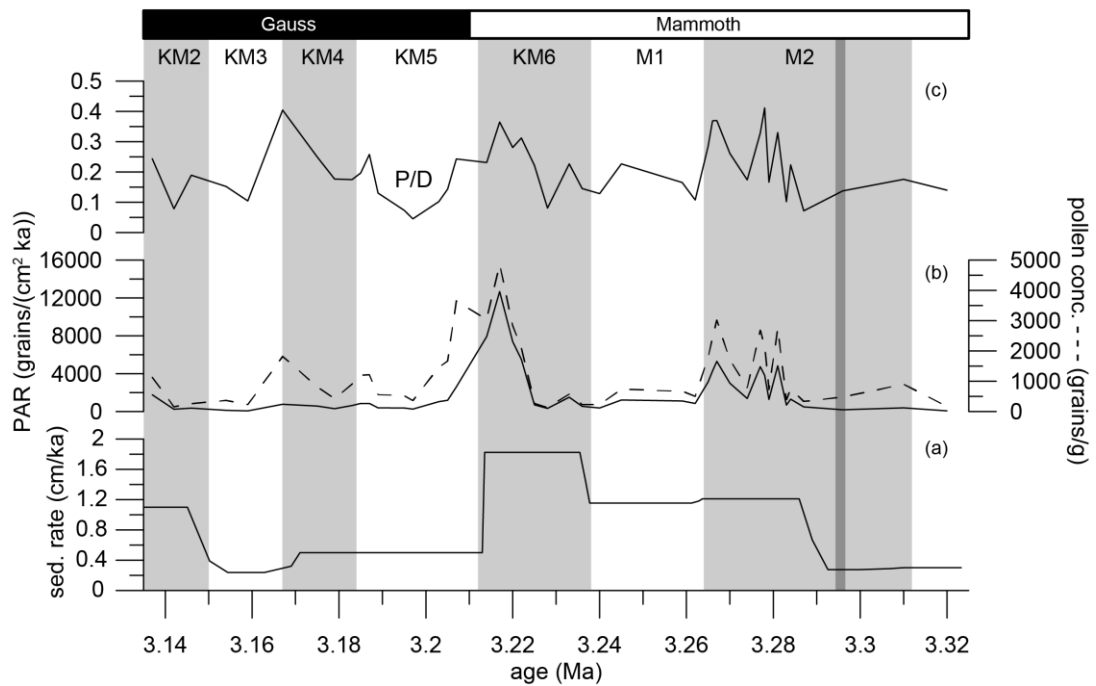
Figure 5.2: Sedimentation rate (a) in comparison to pollen deposition (b–c) at ODP Hole 642B. (b) Pollen accumulation rate (PAR) and pollen concentration, and (c) pollen (P) to dinoflagellate cyst (D) ratio. Dark grey vertical bar indicates the possible presence of an hiatus over the most extreme part of marine isotope stage M2 (Risebrobakken et al., 2016).

3.179 Ma and stay around 5–10% until values drop to <3% at 3.142 Ma within MIS KM2. A clear increase in the relative abundance of *H. tectata* occurs at 3.185 Ma at the end of MIS KM5, continuing throughout MIS KM4 and reaching highest values of 32% at 3.159 Ma in the middle of MIS KM3. Afterwards, proportions of *H. tectata* decline and those of *L. machaerophorum* increase to up to 16%.

Cyst concentrations range between 500 and 5500 cysts/g in the majority of samples (Figure 5.1). Highest concentrations occur between 3.222 and 3.197 with maximum values of 13,000 cysts/g at 3.203 Ma. The DBF shows the same pattern as the cyst concentrations throughout most of the interval. However, the DBF declines sharply between 3.214 and 3.207 Ma while cyst concentrations remain high until 3.197 Ma (Figure 5.1).

The P/D ratio is highly variable with dinocysts always constituting the greater proportion. Relatively high values of up to ~0.4 are reached in the later part of MIS M2, KM6 and MIS KM4 as well as the beginning of KM2 (Figure 5.2).

5.3.2   Arcitarch assemblages

The relative abundance of acritarch taxa and their concentrations are extremely variable, with absolute counts ranging between 28 and 1099 cysts. Twelve taxa were

130
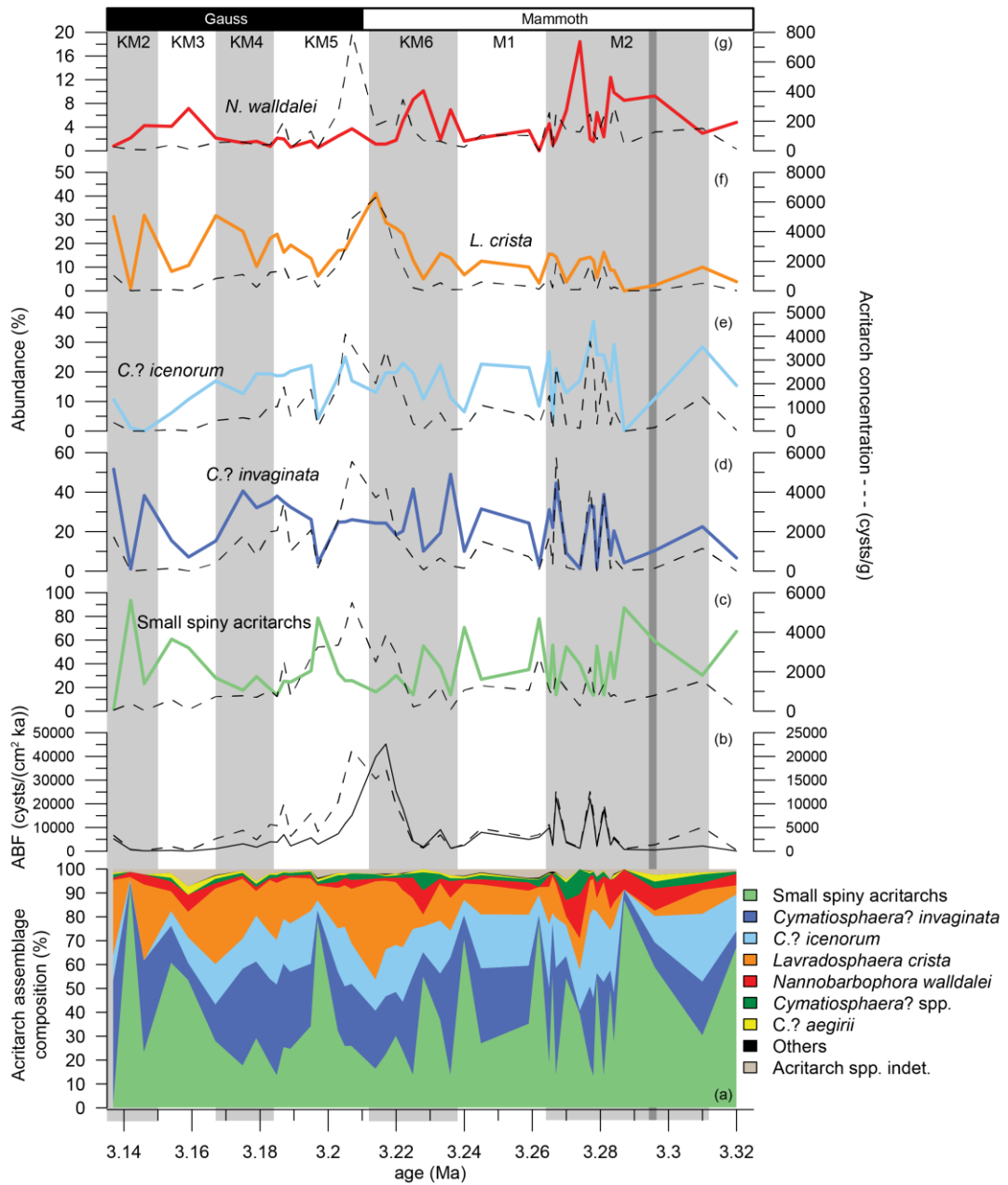
Figure 5.3: Acritarch assemblage changes at ODP Hole 642B. (a) Acritarch assemblage composition; (b) acritarch burial flux (ABF) and total acritarch concentration, and (c–g) abundances and concentrations of selected species. Dark grey vertical bar indicates the possible presence of an hiatus over the most extreme part of marine isotope stage M2 (Risebrobakken et al., 2016).

differentiated with five, *Cymatiosphaera? icenorum*, *C.? invaginata*, *Lavradosphaera crista*, *Nannobarbophora walldalei* and SSA being abundant to dominant (Figure 5.3; Plate 5.4). Abundance changes of SSA, *C.? invaginata* and *C.? icenorum* show no clear trend between 3.320 and 3.137 Ma. However, notable are the higher percentages of *L. crista* in the second half of the record (3.222–3.137 Ma, mid-MIS KM6 to early MIS KM2). Peaks of *N. walldalei* show a continuous decline throughout the studied interval with relative high values during MIS M2, KM6 and KM3.

131

Acritarch concentrations are comparable to dinocyst concentrations for most of the studied interval with values fluctuating between ~140 and 1400 cysts/g. Maximum concentrations of ~16,400–21,300 cysts/g are reached between 3.217 and 3.205 Ma (Figure 5.3). The ABF shows a good correlation to the acritarch concentration with the exception for the early part of MIS KM5 where the ABF declines before the concentration decreases (Figure 5.3).

5.4   Discussion

5.4.1   Palaeoecology of the predominant dinoflagellate cyst species in ODP Hole 642B during the mid-Piacenzian warm period

Of the three most abundant dinocyst species (cysts of *P. reticulatum*, *F. filifera* and *H. tectata*) in the sediments of Hole 642B, only cysts of *P. reticulatum* are still extant. This species is cosmopolitan and tolerates a wide range of temperature and salinity (Zonneveld et al., 2013). It is particularly abundant near shelf edges (Dale and Dale, 2002; Wall et al., 1977) and can be over-represented in fossil assemblages due to high cyst productions (Bolch and Hallegraeff, 1990; Dale, 1976). In the modern North Atlantic, high abundances of cysts of *P. reticulatum* are associated with the nutrient-rich waters of the NAC (Rochon et al., 1999; Zonneveld et al., 2013). Upon entering the Nordic Seas, the distribution of Atlantic water is reflected in the predominance of cysts of *P. reticulatum* (>60%) in modern dinocyst assemblages in the Norwegian Sea, enabling the use of this species as a tracer of Atlantic water in palaeoenvironmental reconstructions (De Schepper et al., 2015; Grøsfjeld et al., 2014, 2009; Hennissen et al., 2014; Knies et al., 2002; Matthiessen, 1995; Rochon et al., 1999). As Hole 642B is located close to the Norwegian shelf and affected by North Atlantic water masses, cyst transport from nearby continental margins and the North Atlantic must be considered when interpreting the dinocyst assemblages. In the Piacenzian samples of Hole 642B, relative abundances of cysts of *P. reticulatum* mostly vary between ~25–45%, suggesting a continuous influence of Atlantic water or water flux from the Norwegian shelf (Figure 5.1). An increased influence of Atlantic water via a well-developed NwAC is indicated by higher percentages (~45–60%) and concentrations during the second half of MIS KM6 and MIS KM5. Higher dinocyst concentrations have previously been associated with higher productivity during glacials of the late Pliocene/early Pleistocene (Hennissen et al., 2014; Versteegh et al., 1996). Here, the increase in concentration can more likely be attributed to the presence of nutrient-rich Atlantic water.

Both *F. filifera* and *H. tectata* became extinct during the Pleistocene (Head, 1996b). According to their stratigraphic records, these species have previously been classified as cold-water tolerant species as they are common elements of Pliocene high-latitude sites in the Northern Hemisphere (Head, 1996b, 1994). However, the high latitudes were markedly warmer than today during the Pliocene, suggesting that these species inhabited relatively mild water masses (Bachem et al., 2016; De Schepper et al., 2015; Robinson, 2009). In the eastern North Atlantic, percentages of *F. filifera* above 5% are associated with Mg/Ca-based (spring-summer) SSTs of >11°C and abundances of *H. tectata* exceeding 30% are indicative of SSTs between 10 and 15°C (De Schepper et al., 2011). These temperature ranges correspond to SST estimates at Hole 642B during the mPWP which vary between ~12–16°C (Figure 5.4) (Bachem et al., 2016). At Hole 642B, abundance changes of *F. filifera* and *H. tectata* are almost continuously reflected in the concentrations (Figure 5.1). Higher abundances and concentrations of *F. filifera* during the first half of MIS M2 suggest an increased water influence from the Arctic in comparison to the second half, and thus a reduction in the northward flow of warm Atlantic water via the NwAC. Alkenone-derived SST estimates from Hole 642B fluctuate between 11.5 and 13°C, which is within the range of Holocene SSTs at the nearby Site MD95-2011 (Figure 5.4) (Bachem et al., 2016). Cold intervals during the first half of MIS KM6, and KM3, with SSTs of ~12–13°C, are characterised by high abundances (>15%) and concentrations of *H. tectata* and accompanied by low proportions of cysts of *P. reticulatum* (<25%), indicating an increased influence of Arctic than Atlantic water (Figure 5.1). Other potential cool-water indicators that are continuously present in low abundances include the extant species *Bitectatodinium tepikiense* and *Impagidinium pallidum* (De Schepper et al., 2011). Relative high abundances of *B. tepikiense* occur during MIS M1, KM3 and KM2 together with high abundances of *F. filifera* and/or *H. tectata* (Figure 5.1). At present, *I. pallidum* is a bi-polar species but its presence at North Atlantic sites during the Pliocene suggests a tolerance of a wider temperature range during the Pliocene, limiting the use of this species as a palaeotemperature indicator (De Schepper et al., 2011). At Hole 642B, this species shows highest abundances during MIS M1 (Figure 5.1).
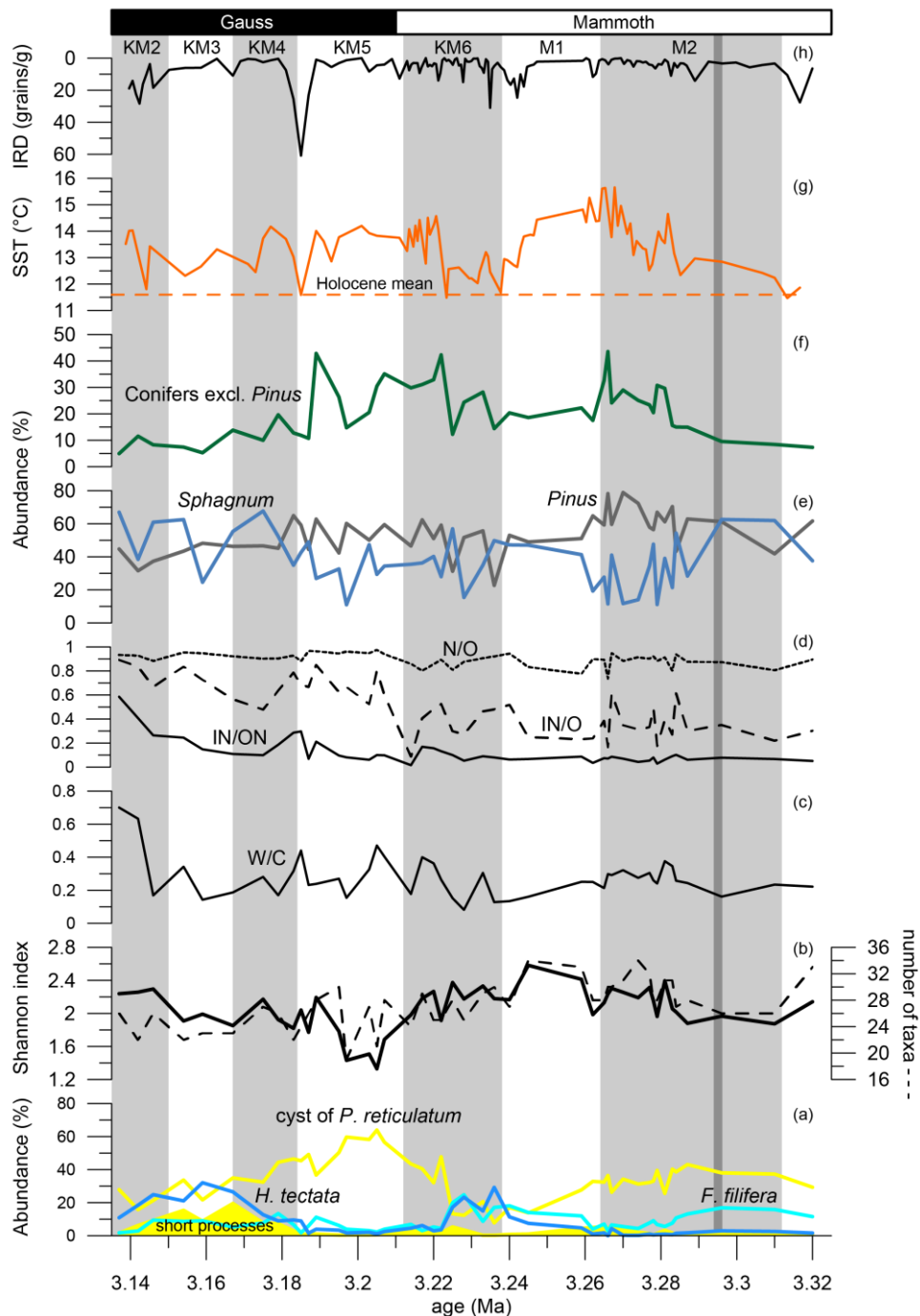
Figure 5.4: Comparison of dinoflagellate cyst (dinocyst) assemblage changes and indices (a–d) to pollen assemblages changes (e–f) (Chapter 3), sea surface temperature (SST) estimates (g) and ice rafted debris (IRD) concentrations (h) (Bachem et al., 2016) from ODP Hole 642B. (a) Relative abundance of cysts of *Protoceratium* (*P*.) *reticulatum* (yellow line), cysts of *P. reticulatum* with short processes (filled yellow area), *Filisphaera* (*F*.) *filifera* (light blue) and *Habibacysta* (*H*.) *tectata* (dark blue); (b) Shannon diversity index and number of taxa; (c) index of warm (W) and cold (C) water indicator species; (d) ratios of inner neritic (IN), outer neritic (ON) and oceanic (O) species; (e–f) relative abundances of *Pinus* pollen (grey), *Sphagnum* spores (blue) and conifers excluding *Pinus* (green); (g) alkenone-based SST estimates (orange) from Bachem et al. (2016) and Holocene mean SST at Site MD95–2011 from Calvo et al. (2002) (orange dashed); (h) IRD concentrations (black). Dark grey vertical bar indicates the possible presence of an hiatus over the most extreme part of marine isotope stage M2 (Risebrobakken et al., 2016).

134

5.4.2 Palaeoceanographic and palaeoenvironmental changes in the Norwegian Sea area

During the mPWP, dinocyst assemblage changes at Hole 642 reveal distinct variations in the influence of Atlantic and Arctic water in the Norwegian Sea and thus changes in the northward heat transport via the NwAC. Here, water masses changes derived from dinocyst assemblage changes are compared to pollen assemblages as a proxy for vegetation and climate changes in Arctic Norway (Chapter 3) and alkenone-based SST estimates (Bachem et al., 2016) from the same site.

5.4.2.1 MIS M2–M1: A glacial-interglacial transition

Glacial MIS M2 has been globally recognised in benthic oxygen isotopes and other marine and terrestrial proxy records as a pronounced cooling event during the warmer-than-present Piacenzian (Brigham-Grette et al., 2013; De Schepper et al., 2014, 2013; Lisiecki and Raymo, 2005; Mudelsee and Raymo, 2005). At Hole 642B, MIS M2 is not as distinctly recorded in the benthic oxygen isotope signal as at other sites, suggesting either the possible presence of a minor hiatus over the most extreme part of MIS M2 (Figure 5.1), or that the event was less pronounced in the Norwegian Sea area (Risebrobakken et al., 2016). During the early part of MIS M2, the moderate abundance of cysts of *P. reticulatum* (25–43%) suggests a constant influence of Atlantic and/or shelf water (Figure 5.1, 5.4). In comparison to DSDP Site 610 and IODP Site U1308 in the northern North Atlantic, where very low abundances of cysts of *P. reticulatum* during this interval indicate the absence of northward warm water transport via the NAC (De Schepper et al., 2013), the relatively high proportions of this species at Hole 642B suggest that its local representation is affected by other factors than the influence of Atlantic water. These factors include influx from the shelf edge and/or higher cyst productions in comparison to the other species (see section 5.4.1). Cysts of *P. reticulatum* might have been able to be perpetually produced in the relatively mild waters of the Norwegian Sea, with temperatures being controlled by higher atmospheric CO_2 concentrations and insolation changes (Bachem et al., 2016). During the first half of MIS M2, alkenone-derived SSTs at Hole 642B are low for the Pliocene and comparable to the Holocene average, with values around 12–13°C (Figure 5.4; Bachem, unpublished data). An increased influence of relatively cooler water masses from the Greenland-Iceland Seas is indicated by the high proportions of *F. filifera* (<17%). The predominance of *Pinus* pollen and *Sphagnum* spores in the pollen assemblages of Hole 642B suggest the prevalence of boreal forests and an extensive distribution of peatlands

similar to the Holocene under subarctic climatic conditions in northern Norway (Figure 5.4). Terrestrial climatic conditions might have been cold enough for the establishment of mountain glaciers despite the lower-than-present height of the Scandinavian mountains (Chapter 3) (Anell et al., 2009; Knies et al., 2014b). Holocene-like climatic conditions in the Norwegian Sea region during the early part of MIS M2 support the notion of a similar-to-present Artic ice sheet extent, possibly as a result of a southward deflected NAC between c. 3.315 and 3.285 Ma (De Schepper et al., 2013). The lack of evidence for a major glacial inception in Scandinavia during MIS M2 in the marine and terrestrial proxy data from Hole 642B may, however, be the result of a hiatus (Risebrobakken et al., 2016).

Between 3.284 and 3.281 Ma, the decline in the relative abundance of *F. filifera* and increase in diversity are indicative of a warming of the water masses (Figure 5.4). The relative abundance of the acritarchs *C.? invaginata*, *C.? icenorum* and *L. crista* as well as the ABF also increase markedly between 3.287 and 3.284 Ma, suggesting enhanced marine productivity (de Vernal and Mudie, 1989a; Schreck et al., 2013). This is accompanied by a rise in alkenone-derived SSTs to highest values (~15–16°C) within the studied interval between 3.285 and 3.283 Ma (Bachem, unpublished data) and followed by a distinct increase in the proportion of other conifer taxa excluding *Pinus* from 12 to 42% between 3.283 and 3.281 Ma (Figure 5.4). The latter is indicative of the establishment of diverse, cool temperate mixed forests and warmer-than-present climatic conditions in northern Norway (Chapter 3). At the same time, the relative abundance of *Sphagnum* spores declines and that of *Pinus* pollen increases, suggesting an expansion of forests at the expense of peatlands. Increased pollen concentrations and PARs may be indicative of a higher terrestrial productivity due to warmer climatic conditions, but increased pollen deposition due to higher sedimentation rates (Figure 5.2) and/or marine productivity (Dupont, 2011) cannot be excluded. The increased pollen influx is also reflected in the P/D ratio which reaches relatively high values during the later part of MIS M2 (Figure 5.2). This warming coincides with the re-establishment of warmer water conditions in the North Atlantic which have been ascribed to a re-invigorated northward heat transport via an active, modern-like NAC around 3.285 Ma (De Schepper et al., 2013; Naafs et al., 2010). In the Norwegian Sea, the warming is not associated with an increase in the relative abundance of cysts of *P. reticulatum* as at Site 610 and U1308 in the northern North Atlantic (De Schepper et al., 2013). This supports the notion that the prevalence of cysts of *P. reticulatum* is partly an

expression of the site location close to the Norwegian shelf edge. On the other hand, the decline in the relative abundance of *F. filifera* is indicative of a warming of the water masses (Figure 5.1). The pronounced increase of alkenone-based SST to values ~5°C higher than the Holocene average suggests that the warming is not only induced by an enhanced Atlantic water inflow but also a response to changes in obliquity (Figure 5.4) (Bachem et al., 2016).

Throughout MIS M1, the relative abundance of cysts of *P. reticulatum* declines while that of *F. filifera* increases stepwise, suggesting further cooling, possibly associated with a reduction in the influence of water from the Atlantic and/or Norwegian shelf (Figure 5.1, 5.4). As Atlantic water is traced by higher abundances of cysts of *P. reticulatum* in the modern Nordic Seas (Matthiessen, 1995), the decline towards lowest values within the Piacenzian record during MIS M1 is interpreted as a reduction of Atlantic water influence. This is supported by lower abundances of cysts of *P. reticulatum* during MIS M1 compared to the end of MIS M2 at the North Atlantic sites 610 and U1308 (De Schepper et al., 2013). The increase in proportions of *F. filifera*, starting at c. 3.262 Ma, is accompanied by an increase in the relative abundance of *Sphagnum* spores which is indicative of an expansion of peatlands at the expense of forests and the establishment of subarctic climatic conditions in northern Norway (Chapter 3). A cooling in alkenone-derived SSTs, however, is not recorded until 3.247 Ma in response to obliquity forcing (Figure 5.4) (Bachem et al., 2016). Concentrations and influxes of dinocysts, acritarchs and pollen and spores are low during MIS M1 (Figure 5.1, 5.2, 5.3), indicating reduced marine and terrestrial productivity. However, lower PARs may be the result of reduced marine productivity, with the latter impeding particle flux to the sea floor (Dupont, 2011). The good correlation of dinocyst and pollen assemblage changes suggests that water mass changes in the Norwegian Sea had a direct impact on terrestrial climate.

The transition between MIS M2 to the mPWP has been suggested to represent a climatic evolution from glacial, similar-to-modern to warmer-than-present conditions driven by a re-invigoration of the NAC in the North Atlantic around 3.285 Ma and accompanied increase in northward heat transport (De Schepper et al., 2013). This warming is reflected in both water mass and vegetation changes in the Norwegian Sea area. Here, the early part of MIS M2 is characterised by alkenone-based SSTs similar or slightly higher compared to the Holocene average (Bachem et al., 2016) and the presence of boreal vegetation in northern Norway also resembles modern conditions

(Figure 5.4; Chapter 3). Cysts of *P. reticulatum* are an abundant component of the dinocyst assemblage together with *Achomosphaera/Spiniferites* spp. and *F. filifera*, with the latter being indicative of Arctic water influence. A brief warming of the water mass, seen via a decline in *F. filifera* and an increase in alkenone-derived SST, is recorded at 3.285–3.284 Ma during the latter half of MIS M2. Terrestrial climatic changes do not occur until 3.283 Ma, suggesting a response to water mass changes in the Norwegian Sea. This warming, marking the MIS M2/mPWP transition is presumably the result of both changes in the position of the NAC in the eastern North Atlantic (De Schepper et al., 2013) and obliquity forcing (Figure 5.1).

5.4.2.2 MIS KM6: Increased inflow of warm Atlantic waters

The cooling that commenced at 3.262 Ma during MIS M1 culminates between 3.236 and 3.222 Ma within the first half of MIS KM6 as seen in the high abundances of *F. filifera* and *H. tectata* which together comprise up to 48% of the assemblage. In contrast, cysts of *P. reticulatum* constitute less than ~20% of the assemblages, suggesting a reduced influence of water from the North Atlantic (Figure 5.1, 5.4). The cooling is also expressed in the W/C index and alkenone-based SST estimates but to a lesser degree in the vegetation changes (Figure 5.4). In the North Atlantic, a reduction in the relative abundance of cysts of *P. reticulatum* is also seen at Site U1308 (De Schepper et al., 2013). As insolation forcing is relatively low during this time, the area might have been influenced by cooler and fresher water masses from the west, with the warm NwAC flowing northward further east and thus closer the coast, resulting in relative warm climatic conditions in northern Norway. At present, changes in the width of the NwAC of up to 300 km are observed in response to changes in atmospheric pressure fields (Blindheim et al., 2000).

A distinct increase in the relative abundance (up to ~48%) and concentrations of cysts of *P. reticulatum* takes place between 3.225 and 3.222 Ma, coinciding with an increase in the proportions of *Pinus* and other conifers that is indicative of the establishment of cool temperate climatic conditions. A rise in alkenone-derived SSTs by ~2.5°C does not occur until 3.223 Ma (Figure 5.4). The increase in the abundance of cysts of *P. reticulatum* is also reflected in its concentrations and corresponds to an increase in the total DBF, suggesting that nutrient-rich water influenced the site and led to enhanced productivity (Figure 5.1) (Hennissen et al., 2014). This is also supported by a steep increase in acritarch concentrations and the ABF, commencing at ~3.225 Ma (Figure 5.3). At the same time, the pollen concentration and PAR increases, possibly as a result

138

of a higher terrestrial and/or marine productivity (Figure 5.1) (Dupont, 2011). These changes suggest that warm, salty Atlantic water masses were transported into the Norwegian Sea via an active NAC, leading to a warmer climate in northern Norway and higher alkenone-derived SSTs in the Norwegian Sea. Bachem et al. (2016) note that the rise in SSTs coincides with an increase in obliquity, indicating a possible response to orbital forcing. The relative abundance of cysts of *P. reticulatum* increases continuously to maximum values of ~64% until 3.205 Ma, with high proportions predominating until 3.197 Ma. This increase is reflected in the dinocyst concentrations (Figure 5.1). However, the DBF and ABF decline sharply between 3.217 and 3.205 Ma across the MIS KM6/KM5 boundary, reflecting a reduction in nutrient availability (Figure 5.1, 5.2). PARs also decline, suggesting reduced terrestrial productivity and/or particle flux to the sea floor (Dupont, 2011). The increase in the abundance of cysts of *P. reticulatum* prior to a rise in alkenone-based SSTs suggests that the latter is at least partly, if not entirely, controlled by water mass changes. Lower alkenone-based SSTs (~14°C) between 3.223 and 3.189 than those reached during the later half of MIS M2 support the notion that radiative forcing exerts a stronger control on SST changes during the early part of the mPWP (Figure 5.4) (Bachem et al., 2016).

5.4.2.3 MIS KM5: Warmer-than-present interglacial conditions

Abundances of cyst of *P. reticulatum* are highest between 3.205 and 3.197 Ma, suggesting an increased influence of Atlantic water and the presence of a well-established NwAC compared to the rest of the studied interval (Figure 5.1). This is supported by the low proportions of *F. filifera* and *H. tectata*. Throughout MIS KM5, alkenone-derived SSTs are ~2°C higher when compared to the Holocene average (Bachem et al., 2016). Relative abundance changes in *Pinus*, other conifers and *Sphagnum* are variable, indicating the presence of mixed to boreal forests, but tend towards more boreal conditions around 3.20 Ma. However, higher proportions of other conifers between 3.222 and 3.205 Ma and at 3.189 Ma suggest that cool temperate climatic conditions prevailed in northern Norway (Figure 5.4). Thus, terrestrial climatic conditions appear to be quite variable in comparison to relatively stable oceanographic conditions. Changes in obliquity and insolation are small around that time, suggesting that they did not control terrestrial climate changes.

At the end of MIS KM5, the relative abundance of conifers excluding *Pinus* declines markedly between 3.189 and 3.187 Ma, suggesting the establishment of boreal forests and subarctic climatic conditions in northern Norway. This cooling corresponds to a

drop in alkenone-derived SSTs of ~2°C between 3.189 and 3.185 Ma and a contemporaneous increase in IRD which most likely comes from sea-terminating ice masses on Greenland (Figure 5.4) (Bachem et al., 2016). Bachem et al. (2016) suggest that the cooling could be linked to weakened obliquity and insolation forcing. An increased influence of water from the Atlantic and/or shelf is suggested by an increase in the abundances of cysts of *P. reticulatum* and decrease in those of *F. filifera* between 3.189 and 3.187 Ma. This is, however, followed by a prolonged increase in the proportions of *H. tectata*, commencing between 3.187 and 3.185 Ma, which is indicative of enhanced Arctic water influence from the Greenland-Iceland Seas (Figure 5.1).

5.4.2.4   MIS KM4–KM2: Cooling of the sea and land

Declining abundances of cysts of *P. reticulatum* and increasing proportions of *H. tectata* are indicative of a reduced influence of Atlantic water and the intrusion of water masses from the eastern Nordic Seas (Figure 5.4). A freshening of the water masses may be inferred from higher proportions of cysts of *P. reticulatum* with short processes (Figure 5.4). In the modern North Atlantic Ocean, the process length of this species shows a positive correlation to salinity and density (Jansson et al., 2014; Mertens et al., 2012, 2010). Alkenone-based SST estimates only show low-amplitude changes, with values fluctuating between 12 and 14°C (Figure 5.4) (Bachem et al., 2016). Both *Pinus* and other conifers show low (<13%) and decreasing abundances throughout MIS KM4 to KM2, reflecting the prevalence of boreal forest in northern Norway. Proportions of *Sphagnum* spores reach values as high as those during the early part of MIS M2 but are still variable, indicating relatively cool conditions and a repeated expansion of peatlands (Figure 5.4; Chapter 3).

During MIS KM2, the decline in proportions of *H. tectata* and increase in those of *L. machaerophorum* suggests a change in water mass composition or taphonomy (Figure 5.1). Species of *L. machaerophorum* are presently mainly found in coastal temperate to equatorial regions with temperatures above 10°C in summer – conditions persisting in the Norwegian Sea during the mPWP (Figure 5.4) (Bachem et al., 2016). During the late Piacenzian, *L. machaerophorum* is a common element in the palynomorph assemblages deposited in the southern North Sea Basin, where it has been used as an indicator for warm temperate conditions (De Schepper et al., 2009b; Head, 1998). In the Norwegian Sea, however, the increase in the abundances of this species is not associated with a pronounced increase in alkenone-based SSTs (Bachem et al., 2016),

excluding a pure temperature response as the sole cause (Figure 5.4). The species tolerates a broad range of salinity and also occurs in high abundances near upwelling cells, below river plumes or in highly stratified waters (Zonneveld et al., 2013). In Norwegian fjords, higher numbers of this species have been associated with increased eutrophication (Dale et al., 1999; Thorsen and Dale, 1997). At Hole 642B, the higher abundances of *L. machaerophorum* are unlikely to be linked to increased nutrient availability due to the contemporaneous low proportions of cysts of *P. reticulatum*, RBCs and low DBF and ABF rates (Figure 5.1, 5.3). As *L. machaerophorum* is a typical neritic species, restricted to the coastal regions and vicinity of continental margins (Zonneveld et al., 2013), the higher abundances at Hole 642B might be an indication of an increased influence of water from the inner shelf area. The higher proportions of this species are reflected in both the IN/ON and IN/O indices (Figure 5.4). The process length of *L. machaerophorum* has also been correlated with salinity (Mertens et al., 2009; Verleye et al., 2009). In this study, specimen with reduced processes were not counted separately but noticed during counting, indicating that cysts may have been produced in fresher, possibly inner shelf, water and were transported to the site.

5.5   Conclusions

A new record of dinocyst assemblage changes from ODP Site 642 for the mPWP reveals variations in the influence of Atlantic and Arctic water masses in the Norwegian Sea and thus northward heat transport via the NwAC between 3.320 and 3.137 Ma. These variations have been derived from the relative abundance changes of cysts of *P. reticulatum*, *F. filifera* and *H. tectata*. The comparison of water mass changes to alkenone-derived SST estimates (Bachem et al., 2016) and vegetation changes in northern Norway based on pollen assemblage changes (Chapter 3) from the same site show climate changes in response to variations in the influence of Atlantic water and changes in obliquity. The NwAC is characterised by a high variability on glacial-interglacial timescales:

- **MIS M2**: During the first half, Arctic water influence is relatively high, as indicated by high abundance of *F. filifera*, and northward heat transport reduced, with Holocene-like SSTs and boreal forest prevailing in northern Norway. The consistent presence of cysts *P. reticulatum* in the Norwegian Sea may be an expression of water fluxes from the Norwegian shelf edge. The full glacial conditions may be missing. Investigation of an unquestionably complete section

across MIS M2 in the Norwegian Sea is needed to confirm or disprove this alternative.

- **MIS M2/M1 transition**: Warming around 3.285–3.284 Ma that is evident in a decline in the abundances of *F. filifera*, rise in alkenone-derived SSTs and the presence of cool temperate forest in northern Norway is indicative of an increased influence of Atlantic water and well-established NwAC. Water mass changes precede terrestrial climate changes, suggesting that the warming on land is at least partly driven by a re-invigorated NwAC. Highest alkenone-derived SSTs within the studied interval suggest that the warming is not only forced by water mass changes but also orbitally-induced insolation variations.

- **MIS M1**: Enhanced water influx from the Arctic and less well-developed NwAC corresponds to boreal climatic conditions in northern Norway. A delayed decline in alkenone-based SSTs coincides with a decrease in obliquity.

- **MIS KM6**: Cooling culminates in the first half, suggesting a relatively weak NwAC and a more pronounced influence of Arctic water. An increased influence of nutrient-rich, warm Atlantic water leads to a re-establishment of an active NwAC between 3.225–3.222 Ma. A distinct warming is also seen in the rise of alkenone-derived SSTs, the development of cool temperate forests in northern Norway and marine as well as terrestrial productivity indicators.

- **MIS KM5**: Atlantic water influence stays high as inferred from highest abundances of cysts of *P. retilulatum*. Alkenone-based SSTs are 2°C higher than the Holocene average, presumably resulting from a combination of the emergence of warmer Atlantic water and radiative forcing. Boreal to cool temperate forests prevail in northern Norway, suggesting variable terrestrial climatic conditions.

- **MIS KM4–KM2**: A gradual increase in Arctic water influence is reflected in high abundances of *H. tectata* and corresponds to the prevalence of boreal forest and a repeated expansion of peatlands in northern Norway. Estimates of SSTs are relatively stable and slightly higher than the Holocene mean. An increase in the abundances of *L. machaerophorum* may be indicative of an increased water flux from the inner shelf.

Chapter 6: Conclusions and Outlook

6.1   Summary of the research project

This research project investigated Piacenzian climate variability and the extent of vegetation changes in northern Norway between 3.60–3.14 Ma (Chapter 3), the long-term evolution of Pliocene vegetation and climate between 5.03 and 3.14 Ma (Chapter 4) and the variability of the NwAC between 3.32 and 3.14 Ma, covering the mPWP (Chapter 5). The reconstructions are based on the analysis of terrestrial and marine palynomorphs in the Pliocene sediments of ODP Hole 642B in the Norwegian Sea. As the climate of the Pliocene Epoch (5.33–2.59 Ma) exhibits similarities to climatic conditions projected for the end of the 21st century, Pliocene environmental reconstructions can advance our understanding of the temporal variability and magnitude of climatic changes in a warmer-than-present world. The high latitudes are particularly sensitive to climatic changes, partly due to positive feedback mechanisms – a phenomenon known as Arctic amplification. The low resolution, poor age control and/or low temporal coverage of existing Pliocene high-latitude vegetation records in the North Atlantic region has hampered the detection of sub-orbital climate variability, and identification of forcings. The effect of palaeogeographic (i.e. the shoaling of the CAS during the Zanclean) and palaeoceanographic changes (i.e. variations in the northward heat transport via the NAC) during the Pliocene on vegetation and climate are unclear. This thesis presents a new Pliocene high-resolution pollen record on sub-orbital timescales for the North Atlantic region, documenting vegetation and climate changes in northern Norway. It also presents a new record of variations in the influence of Atlantic/Arctic water in the Norwegian Sea during the mPWP derived from dinocyst assemblage changes. The dinocyst record is compared to vegetation changes in northern Norway, allowing the analysis of the link between marine and terrestrial environmental changes.

6.1.1   Piacenzian vegetation, and climate variability in northern Norway

Between 3.60 and 3.14 Ma, vegetation fluctuated between diverse cool temperate forests and boreal forests with tundra vegetation at higher altitudes of the Scandinavian mountains which reached elevations of 500–1000m in northern Norway, being 500–1000m lower than present (Chapter 3). Cool temperate forests, which persisted during warmer-than-present intervals, consisted of *Alnus*, *Betula*, *Carpinus*, *Carya*, *Picea*, *Pinus*, *Sciadopitys*, *Tsuga* and *Quercus*. The presence of thermophilous species (e.g.

Sciadopitys and *Quercus*) in northern Norway suggests a northward shift of the northern boundary of the mixed to deciduous forest zone by 4–8° latitude. During cooler intervals, the forest composition resembled that of today, with *Pinus* being the predominant species. The appearance of herbs (i.e. Asteraceae pollen) and mosses (i.e. *Sphagnum* spores) during those intervals is inferred to reflect an opening of the vegetation and the development of herb fields and peatlands at higher altitudes. Mountain glaciers likely did not establish during cooler intervals due to the lower-than-present height of the Scandinavian mountains. However, during intervals with an extensive, possibly wider than present, distribution of peatlands, climatic conditions might have been cold enough to allow for the establishment for mountain glaciers. Quantitative climate estimates based on the CA suggest that MATs and WMTs were on average 5–14°C and 8–14°C higher than present during warmer-than-present intervals, respectively, in comparison to climate data from near-coastal meteorological reference stations.

6.1.2 Controls on Pliocene vegetation and climate evolution in northern Norway

The Pliocene pollen record (5.03–3.14 Ma) reveals a long-term cooling trend that is superimposed on shifts between distinct c. 520 to 120 ka-long climate phases characterised by the prevalence of cool temperate and boreal conditions in northern Norway (Chapter 4). The long-term cooling is inferred from the continuous decline in the relative abundance of the temperate taxon *Sciadopitys* throughout subsequent warm intervals, which is in agreement with Pliocene records showing decreasing atmospheric CO_2 concentrations and the notion of the Pliocene representing the later stage of a late Neogene cooling trajectory. Spectral analysis of the relative abundance changes of *Pinus* pollen between 4.36 and 3.14 Ma suggests that cooler intervals between c. 4.2 and 4.0 Ma and 3.3 and 3.1 Ma occurred in response to the concurrence of eccentricity (400 ka) minima and low-amplitude obliquity and precession variations. The expression of the 400-ka eccentricity cycle in the Pliocene pollen record of Hole 642B is, however, obscured by palaeogeographic and palaeoceanographic changes.

During the early Zanclean, PARs are highest. A distinct decline in PARs is observed at 4.56 Ma, with pollen deposition not recovering until 4.35 Ma and values remaining below those reached during the early Zanclean. The decline in PARs may be linked to reduced marine primary productivity after 4.56 Ma, hampering the sinking of pollen to the sea floor. Alternatively, climate model outputs obtained from model experiments

run by the Pliocene palaeoclimate model community at the University of Leeds and Bristol suggest that the shoaling of the CAS between 4.7 and 4.2 Ma resulted in atmospheric circulation changes from prevailing southeasterlies to southwesterlies, with the latter creating unfavourable conditions for offshore pollen transport. During the late Zanclean and Piacenzian, vegetation changes in northern Norway correspond to changes in the strength/position of the North Atlantic Current, suggesting that variations in northward heat transport affected terrestrial climate changes in Scandinavia.

6.1.3   Norwegian Atlantic Current variability during the mid-Piacenzian warm period and its impact on Scandinavian vegetation changes

Dinocyst assemblage changes at Hole 642B reveal variations in the influence of Atlantic and Arctic water between 3.320 and 3.137 Ma, covering MIS M2 to KM2 (Chapter 5). The extant cysts of *Protoceratium reticulatum* are used as a tracer of Atlantic water in the Nordic Seas. The extinct species *Filisphaera filifera* and *Habibacysta tectata* are indicative of Arctic water influence from the Greenland-Iceland Seas. High abundances of *F. filifera* and *H. tectata* during the first half of MIS M2, MIS M1 and the first half of KM6, and KM4 to KM2 suggest influence of Arctic water and coincide with the prevalence of boreal forest and similar-to-present climatic conditions in northern Norway. Two warming events are evident in the dinocyst assemblage changes during the studied interval. The first warming at 3.284 Ma is evident in declining abundances of *F. filifera*, suggesting reduced Arctic water influence. In northern Norway, cool temperate forests and thus warmer-than-present climatic conditions establish at 3.283 Ma, suggesting a lacked response of terrestrial climatic changes to water mass changes. The warming coincides with an increase in obliquity, indicating a possible response to orbital forcing. The second warming event around 3.225 Ma is marked by an increase in the relative abundance of cysts of *P. reticulatum*, indicating increased Atlantic water influence and a well-established NwAC. This warming is concurrently seen in the establishment of cool temperate forests and warmer-than-present climatic conditions in northern Norway, suggesting a direct response of terrestrial climatic changes to the emergence of Atlantic water.

6.2   Summary conclusions

This thesis provides new high-resolution Pliocene (5.03–3.14) pollen and Piacenzian (3.32–3.14 Ma) dinocyst records for ODP Hole 642B (Norwegian Sea), documenting vegetation changes in northern Norway and variations in the inflow of Atlantic water into the Norwegian Sea, respectively. The main findings of this study are:

- In northern Norway, vegetation fluctuated between cool temperate forests and boreal forests with herb fields/peatlands at higher altitudes during the Piacenzian, indicating warmer-than-present and similar-to-present climatic conditions, respectively (Chapter 3). During warmer-than-present intervals, MATs were 5–14°C higher than present and WMTs 8–14°C. The Piacenzian vegetation changes correlate with other marine and terrestrial records across the Northern Hemispheric, suggesting a hemispheric-wide impact of climatic changes superimposed on region-specific changes. The expansion of peatlands at the end of the record may be a major control on climatic cooling through the drawdown of atmospheric CO_2 and vegetation-snow albedo feedbacks, contributing to the Earth's system shifting into the highly variable Pleistocene.

- The first long-term high-resolution Pliocene pollen record is indicative of a gradual climate cooling in northern Norway in response to declining atmospheric CO_2 concentrations, continuing the long-term cooling trend that followed the mid-Miocene climatic optimum (17–14.5 Ma). Distinct climate phases characterised by boreal or cool temperate climatic conditions interrupt this gradual cooling trend. Cooler intervals are presumably partly driven by minima in the long eccentricity (400 ka) cycle and concurrent low-amplitude variations in obliquity and precession. During the early Zanclean, oceanographic and/or atmospheric circulation changes occur as a result of the shoaling of the CAS. Boreal conditions establish in northern Norway in response to the development of a modern-like NwAC. Subsequent variations in the position/strength of the NAC and thus northward heat transport via the NwAC control vegetation and climate changes in northern Norway. This is the first such evidence for both orbital and atmospheric controls on Pliocene vegetation and climate changes, and major atmospheric circulation shifts in the Nordic Seas region.

- During the mPWP, northward heat transport via the NwAC varies on glacial-interglacial timescales. Increased Atlantic and Arctic water influence corresponds to cool temperate and boreal climatic conditions in northern Norway, respectively. Warming events at 3.285 Ma and 3.225 Ma follow the obliquity trend, suggesting an additional orbital control. The good correlation between marine and terrestrial proxy records highlights the value of combining the two, to better understand processes and controls on both oceanographic and atmospheric environmental changes.

6.3   Outlook

This research project has provided the first high-resolution pollen record for the entire Pliocene and a detailed land-sea correlation by comparing pollen and dinocyst assemblage changes for the mPWP. Implications for future research are outlined below:

- The high-resolution Piacenzian pollen record reveals a development of peatlands before the onset of NHG. The hypothesis of peatlands expansion and/or tundra development acting as a positive feedback mechanism with regard to atmospheric CO_2 drawdown and vegetation-snow feedbacks needs to be assessed via future high-resolution vegetation reconstructions in the (sub)Arctic region. Furthermore, such studies would allow for the greater comparison to identify major controls on vegetation and climate changes on regional to hemispheric-scales.

- The new Pliocene pollen record provides insights into the controlling mechanisms behind vegetation and climate changes. To fully understand the effect of apparent global (e.g. atmospheric CO_2 changes and orbital forcing), hemispheric-wide (e.g. shoaling/closure of CAS and related AMOC changes) and regional (e.g. NwAC changes and (sea) ice feedbacks) controls on terrestrial climate changes as identified in this record, further comparable studies are required. These would allow for the determination of the spatial impact of the above mentioned processes. As a specific example, an expansion of peatlands does not only occur at the end of the record but also during a previous cooler climate phase without being followed by global climatic cooling. This either suggests that the expansion of peatlands is specific to Scandinavia or that the two cooling phases are controlled by different scale climate forcings.

- The integration of terrestrial and marine palaeoenvironmental proxies from the same site for the mPWP highlights the value of combining those two to gain a better understanding of the interaction of environmental changes on land and in the sea. Furthermore, such studies enable the identification of oceanographic and/or atmospheric forcing mechanisms behind the observed climatic changes. The Pliocene environmental reconstruction for the Norwegian Sea region would benefit from a high-resolution extension of the dinocyst record to track the NwAC variability over the whole epoch.

References

Andreassen, L.M., Winsvold, S.H., Paul, F., Hausberg, J.E., 2012. Inventory of Norwegian Glaciers. Norwegian Water Resources and Energy Directorate, Oslo.

Andreev, A.A., Tarasov, P.E., Wennrich, V., Raschke, E., Herzschuh, U., Nowaczyk, N.R., Brigham-Grette, J., Melles, M., 2014. Late Pliocene and Early Pleistocene vegetation history of northeastern Russian Arctic inferred from the Lake El'gygytgyn pollen record. Clim. Past 10, 1017–1039. doi:10.5194/cp-10-1017-2014

Andrew, R., West, R.G., 1977. Pollen spectra from Pliocene crag at Orford, Suffolk. New Phytol. 78, 709–714.

Anell, I., Thybo, H., Artemieva, I.M., 2009. Cenozoic uplift and subsidence in the North Atlantic region: Geological evidence revisited. Tectonophysics 474, 78–105. doi:10.1016/j.tecto.2009.04.006

Archibold, O.W., 1995. Ecology of World Vegetation. Chapman & Hall, London.

Bachem, P.E., Risebrobakken, B., McClymont, E.L., 2016. Sea surface temperature variability in the Norwegian Sea during the late Pliocene linked to subpolar gyre strength and radiative forcing. Earth Planet. Sci. Lett. 446, 113–122. doi:10.1016/j.epsl.2016.04.024

Badger, M.P.S., Schmidt, D.N., Mackensen, A., Pancost, R.D., 2013. High-resolution alkenone palaeobarometry indicates relatively stable pCO_2 during the Pliocene (3.3-2.8 Ma). Philos. Trans. A. Math. Phys. Eng. Sci. 371, 20130094. doi:10.1098/rsta.2013.0094

Ballantyne, A.P., Greenwood, D.R., Sinninghe Damsté, J.S., Csank, A.Z., Eberle, J.J., Rybczynski, N., 2010. Significantly warmer Arctic surface temperatures during the Pliocene indicated by multiple independent proxies. Geology 38, 603–606. doi:10.1130/G30815.1

Ballantyne, A.P., Rybczynski, N., Baker, P.A., Harington, C.R., White, D., 2006. Pliocene Arctic temperature constraints from the growth rings and isotopic composition of fossil larch. Palaeogeogr. Palaeoclimatol. Palaeoecol. 242, 188–200. doi:10.1016/j.palaeo.2006.05.016

Bartlein, P.J., Harrison, S.P., Brewer, S., Connor, S., Davis, B.A.S., Gajewski, K., Guiot, J., Harrison-Prentice, T.I., Henderson, A., Peyron, O., Prentice, I.C., Scholze, M., Seppä, H., Shuman, B., Sugita, S., Thompson, R.S., Viau, A.E., Williams, J., Wu, H., 2011. Pollen-based continental climate reconstructions at 6 and 21 ka: A global synthesis. Clim. Dyn. 37, 775–802. doi:10.1007/s00382-010-0904-1

Bartoli, G., Hönisch, B., Zeebe, R.E., 2011. Atmospheric CO2 decline during the Pliocene intensification of Northern Hemisphere glaciations. Paleoceanography 26, PA4213. doi:10.1029/2010PA002055

Bennike, O., Abrahamsen, N., Bak, M., Israelson, C., Konradi, P., Matthiessen, J., Witkowski, A., 2002. A multi-proxy study of Pliocene sediments from Île de France, North-East Greenland. Palaeogeogr. Palaeoclimatol. Palaeoecol. 186, 1–23.

Beug, H.J., 2004. Leitfaden der Pollenbestimmung für Mitteleuropa und angrenzende Gebiete. Dr. Friedrich Pfeil, München.

Birks, H.J.B., 2010. Strengths and Weaknesses of Quantitative Climate Reconstructions Based on Late-Quaternary Biological Proxies. Open Ecol. J. 3, 68–110. doi:10.2174/1874213001003020068

Birks, H.J.B., 1998. D.G. Frey and E.S. Deevey Review #1: Numerical tools in palaeolimnology - Progress, potentialities, and problems. J. Paleolimnol. 20, 307–332. doi:10.1023/A:1008038808690

Birks, H.J.B., Line, J.M., 1992. The use of rarefaction analysis for estimating palynological richness from Quaternary pollen-analytical data. Holocene 2, 1–10. doi:10.1177/095968369200200101

Birks, H.J.B., Lotter, A.F., Juggins, S., Smol, J.P. (Eds.), 2012. Tracking Environmental Change Using Lake Sediments. Springer, Dordrecht Heidelberg New York London.

Bjune, A., Birks, H.J.B., Seppä, H., 2004. Holocene vegetation and climate history on a continental-oceanic transect in northern Fennoscandia based on pollen and plant macrofossils. Boreas 33, 211–223. doi:10.1080/03009480410001244

Bjune, A.E., 2005. Holocene vegetation history and tree-line changes on a north–south transect crossing major climate gradients in southern Norway—evidence from pollen and plant macrofossils in lake sediments. Rev. Palaeobot. Palynol. 133, 249–275. doi:10.1111/j.1502-3885.2004.tb01142.x

Bjune, A.E., Birks, H.J.B., 2008. Holocene vegetation dynamics and inferred climate changes at Svanåvatnet, Mo i Rana, northern Norway. Boreas 37, 146–156. doi:10.1111/j.1502-3885.2007.00006.x

Bleil, U., 1989. 40. Magnetostratigraphy of Neogene and Quaternary Sediment Series from the Norwegian Sea: Ocean Drilling Program, Leg 104. Proc. Ocean Drill. Program, Sci. Results 104, 829–901.

Blindheim, J., Borovkov, V., Hansen, B., Malmberg, S.-A., Turrell, W.R., Østerhus, S., 2000. Upper layer cooling and freshening in the Norwegian Sea in relation to atmospheric forcing. Deep Sea Res. Part I Oceanogr. Res. Pap. 47, 655–680. doi:10.1016/S0967-0637(99)00070-9

Blindheim, J., Østerhus, S., 2005. The Nordic Seas, Main Oceanographic Features. Geophys. Monogr. Ser. 158, 11–37. doi:10.1029/158GM03

Bolch, C.J., Hallegraeff, G.M., 1990. Dinoflagellate Cysts in Recent Marine Sediments from Tasmania, Australia. Bot. Mar. 33, 173–192. doi:10.1515/botm.1990.33.2.173

Bonnet, S., de Vernal, A., Hillaire-Marcel, C., Radi, T., Husum, K., 2010. Variability of sea-surface temperature and sea-ice cover in the Fram Strait over the last two millennia. Mar. Micropaleontol. 74, 59–74. doi:10.1016/j.marmicro.2009.12.001

Bottema, S., Van Straaten, L.M.J.U., 1966. Malacology and palynology of two cores from the Adriatic sea floor. Mar. Geol. 4, 553–564.

Boulter, M.C., Manum, S.B., 1997. A lost continent in a temperate Arctic. Endeavour 21, 105–108. doi:10.1016/S0160-9327(97)80218-9

Brierley, C.M., Fedorov, A. V, Liu, Z., Herbert, T.D., Lawrence, K.T., LaRiviere, J.P., 2009. Greatly Expanded Tropical Warm Pool and Weakened Hadley Circulation in the Early Pliocene. Science (80-.). 323, 1714–1718. doi:10.1126/science.1167625

Brigham-Grette, J., Melles, M., Minyuk, P., Andreev, A., Tarasov, P., DeConto, R.,

Koenig, S., Nowaczyk, N., Wennrich, V., Rosén, P., Haltia, E., Cook, T., Gebhardt, C., Meyer-Jacob, C., Snyder, J., Herzschuh, U., 2013. Pliocene Warmth, Polar Amplification, and Stepped Pleistocene Cooling Recorded in NE Arctic Russia. Science 340, 1421–1427. doi:10.1126/science.1233137

Bruch, A.A., Utescher, T., Mosbrugger, V., 2011. Precipitation patterns in the Miocene of Central Europe and the development of continentality. Palaeogeogr. Palaeoclimatol. Palaeoecol. 304, 202–211. doi:10.1016/j.palaeo.2010.10.002

Budikova, D., 2009. Role of Arctic sea ice in global atmospheric circulation: A review. Glob. Planet. Change 68, 149–163. doi:10.1016/j.gloplacha.2009.04.001

Butt, F.A., Drange, H., Elverhøi, A., Otterå, O.H., Solheim, A., 2002. Modelling Late Cenozoic isostatic elevation changes in the Barents Sea and their implications for oceanic and climatic regimes: Preliminary results. Quat. Sci. Rev. 21, 1643–1660. doi:10.1016/S0277-3791(02)00018-5

Calvo, E., Grimalt, J., Jansen, E., 2002. High resolution UK37 sea surface temperature reconstruction in the Norwegian Sea during the Holocene. Quat. Sci. Rev. 21, 1385–1394. doi:10.1016/S0277-3791(01)00096-8

Cheddadi, R., Lamb, H.F., Guiot, J., Van Der Kaars, S., 1998a. Holocene climatic change in Morocco: A quantitative reconstruction from pollen data. Clim. Dyn. 14, 883–890. doi:10.1007/s003820050262

Cheddadi, R., Mamakowa, K., Guiot, J., De Beaulieu, J.L., Reille, M., Andrieu, V., Granoszewski, W., Peyron, O., 1998b. Was the climate of the Eemian stable? A quantitative climate reconstruction from seven European pollen records. Palaeogeogr. Palaeoclimatol. Palaeoecol. 143, 73–85. doi:10.1016/S0031-0182(98)00067-4

Clarke, K.R., Gorley, R.N., 2006. PRIMER v6: User Manual/Tutorial.

Clemens, S.C., Tiedemann, R., 1997. Eccentricity forcing of Pliocene–Early Pleistocene climate revealed in a marine oxygen-isotope record. Nature 385, 801–804. doi:10.1038/385801a0

Costin, A.B., Gray, M., Totterdell, C.J., Wimbush, D.J., 2000. Kosciuszko Alpine Flora. CSIRO publishing, Melbourne, Australia.

Crowley, T.J., 1996. Pliocene climates: the nature of the problem. Mar. Micropaleontol. 27, 3–12. doi:10.1016/0377-8398(95)00049-6

Csank, A.Z., Patterson, W.P., Eglington, B.M., Rybczynski, N., Basinger, J.F., 2011. Climate variability in the Early Pliocene Arctic: Annually resolved evidence from stable isotope values of sub-fossil wood, Ellesmere Island, Canada. Palaeogeogr. Palaeoclimatol. Palaeoecol. 308, 339–349.

Dale, B., 1976. Cyst formation, sedimentation, and preservation: factors affecting dinoflagellate assemblages in recent sediments from Trondheimsfjord, Norway. Rev. Palaeobot. Palynol. 22, 39–60.

Dale, B., Dale, A.L., 2002. Environmental applications of dinoflagellate cysts and acritarchs, in: Haslett, S.K. (Ed.), Quaternary Environmental Micropalaeontology. Arnold, London, pp. 207–240.

Dale, B., Dale, A.L., 1992. Dinoflagellate Contributions to the Deep Sea, Ocean Biocoenosis Series. Woods Hole Oceanographic Insitution, Woods Hole, MA.

Dale, B., Thorsen, T.A., Fjellsa, A., 1999. Dinoflagellate Cysts as Indicators of Cultural Eutrophication in the Oslofjord, Norway. Estuar. Coast. Shelf Sci. 48, 371–382. doi:10.1006/ecss.1999.0427

Davis, B.A.S., Brewer, S., Stevenson, A.C., Guiot, J., Allen, J., Almqvist-Jacobson, H., Ammann, B., Andreev, A.A., Argant, J., Atanassova, J., Balwierz, Z., Barnosky, C.D., Bartley, D.D., De Beaulieu, J.L., Beckett, S.C., Behre, K.E., Bennett, K.D., Berglund, B.E.B., Beug, H.J., Bezusko, L., Binka, K., Birks, H.H., Birks, H.J.B., Björck, S., Bliakhartchouk, T., Bogdel, I., Bonatti, E., Bottema, S., Bozilova, E.D.B., Bradshaw, R., Brown, A.P., Brugiapaglia, E., Carrion, J., Chernavskaya, M., Clerc, J., Clet, M., Coûteaux, M., Craig, A.J., Cserny, T., Cwynar, L.C., Dambach, K., De Valk, E.J., Digerfeldt, G., Diot, M.F., Eastwood, W., Elina, G., Filimonova, L., Filipovitch, L., Gaillard-Lemdhal, M.J., Gauthier, A., Göransson, H., Guenet, P., Gunova, V., Hall, V.A.H., Harmata, K., Hicks, S., Huckerby, E., Huntley, B., Huttunen, A., Hyvärinen, H., Ilves, E., Jacobson, G.L., Jahns, S., Jankovská, V., Jóhansen, J., Kabailiene, M., Kelly, M.G., Khomutova, V.I., Königsson, L.K., Kremenetski, C., Kremenetskii, K. V., Krisai, I., Krisai, R., Kvavadze, E., Lamb, H., Lazarova, M.A., Litt, T., Lotter, A.F., Lowe, J.J., Magyari, E., Makohonienko, M., Mamakowa, K., Mangerud, J., Mariscal, B.,

Markgraf, V., McKeever, Mitchell, F.J.G., Munuera, M., Nicol-Pichard, S., Noryskiewicz, B., Odgaard, B. V., Panova, N.K., Pantaleon-Cano, J., Paus, A.A., Pavel, T., Peglar, S.M., Penalba, M.C., Pennington, W., Perez-Obiol, R., Pushenko, M., Ralska-Jasiewiszowa, M., Ramfjord, H., Regnell, J., Rybnickova, E., Rybnickova, M., Saarse, L., Sanchez Gomez, M.F., Sarmaja-Korjonen, K., Sarv, A., Seppä, H., Sivertsen, S., Smith, A.G., Spiridonova, E.A., Stancikaite, M., Stefanova, J., Stewart, D.A., Suc, J.P., Svobodova, H., Szczepanek, K., Tarasov, P., Tobolski, K., Tonkov, S.P., Turner, J., Van der Knaap, W.O., Van Leeuwen, J.F.N., Vasari, A., Vasari, Y., Verbruggen, C., Vergne, V., Veski, S., Visset, L., Vuorela, I., Wacnik, A., Walker, M.J.C., Waller, M.P., Watson, C.S., Watts, W.A., Whittington, G., Willis, K.J., Willutzki, H., Yelovicheva, Y., Yll, E.I., Zelikson, E.M., Zernitskaya, V.P., 2003. The temperature of Europe during the Holocene reconstructed from pollen data. Quat. Sci. Rev. 22, 1701–1716. doi:10.1016/S0277-3791(03)00173-2

Davis, B.A.S., Zanon, M., Collins, P., Mauri, A., Bakker, J., Barboni, D., Barthelmes, A., Beaudouin, C., Bjune, A.E., Bozilova, E., Bradshaw, R.H.W., Brayshay, B.A., Brewer, S., Brugiapaglia, E., Bunting, J., Connor, S.E., de Beaulieu, J.L., Edwards, K., Ejarque, A., Fall, P., Florenzano, A., Fyfe, R., Galop, D., Giardini, M., Giesecke, T., Grant, M.J., Guiot, J., Jahns, S., Jankovská, V., Juggins, S., Kahrmann, M., Karpińska-Kołaczek, M., Kołaczek, P., Kühl, N., Kuneš, P., Lapteva, E.G., Leroy, S.A.G., Leydet, M., Guiot, J., Jahns, S., Jankovská, V., Juggins, S., Kahrmann, M., Karpińska-Kołaczek, M., Kołaczek, P., Kühl, N., Kuneš, P., Lapteva, E.G., Leroy, S.A.G., Leydet, M., López Sáez, J.A., Masi, A., Matthias, I., Mazier, F., Meltsov, V., Mercuri, A.M., Miras, Y., Mitchell, F.J.G., Morris, J.L., Naughton, F., Nielsen, A.B., Novenko, E., Odgaard, B., Ortu, E., Overballe-Petersen, M.V., Pardoe, H.S., Peglar, S.M., Pidek, I.A., Sadori, L., Seppä, H., Severova, E., Shaw, H., Świeta-Musznicka, J., Theuerkauf, M., Tonkov, S., Veski, S., van der Knaap, W.O., van Leeuwen, J.F.N., Woodbridge, J., Zimny, M., Kaplan, J.O., 2013. The European Modern Pollen Database (EMPD) project. Veg. Hist. Archaeobot. 22, 521–530. doi:10.1007/s00334-012-0388-5

de Boer, B., Lourens, L.J., Wal, R.S.W. Van De, 2014. Persistent 400,000-year variability of Antarctic ice volume and the carbon cycle is revealed throughout the Plio-Pleistocene. Nat. Commun. 5, 1–8. doi:10.1038/ncomms3999

De Schepper, S., Fischer, E.I., Groeneveld, J., Head, M.J., Matthiessen, J., 2011. Deciphering the palaeoecology of Late Pliocene and Early Pleistocene dinoflagellate cysts. Palaeogeogr. Palaeoclimatol. Palaeoecol. 309, 17–32. doi:10.1016/j.palaeo.2011.04.020

De Schepper, S., Gibbard, P.L., Salzmann, U., Ehlers, J., 2014. A global synthesis of the marine and terrestrial evidence for glaciation during the Pliocene Epoch. Earth-Science Rev. 135, 83–102. doi:10.1016/j.earscirev.2014.04.003

De Schepper, S., Groeneveld, J., Naafs, B.D.A., Van Renterghem, C., Hennissen, J., Head, M.J., Louwye, S., Fabian, K., 2013. Northern Hemisphere Glaciation during the Globally Warm Early Late Pliocene. PLoS One 8, e81508. doi:10.1371/journal.pone.0081508

De Schepper, S., Head, M.J., 2014. New late Cenozoic acritarchs: evolution, palaeoecology and correlation potential in high latitude oceans. J. Syst. Palaeontol. 12, 493–519. doi:10.1080/14772019.2013.783883

De Schepper, S., Head, M.J., 2009. Pliocene and Pleistocene Dinoflagellate Cyst and Acritarch Zonation of DSDP Hole 610a, Eastern North Atlantic. Palynology 33, 179–218. doi:10.2113/gspalynol.33.1.179

De Schepper, S., Head, M.J., 2008a. New dinoflagellate cyst and acritarch taxa from the Pliocene and Pleistocene of the Eastern North Atlantic (DSDP Site 610). J. Syst. Palaeontol. 6, 101–117. doi:10.1017/S1477201907002167

De Schepper, S., Head, M.J., 2008b. Age calibration of dinoflagellate cyst and acritarch events in the Pliocene-Pleistocene of the eastern North Atlantic (DSDP Hole 610A). Stratigraphy 5, 137–161.

De Schepper, S., Head, M.J., Groeneveld, J., 2009a. North Atlantic Current variability through marine isotope stage M2 (circa 3.3 Ma) during the mid-Pliocene. Paleoceanography 24, PA4206.

De Schepper, S., Head, M.J., Louwye, S., 2009b. Pliocene dinoflagellate cyst stratigraphy, palaeoecology and sequence stratigraphy of the Tunnel-Canal Dock, Belgium. Geol. Mag. 146, 92–112. doi:10.1017/S0016756808005438

De Schepper, S., Head, M.J., Louwye, S., 2004. New Dinoflagellate Cyst and Incertae

Sedis Taxa From the Pliocene of Northern Belgium, Southern North Sea Basin. J. Paleontol. 78, 625–644. doi:10.1666/0022-3360(2004)078<0625:NDCAIS>2.0.CO;2

De Schepper, S., Schreck, M., Beck, K., Matthiessen, J., 2015. Early Pliocene onset of modern Nordic Seas circulation due to ocean gateway changes. Nat. Commun. 6, 1–8. doi:10.1038/ncomms9659

de Vernal, A., Henry, M., Matthiessen, J., Mudie, P.J., Rochon, A., Boessenkool, K.P., Eynaud, F., Grøsfjeld, K., Guiot, J., Hamel, D., Harland, R., Head, M.J., Kunz-Pirrung, M., Levac, E., Loucheur, V., Peyron, O., Pospelova, V., Radi, T., Turon, J.L., Voronina, E., 2001. Dinoflagellate cyst assemblages as tracers of sea-surface conditions in the Northern North Atlantic, Arctic and sub-Arctic seas: The new "n = 677" data base and its application for quantitative palaeoceanographic reconstruction. J. Quat. Sci. 16, 681–698. doi:10.1002/jqs.659

de Vernal, A., Hillaire-Marcel, C., Rochon, A., Fréchette, B., Henry, M., Solignac, S., Bonnet, S., 2013a. Dinocyst-based reconstructions of sea ice cover concentration during the Holocene in the Arctic Ocean, the northern North Atlantic Ocean and its adjacent seas. Quat. Sci. Rev. 79, 111–121. doi:10.1016/j.quascirev.2013.07.006

de Vernal, A., Mudie, P.J., 1989a. Pliocene and Pleistocene palynostratigraphy at ODP Sites 646 and 647, eastern and southern Labrador Sea, in: Proceedings of the Ocean Drilling Program, Scientific Results. Ocean Drilling Program College Station, Texas, pp. 401–422.

de Vernal, A., Mudie, P.J., 1989b. Late Pliocene to Holocene palynostratigraphy at ODP Site 645, Baffin Bay, in: Proceedings of the Ocean Drilling Program, Scientific Results. pp. 387–399.

de Vernal, A., Rochon, A., Fréchette, B., Henry, M., Radi, T., Solignac, S., 2013b. Reconstructing past sea ice cover of the Northern Hemisphere from dinocyst assemblages: Status of the approach. Quat. Sci. Rev. 79, 122–134. doi:10.1016/j.quascirev.2013.06.022

de Vernal, A., Rochon, A., Turon, J.-L., Matthiessen, J., 1998. Organic-walled dinoflagellate cysts: Palynological tracers of sea-surface conditions in middle to high latitude marine environments. Geobios 30, 905–920. doi:10.1016/S0016-

6995(97)80215-X

de Vernal, A., Rosell-Melé, A., Kucera, M., Hillaire-Marcel, C., Eynaud, F., Weinelt, M., Dokken, T., Kageyama, M., 2006. Comparing proxies for the reconstruction of LGM sea-surface conditions in the northern North Atlantic. Quat. Sci. Rev. 25, 2820–2834. doi:10.1016/j.quascirev.2006.06.006

DeConto, R.M., Pollard, D., Wilson, P.A., Pälike, H., Lear, C.H., Pagani, M., 2008. Thresholds for Cenozoic bipolar glaciation. Nature 455, 652–656. doi:10.1038/nature07337

Delworth, T., Dixon, K., 2000. Implications of the recent trend in the Arctic/North Atlantic oscillation for the North Atlantic thermohaline circulation. J. Clim. 13, 3721–3727.

Demske, D., Mohr, B., Oberhänsli, H., 2002. Late Pliocene vegetation and climate of the Lake Baikal region, southern East Siberia, reconstructed from palynological data. Palaeogeogr. Palaeoclimatol. Palaeoecol. 184, 107–129.

Demske, D., Tarasov, P.E., Nakagawa, T., 2013. Atlas of pollen, spores and further non-pollen palynomorphs recorded in the glacial-interglacial late Quaternary sediments of Lake Suigetsu, central Japan. Quat. Int. 290-291, 164–238. doi:10.1016/j.quaint.2012.02.002

Diekmann, M., 1994. Deciduous forest vegetation in Boreo-nemoral Scandinavia. Acta Phytogeogr. Suec. 80, 1–112.

Donders, T.H., Kloosterboer-van Hoeve, M.L., Westerhoff, W., Verreussel, R.M.C.H., Lotter, A.F., 2007. Late Neogene continental stages in NW Europe revisited. Earth-Science Rev. 85, 161–186. doi:10.1016/j.earscirev.2007.06.004

Dowsett, H., Dolan, A., Rowley, D., Pound, M., Salzmann, U., Robinson, M., Chandler, M., Foley, K., Haywood, A., 2016. The PRISM4 (mid-Piacenzian) palaeoenvironmental reconstruction. Clim. Past 12, 1519–1538.

Dowsett, H., Robinson, M., Foley, K., 2015. A global planktic foraminifer census data set for the Pliocene ocean. Sci. Data 2, 150076. doi:10.1038/sdata.2015.76

Dowsett, H., Robinson, M., Haywood, A.M., Salzmann, U., Hill, D., Sohl, L.E., Chandler, M., Williams, M., Foley, K., Stoll, D.K., 2010. The PRISM3D

paleoenvironmental reconstruction. Stratigraphy 7, 123–139.

Dowsett, H.J., 2007. The PRISM palaeoclimate reconstruction and Pliocene sea-surface temperature, in: Williams, M., Haywood, A.M., Gregory, F.J., Schmidt, D.N. (Eds.), Deep-Time Perspectives on Climate Change: Marrying the Signal from Computer Models and Biological Proxies. pp. 459–480.

Dowsett, H.J., Barron, J.A., Poore, R.Z., Thompson, R.S., Cronin, T.M., Ishman, S.E., Willard, D.A., 1999. Middle Pliocene paleoenvironmental reconstruction: PRISM2. USGS Open File Rep.

Dowsett, H.J., Cronin, T.M., Poore, R.Z., Thompson, R.S., Whatley, R.C., Wood, A.M., 1992. Micropaleontological Evidence for Increased Meridional Heat Transport in the North Atlantic Ocean During the Pliocene. Science (80-.). 258, 1133–1135. doi:10.1126/science.258.5085.1133

Dowsett, H.J., Foley, K.M., Stoll, D.K., Chandler, M.A., Sohl, L.E., Bentsen, M., Otto-Bliesner, B.L., Bragg, F.J., Chan, W.-L., Contoux, C., Dolan, A.M., Haywood, A.M., Jonas, J.A., Jost, A., Kamae, Y., Lohmann, G., Lunt, D.J., Nisancioglu, K.H., Abe-Ouchi, A., Ramstein, G., Riesselman, C.R., Robinson, M.M., Rosenbloom, N.A., Salzmann, U., Stepanek, C., Strother, S.L., Ueda, H., Yan, Q., Zhang, Z., 2013a. Sea Surface Temperature of the mid-Piacenzian Ocean: A Data-Model Comparison. Sci. Rep. 3, 1–8. doi:10.1038/srep02013

Dowsett, H.J., Robinson, M.M., Foley, K.M., 2009. Pliocene three-dimensional global ocean temperature reconstruction. Clim. Past 5, 769–783. doi:10.5194/cpd-5-1901-2009

Dowsett, H.J., Robinson, M.M., Stoll, D.K., Foley, K.M., Johnson, A.L.A., Williams, M., Riesselman, C.R., 2013b. The PRISM (Pliocene palaeoclimate) reconstruction: time for a paradigm shift. Philos. Trans. A. Math. Phys. Eng. Sci. 371, 20120524. doi:10.1098/rsta.2012.0524

Driscoll, N.W., Haug, G., 1998. A Short Circuit in Thermohaline Circulation: A Cause for Northern Hemisphere Glaciation? Science (80-.). 282, 436–438. doi:10.1126/science.282.5388.436

Dupont, L., 2011. Orbital scale vegetation change in Africa. Quat. Sci. Rev. 30, 3589–3602. doi:10.1016/j.quascirev.2011.09.019

Eidvin, T., Riis, F., Rasmussen, E.S., 2014. Oligocene to Lower Pliocene deposits of the Norwegian continental shelf, Norwegian Sea, Svalbard, Denmark and their relation to the uplift of Fennoscandia: A synthesis. Mar. Pet. Geol. 56, 184–221. doi:10.1016/j.marpetgeo.2014.04.006

Eldrett, J.S., Greenwood, D.R., Polling, M., Brinkhuis, H., Sluijs, A., 2014. A seasonality trigger for carbon injection at the Paleocene-Eocene Thermal Maximum. Clim. Past 10, 759–769. doi:10.5194/cp-10-759-2014

Erdtman, G., Berglund, B., Praglowski, J., 1961. An introduction to a Scandinavian pollen flora. Almqvist & Wiksells, Uppsala.

Evitt, W.R., 1985. Sporopollenin dinoflagellate cysts: their morphology and interpretation. American Association of Stratigraphic Palynologists Foundation, Dallas, TX.

Expedition 302 Scientists, 2006. Expedition 302 summary, Proceedings of the Integrated Ocean Drilling Program. Integrated Ocean Drilling Program Management International, Inc., Edinburgh. doi:10.2204/iodp.proc.302.101.2006

Faegri, K., Iversen, J., 1989. Textbook of Pollen Analysis. Wiley&Sons, Chichester.

Fauquette, S., Guiot, J., Suc, J.-P., 1998. A method for climatic reconstruction of the Mediterranean Pliocene using pollen data. Palaeogeogr. Palaeoclimatol. Palaeoecol. 144, 183–201.

Fauquette, S., Suc, J.-P., Guiot, J., Diniz, F., Feddi, N., Zheng, Z., Bessais, E., Drivaliari, A., 1999. Climate and biomes in the West Mediterranean area during the Pliocene. Palaeogeogr. Palaeoclimatol. Palaeoecol. 152, 15–36. doi:http://dx.doi.org/10.1016/S0031-0182(99)00031-0

Fedorov, A. V, Brierley, C.M., Lawrence, K.T., Liu, Z., Dekens, P.S., Ravelo, A.C., 2013. Patterns and mechanisms of early Pliocene warmth. Nature 496, 43–49.

Fensome, R.A., MacRae, R.A., Williams, G.L., 2008. DINOFLAJ2, Version1 [WWW Document]. Am. Assoc. Stratigr. Palynol. Data Ser. No. 1. URL http://dinoflaj.smu.ca/wiki/Main_Page (accessed 26.9.16).

Ferguson, D.K., Knobloch, E., 1998. A fresh look at the rich assemblage from the Pliocene sink-hole of Willershausen, Germany. Rev. Palaeobot. Palynol. 101, 271–

286.

Figueiral, I., Mosbrugger, V., Rowe, N.P., Ashraf, A.R., Utescher, T., Jones, T.P., 1999. The miocene peat-forming vegetation of northwestern Germany: An analysis of wood remains and comparison with previous palynological interpretations. Rev. Palaeobot. Palynol. 104, 239–266. doi:10.1016/S0034-6667(98)00059-1

Fronval, T., Jansen, E., 1996. Late Neogene paleoclimates and paleoceanography in the Iceland-Norwegian Sea: evidence from the Iceland and Vøring Plateaus. Proc. Ocean Drill. Program, Sci. Results 151, 455–468.

Furevik, T., 2000. Large-scale atmospheric circulation variability and its impacts on the Nordic seas ocean climate: A review. Nord. Seas An Integr. Perspect. Geophys. Monogr. Ser. 158, 105–136.

Gajewski, K., Viau, A., Sawada, M., Atkinson, D., Wilson, S., 2001. Sphagnum peatland distribution in North America and Eurasia during the past 21,000 years. Global Biogeochem. Cycles 15, 297–310. doi:10.1029/2000GB001286

Gallimore, R.G., Kutzbach, J.E., 1996. Role of orbitally induced changes in tundra area in the onset of glaciation. Nature 381, 503–505. doi:10.1038/381503a0

Gao, C., McAndrews, J.H., Wang, X., Menzies, J., Turton, C.L., Wood, B.D., Pei, J., Kodors, C., 2012. Glaciation of North America in the James Bay Lowland, Canada, 3.5 Ma. Geology 40, 975–978.

Gibbard, P.L., Head, M.J., Walker, M.J.C., 2010. Formal ratification of the Quaternary System/Period and the Pleistocene Series/Epoch with a base at 2.58 Ma. J. Quat. Sci. 25, 96–102. doi:10.1002/jqs.1338

Gladenkov, A.Y., Oleinik, A.E., Marincovich Jr., L., Barinov, K.B., 2002. A refined age for the earlier opening of Bering Strait. Paleogeography, Paleclimatology, Paleoecol. 183, 321–328.

Gordon, C., Cooper, C., Senior, C.A., Banks, H., Gregory, J.M., Johns, T.C., Mitchell, J.F.B., Wood, R.A., 2000. The simulation of SST, sea ice extents and ocean heat transports in a version of the Hadley Centre coupled model without flux adjustments. Clim. Dyn. 16, 147–168. doi:10.1007/s003820050010

Grimm, E.C., 1990. TILIA and TILIA* GRAPH. PC spreadsheet and graphics software

for pollen data. INQUA, Work. Gr. Data-Handling Methods Newsl. 4, 5–7.

Grimm, E.C., 1987. CONISS: a FORTRAN 77 program for stratigraphically constrained cluster analysis by the method of incremental sum of squares. Comput. Geosci. 13, 13–35.

Grimm, G.W., Denk, T., 2012. Reliability and resolution of the coexistence approach — A revalidation using modern-day data. Rev. Palaeobot. Palynol. 172, 33–47. doi:10.1016/j.revpalbo.2012.01.006

Grimm, G.W., Potts, A.J., 2016. Fallacies and fantasies: The theoretical underpinnings of the Coexistence Approach for palaeoclimate reconstruction. Clim. Past 12, 611–622. doi:10.5194/cp-12-611-2016

Grøsfjeld, K., De Schepper, S., Fabian, K., Husum, K., Baranwal, S., Andreassen, K., Knies, J., 2014. Dating and palaeoenvironmental reconstruction of the sediments around the Miocene/Pliocene boundary in Yermak Plateau ODP Hole 911A using marine palynology. Palaeogeogr. Palaeoclimatol. Palaeoecol. 414, 382–402. doi:10.1016/j.palaeo.2014.08.028

Grøsfjeld, K., Harland, R., Howe, J., 2009. Dinoflagellate cyst assemblages inshore and offshore Svalbard reflecting their modern hydrography and climate. Nor. J. Geol. 89, 121–134.

Guiot, J., 1990. Methodology of the last climatic cycle reconstruction in France from pollen data. Palaeogeogr. Palaeoclimatol. Palaeoecol. 80, 49–69. doi:10.1016/0031-0182(90)90033-4

Guiot, J., Pons, A., de Beaulieu, J.L., Reille, M., 1989. A 140,000-year continental climate reconstruction from two European pollen records. Nature 338, 309–313. doi:10.1038/338309a0

Gurevitch, J., Scheiner, S.M., Fox, G.A., 2002. The ecology of plants.

Hall, C.M., 2003. High-latitude mesospheric mean winds: A comparison between Tromsø (69°N) and Svalbard (78°N). J. Geophys. Res. 108, 1–12. doi:10.1029/2003JD003509

Hammer, Ø., Harper, D. a. T., Ryan, P.D., 2001. Paleontological statistics software package for education and data analysis. Palaeontol. Electron. 4, 9–18.

doi:10.1016/j.bcp.2008.05.025

Hansen, B., Østerhus, S., 2000. North Atlantic–Nordic Seas exchanges. Prog. Oceanogr. 45, 109–208. doi:10.1016/S0079-6611(99)00052-X

Haug, G.H., Tiedemann, R., 1998. Effect of the formation of the Isthmus of Panama on Atlantic Ocean thermohaline circulation. Nature 393, 673–676.

Haug, G.H., Tiedemann, R., Zahn, R., Ravelo, A.C., 2001. Role of Panama uplift on oceanic freshwater balance. Geology 29, 207–210. doi:10.1130/0091-7613(2001)029<0207:ROPUOO>2.0.CO;2

Haywood, A.M., Dolan, A.M., Pickering, S.J., Dowsett, H.J., McClymont, E.L., Prescott, C.L., Salzmann, U., Hill, D.J., Hunter, S.J., Lunt, D.J., 2013a. On the identification of a Pliocene time slice for data–model comparison. Philos. Trans. R. Soc. A Math. Phys. Eng. Sci. 371, 1–21.

Haywood, A.M., Dowsett, H.J., Dolan, A.M., 2016. Integrating geological archives and climate models for the mid-Pliocene warm period. Nat. Commun. 7, 10646. doi:10.1038/ncomms10646

Haywood, A.M., Hill, D.J., Dolan, A.M., Otto-Bliesner, B.L., Bragg, F., Chan, W.-L., Chandler, M.A., Contoux, C., Dowsett, H.J., Jost, A., Kamae, Y., Lohmann, G., Lunt, D.J., Abe-Ouchi, A., Pickering, S.J., Ramstein, G., Rosenbloom, N.A., Salzmann, U., Sohl, L., Stepanek, C., Ueda, H., Yan, Q., Zhang, Z., 2013b. Large-scale features of Pliocene climate: results from the Pliocene Model Intercomparison Project. Clim. Past 9, 191–209. doi:10.5194/cp-9-191-2013

Haywood, A.M., Ridgwell, A., Lunt, D.J., Hill, D.J., Pound, M.J., Dowsett, H.J., Dolan, A.M., Francis, J.E., Williams, M., 2011. Are there pre-Quaternary geological analogues for a future greenhouse warming? Philos. Trans. R. Soc. A Math. Phys. Eng. Sci. 369, 933–956.

Haywood, A.M., Sellwood, B.W., Valdes, P.J., 2000. Regional warming: Pliocene (3 Ma) paleoclimate of Europe and the Mediterranean. Geology 28, 1063–1066.

Haywood, A.M., Valdes, P.J., 2004. Modelling Pliocene warmth: contribution of atmosphere, oceans and cryosphere. Earth Planet. Sci. Lett. 218, 363–377.

Head, M.J., 2003. Neogene Occurrences of the Marine Acritarch Genus

Nannobarbophora Habib and Knapp, 1982 Emend., and the New Species N. Gedlii. J. Paleontol. 77, 382–385. doi:10.1666/0022-3360(2003)077<0382:NOOTMA>2.0.CO;2

Head, M.J., 1998. Pollen and dinoflagellates from the Red Crag at Walton-on-the-Naze, Essex: evidence for a mild climatic phase during the early Late Pliocene of eastern England. Geol. Mag. 135, 803–817.

Head, M.J., 1997. Thermophilic Dinoflagellate Assemblages from the Mid Pliocene of Eastern England. J. Paleontol. 71, 165–193.

Head, M.J., 1996a. Chapter 30. Modern dinoflagellate cysts and their biological affinities, in: Jansonius, J., McGregor, D.C. (Eds.), Palynology: Principles and Applications. American Association of Stratigraphic Palynologists Foundation, Dallas, TX, pp. 1197–1248.

Head, M.J., 1996b. Late Cenozoic Dinoflagellates from the Royal Society Borehole at Ludham, Norfolk, Eastern England. J. Paleontol. 70, 543–570.

Head, M.J., 1994. Morphology and Paleoenvironmental Significance of the Cenozoic Dinoflagellate Genera Tectatodinium and Habibacysta. Micropaleontology 40, 289–321.

Head, M.J., 1993. Dinoflagellates, Sporomorphs, and Other Palynomorphs from the Upper Pliocene St. Erth Beds of Cornwall, Southwestern England. Mem. (The Paleontol. Soc. 67, 1–62.

Head, M.J., Norris, G., 2003. New Species of Dinoflagellate Cysts and Other Palynomorphs From the Latest Miocene and Pliocene of DSDP Hole 603C, Western North Atlantic. J. Paleontol. 77, 1–15. doi:10.1666/0022-3360(2003)077<0001:NSODCA>2.0.CO;2

Head, M.J., Westphal, H., 1999. Palynology and Paleoenvironments of a Pliocene Carbonate Platform: The Clino Core, Bahamas. J. Paleontol. 73, 1–25.

Hennissen, J.A.I., Head, M.J., De Schepper, S., Groeneveld, J., 2014. Palynological evidence for a southward shift of the North Atlantic Current at ~2.6 Ma during the intensification of late Cenozoic Northern Hemisphere glaciation. Paleoceanography 29, 564–580. doi:10.1002/2013PA002543

Herbert, T.D., Ng, G., Cleaveland Peterson, L., 2015. Evolution of Mediterranean sea surface temperatures 3.5–1.5 Ma: Regional and hemispheric influences. Earth Planet. Sci. Lett. 409, 307–318. doi:10.1016/j.epsl.2014.10.006

Herbert, A. V., Harrison, S.P., 2016. Evaluation of a modern-analogue methodology for reconstructing Australian palaeoclimate from pollen. Rev. Palaeobot. Palynol. 226, 65–77. doi:10.1016/j.revpalbo.2015.12.006

Herzschuh, U., Birks, H.J.B., Laepple, T., Andreev, A., Melles, M., Brigham-Grette, J., 2016. Glacial legacies on interglacial vegetation at the Pliocene-Pleistocene transition in NE Asia. Nat. Commun. 7, 11967. doi:10.1038/ncomms11967

Herzschuh, U., Birks, H.J.B., Mischke, S., Zhang, C., Böhner, J., 2010. A modern pollen-climate calibration set based on lake sediments from the tibetan plateau and its application to a late quaternary pollen record from the qilian mountains. J. Biogeogr. 37, 752–766. doi:10.1111/j.1365-2699.2009.02245.x

Heusser, L., Balsam, W.L., 1977. Pollen distribution in the northeast Pacific Ocean. Quat. Res. 7, 45–62.

Heusser, L.E., 1983. Pollen distribution in the bottom sediments of the western North Atlantic ocean. Mar. Micropaleontol. 8, 77–88.

Heusser, L.E., Balsam, W.L., 1985. Pollen sedimentation in the Northwest Atlantic: effects of the western boundary undercurrent. Mar. Geol. 69, 149–153.

Hilgen, F.J., Lourens, L.J., Van Dam, J.A., 2012. Chapter 29 - The Neogene Period, in: The Geologic Time Scale. Elsevier, Burlington, MA, USA, pp. 923–978. doi:10.1016/B978-0-444-59425-9.00029-9

Hill, D.J., 2015. The non-analogue nature of Pliocene temperature gradients. Earth Planet. Sci. Lett. 425, 232–241. doi:10.1016/j.epsl.2015.05.044

Hooghiemstra, H., Lézine, A.-M., Leroy, S.A.G., Dupont, L., Marret, F., 2006. Late Quaternary palynology in marine sediments: A synthesis of the understanding of pollen distribution patterns in the NW African setting. Quat. Int. 148, 29–44. doi:10.1016/j.quaint.2005.11.005

IPCC, 2013. Summary for Policymakers, in: Stocker, T.F., Qin, D., Plattner, G.-K., Tignor, M., Allen, S.K., Boschung, J., Nauels, A., Xia, Y., Bex, V., Midgley, P.M.

(Eds.), Climate Change 2013: The Physical Science Basis. Contribution of Working Group I to the Fifth Assessment Report of the Intergovemmental Panel on Climate Change. Cambridge University Press, Cambridge, United Kingdom and New York, NY, USA.

Ishikawa, S., Watanabe, N., 1986. An ecological study on the Sciadopitys verticillata forest and other natural forests of Mt. Irazu, southern Shikoku, Japan. Mem. - Fac. Sci. Kochi Univ. Ser. D Biol. 7, 63–66.

Ivanov, D.A., Ashraf, A.R., Mosbrugger, V., 2007. Late Oligocene and Miocene climate and vegetation in the Eastern Paratethys area (northeast Bulgaria), based on pollen data. Palaeogeogr. Palaeoclimatol. Palaeoecol. 255, 342–360. doi:10.1016/j.palaeo.2007.08.003

Jansen, E., Fronval, T., Rack, F., Channell, J.E.T., 2000. Pliocene-Pleistocene ice rafting history and cyclicity in the Nordic seas during the last 3.5 Myr. Paleoceanography 15, 709–721. doi:10.1029/1999PA000435

Jansen, E., Sjøholm, J., 1991. Reconstruction of Glaciation over the Past 6 Myr from Ice-Borne Deposits in the Norwegian Sea. Lett. to Nat. 349, 600–603.

Jansson, I.M., Mertens, K.N., Head, M.J., de Vernal, A., Londeix, L., Marret, F., Matthiessen, J., Sangiorgi, F., 2014. Statistically assessing the correlation between salinity and morphology in cysts produced by the dinoflagellate Protoceratium reticulatum from surface sediments of the North Atlantic Ocean, Mediterranean-Marmara-Black Sea region, and Baltic-Kattegat-Skage. Palaeogeogr. Palaeoclimatol. Palaeoecol. 399, 202–213. doi:10.1016/j.palaeo.2014.01.012

Jiménez-Moreno, G., Burjachs, F., Expósito, I., Oms, O., Carrancho, A., Villalaín, J.J., Agustí, J., Campeny, G., Gómez de Soler, B., van der Made, J., 2013. Late Pliocene vegetation and orbital-scale climate changes from the western Mediterranean area. Glob. Planet. Change.

Juggins, S., Birks, H.J.B., 2012. Quantitative Environmental Reconstructions from Biological Data, in: Birks, H.J.B., Lotter, A.F., Juggins, S., Smol, J.P. (Eds.), Tracking Environmental Change Using Lake Sediments. Dordrecht Heidelberg New York London, pp. 431–494.

Keil, R.G., Hu, F.S., Tsamakis, E.C., Hedges, J.I., 1994. Pollen in marine sediments as

an indicator of oxidation of organic matter. Nature 369, 639–641. doi:10.1038/369639a0

Khélifi, N., Sarnthein, M., Naafs, B.D.A., 2012. Technical note: Late Pliocene age control and composite depths at ODP Site 982, revisited. Clim. Past 8, 79–87. doi:10.5194/cp-8-79-2012

Kleiven, H., Jansen, E., Fronval, T., Smith, T.M., 2002. Intensification of Northern Hemisphere glaciations in the circum Atlantic region (3.5-2.4 Ma) - ice-rafted detritus evidence. Palaeogeogr. Palaeoclimatol. Palaeoecol. 184, 213–223.

Knies, J., Cabedo-Sanz, P., Belt, S.T., Baranwal, S., Fietz, S., Rosell-Melé, A., 2014a. The emergence of modern sea ice cover in the Arctic Ocean. Nat. Commun. 5, 5608. doi:10.1038/ncomms6608

Knies, J., Matthiessen, J., Vogt, C., Laberg, J.S., Hjelstuen, B.O., Smelror, M., Larsen, E., Andreassen, K., Eidvin, T., Vorren, T.O., 2009. The Plio-Pleistocene glaciation of the Barents Sea–Svalbard region: a new model based on revised chronostratigraphy. Quat. Sci. Rev. 28, 812–829. doi:10.1016/j.quascirev.2008.12.002

Knies, J., Matthiessen, J., Vogt, C., Stein, R., 2002. Evidence of "Mid-Pliocene (~3 Ma) global warmth" in the eastern Arctic Ocean and implications for the Svalbard / Barents Sea ice sheet during the late Pliocene and early Pleistocene (~3–1.7 Ma). Boreas 31, 82–93.

Knies, J., Mattingsdal, R., Fabian, K., Grøsfjeld, K., Baranwal, S., Husum, K., De Schepper, S., Vogt, C., Andersen, N., Matthiessen, J., Andreassen, K., Jokat, W., Nam, S.-I., Gaina, C., 2014b. Effect of early Pliocene uplift on late Pliocene cooling in the Arctic–Atlantic gateway. Earth Planet. Sci. Lett. 387, 132–144. doi:10.1016/j.epsl.2013.11.007

Koenig, S.J., DeConto, R.M., Pollard, D., 2011. Late Pliocene to Pleistocene sensitivity of the Greenland Ice Sheet in response to external forcing and internal feedbacks. Clim. Dyn. 37, 1247–1268. doi:10.1007/s00382-011-1050-0

Koreneva, E. V., Zaklinskaya, E.D., Bratseva, G.M., 1976. 32. Palynology studies of sites 336, 338, 345, and 348, DSDP Leg 38. Initial Reports Deep Sea Drill. Proj. 38 1169–1193.

Kotthoff, U., Greenwood, D.R., McCarthy, F.M.G., Müller-Navarra, K., Prader, S., Hesselbo, S.P., 2014. Late Eocene to middle Miocene (33 to 13 million years ago) vegetation and climate development on the North American Atlantic Coastal Plain (IODP Expedition 313, Site M0027). Clim. Past 10, 1523–1539. doi:10.5194/cp-10-1523-2014

LaRiviere, J.P., Ravelo, A.C., Crimmins, A., Dekens, P.S., Ford, H.L., Lyle, M., Wara, M.W., 2012. Late Miocene decoupling of oceanic warmth and atmospheric carbon dioxide forcing. Nature 486, 97–100. doi:10.1038/nature11200

Larsson, L.M., Dybkjær, K., Rasmussen, E.S., Piasecki, S., Utescher, T., Vajda, V., 2011. Miocene climate evolution of northern Europe: A palynological investigation from Denmark. Palaeogeogr. Palaeoclimatol. Palaeoecol. 309, 161–175. doi:10.1016/j.palaeo.2011.05.003

Laskar, J., Robutel, P., Joutel, F., Gastineau, M., Correia, A.C.M., Levrard, B., 2004. A long-term numerical solution for the insolation quantities of the Earth. Astron. Astrophys. 428, 261–285. doi:10.1051/0004-6361:20041335

Lawrence, K.T., Bailey, I., Raymo, M.E., 2013. Re-evaluation of the age model for North Atlantic Ocean Site 982 - Arguments for a return to the original chronology. Clim. Past 9, 2391–2397. doi:10.5194/cp-9-2391-2013

Lawrence, K.T., Herbert, T.D., Brown, C.M., Raymo, M.E., Haywood, A.M., 2009. High-amplitude variations in North Atlantic sea surface temperature during the early Pliocene warm period. Paleoceanography 24, PA2218. doi:10.1029/2008PA001669

Lebreton, V., Messager, E., Marquer, L., Renault-Miskovsky, J., 2010. A neotaphonomic experiment in pollen oxidation and its implications for archaeopalynology. Rev. Palaeobot. Palynol. 162, 29–38. doi:10.1016/j.revpalbo.2010.05.002

Legendre, P., Birks, H.J.B., 2012. From classical to canonical ordination, in: Birks, H.J.B., Lotter, A.F., Juggins, S., Smol, J.P. (Eds.), Tracking Environmental Change Using Lake Sediments. Springer, Dordrecht, pp. 201–248.

Leroy, S., Dupont, L., 1994. Development of vegetation and continental aridity in northwestern Africa during the Late Pliocene: the pollen record of ODP site 658.

166

Palaeogeogr. Palaeoclimatol. Palaeoecol. 109, 295–316. doi:10.1016/0031-0182(94)90181-3

Leroy, S.A.G., Dupont, L.M., 1997. Marine palynology of the ODP Site 658 (N-W Africa) and its contribution to the stratigraphy of late Pliocene. GEOBIOS 30, 351–359.

Li, X., Jiang, D., Zhang, Z., Zhang, R., Tian, Z., Yan, Q., 2015. Mid-Pliocene westerlies from PlioMIP simulations. Adv. Atmos. Sci. 32, 909–923. doi:10.1007/s00376-014-4171-7

Li, Y., Xu, Q., Liu, J., Yang, X., Nakagawa, T., 2007. A transfer-function model developed from an extensive surface-pollen data set in northern China and its potential for palaeoclimate reconstructions. The Holocene 17, 897–905. doi:10.1177/0959683607082404

Lisiecki, L.E., Raymo, M.E., 2005. A Pliocene-Pleistocene stack of 57 globally distributed benthic δ18O records. Paleoceanography 20, PA1003.

Louwye, S., Head, M.J., De Schepper, S., 2004. Dinoflagellate cyst stratigraphy and palaeoecology of the Pliocene in northern Belgium, southern North Sea Basin. Geol. Mag. 141, 353–378. doi:10.1017/S0016756804009136

Lozier, M.S., Owens, W.B., Curry, R.G., 1995. The climatology of the North Atlantic. Prog. Oceanogr. 36, 1–44. doi:10.1016/0079-6611(95)00013-5

Lunt, D.J., Foster, G.L., Haywood, A.M., Stone, E.J., 2008a. Late Pliocene Greenland glaciation controlled by a decline in atmospheric CO2 levels. Nature 454, 1102–1105.

Lunt, D.J., Haywood, A.M., Schmidt, G.A., Salzmann, U., Valdes, P.J., Dowsett, H.J., Loptson, C.A., 2012. On the causes of mid-Pliocene warmth and polar amplification. Earth Planet. Sci. Lett. 321-322, 128–138. doi:10.1016/j.epsl.2011.12.042

Lunt, D.J., Valdes, P.J., Haywood, A., Rutt, I.C., 2008b. Closure of the Panama Seaway during the Pliocene: implications for climate and Northern Hemisphere glaciation. Clim. Dyn. 30, 1–18. doi:10.1007/s00382-007-0265-6

MacDonald, G.M., Beilman, D.W., Kremenetski, K. V, Sheng, Y., Smith, L.C.,

Velichko, A.A., 2006. Rapid Early Development of Circumarctic Peatlands and Atmospheric CH4 and CO2 Variations. Science 314, 285–288. doi:10.1126/science.1131722

Mangerud, J., Jansen, E., Landvik, J.Y., 1996. Late Cenozoic history of the Scandinavian and Barents Sea ice sheets. Glob. Planet. Change 12, 11–26. doi:10.1016/0921-8181(95)00009-7

Marret, F., Zonneveld, K.A.F., 2003. Atlas of modern organic-walled dinoflagellate cyst distribution. Rev. Palaeobot. Palynol. 125, 1–200. doi:10.1016/S0034-6667(02)00229-4

Martínez-Botí, M.A., Foster, G.L., Chalk, T.B., Rohling, E.J., Sexton, P.F., Lunt, D.J., Pancost, R.D., Badger, M.P.S., Schmidt, D.N., 2015. Plio-Pleistocene climate sensitivity evaluated using high-resolution CO2 records. Nature 518, 49–54. doi:10.1038/nature14145

Matthiessen, J., 1995. Distribution patterns of dinoflagellate cysts and other organic-walled microfossils in recent Norwegian-Greenland Sea sediments. Mar. Micropaleontol. 24, 307–334. doi:10.1016/0377-8398(94)00016-G

Matthiessen, J., Brenner, W., 1996. 13. Dinoflagellate cyst ecostratigraphy of Pliocene-Pleistocene sediments from the Yermak Plateau (Arctic Ocean, Hole 911A). Proc. Ocean Drill. Program, Sci. Results 151, 243–253.

Matthiessen, J., de Vernal, A., Head, M., Okolodkov, Y., Zonneveld, K., Harland, R., 2005. Modern organic-walled dinoflagellate cysts in Arctic marine environments and their (paleo-) environmental significance. Paläontologische Zeitschrift 79, 3–51. doi:10.1007/BF03021752

Matthiessen, J., Knies, J., Vogt, C., Stein, R., 2009. Pliocene palaeoceanography of the Arctic Ocean and subarctic seas. Philos. Trans. A. Math. Phys. Eng. Sci. 367, 21–48. doi:10.1098/rsta.2008.0203

Mattingsdal, R., Knies, J., Andreassen, K., Fabian, K., Husum, K., Grøsfjeld, K., De Schepper, S., 2013. A new 6 Myr stratigraphic framework for the Atlantic–Arctic Gateway. Quat. Sci. Rev. 92, 170–178. doi:10.1016/j.quascirev.2013.08.022

McClymont, E., Dekens, P., Dowsett, H.J., Dupont, L.M., Haywood, A.M., Salzmann,

U., 2015. Pliocene climate variability over glacial-interglacial timescales (PlioVAR) working group. PAGES Mag. 23, 2015.

Mertens, K.N., Bringué, M., Van Nieuwenhove, N., Takano, Y., Pospelova, V., Rochon, A., De Vernal, A., Radi, T., Dale, B., Patterson, R.T., Weckström, K., Andrén, E., Louwye, S., Matsuoka, K., 2012. Process length variation of the cyst of the dinoflagellate Protoceratium reticulatum in the North Pacific and Baltic-Skagerrak region: Calibration as an annual density proxy and first evidence of pseudo-cryptic speciation. J. Quat. Sci. 27, 734–744. doi:10.1002/jqs.2564

Mertens, K.N., Dale, B., Ellegaard, M., Jansson, I., Godhe, A., 2010. Process length variation in cysts of the dinoflagellate Protoceratium reticulatum, from surface sediments of the Baltic–Kattegat–Skagerrak estuarine system: a regional salinity proxy. Boreas 40, 242–255. doi:10.1111/j.1502-3885.2010.00193.x

Mertens, K.N., González, C., Delusina, I., Louwye, S., 2009. 30 000 years of productivity and salinity variations in the late Quaternary Cariaco Basin revealed by dinoflagellate cysts. Boreas 38, 647–662. doi:10.1111/j.1502-3885.2009.00095.x

Miller, G.H., Alley, R.B., Brigham-Grette, J., Fitzpatrick, J.J., Polyak, L., Serreze, M.C., White, J.W.C., 2010. Arctic amplification: can the past constrain the future? Quat. Sci. Rev. 29, 1779–1790. doi:10.1016/j.quascirev.2010.02.008

Moe, D., 1974. Identification Key for Trilete Microspores of Fennoscandian Pteridophyta. Grana 14, 132–142.

Moen, A., 1999. National Atlas of Norway: vegetation. Norwegian Mapping Authority, Hønefoss, Norway.

Moen, A., 1987. The regional vegetation of Norway; that of central Norway in particular. Nord. Geogr. Tidsskr. 41, 179–226.

Mohr, B., 1986. Die Mikroflora der Oberpliozänen Tone von Willershausen (Kreis Northeim, Niedersachen). Palaeontogr. Abt. B 198, 133–156.

Mohr, B., 1984. Die Mikroflora der Obermiozänen bis Unterpliozänen Deckschichten der rheinischen Braunkohle. Palaeontogr. Abt. B 191, 29–133.

Molnar, P., 2008. Closing of the Central American Seaway and the Ice Age: A critical

review. Paleoceanography 23, PA2201.

Montade, V., Nebout, N.C., Kissel, C., Mulsow, S., 2011. Pollen distribution in marine surface sediments from Chilean Patagonia. Mar. Geol. 282, 161–168. doi:10.1016/j.margeo.2011.02.001

Montes, C., Cardona, A., Jaramillo, C., Pardo, A., Silva, J.C., Valencia, V., Ayala, C., Pérez-Angel, L.C., Rodriquez-Parra, L.A., Ramirez, V., Niño, H., 2015. Middle Miocene closure of the Central American Seaway. Science (80). 348, 226–229.

Mork, M., 1981. Circulation phenomena and frontal dynamics of the Norwegian coastal current. Philos. Trans. R. Soc. London 302, 635–647.

Mosbrugger, V., Gee, C.T., Belz, G., Ashraf, A.R., 1994. Three-dimensional reconstruction of an in-situ Miocene peat forest from the Lower Rhine Embayment, northwestern Germany—new methods in palaeovegetation analysis. Palaeogeogr. Palaeoclimatol. Palaeoecol. 110, 295–317. doi:10.1016/0031-0182(94)90089-2

Mosbrugger, V., Utescher, T., 1997. The coexistence approach - a method for quantitative reconstructions of Tertiary terrestrial palaeoclimate data using plant fossils. Palaeogeogr. Palaeoclimatol. Palaeoecol. 134, 61–86.

Mudelsee, M., Bickert, T., Lear, C.H., Lohmann, G., 2014. Cenozoic climate changes: A review based on time series analysis of marine benthic $\delta 18O$ records. Rev. Geophys. 52, 333–374. doi:10.1002/2013RG000440.Received

Mudelsee, M., Raymo, M.E., 2005. Slow dynamics of the Northern Hemisphere glaciation. Paleoceanography 20, PA4022.

Mudie, P.J., 1982. Pollen distribution in recent marine sediments, eastern Canada. Can. J. Earth Sci. 19, 729–747.

Mudie, P.J., McCarthy, F.M.G., 2006. Marine palynology: potentials for onshore - offshore correlation of Pleistocene - Holocene records. Trans. R. Soc. South Africa 61, 139–157.

Mudie, P.J., McCarthy, F.M.G., 1994. Late Quaternary pollen transport processes, western North Atlantic: Data from box models, cross-margin and N-S transects. Mar. Geol. 118, 79–105.

Müller, P.J., Suess, E., 1979. Productivity, sedimentation rate, and sedimentary organic matter in the oceans - I. Organic carbon preservation. Deep Sea Res. Part A, Oceanogr. Res. Pap. 26, 1347–1362. doi:10.1016/0198-0149(79)90003-7

Naafs, B.D.A., Stein, R., Hefter, J., Khélifi, N., De Schepper, S., Haug, G.H., 2010. Late Pliocene changes in the North Atlantic Current. Earth Planet. Sci. Lett. 298, 434–442. doi:10.1016/j.epsl.2010.08.023

Nilsen, J.E.Ø., Nilsen, F., 2007. The Atlantic Water flow along the Vøring Plateau: Detecting frontal structures in oceanic station time series. Deep Sea Res. Part I 54, 297–319. doi:10.1016/j.dsr.2006.12.012

Norwegian Meteorological Institute, Norwegian Broadcasting Corporation, 2014. YR [WWW Document]. URL http://www.yr.no/ (accessed 1.3.15).

Numata, M., 1974. The flora and vegetation of Japan. Tokyo etc., Kodansha x, 294pp.. Illus. maps Geog 2.

Olivares, C.A., Antón, M.G., Manzaneque, F.G., Juaristi, C.M., 2004. Palaeoenvironmental interpretation of the Neogene locality Caranceja (Reocín, Cantabria, N Spain) from comparative studies of wood, charcoal, and pollen. Rev. Palaeobot. Palynol. 132, 133–157. doi:10.1016/j.revpalbo.2004.05.004

Olson, D.M., Dinerstein, E., Wikramanayake, E.D., Burgess, N.D., Powell, G.V.N., Underwood, E.C., D'amico, J.A., Itoua, I., Strand, H.E., Morrison, J.C., Loucks, C.J., Allnutt, T.F., Ricketts, T.H., Kura, Y., Lamoreux, J.F., Wettengel, W.W., Hedao, P., Kassem, K.R., 2001. Terrestrial Ecoregions of the World: A New Map of Life on Earth. Bioscience 51, 933–938. doi:10.1641/0006-3568(2001)051[0933:TEOTWA]2.0.CO;2

Orvik, K.A., Niiler, P., 2002. Major pathways of Atlantic water in the northern North Atlantic and Nordic Seas toward Arctic. Geophys. Res. Lett. 29, 2–1–2–4. doi:10.1029/2002GL015002

Osborne, A.H., Newkirk, D.R., Groeneveld, J., Martin, E.E., Tiedemann, R., Frank, M., 2014. The seawater neodymium and lead isotope record of the final stages of Central American Seaway closure. Paleoceanography 29, 715–729. doi:10.1002/2014PA002676

Ottersen, G., Planque, B., Belgrano, A., Post, E., Reid, P.C., Stenseth, N.C., 2001. Ecological effects of the North Atlantic Oscillation. Oecologia 128, 1–14. doi:10.1007/s004420100655

Paez-Reyes, M., Head, M.J., 2013. The Cenozoic Gonyaulacacean Dinoflagellate Genera Operculodinium Wall, 1967 and Protoceratium Bergh, 1881 and Their Phylogenetic Relationships. J. Paleontol. 87, 786–803. doi:10.1666/12-103

Pagani, M., Liu, Z., LaRiviere, J., Ravelo, A.C., 2010. High Earth-system climate sensitivity determined from Pliocene carbon dioxide concentrations. Nat. Geosci. 3, 27–30.

Palmer, A.R., 1983. The Decade of North American Geology 1983 Geologic Time Scale. Geology 11, 503–504. doi:10.1130/0091-7613(1983)11<503

Pearson, R.G., Phillips, S.J., Loranty, M.M., Beck, P.S.A., Damoulas, T., Knight, S.J., Goetz, S.J., 2013. Shifts in Arctic vegetation and associated feedbacks under climate change. Nat. Clim. Chang. 3, 673–677. doi:10.1038/nclimate1858

Peyron, O., Guiot, J., Cheddadi, R., Tarasov, P., Reille, M., de Beaulieu, J.-L., Bottema, S., Andrieu, V., 1998. Climatic Reconstruction in Europe for 18,000 YR B.P. from Pollen Data. Quat. Res. 49, 183–196. doi:http://dx.doi.org/10.1006/qres.1997.1961

Philippe, M., Méon, H., Lambert, G., Erdei, B., Thevenard, F., Gomez, B., 2002. A palm-tree and Sciadopitys swamp-forest from the Neogene of Bresse (eastern France). Comptes Rendus Palevol 1, 221–225. doi:10.1016/S1631-0683(02)00035-0

Poore, H.R., Samworth, R., White, N.J., Jones, S.M., McCave, I.N., 2006. Neogene overflow of Northern Component Water at the Greenland-Scotland Ridge. Geochemistry, Geophys. Geosystems 7. doi:10.1029/2005GC001085

Popescu, S.-M., 2001. Repetitive changes in Early Pliocene vegetation revealed by high-resolution pollen analysis: revised cyclostratigraphy of southwestern Romania. Rev. Palaeobot. Palynol. 120, 181–202.

Popescu, S.-M., Biltekin, D., Winter, H., Suc, J.-P., Melinte-Dobrinescu, M.C., Klotz, S., Rabineau, M., Combourieu-Nebout, N., Clauzon, G., Deaconu, F., 2010. Pliocene and Lower Pleistocene vegetation and climate changes at the European

scale: Long pollen records and climatostratigraphy. Quat. Int. 219, 152–167.

Popescu, S.M., Suc, J.P., Loutre, M.F., 2006. Early Pliocene vegetation changes forced by eccentricity-precession. Example from Southwestern Romania. Palaeogeogr. Palaeoclimatol. Palaeoecol. 238, 340–348. doi:10.1016/j.palaeo.2006.03.032

Potter, P.E., Szatmari, P., 2009. Global Miocene tectonics and the modern world. Earth-Science Rev. 96, 279–295. doi:10.1016/j.earscirev.2009.07.003

Pound, M.J., Haywood, A.M., Salzmann, U., Riding, J.B., 2012. Global vegetation dynamics and latitudinal temperature gradients during the Mid to Late Miocene (15.97–5.33Ma). Earth-Science Rev. 112, 1–22. doi:10.1016/j.earscirev.2012.02.005

Pound, M.J., Lowther, R.I., Peakall, J., Chapman, R.J., Salzmann, U., 2015. Palynological evidence for a warmer boreal climate in the Late Pliocene of the Yukon Territory, Canada. Palynology 39, 91–102. doi:10.1080/01916122.2014.940471

Pound, M.J., Riding, J.B., 2015. Palaeoenvironment, palaeoclimate and age of the Brassington Formation (Miocene) of Derbyshire, UK. J. Geol. Soc. London. doi:10.1144/jgs2015-050

Pound, M.J., Tindall, J., Pickering, S.J., Haywood, A.M., Dowsett, H.J., Salzmann, U., 2014. Late Pliocene lakes and soils: a global data set for the analysis of climate feedbacks in a warmer world. Clim. Past 10, 167–180. doi:10.5194/cp-10-167-2014

Prescott, C.L., Haywood, A.M., Dolan, A.M., Hunter, S.J., Pope, J.O., Pickering, S.J., 2014. Assessing orbitally-forced interglacial climate variability during the mid-Pliocene Warm Period. Earth Planet. Sci. Lett. 400, 261–271. doi:10.1016/j.epsl.2014.05.030

Quan, C., Liu, Y.-S.C., Tang, H., Utescher, T., 2014. Miocene shift of European atmospheric circulation from trade wind to westerlies. Sci. Rep. 4, 5660. doi:10.1038/srep05660

Radi, T., de Vernal, A., 2008. Dinocysts as proxy of primary productivity in mid-high latitudes of the Northern Hemisphere. Mar. Micropaleontol. 68, 84–114.

doi:10.1016/j.marmicro.2008.01.012

Ravelo, A.C., Andreasen, D.H., 2000. Enhanced circulation during a warm period. Geophys. Res. Lett. 27, 1001–1004. doi:10.1029/1999GL007000

Ravelo, A.C., Andreasen, D.H., Lyle, M., Olivarez Lyle, A., Wara, M.W., 2004. Regional climate shifts caused by gradual global cooling in the Pliocene epoch. Nature 429, 263–267. doi:10.1038/nature02567

Raymo, M.E., Grant, B., Horowitz, M., Rau, G.H., 1996. Mid-Pliocene warmth: stronger greenhouse and stronger conveyor. Mar. Micropaleontol. 27, 313–326. doi:10.1016/0377-8398(95)00048-8

Raymo, M.E., Rind, D., Ruddimann, W.F., 1990. Climate effects of reduced Arctic sea-ice limits in the GISS II general circulation model. Paleoceanography 5, 367–382.

Reid, P.C., 1977. Peridiniacean and glenodiniacean dinoflagellate cysts from the British Isles. Nov. Hedwigia 29, 429–463.

Risebrobakken, B., Andersson, C., De Schepper, S., McClymont, E.L., 2016. Low frequency Pliocene climate variability on the eastern Nordic Seas. Paleoceanography 31, 1154–1175. doi:10.1002/2015PA002918

Robinson, M.M., 2009. New quantitative evidence of extreme warmth in the Pliocene Arctic. Stratigraphy 6, 265–275.

Robinson, M.M., Dowsett, H.J., Dwyer, G.S., Lawrence, K.T., 2008. Reevaluation of mid-Pliocene North Atlantic sea surface temperatures. Paleoceanography 23, PA3213. doi:10.1029/2008pa001608

Robinson, M.M., Valdes, P.J., Haywood, A.M., Dowsett, H.J., Hill, D.J., Jones, S.M., 2011. Bathymetric controls on Pliocene North Atlantic and Arctic sea surface temperature and deepwater production. Palaeogeogr. Palaeoclimatol. Palaeoecol. 309, 92–97. doi:10.1016/j.palaeo.2011.01.004

Rochon, A., de Vernal, A., Turon, J.-L., Matthiessen, J., Head, M.J., 1999. Distribution of recent dinoflagellate cysts in surface sediments from the North Atlantic Ocean and adjacent seas in relation to sea-surface parameters. Am. Assoc. Stratigr. Palynol. 35, 1–146. doi:10.1016/0377-8398(94)00016-G

Romero-Wetzel, M.B., 1989. Struktur und Bioturbation des Makrobenthos auf dem Vöring-Plateau (Norwegische See). Berichte Sonderforschungsbereich 313 Univ. Kiel 13, 1–204.

Rousseau, D.-D., Bachiri-Taoufiq, N., Petit, C., Farjanel, G., Méon, H., Puisségur, J.-J., 1992. Continental late Pliocene paleoclimatic history recorded in the Bresse Basin (France). Palaeogeogr. Palaeoclimatol. Palaeoecol. 95, 253–261.

Rousseau, D.-D., Parra, I., Cour, P., Clet, M., 1995. Continental climatic changes in Normandy (France) between 3.3 and 2.3 Myr BP. Palaeogeogr. Palaeoclimatol. Palaeoecol. 113, 373–383.

Rybczynski, N., Gosse, J.C., Harington, C.R., Wogelius, R.A., Hidy, A.J., Buckley, M., 2013. Mid-Pliocene warm-period deposits in the High Arctic yield insight into camel evolution. Nat. Commun. 4, 1550. doi:10.1038/ncomms2516

Salzmann, U., Dolan, A.M., Haywood, A.M., Chan, W.-L., Voss, J., Hill, D.J., Abe-Ouchi, A., Otto-Bliesner, B., Bragg, F.J., Chandler, M.A., Contoux, C., Dowsett, H.J., Jost, A., Kamae, Y., Lohmann, G., Lunt, D.J., Pickering, S.J., Pound, M.J., Ramstein, G., Rosenbloom, N.A., Sohl, L., Stepanek, C., Ueda, H., Zhang, Z., 2013. Challenges in quantifying Pliocene terrestrial warming revealed by data-model discord. Nat. Clim. Chang. 3, 969–974.

Salzmann, U., Haywood, A.M., Lunt, D.J., 2009. The past is a guide to the future? Comparing Middle Pliocene vegetation with predicted biome distributions for the twenty-first century. Philos. Trans. R. Soc. A Math. Phys. Eng. Sci. 367, 189–204.

Salzmann, U., Haywood, A.M., Lunt, D.J., Valdes, P.J., Hill, D.J., 2008. A new global biome reconstruction and data-model comparison for the middle Pliocene. Glob. Ecol. Biogeogr. 17, 432–447.

Salzmann, U., Williams, M., Haywood, A.M., Johnson, A.L.A., Kender, S., Zalasiewicz, J., 2011. Climate and environment of a Pliocene warm world. Palaeogeogr. Palaeoclimatol. Palaeoecol. 309, 1–8. doi:10.1016/j.palaeo.2011.05.044

Sarnthein, M., Bartoli, G., Prange, M., Schmittner, A., Schneider, B., Weinelt, M., Andersen, N., Garbe-Schönberg, D., 2009. Mid-Pliocene shifts in ocean overturning circulation and the onset of Quaternary-style climates. Clim. Past 5,

269–283.

Schneider, W., 1995. Palaeohistological studies on Miocene brown coals of Central Europe. Int. J. Coal Geol. 28, 229–248. doi:10.1016/0166-5162(95)00019-4

Schreck, M., Matthiessen, J., 2013. Batiacasphaera micropapillata: Palaeobiogeographic distribution and palaeoecological implications of a critical Neogene species complex, in: Lewis, J., Marret, F., Bradley, L. (Eds.), Biological and Geological Perspectives of Dinoflagellates. The Micropalaeontological Society, Special Publications. Geological Society, London, pp. 293–306.

Schreck, M., Matthiessen, J., Head, M.J., 2012. A magnetostratigraphic calibration of Middle Miocene through Pliocene dinoflagellate cyst and acritarch events in the Iceland Sea (Ocean Drilling Program Hole 907A). Rev. Palaeobot. Palynol. 187, 66–94. doi:10.1016/j.revpalbo.2012.08.006

Schreck, M., Meheust, M., Stein, R., Matthiessen, J., 2013. Response of marine palynomorphs to Neogene climate cooling in the Iceland Sea (ODP Hole 907A). Mar. Micropaleontol. 101, 49–67. doi:10.1016/j.marmicro.2013.03.003

Schulz, C., Stutzel, T., 2007. Evolution of taxodiaceous Cupressaceae (Coniferopsida). Org. Divers. Evol. 7, 124–135. doi:10.1016/j.ode.2006.03.001

Screen, J., Simmonds, I., 2010. The central role of diminishing sea ice in recent Arctic temperature amplification. Nature.

Seki, O., Foster, G.L., Schmidt, D.N., Mackensen, A., Kawamura, K., Pancost, R.D., 2010. Alkenone and boron-based Pliocene pCO2 records. Earth Planet. Sci. Lett. 292, 201–211.

Seppä, H., Bennett, K.D., 2003. Quaternary pollen analysis: recent progress in palaeoecology and palaeoclimatology. Prog. Phys. Geogr. 27, 548–579. doi:10.1191/0309133303pp394oa

Seppä, H., Birks, H.J.B., 2001. July mean temperature and annual precipitation trends during the Holocene in the Fennoscandian tree-line area: pollen-based climate reconstructions. The Holocene 11, 527–539. doi:10.1191/095968301680223486

Seppä, H., Birks, H.J.B., Odland, A., Poska, A., Veski, S., 2004. A modern pollen-climate calibration set from northern Europe: Developing and testing a tool for

palaeoclimatological reconstructions. J. Biogeogr. 31, 251–267. doi:10.1111/j.1365-2699.2004.00923.x

Serreze, M.C., Francis, J.A., 2006. The arctic amplification debate. Clim. Change 76, 241–264. doi:10.1007/s10584-005-9017-y

Shipboard Scientific Party, 1987. 4. Site 642: Norwegian Sea, in: Eldholm, O., Thiede, J., Taylor, E. (Eds.), . Init. Repts., 104: College Station, TX (Ocean Drilling Program), pp. 53–453.

Simpson, G.L., 2012. Analogue Methods in Palaeolimnology, in: Birks, H.J.B., Lotter, A.F., Juggins, S., Smol, J.P. (Eds.), Tracking Environmental Change Using Lake Sediments. Springer, Dordrecht Heidelberg New York London, pp. 495–522.

Sniderman, J.M.K., Woodhead, J.D., Hellstrom, J., Jordan, G.J., Drysdale, R.N., Tyler, J.J., Porch, N., 2016. Pliocene reversal of late Neogene aridification. Proc. Natl. Acad. Sci. 201520188. doi:10.1073/pnas.1520188113

Sohl, L.E., Chandler, M.A., Schmunk, R.B., Mankoff, K., Jonas, J.A., Foley, K.M., Dowsett, H.J., 2009. PRISM3/GISS Topographic Reconstruction. U.S. Geol. Surv. Data Ser. 419 6 pp.

Steph, S., Tiedemann, R., Prange, M., Groeneveld, J., Nürnberg, D., Reuning, L., Schulz, M., Haug, G.H., 2006. Changes in Caribbean surface hydrography during the Pliocene shoaling of the Central American Seaway. Paleoceanography 21, PA4221. doi:10.1029/2004PA001092

Steph, S., Tiedemann, R., Prange, M., Groeneveld, J., Schulz, M., Timmermann, A., Nürnberg, D., Rühlemann, C., Saukel, C., Haug, G.H., 2010. Early Pliocene increase in thermohaline overturning: A precondition for the development of the modern equatorial Pacific cold tongue. Paleoceanography 25, 1–17. doi:10.1029/2008PA001645

Stockmarr, J., 1971. Tablets with spores used in absolute pollen analysis. Pollen et spores 13, 615–621.

Suc, J.-P., Bertini, A., Combourieu-Nebout, N., Diniz, F., Leroy, S., Russo-Ermolli, E., Zheng, Z., Bessais, E., 1995a. Structure of West Mediterranean vegetation and climate since 5.3 ma. Acta zool. cracov. 38, 3–16.

Suc, J.-P., Diniz, F., Leroy, S., Poumot, C., Bertini, A., Dupont, L., Clet, M., Bessais, E., Zheng, Z., Fauquette, S., Ferrier, J., 1995b. Zanclean (~Brunssumian) to early Piacenzian (~early-middle Reuverian) climate from 4° to 54° north latitude (West Africa, West Europe and West Mediterranean areas). Meded. Rijks Geol. D. 52, 43–56.

Svenning, J.C., 2003. Deterministic Plio-Pleistocene extinctions in the European cool-temperate tree flora. Ecol. Lett. 6, 646–653. doi:10.1046/j.1461-0248.2003.00477.x

Swift, J.H., 1986. The Arctic Waters, in: Hurdle, B.G. (Ed.), The Nordic Seas. Springer-Verlag New York Inc., New York, pp. 129–154.

Tarasov, P.E., Andreev, A.A., Anderson, P.M., Lozhkin, A. V., Leipe, C., Haltia, E., Nowaczyk, N.R., Wennrich, V., Brigham-Grette, J., Melles, M., 2013. A pollen-based biome reconstruction over the last 3.562 million years in the Far East Russian Arctic – new insights into climate–vegetation relationships at the regional scale. Clim. Past 9, 2759–2775. doi:10.5194/cp-9-2759-2013

Tarasov, P.E., Nakagawa, T., Demske, D., Österle, H., Igarashi, Y., Kitagawa, J., Mokhova, L., Bazarova, V., Okuda, M., Gotanda, K., Miyoshi, N., Fujiki, T., Takemura, K., Yonenobu, H., Fleck, A., 2011. Progress in the reconstruction of Quaternary climate dynamics in the Northwest Pacific: A new modern analogue reference dataset and its application to the 430-kyr pollen record from Lake Biwa. Earth-Science Rev. 108, 64–79. doi:10.1016/j.earscirev.2011.06.002

Thompson, R.S., Anderson, K.H., Bartleain, P.J., 1999. Atlas of Relations between Climatic Parameters and Distributions of Important Trees and Shrubs in North America. U.S. Geol. Surv. Prof. Pap. 1650A, 269. doi:http://pubs.usgs.gov/pp/p1650-a/pages/conifers.html

Thompson, R.S., Anderson, K.H., Pelltier, R.T., Strickland, L.E., Bartlein, P.J., Shafer, S.L., 2012. Quantitative estimation of climatic parameters from vegetation data in North America by the mutual climatic range technique. Quat. Sci. Rev. 51, 18–39. doi:10.1016/j.quascirev.2012.07.003

Thompson, R.S., Fleming, R.F., 1996. Middle Pliocene vegetation: Reconstructions, paleoclimatic inferences, and boundary conditions for climate modeling. Mar.

Micropaleontol. 27, 27–49. doi:10.1016/0377-8398(95)00051-8

Thorsen, T.A., Dale, B., 1997. Dinoflagellate cysts as indicators of pollution and past climate in a Norwegian fjord. Holocene 7, 433–446. doi:10.1177/095968369700700406

Trigo, R.M., Osborn, T.J., Corte-real, J.M., 2002. The North Atlantic Oscillation influence on Europe: climate impacts and associated physical mechanisms. Clim. Res. 20, 9–17. doi:10.3354/cr020009

Tripati, A.K., Roberts, C.D., Eagle, R.A., 2009. Coupling of CO2 and ice sheet stability over major climate transitions of the last 20 million years. Science 326, 1394–1397. doi:10.1126/science.1178296

Uhl, D., Klotz, S., Traiser, C., Thiel, C., Utescher, T., Kowalski, E., Dilcher, D.L., 2007. Cenozoic paleotemperatures and leaf physiognomy — A European perspective. Palaeogeogr. Palaeoclimatol. Palaeoecol. 248, 24–31. doi:10.1016/j.palaeo.2006.11.005

Utescher, T., Ashraf, A.R., Dreist, A., Dybkjaer, K., Mosbrugger, V., Pross, J., Wilde, V., 2012. Variability of Neogene Continental Climates in Northwest Europe - a detailed study based on Microfloras. Turkish J Earth Sci 21, 289–314.

Utescher, T., Bruch, A.A., Erdei, B., François, L., Ivanov, D., Jacques, F.M.B., Kern, A.K., Liu, Y.-S. (C. ., Mosbrugger, V., Spicer, R.A., 2014. The Coexistence Approach - Theoretical background and practical considerations of using plant fossils for climate quantification. Palaeogeogr. Palaeoclimatol. Palaeoecol. 410, 58–73. doi:10.1016/j.palaeo.2014.05.031

Utescher, T., Mosbrugger, V., 2013. The Palaeoflora Database [WWW Document]. URL http://www.palaeoflora.de (accessed 21.9.15).

Utescher, T., Mosbrugger, V., Ashraf, A.R., 2000. Terrestrial climate evolution in northwest Germany over the last 25 million years. Palaios 15, 430–449.

van der Kaars, S., De Deckker, P., 2003. Pollen distribution in marine surface sediments offshore Western Australia. Rev. Palaeobot. Palynol. 124, 113–129. doi:10.1016/S0034-6667(02)00250-6

Van Nieuwenhove, N., Baumann, A., Matthiessen, J., Bonnet, S., de Vernal, A., 2016.

Sea surface conditions in the southern Nordic Seas during the Holocene based on dinoflagellate cyst assemblages. The Holocene 26, 722–735. doi:10.1177/0959683615618258

Verhoeven, K., Louwye, S., 2013. Palaeoenvironmental reconstruction and biostratigraphy with marine palynomorphs of the Plio–Pleistocene in Tjörnes, Northern Iceland. Palaeogeogr. Palaeoclimatol. Palaeoecol. 376, 224–243. doi:10.1016/j.palaeo.2013.03.002

Verhoeven, K., Louwye, S., 2012. Selenopemphix islandensis sp. nov.: a new organic-walled dinoflagellate cyst from the Lower Pliocene Tjörnes beds, northern Iceland. Palynology 36, 10–25. doi:10.1080/01916122.2011.593573

Verhoeven, K., Louwye, S., Eiríksson, J., 2013. Plio-Pleistocene landscape and vegetation reconstruction of the coastal area of the Tjörnes Peninsula, Northern Iceland. Boreas 42, 108–122. doi:10.1111/j.1502-3885.2012.00279.x

Verhoeven, K., Louwye, S., Eiríksson, J., De Schepper, S., 2011. A new age model for the Pliocene-Pleistocene Tjörnes section on Iceland: Its implication for the timing of North Atlantic-Pacific palaeoceanographic pathways. Palaeogeogr. Palaeoclimatol. Palaeoecol. 309, 33–52. doi:10.1016/j.palaeo.2011.04.001

Verleye, T.J., Mertens, K.N., Louwye, S., Arz, H.W., 2009. Holocene Salinity Changes in the Southwestern Black Sea: a Reconstruction Based on Dinoflagellate Cysts. Palynology 33, 77–100. doi:10.2113/gspalynol.33.1.77

Versteegh, G.J.M., Brinkhuis, H., Visscher, H., Zonneveld, K.A.F., 1996. The relation between productivity and temperature in the Pliocene North Atlantic at the onset of northern hemisphere glaciation: A palynological study. Glob. Planet. Change 11, 155–165. doi:10.1016/0921-8181(95)00054-2

Versteegh, G.J.M., Zonneveld, K.A.F., 1994. Determination of (palaeo-)ecological preferences of dinoflagellates by applying Detrended and Canonical Correspondence analysis to Late Pliocene dinoflagellate cyst assemblages of the south Italian Singa section. Rev. Palaeobot. Palynol. 84, 181–199. doi:10.1016/0034-6667(94)90050-7

Wall, D., Dale, B., 1966. "Living fossils" in western Atlantic plankton. Nature 211, 1025–1026. doi:10.1038/211676a0

Wall, D., Dale, B., Lohmann, G.P., Smith, W.K., 1977. The environmental and climatic distribution of dinoflagellate cysts in modern marine sediments from regions in the North and South Atlantic Oceans and adjacent seas. Mar. Micropaleontol. 2, 121–200.

Wen, J., 1999. Evolution of Eastern Asian and Eastern North American Disjunct Distributions in Flowering Plants. Annu. Rev. Ecol. Syst. 30, 421–455. doi:10.1146/annurev.ecolsys.30.1.421

Westerhold, T., Bickert, T., Röhl, U., 2005. Middle to late Miocene oxygen isotope stratigraphy of ODP site 1085 (SE Atlantic): New constrains on Miocene climate variability and sea-level fluctuations. Palaeogeogr. Palaeoclimatol. Palaeoecol. 217, 205–222. doi:10.1016/j.palaeo.2004.12.001

Whitmore, J., Gajewski, K., Sawada, M., Williams, J.W., Shuman, B., Bartlein, P.J., Minckley, T., Viau, A.E., Webb, T., Shafer, S., Anderson, P., Brubaker, L., 2005. Modern pollen data from North America and Greenland for multi-scale paleoenvironmental applications. Quat. Sci. Rev. 24, 1828–1848. doi:10.1016/j.quascirev.2005.03.005

Willard, D.A., 1996. Pliocene-Pleistocene pollen assemblages from the Yermak Plateau, Arctic Ocean: Sites 910 and 911. Proc. Ocean Drill. Program, Sci. Results 151, 297–305.

Willard, D.A., 1994. Palynological record from the North Atlantic region at 3 Ma: vegetational distribution during a period of global warmth. Rev. Palaeobot. Palynol. 83, 275–297. doi:10.1016/0034-6667(94)90141-4

Willard, D.A., Cronin, T.M., Scott, E.I., Litwin, R.J., 1993. Terrestrial and marine records of climatic and environmental changes during the Pliocene in subtropical Florida. Geology 21, 679–682.

Willard, D.A., Weimer, L.M., Riegel, W.L., 2001. Pollen assemblages as paleoenvironmental proxies in the Florida Everglades. Rev. Palaeobot. Palynol. 113, 213–235. doi:10.1016/S0034-6667(00)00042-7

Williams, M., Haywood, A.M., Harper, E.M., Johnson, A.L.A., Knowles, T., Leng, M.J., Lunt, D.J., Okamura, B., Taylor, P.D., Zalasiewicz, J., 2009. Pliocene climate and seasonality in North Atlantic shelf seas. Philos. Trans. R. Soc. A Math. Phys.

Eng. Sci. 367, 85–108.

Willis, K.J., Kleczkowski, A., Briggs, K.M., Gilligan, C.A., 1999a. The role of sub-Milankovitch climatic forcing in the initiation of the Northern Hemisphere glaciation. Science (80-.). 285, 568–571.

Willis, K.J., Kleczkowski, A., Crowhurst, S.J., 1999b. 124,000-year periodicity in terrestrial vegetation change during the late Pliocene epoch. Nature 397, 685–688.

Wrenn, J.H., 1988. Differentiating species of the dinoflagellate cyst genus Nematosphaeropsis Deflandre & Cookson 1955. Palynology 12, 129–150.

Xing, Y., Gandolfo, M.A., Linder, H.P., 2015. The Cenozoic biogeographical evolution of woody angiosperms inferred from fossil distributions. Glob. Ecol. Biogeogr. 1290–1301. doi:10.1111/geb.12383

Zachos, J., Pagani, M., Sloan, L., Thomas, E., Billups, K., 2001. Trends, rhythms, and aberrations in global climate 65 Ma to present. Science 292, 686–93. doi:10.1126/science.1059412

Zachos, J.C., Dickens, G.R., Zeebe, R.E., 2008. An early Cenozoic perspective on greenhouse warming and carbon-cycle dynamics. Nature 451, 279–283. doi:10.1038/nature06588

Zagwijn, W.H., 1992. The beginning of the Ice Age in Europe and its major subdivisions. Quat. Sci. Rev. 11, 583–591.

Zagwijn, W.H., 1960. Aspects of the Pliocene and Early Pleistocene vegetation in the Netherlands. Meded. van Geol. Sticht. 3, 1–78.

Zhang, Z.S., Nisancioglu, K.H., Chandler, M.A., Haywood, A.M., Otto-Bliesner, B.L., Ramstein, G., Stepanek, C., Abe-Ouchi, A., Chan, W.L., Bragg, F.J., Contoux, C., Dolan, A.M., Hill, D.J., Jost, A., Kamae, Y., Lohmann, G., Lunt, D.J., Rosenbloom, N.A., Sohl, L.E., Ueda, H., 2013a. Mid-Pliocene Atlantic Meridional Overturning Circulation not unlike modern. Clim. Past 9, 1495–1504. doi:10.5194/cp-9-1495-2013

Zhang, Z.S., Nisancioglu, K.H., Ninnemann, U.S., 2013b. Increased ventilation of Antarctic deep water during the warm mid-Pliocene. Nat. Commun. 4, 1499. doi:10.1038/ncomms2521

Zonneveld, K.A.F., Bockelmann, F., Holzwarth, U., 2007. Selective preservation of organic-walled dinoflagellate cysts as a tool to quantify past net primary production and bottom water oxygen concentrations. Mar. Geol. 237, 109–126. doi:10.1016/j.margeo.2006.10.023

Zonneveld, K.A.F., Marret, F., Versteegh, G.J.M., Bogus, K., Bonnet, S., Bouimetarhan, I., Crouch, E., de Vernal, A., Elshanawany, R., Edwards, L., Esper, O., Forke, S., Grøsfjeld, K., Henry, M., Holzwarth, U., Kielt, J.F., Kim, S.Y., Ladouceur, S., Ledu, D., Chen, L., Limoges, A., Londeix, L., Lu, S.H., Mahmoud, M.S., Marino, G., Matsouka, K., Matthiessen, J., Mildenhal, D.C., Mudie, P., Neil, H.L., Pospelova, V., Qi, Y., Radi, T., Richerol, T., Rochon, A., Sangiorgi, F., Solignac, S., Turon, J.L., Verleye, T., Wang, Y., Wang, Z., Young, M., 2013. Atlas of modern dinoflagellate cyst distribution based on 2405 data points. Rev. Palaeobot. Palynol. 191, 1–197. doi:10.1016/j.revpalbo.2012.08.003